Continuous Gauging of Electric Traction Contact Wire.

BY

A. R. TIMM

PRESENTED FOR THE DEGREE OF

MASTER OF SCIENCE

IN

ELECTRICAL ENGINEERING

AT THE

UNIVERSITY OF CAPE TOWN

DECEMBER 1975

The copyright of this thesis vests in the author. No quotation from it or information derived from it is to be published without full acknowledgement of the source. The thesis is to be used for private study or non-commercial research purposes only.

Published by the University of Cape Town (UCT) in terms of the non-exclusive license granted to UCT by the author.

University of Cape Town

Acknowledgement

I should like to express my sincere thanks to Prof.J.L.Besseling and Mr.J.H.van Nierop for their supervisory assistance, and to Mr.D.J.B.Kenyon for his labours in the Workshop.

Thanks are also due to Messers Ackermann and Louwrens of the South African Railways for their assistance in supplying information, and to Mr. Krynauw for his advice and co-operation in the testing of the device.

Finally I should like to express my gratitude to Heinke Hoffmann for undertaking the typing, and to my wife Jill for her patience and moral support over the duration of the project.

ABSTRACT

In this system the electric traction overhead contact wire wear is continuously measured. A GaAs LED and lens combination produces a collimated beam of light along the pantograph pan. The beam, through which the contact wire slides, is monitored by a vertical array of phototransistors spaced at equal intervals. The number of phototransistors in shadow at any instant is proportional to the contact wire thickness. A fibre-optic data link conveys the encoded information from the pan at high tension to the locomotive at ground potential.

The uncertainty of measurement, defined by the detector spacing, is 1½ mm (or 10% of the new contact wire). By using an integrated detector array, a resolution of ⅛ mm could be achieved (0,8% accuracy).

The electromagnetic screening against the large fields associated with the currents in the live contact wire proved adequate.

The prototype operated satisfactorally at speeds up to 60 Km/hr, in tests on the live 3 kV D.C. South African Railway's overhead contact wire system. Its dynamic performance can be improved by making the box for the circuitry smaller, and constructing a special streamlined pan from a lightweight alloy.

ERRATA

Section	Page	Paragraph	Line	
1-10	1	4	2 :	... cause to doubt the validity of ...
1-24b	9	3	5 :	... smooth running conditions ...
1-42b	25	3	3 :	... continually carries the arc ...
1-42c	25	4	4 :	... is to the arc spot, and ...
3-31b	83	5	2 :	... at currents of almost ...
4-10	102	5	8 :	... C_2 is charged up via R_{10} ...
4-21b	117	3	1 :	... expression exists for $R(\lambda)$, it is ...
4-21b	119	3	1 :	... pu effectiveness of the sun's radiation ...
4-22b	124	2	2 :	... of about 0,07 mW/cm^2.
4-64	174	7	5 :	... and capicitor combination R_1 and C_1 .
6-20g	195	7	1 :	... the pen recorder were run ...
I-2	204	1	2 :	... cause the tension mountings of ...
III-1a	219	7	2 :	The Zener diode Z_1 ...
III-1b	223	7	1 :	... collector current of T_2 is then ...

Fig 1-14 27 : ... on Japanese New Tocaido Line.

Fig 4-2 117 : ... under a curve by Simpson's Rule.

I N D E X

1		INTRODUCTION	1
	1-10	General	1
	1-20	Details of Overhead System	4
	1-21	Overhead Contact Wire	
	1-22	Overhead Catenary System	
	1-23	Supporting Structures	
	1-24	General Design Considerations	
	1-30	The Pantograph	13
	1-31	General Description	
	1-32	Dynamic Behaviour	
	1-33	Present and Future Trends	
	1-40	Contact Wire Wear	22
	1-41	The Phenomenon of Current Collection	
	1-42	Normal Contact Wire Wear	
	1-43	Hard Spots and Other Phenomena	
	1-44	Permissible Wear	
2		THE SYSTEM	33
	2-10	General	33
	2-20	Wear Measurement by Optical Scanning of Contact Wire Profile	34
3		FEASIBILITY STUDY	39
	3-10	Components	39
	3-11	Choice of Light Source	
	3-12	Choice of Detector	
	3-13	Design of Lens	
	3-20	Accuracy	53
	3-21	Lens Limitations	
	3-22	Deciding at what Intensity Level to Recognise Presence of Light	
	3-23	Setting Light Source at Focal Point of Lens	
	3-24	Resolution	
	3-30	Electrical Considerations	80
	3-31	Mode of Operation	
	3-32	Noise Statistics	
4		ELECTRICAL DESIGN DETAIL	100
	4-10	Design of LED Pulsing Circuit	102
	4-20	Design of Photodetector Circuit	116
	4-21	Circuit Sensitivity	
	4-22	Circuit Design	
	4-30	Digital Manipulation of Data at 3 kV	145

4-31	Data Decoding	
4-32	Circuit Realisation	
4-40	Power Supply for System on Pantograph	155
4-50	Data Transmission Across 3 kV	156
4-60	Data Decoding and Display	161
4-61	Data Reception	
4-62	Data Interrogation	
4-63	Data Display and Recording	
4-63	Alarm Circuit	
4-70	Power Supply for System on Ground	175
5	RESULTS	177
5-10	Performance in the Laboratory	177
5-11	Accuracy	
5-12	Noise Immunity	
5-20	Assessment in the Field	181
5-21	As a Measuring Device	
5-22	Mechanical Features	
5-23	Electrical Features	
6	CONCLUSION	192
6-10	General	192
6-20	Improvements for Future Models.	194

APPENDICES

I	REJECTED METHODS OF CONTACT WIRE WEAR MEASUREMENT	197
I-1	Resistance Measurement	197
I-2	Deflection Measurement	200
I-3	Using Television	205
I-4	Using Ultrasonics	208
II	METHODS OF SETTING THE LIGHT SOURCE AT THE FOCAL POINT OF THE LENS	210
II-1	Method 1	210
II-2	Method 2	216

III/

CHAPTER I
INTRODUCTION

1-10 GENERAL

The project aims to devise a system which will measure the wear of the South African Railways overhead contact wire.

Such a device would prove invaluable, as it would greatly reduce the overhead system maintenance costs. At present a vast labour force is employed to continuously inspect every metre of the high voltage 3 kV contact wire throughout the electrified system. Visual checks are carried out almost continuously, while accurate spot checks are performed at six-monthly intervals. Previously these were done by micrometer, but in 1972 a "slide on" contact wire thickness gauge* was developed by Mr D. Louwrens of the S.A.R., which has proved more efficient. See Fig 1-1.

However, there is still the need for a mechanised device which can take a continuous, accurate measurement of the contact wire thickness. With the country's expanding rail electrification program, the problem of overhead maintenance is becoming increasingly burdensome. Countries with much larger electrified systems, e.g. Japan, quote figures of 20% of the total man-hours devoted to line inspection, being spent on contact wire measurement alone.[1]

Apart from the enormous cost of maintaining the labour force, there is often cause to double the validity of some of the readings recorded because of the human factor - boredom. Such repetitive work is tailor-made for a machine since it cannot become careless.

There is also the question of honesty. A certain worthy, responsible for keeping record of the contact wire thickness, decided it was far easier to estimate this figure, rather than measure it. On his falling ill one day, it was discovered to his chagrin, that the readings taken by his "stand in", bore little correlation to those recorded by him!

It is important to avoid this type of situation, for several reasons. Firstly it is economically prudent to be able to plan overhead replacements in an orderly fashion, before

* S.A.R. Reference Number: WE 2270/5

BREAKS/

breaks occur, (rather than also paying the costs of the damages). Secondly, there is the danger aspect - anyone in the vicinity of a break is liable to sustain a lethal 3 kV electric shock.

Another relevant point is that much of the routine overhead maintenance (e.g. insulator replacement and contact wire thickness measurement) is performed under live electrical conditions.[2] Cutting the power for such tasks would cause continual disruption of rail traffic. Those concerned however, have little to fear provided they are careful - but if they are caught unexpectedly by a sudden gust of wind, while precariously perched on the top of a wooden ladder, the results can be disastrous.

(The author was priviliged to meet a foreman of the works who claims to have been a victim of such an incident. On losing his balance when a squall struck, he clutched at the proverbial straw and managed to make contact with the adjacent supporting structure while touching the live contact wire. Fortunately he was revived by mouth-to-mouth resuscitation. The white scars on his hands bore witness to his tale.)

Hence it is important to give careful consideration to the safety aspect.

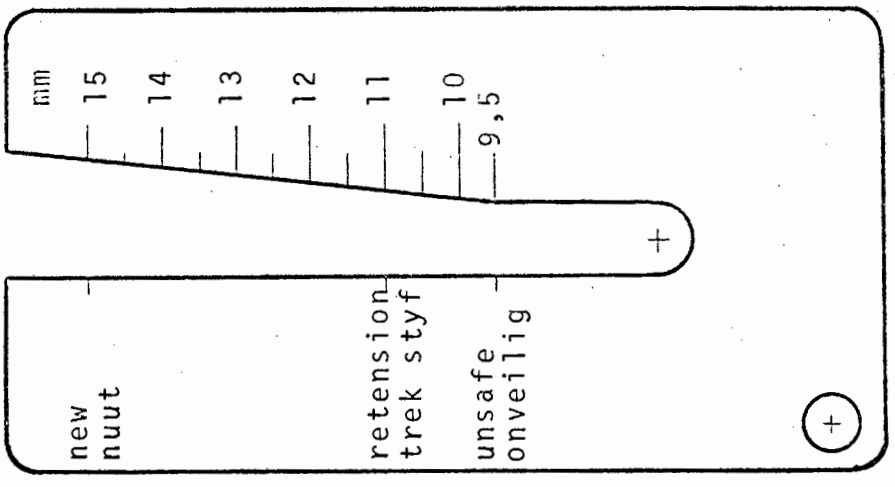

Fig 1-1: Contact Wire Thickness Gauge
(Courtesty of the S.A.R.)

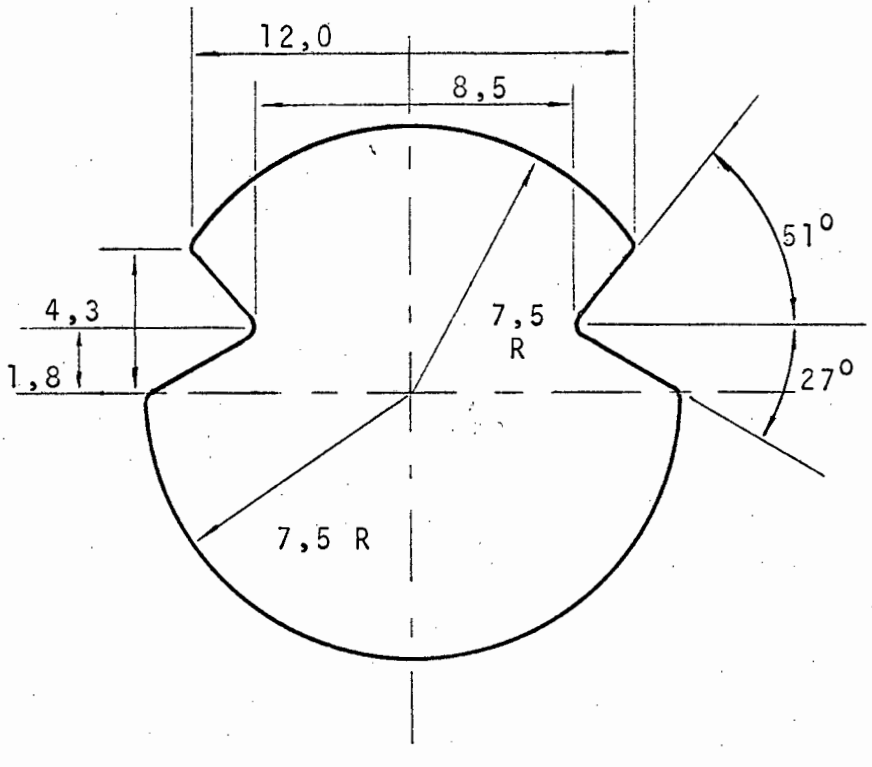

Fig 1-2: Cross Section of Overhead Contact Wire
(5x Full Scale) (All Dimensions in mm)

1-20 DETAILS OF OVERHEAD SYSTEM

A thorough knowledge of the overhead system is necessary to appreciate the problems involved in the construction of the proposed device. Generally the overhead construction is in accordance with British Standard specifications.

1-21 Overhead Contact Wire

The following is a summary of relevant extracts from the basic specifications[3] laid down by the South African Railways, for the overhead contact wire. These comply with the British Standard (B.S.) 23. A cross-section view of the contact wire is shown in Fig 1-2.

The wire shall be made of high conductivity copper, be hard drawn* and grooved, and supplied in lengths of 1830 metres, (6 000 ft) free of kinks, twists or other defects. These lengths shall be wound evenly on drums in such a manner that the vertical axis of the wire is at right angles to the axis of the drum, and "the contact surface of the wire shall be to the bottom when the wire is unreeled off the top of the drum".

All joints in the wire shall be made before drawing (either by electric welding or with hard silver solder), and the properties of the joints shall comply with those of the wire in general, in accordance with B.S. 23, which are:

i	Mass per 1830 metres (± 3% tolerance)	- 2623 Kg
ii	Resistance at 20°C per 1830 metres	- 0,2056 ohm (max)
iii	Ultimate tensile strength	- 3150 Kg/cm^2 (min)
iv	Percentage elongation in gauge length of 25 cm	- 4,5% (min)
v	Number of torsions in 25 cm	- 4 (min)
vi	Number of 90° bends	- 6 (min)
vii	Brinell Hardness Number	- 96) (min)
	Rockwell "B" Hardness Number	- 50)
viii	Coefficient of linear expansion per degree C	- 17 x 10^{-6}
ix	Modulus of elasticity	- 1,27 x 10^6 Kg/cm^2
x	Cross-section area	- 1,61 cm^2

* Cadmium copper is now used in preference to the hard drawn variety, which was prone to the accumulation of "permanent stretch", and hence required periodic re-tensioning.

OVERHEAD/

1-22 Overhead Catenary System

Here too, as in most Railway designs, South Africa has adopted British standards.

Various possible catenary systems are listed below.[4a]

(a) One single-contact wire (tramway construction).
(b) A main catenary supporting a single-contact wire.
(c) One contact wire supported by an auxiliary catenary which is in turn supported by a main catenary.
(d) A single catenary supporting two contact wires.
(e) Two contact wires supported by an auxiliary catenary which is supported by a main catenary.

Currently in use in South Africa is the second system (b), which gives sufficient flexibility to the contact wire for the speeds sustained in this country, while not being too compli= cated in construction. See Fig 1-3.

(At present locomotive speeds are limited to less than 100 Km/hr[5], but a feasibility study is being conducted with regard to the introduction of a high speed line. It is likely that if the present catenary system proves to be inadequate, then the third type (c) mentioned above will be used in preference to (d) or (e), as a single robust contact wire is generally recommended as being satisfactory.[4b] This in fact is used in most overseas countries.

The envisaged system will use 25 kV (a.c.)on the overhead line instead of the present 3 kV (d.c.) and will result in smaller currents being drawn by the locomotives. Hence the overhead contact wire need not be as thick as it is at present, so less copper will be used. This will reduce construction costs.)

The catenary is usually made of stranded cables of hard-drawn copper to achieve maximum conductivity for minimum weight. It is in electrical contact with the contact wire via feeder connections, and also, though to a lesser extent, via the droppers.

The droppers[4c] consist of looped conductors which when in tension, keep the contact wire at the required height above the ground, yet do not add any downward force to it when it is lifted by a passing pantograph. They are made of flexible stranded wires, or, in industrial areas where individual strands have been found to deteriorate rapidly, of semi-hard-

Fig 1-3: Different Catenary Systems

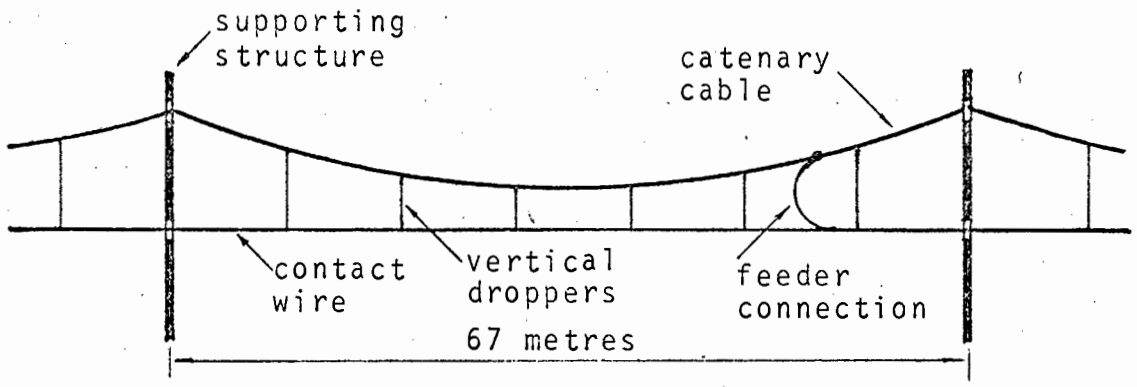

(a) Longitudinal Elevation of Normal Span
(Single Catenary and Contact Wire)

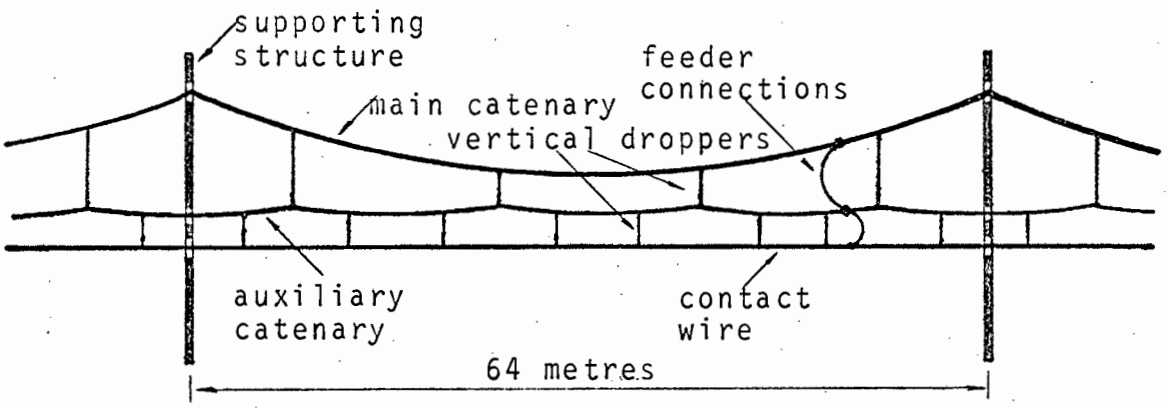

(b) Longitudinal Elevation of Normal Span
(Main and Auxiliary Catenaries and Contact Wire)

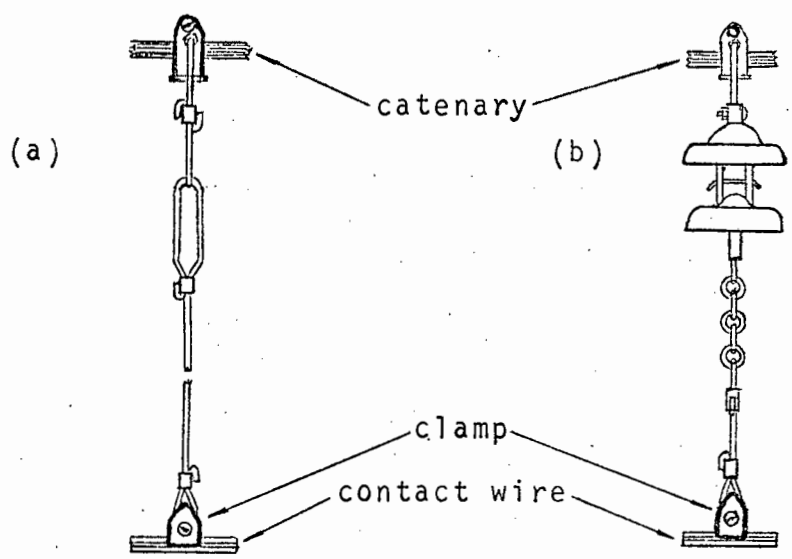

Fig 1-4: (a) Conducting and (b) Non-conducting dropper

drawn solid copper wire. Bolted clips are used to attach them to the catenary and to the contact wire. See Fig 1-4.

Some droppers are purposely designed to isolate the contact wire from whatever else they are connected to. These find a use under bridges where clearances are such that only the contact wire may be carried through.[4d] The main catenary is then terminated at each of the bridge faces and jumpered across by means of an insulated cable.

1-23 Supporting Structures

Supporting structures are usually made of steel, with the high voltage overhead wires attached to them by means of insulators. They are spaced about 67 metres apart, and their design usually depends on such things as required clearance from the track, allowance on curves, and generally the particular railway in question. A typical supporting structure with independent registration fittings is shown in Fig 1-5.

With high speed traffic, hard spots tend to form at each registration point. To counter this, the steady arms are made as light and as short as possible, and their hinges are brought down approximately to the level of the contact wire. This brings them in line with the centrifugal forces experienced when going around curves, and also with the transverse frictional components due to contact wire stagger. A horizontal hinge allows any movement along the track, which may occur from periodic re-tensioning of the contact wires, or even from the stroking effect of a passing pantograph.

1-24 General Design Considerations

(a) Span Length and Stagger

To avoid the contact wire being blown off the pantograph in high winds, span lengths are limited to about 67 metres (220 ft).[4e] On maximum length spans, the contact wire must be central on the pantograph at mid-span, but as the span length is decreased (for instance around curves), an increasing offset at mid-span is allowed.

On straight sections of track, the contact wire is displaced at the supporting structures, alternatively to one side of the track centre and then to the other. This "staggering" of the contact wire ensures even wear and prevents "tracking"

ON/

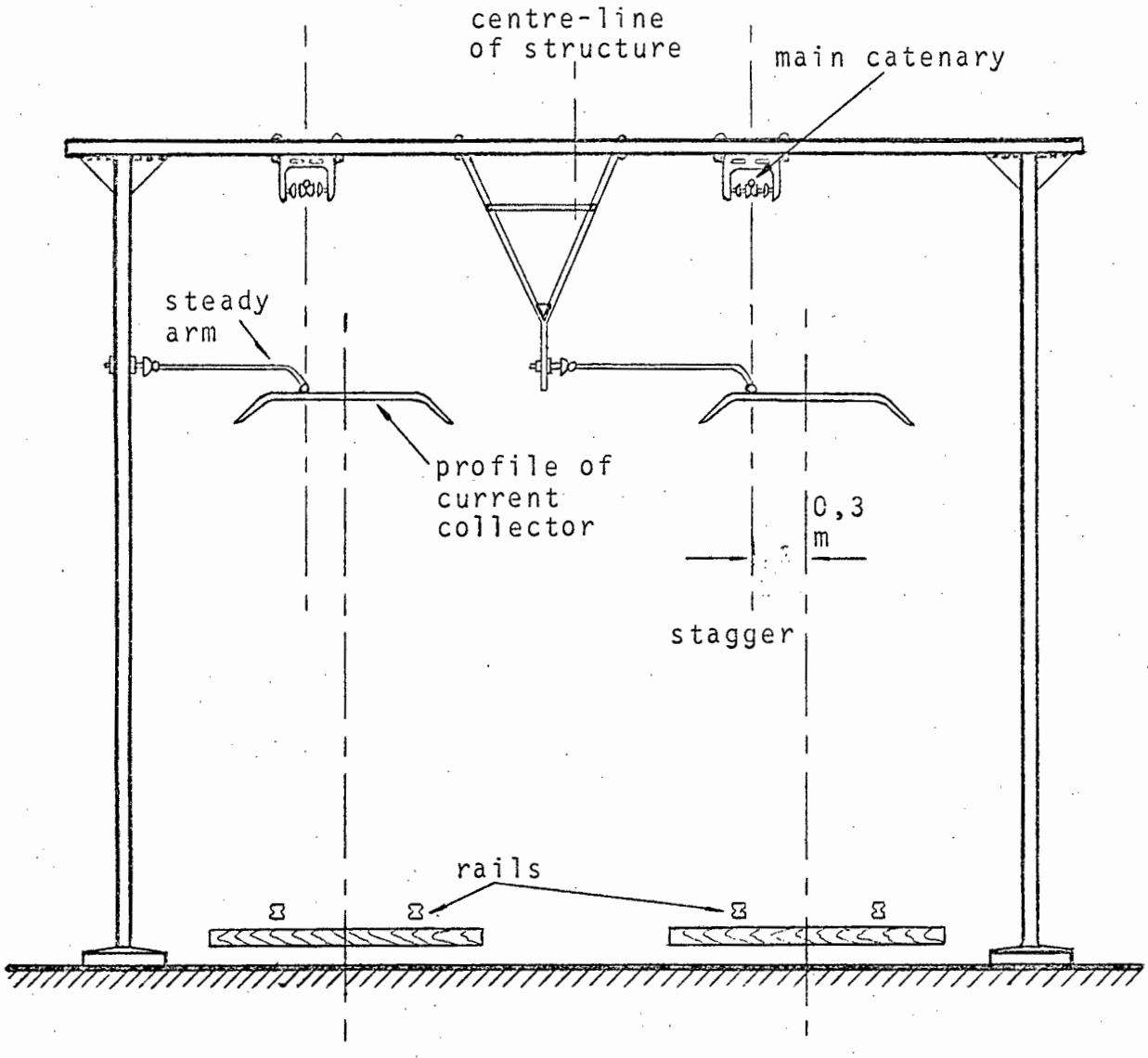

Fig 1-5: Typical Supporting Structure with Independent Registration Fittings

on the current collecting surface of the pantograph "pan". The normal stagger amplitude is about 30 cm,[4f] while the maximum offset on curves is limited to almost 40 cm.

(b) Tensioning

Correct tensioning of the contact wire is important for smooth running, since ambient temperature variations cause expansions and contractions in its length. If the normal tension is set too high, then a severe strain is imparted to the registration fittings on cold days - especially around curves of small radius and at terminal structures.

In addition if the sag in the catenary is too small, the contraction or expansion along its length causes the contact wire to "hog" or "droop". This is unsatisfactory for high speed running. Generally a catenary sag of 1,5 metres to 1,8 metres[4g] is advocated for smooth funning conditions at all speeds. A 10% error in catenary tension produces an error in the contact wire sag of about 6 cm.

With increasing rail speeds, correct tensioning[6] of the contact wire assumes greater importance, as oscillations are set up when the pantograph reaches certain critical speeds. Resonance occurs when the velocity of the pantograph equals the group velocity of the wire - which is different for each harmonic of the wave induced by the pantograph. These critical speeds are proportional to the square root of the contact wire tension,[7] and the amplitude of oscillation is found to increase markedly with tension[8]. Research by the Japanese National Railways indicates that this phenomenon is only experienced at velocities of the order of 200 Km/hr and beyond - depending on the tension and the nature of the equipment used. With the relatively slow rail speeds currently used in South Africa however, this is not yet a problem.

Tension lengths are restricted to about 1,8 kilometres (the length in which the contact wire is supplied), both for convenience in manufacturing and for electrical sectioning and maintenance. To ensure a smooth transition of the panto= graph from one tension length to the next, the contact wires are overlapped for a short distance at adjoining sections. Sometimes these overlapping sections are clamped solidly together in electrical contact, or they may be insulated and fitted with jumpers or they may be insulated and switched.

THE/

The tension in the contact wire is measured using a de= flection device commonly known as the "Hans Schmidt Gauge".

Figure 1-6 shows the principle of operation of the device. It makes contact with the wire at three points spaced half-a-metre apart. A spring at the centre contact point causes the wire to deflect by an amount δ, which is registered on the dial. A table[9] is then used to determine the tension T from the contact wire thickness t, and the deflection δ.

(The minimum tension registered on the gauge chart is 1 000 lb.wt. while the maximum is 4 000 lb.wt. In practice the setting is kept well away from either limit.)

Automatic tensioning is employed on the Continent and especially in Sweden where temperature conditions are extreme. Since this is also only effective where the overhead system is light,it has not found favour in this country. Other factors against it are its expense and the limitation it imposes on the tension length.

(c) Contact Wire Height

The normal contact wire height above rail level is 4,88 metres (16 ft),[4h] but over public level crossings it is increased to 5,49 metres (18 ft). In sidings where there is a danger to men working on wagons, a height of 6,10 metres (20 ft) is advocated.

The minimum height is dependent on the loading gauge and the required electrical clearance to rolling stock. This problem is found at bridges and tunnels where usually only very small clearances are available.

The accepted criterion is that a minimum space of 32 cm must be available in order to pass all the wires (catenaries and contact wire) under flat-soffit bridges, while only 22 cm is required for bridges of the jack-arch type.[4i] This minimum-clearance construction permits a possible free lift of 7 cm, which is sufficient even when the upward panto= graph force is almost doubled - which is almost the case when very heavy trains require two locomotives in tandem to pull them.

Some stations also have a very small clearance. In Cape Town Station, for instance, the pantograph current collector is forced almost right down on to its mountings by the

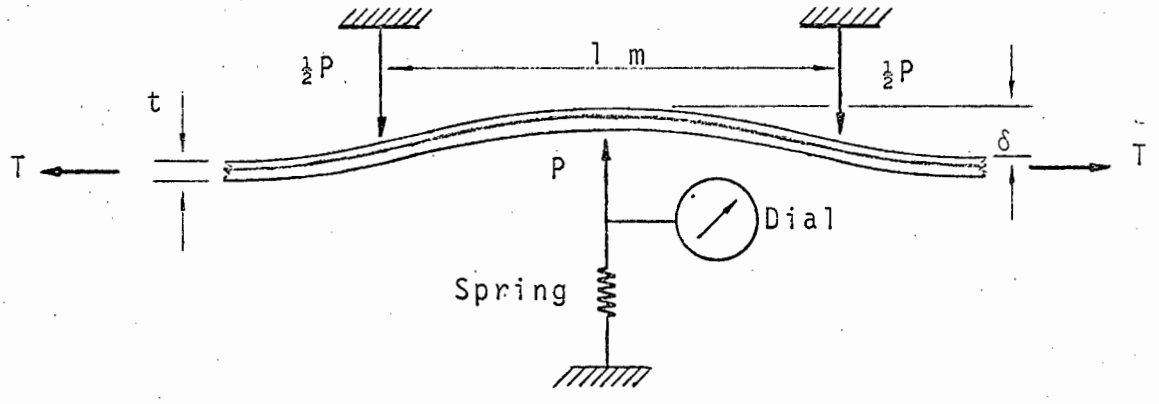

Fig 1-6: Principle of Operation of Hans Schmidt Gauge

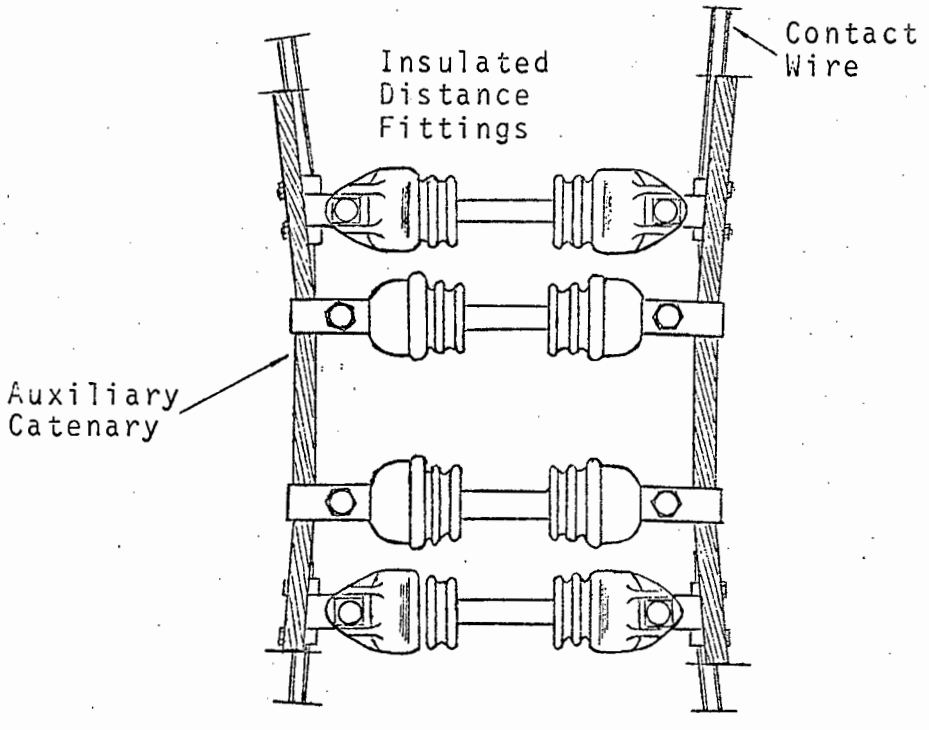

Fig 1-7: Plan View of Insulated Knuckle connecting Contact Wires and Auxiliary Catenaries

contact wire. This is acceptable because the speed there is so low. For high speed running the change of grade of the contact wire relative to the rail must not exceed 1 in 300 for main-line operation.

(d) Multiple-Track Construction

For main-line multiple-track constructions, the electrical equipment of each line is paralleled at substations and track sectioning cabins. They are otherwise insulated from one another. This enables any one track to be isolated in the event of a fault.

Where cross-overs exist between main lines, an "insulated knuckle"[4j] (see Fig 1-7) is used to isolate the two overhead systems, while allowing a locomotive to pass from the one to the other with little reduction in speed. Although "hard spots"(points on the contact wire where excessive localised wear occurs) are created at these places, they are not unduly serious.

1-30 THE PANTOGRAPH

1-31 General Description

The relatively low potential (3 kV D.C.) used by the South African Railways on their overhead system, necessitates large currents (of the order of kilo-amps) being drawn by such units as the Class 4E locomotives of the Cape Western System.[5]

Heavy current collectors are therefore required (they weigh about 12 kg), and hence the whole pantogtaph must be of a robust construction. Because of the associated inertia, the contact force between the current collector and the contact wire must be sufficiently large to ensure that as little contact loss as possible occurs between them. This is an important criterion for good current collection. However a compromise must be made, since overmuch force causes excessive wear on both contact strips and contact wire. In practice a contact force of about 7,3 kg (16 lb)[2] is typical.

The contact strips[10a] (see Fig 1-8) used by the S.A.R. on their pantograph heads were made of hard drawn copper.* This ensures an adequate rating for the current path.

It is common practice to lubricate the contact wire with castor oil, and some of the locomotives carry axil-driven pumps which feed oil from a reservoir on the underframe of the pan head. By planned routing of these locomotives the contact wire is kept well lubricated.

A disadvantage of copper contact strips is that they tend to become welded to the contact wire when under heavy load.[11a] South Africa seems to be almost the only country employing such strips. Other countries prefer such materials as carbon, metallised carbon, sintered iron, steel, hard steel, and even aluminium.[10b] However, since most overseas countries use higher voltage a.c. systems, where they do not have to draw such large currents, it is difficult to make a fair comparison.

Single-pan current collectors mounted on to diamond frame pantographs are used on the suburban locomotives in the Cape Western system. The pan is bow-shaped as shown in Fig 1-8,

* Cadmium copper is now used in preference to hard drawn copper.

THE END/

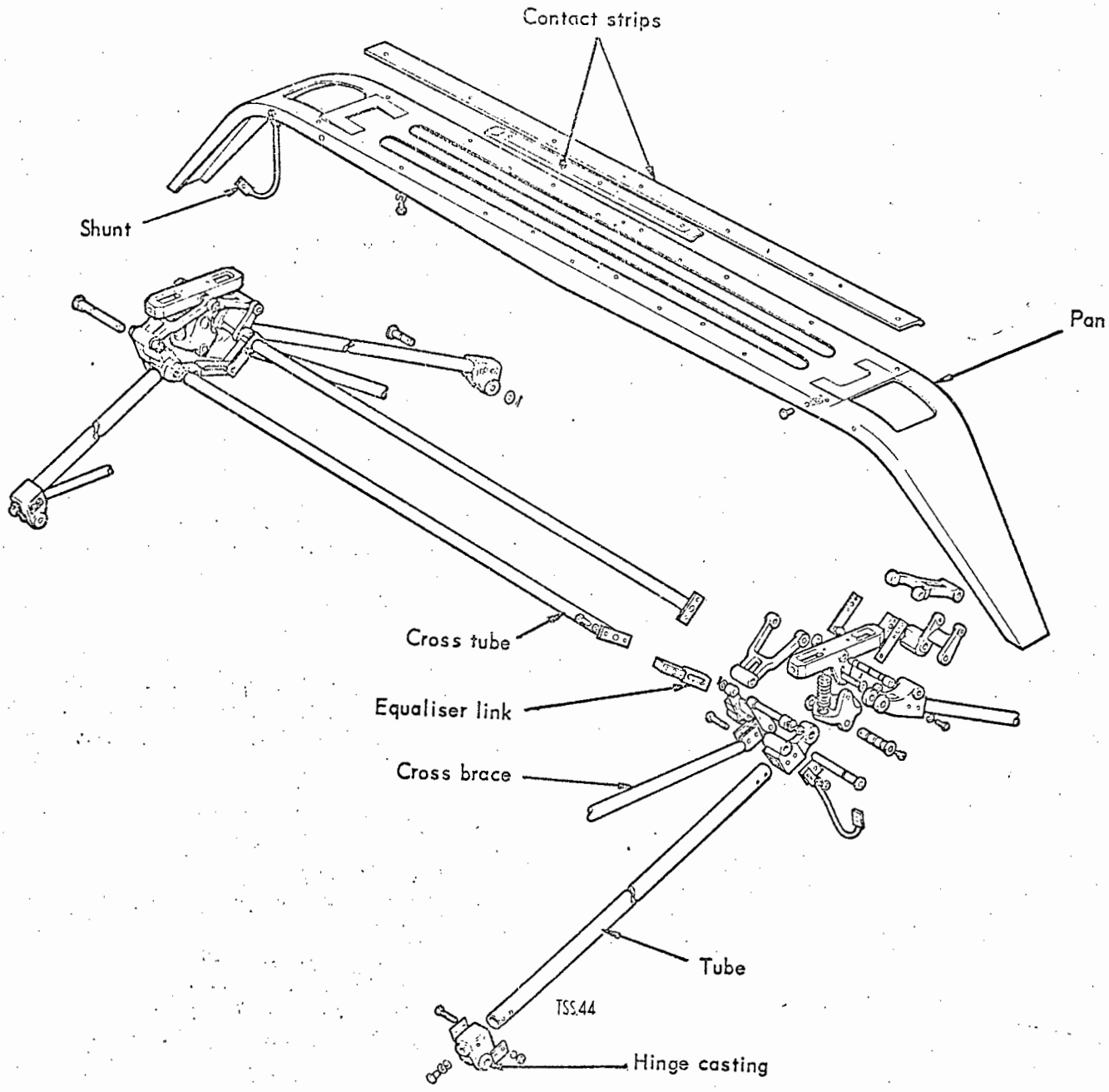

Fig 1-8: UPPER MOVING FRAME AND PAN ASSEMBLY
(Courtesy of the S.A.R.)

the end horns preventing the contact wire from sliding under the pantograph head. This might otherwise happen at points and cross-overs, where a transfer must be made from one wire to another. A gentle slope must therefore exist between the horns and the pan's middle section, and the contact wire's height must be properly adjusted. This ensures a smooth tran= sition of the point of contact.

Other factors that can cause the pan to hook itself over the wire are combinations of "throw-over" (due to centrifugal force), "blow-off" (caused by strong winds), and wire stagger.

The length of the pantograph shoe should be great enough to eliminate these possibilities, but it is limited by the structure gauge of bridges and tunnels on the system. Suf= ficient electrical clearance must also exist between the extreme transverse position of the current collector and the overhead supporting structures; as well as between the collector head and low contact wires when the pantograph is fully lowered.

The structure of the diamond-frame pantograph is such that the lower members are much sturdier than the upper ones. Hence in the event of a collision with anything on the over= head system, the top half of the pantograph will buckle while the bottom half should remain intact. The object is also to allow the pantograph to "give" - rather than have it ripping away the overhead cable. See Fig 1-9.

(Even on the best-maintained catenaries, pantographs are subject to this type of treatment. Any one of the numerous droppers, (each weighing something of the order of 75 grams), may become detached from the catenary due to some material defect. At a train speed of 100 km/hr, this will strike the current collector with a force of up to 300 kg provided the pantograph head is able either to recoil by 20 mm or to suffer a permanent deformation of this order of magnitude.[11b]

1-32 Dynamic Behaviour

Much work has been done in devising mathematical models, both theoretical and empirical, to predict the dynamic behaviour of pantographs, and the vibrations they cause on the overhead wires.[7,8,12]

A small model electric locomotive[6, 13] on a miniature rail=

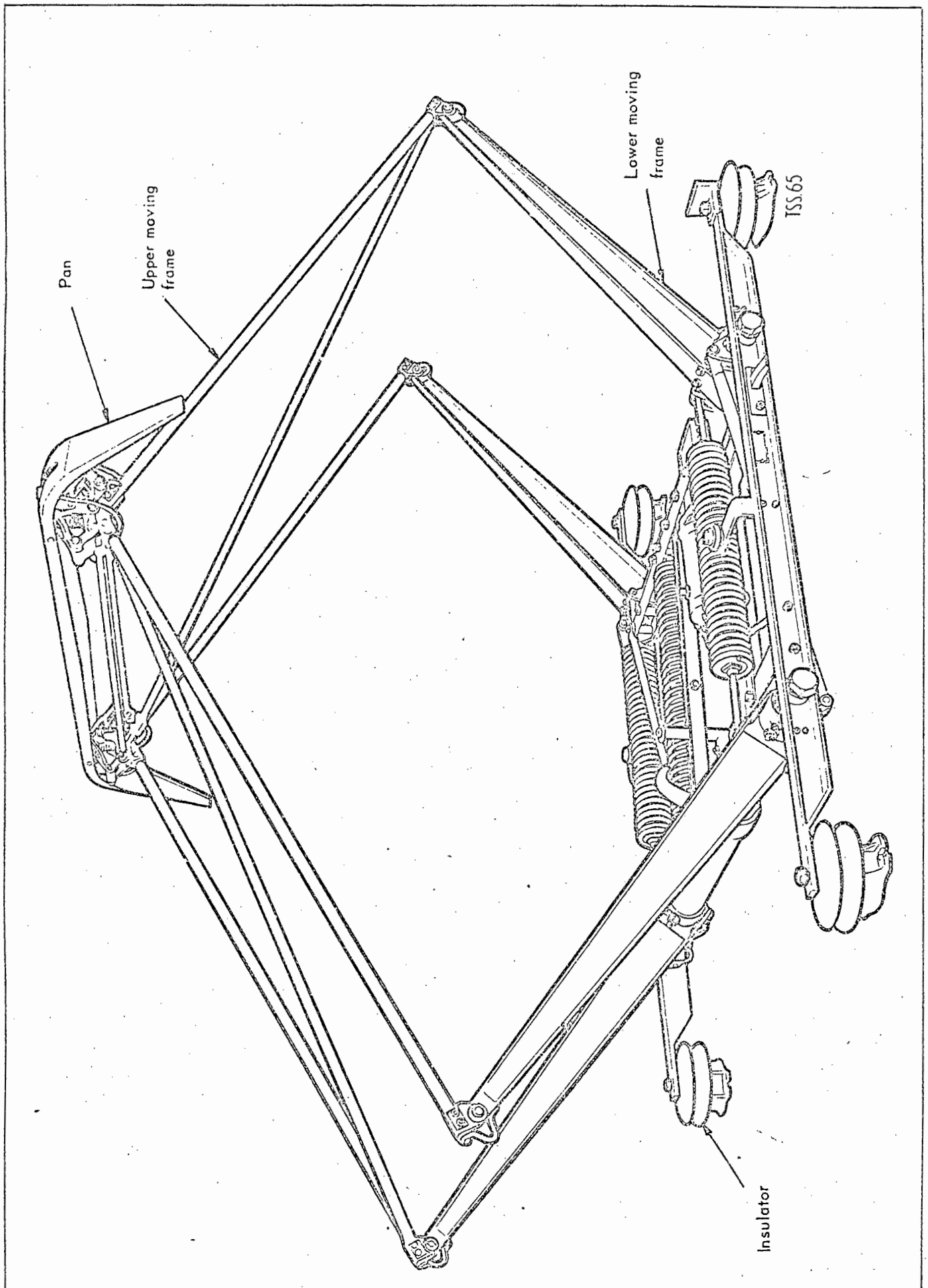

Fig. 1-9 GENERAL LAYOUT OF PANTOGRAPH
(Courtesy of the S.A.R.)

way, has even been built to simulate the behaviour of the over= head equipment under various conditions; and such features as pantograph trajectory and contact loss have been studied in great detail.

All come to the same basic conclusions:-

(a) The motion of the pantograph is characterised by vertical oscillations, which reach dangerously large amplitudes at cer= tain velocities. These velocities are equal to the speeds of the different harmonics of the waves induced in the contact wire. The problem can be overcome to a certain extent by the correct tensioning of the contact wire, since the group velo= city of waves in a wire is proportional to the square root of the tension.

Setting the correct sag in the contact wire is also vitally important, and a first approximation to this end is to droop it in a mirror image of the pantograph static characteristic. The object is to achieve as level a trajec= tory as possible. This raises the maximum permissible speed considerably above the 120 km/hr limit imposed for level wire.[6]

Hydraulic damping[10c] can also be used to counter the oscillations. This can be applied either to the overhead wire or to the pantograph - the latter arrangement being the more economically viable. It is advocated in preference to relying solely on the frictional damping at the bearings of the frame. This prevents the build-up of large amplitude oscillations, which reduce bearing life. The damping constant must not be set too high though, as this will cause excessive pressure to be exerted on the contact wire, and the pantograph will find difficulty in following rapidly varying wire heights. With optimum design however, the life of the contact materials can be prolonged by the smoothing out of the fluctuations in the contact pressures.

(b) The extent of contact loss increases with speed, and peaks are found at the resonant speeds. For good current collection an arbitrary acceptance limit of 2,5% [6] has been suggested. The"skipping distance", which is the distance covered by the pantograph when not in contact with the

overhead wire, increases almost as the fourth power of the running speed.[11c]

The weight[11d] of the contact piece is also important in this regard. The catenary system, having a varying elasticity and mass distribution, continually subjects the pantograph to rapid, irregular, vertical movements. In order to maintain an acceptable contact characteristic, the acceleration of the current collector (the quotient of contact pressure and collector mass), must therefore be sufficiently large. Since limitations exist on the contact pressure, it is essential to keep the mass as low as possible. Tests conclusively prove that the wear on contact strips increases considerably with the weight of the contact piece.[19] However it must not be made so light as to impair the transverse rigidity of the collector. This applies especially to the high speed pantographs used on high voltage a.c. systems.

(c) The aerodynamic behaviour of the pantograph is another factor to be considered - the aerodynamic force being defined as the sum of the static force and the force due to the action of the air stream on the articulated frame and collector head.[10d] The latter is generally found to be proportional to the square of the speed.

In pantograph design it is important to ensure that the maximum pressure on the contact wire is not exceeded, as this causes excessive wear.

The current collecting characteristic is also affected by the action of the air stream, and the quotient

$$\frac{\text{Effective Dynamic Mass of one Pantograph (Mdyn)}}{\text{Aerodynamic upward Force (F aerodyn)}}^{10e} \quad \ldots(1\text{-}1)$$

can be used as a criterion to determine the quality of current collection. (This is assessed by the number of contact interruptions made). A series of tests conducted by O.R.E. found that the quotient varied between 1,5 and 4,0 depending on the contact pressure, speed and type of overhead in use. The aerodynamic force should be such that the required quality index is obtained as a function of the effective mass without exceeding the maximum upward force allowed on the particular overhead system.

1-33 Present and Future Trends

Figure 1-10 shows how the weight of the pantograph head has decreased since electric traction first came into its own. For optimum current collection and less pantograph maintenance it must decrease even more. With the development of light= weight robust materials such as "carbon reinforced resin bon= ded glass fibre", and "carbon reinforced plastic",[10f] the prospect becomes more promising, and overhead equipment weighing 30 - 40% less than the equivalent metal ones are definite possibilities.

To reduce aerodynamic resistance, the surface area of pantograph heads have become increasingly smaller, and light= weight flattened rods, assembled and bent to the required shape, have found favour over the metal sheets of yesterday. Figure 1-11 shows a typical pantograph of modern design which is used by the German State Railways on their high speed E0 3 locomotives.[10h]

The Japanese have also had a measure of success in the development of high speed pantographs. Figure 1-12 shows some of the schemes they have tried.[14]

The head of "type A" consists of main and auxiliary contact strips which follow the slow and fast contact wire fluctuations respectively.

"Type Y" has each strip elastically supported on the pan, which is in turn supported on springs. Its construction aims at reducing the mass in direct contact with the overhead wire.

The two contact strips of "type K" and "K special" are individually supported by paralled leaf springs. This design also aims at reduction in weight, while allowing the contact strips to move independently of one another.

Tests showed that "type A" had the best response charac= teristic to applied vibrations, but that all of them were better than their old "type PS200" pantograph which was used as a standard in these experiments.

The result of such research must surely lead to a longer con= tact wire life. However even if it increases by one or two orders of magnitude, the necessity to monitor the wire thick= ness will always remain since rapid localised wear will still take place. Also the extent of damage caused by a break be= comes more pronounced as speeds increase.

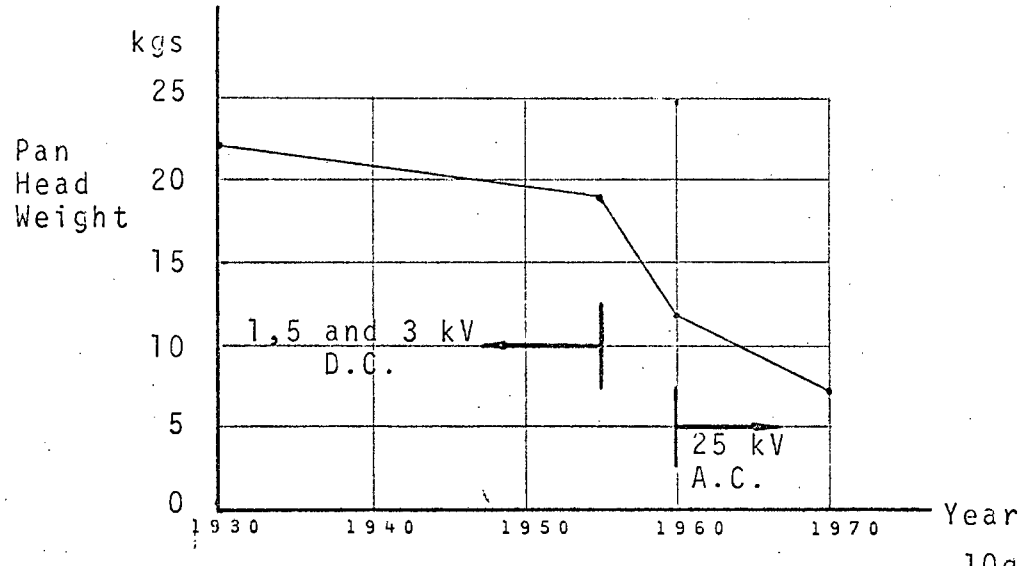

Fig 1-10: Comparison of B.R. pantograph heads over the Period 1930 to 1970.
(Courtesy of the I. Mech. Eng. Railway Div.)

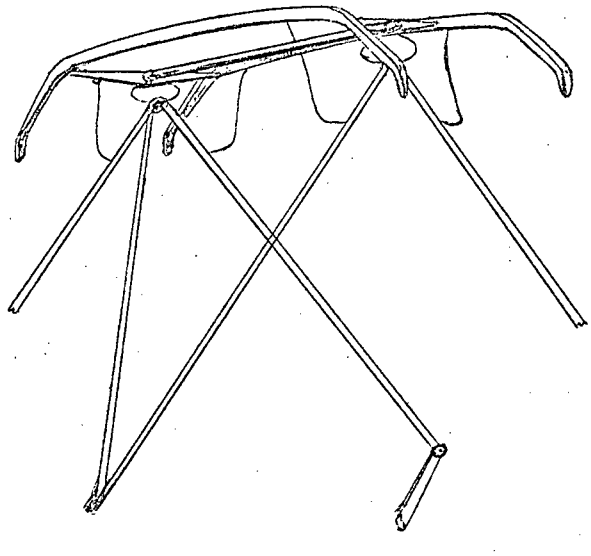

Fig 1-11: Wanisch Pan Head with Rubber Block Damping and Leaf Springs used by the German State Railways.

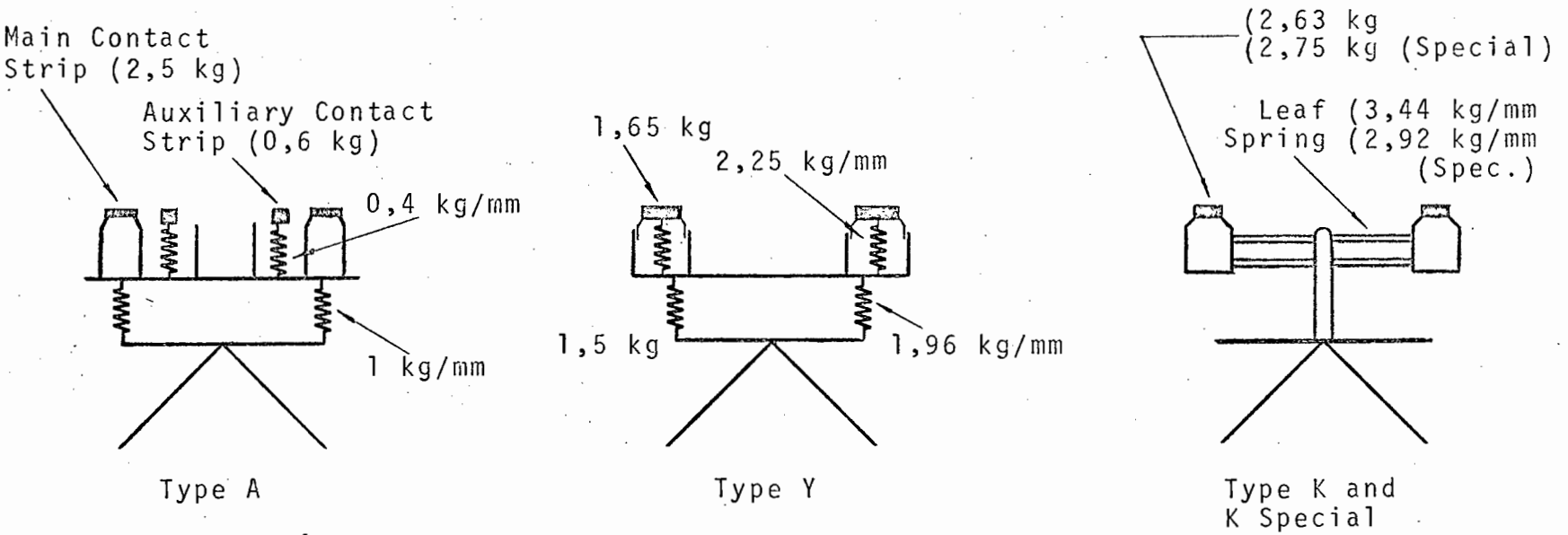

Fig 1-12: Prototype Designs of Pantographs for High Speed Current Collection Developed by the Japanese. (Courtesy J.R.T.R.I.).

1-40 CONTACT WIRE WEAR

1-41 The Phenomenon of Current Collection

Contact wire wear is a very complicated phenomenon, and is probably the most important problem in the maintenance of overhead electrical systems. Constant vigilance is necessary to ensure smooth running, since the rate of wear is so unpre= dictable. Moreover the life of the overhead cable is not determined by its average rate of wear, but rather by the wear at its "hard spots". This can be extremely rapid and will be discussed later in more detail.

First it is important to understand the mechanism of cur= rent collection.[11e] If the pressure between contact wire and contact strips is adequate, then current will flow from the one to the other via a few continually changing contact points, forming "current bridges" of high conductivity. With a stationary pantograph, a bridge continues conducting until enough localised heat is generated to vapourise the metal at that point. Contact there is then broken and another point takes over. With increasing current, the changes become more and more frequent, until finally the destruction of the material extends over the whole contact area.

Under dynamic conditions, new contact points continuously become affective without the occurrence of previous overload, so electrical wear is minimal. With heavier currents the same vaporisation processes do occur, but they are accompanied by a phenomenon known as "current lubrication",[11f] which causes the frictional wear to be less severe. Naturally it is more apparent on low voltage systems than on high voltage ones.

When the two contact pieces become mechanically separated, the current passing between contact points flows through a zone of incandescent gas. The temperatures associated with such an arc are very high, so a great deal more material is lost by vaporisation than in the previous cases.

1-42 Normal Contact Wire Wear

A study made by the Japanese Railway Research institute indicates that the total wear resulting from normal running can

BE EXPRESSED/

be expressed by the following equation.[15, 16]

(This was actually developed to explain the wear on the pantograph contact strips, but so closely allied to this is contact wire wear, that it is still acceptable. The main difference is that the contact point on the overhead cable changes rapidly as the pantograph runs along it, compared with the relatively slow sideways movement of the wire on the contact strips due to stagger.)

$$W = W_1 + W_2 + W_3 \qquad (1\text{-}2)$$

where

W_1 is the wear caused by sliding friction when current is being drawn, but in the absence of arcing.

W_2 is the electrothermal wear due to arcing.

W_3 is the increased mechanical wear resulting from arcing (This is the worst offender.)

(a) W_1 can be considerably reduced by lubrication, and is generally found to be much less than W_2 or W_3. The coefficient of friction is dependent on many factors, including sliding speed and current density, as well as contact wire tension, polish and composition. Natural lubricants such as moisture from fog, heavy dew and rain also tend to reduce it, but their presence is accompanied by greater contact resistance and increased contact loss, which causes sparking. Lubrication by oil or grease, ensures a reduction in friction under all weather conditions, but has the same adverse effects. In addition, summer temperatures cause the lubricant to become less viscous, resulting in the roofs of locomotives and carriages becoming caked with it.

On the other hand, insufficient lubrication causes increased mechanical wear, resulting in copper dust being deposited on the roofs in such quantities that the high tension insulators of the pantographs and roof conductors are liable to become punctured.[11g]

Another detrimental effect of friction is that it causes oscillations in the contact wire. These are aggravated by its zig-zag alignment and the rocking motion of the pantograph, and result in increased contact loss and sparking. (The German

Federal Railways quote measured catenary oscillations of up to 1 300 c/s).[11h]

Standing waves have also been known to occur on the line, causing a marked deterioration in contact conditions - especially if the oscillations are too fast for the pantograph to follow. Experience shows that they are particularly bad on stretches of line where trains all run at similar speeds. The German Reichsbahn quotes a case where the resultant corrugations had a wavelength of 40 mm,[11i] and wear was so rapid that the wire had to be replaced after comparatively short periods of service. This effect was eventually countered by improved pantograph designs.

(b) The electrothermal component of wear, W_2, is not as severe as the increased frictional wear, W_3, that occurs in conjunction with it. Both are caused by arcing, which, unless checked, can result in a very short overhead wire life.

In general the effect of arcing is worse on low voltage d.c.systems than on high voltage a.c. ones, for the following two reasons:

(i) When contact is lost between wire and pantograph the current that is broken is much larger in the case of the former than the latter.

(ii) By the very nature of "a.c.", the arc has greater difficulty in sustaining itself, since it is ex= tinguished each time there is a current zero-cros= sing.

This explains the severity of the problem in South Africa.

Research conducted by the Japanese offers the following explanation for the mechanism of electrothermal wear:[16]

When the temperature of any part of the metal is instan= taneously increased to beyond its melting point by an arc being struck, a violent "scattering" of material occurs due to the sudden excitation of its molecules. The extent of wear is then dependent on the area that is heated,on the temperature distribution in the vicinity of the arc spot, and on the duration of the arc.

For arcs of short duration (of the order of 10 ms), the thermal gradient in this vicinity is extremely large, and temperatures capable of causing vaporisation are confined

ALMOST/

almost entirely to the region defined by the arc current. This area is also found to be directly proportional to the arc current.

For arcs of longer duration the high temperature area extends beyond the arc spot, and becomes proportional to the square of of the current. (Also the area enclosed by a boundary of constant temperature T is inversely proportional to the square of T.) The wear here is far more severe, especially on the contact strips.

As far as the contact wire is concerned however, there is very little difference between the two cases, since the motion of the locomotive continually carried the arc into a cooler region. Hence no one point is allowed to remain hot for too long.

(c) The third component of wear, W_3, occurs mainly when frictional contact is again made between pantograph and contact wire. Its severity is dependent on how close the re-contact point is to the arc, and wear is caused by scattering when the two very hot surfaces strike and rub against each other. The spraying of the molten metal also causes a deterioration in the smoothness of the contact surfaces, resulting in increased frictional wear. Of the three, this is the most serious type of wear.

Factors influencing it include contact pressure and lubrication. In general, the greater the contact pressure, the less the wear, since the chances of arcing are reduced. Excessive lubrication, on the other hand, causes an increase in contact resistance, resulting in an increased contact voltage drop and hence increased heating. (Tests by the Japanese Railways indicate that contact voltage drops exceeding 0,3 volts[16] result in wide and rough scars being left on the contact surfaces. Strangely enough, this limiting value seems to be independent of current).

Unhappily, both the above factors are in direct conflict with W_1, so a balance has to be struck.

1-43 Hard Spots and other Phenomena

(a) "Hard spots" are isolated points on the contact wire where wear is extremely rapid. They abound at stations where starting currents (and hence arcing currents) are high, and at cross-overs where pantographs passing from one line to another always strike the wire at the same place. Since abnormal wear is expected at these places however, it is relatively easy to effect repairs. More serious is the sporadic occurrence of hard spots on the open line as this necessitates a constant vigilance over long stretches between towns and stations.

Their causes include repetitive impact (as at cross-overs), repetitive arcing (due to pantographs bouncing at the same point on the line, possibly because of some defect on the track), and excessive localised weight on the overhead wire resulting in an increased contact pressure at that point.

Fig 1-13 shows a typical wear waveform in the vicinity of an artificially created hard spot, obtained in an experiment performed by the Japanese Railways Technical Research Institute.[15] The wear recorded is due to sliding friction alone, since the test pantograph drew no current. This explains the pronounced reduction in wear immediately after the hard spot, as contact between wire and pantograph was lost there. Had current been drawn, this would have been accompanied by arcing and extreme wear would have resulted. It is interesting to note the presence of the so-called "weightless hard spots" at points a, b and c, where wear is almost as severe as at the real hard spot. These are due to oscillations in the overhead line, which appear to be caused by the added weight, since peaks only exist before it and not after it.

(b) The Japanese Railways make mention of a case where the wear on a 25 kV a.c. line was actually greater than on a 1,5 kV d.c. one. This occurred on their Tokaido Line,[17] which was opened in 1964, to cater for speeds of the order of 200 km/hr.

The unusual wear rate was probably due to their unfamiliarity with high speed traffic at the time, as they attributed it to the differences in operating conditions, such as

SPEED,/

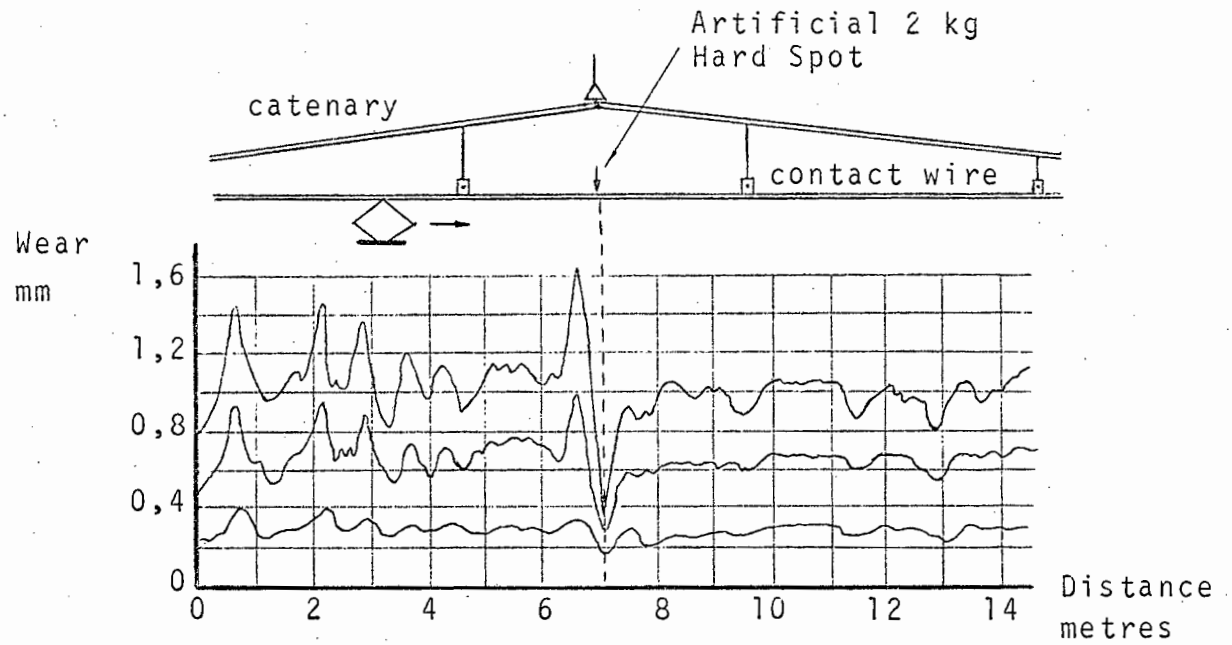

Fig 1-13: Wear Waveform in the Vicinity of an Artificial Hard Spot (No Current Drawn) (Courtesy of the J.R.T.R.I.)

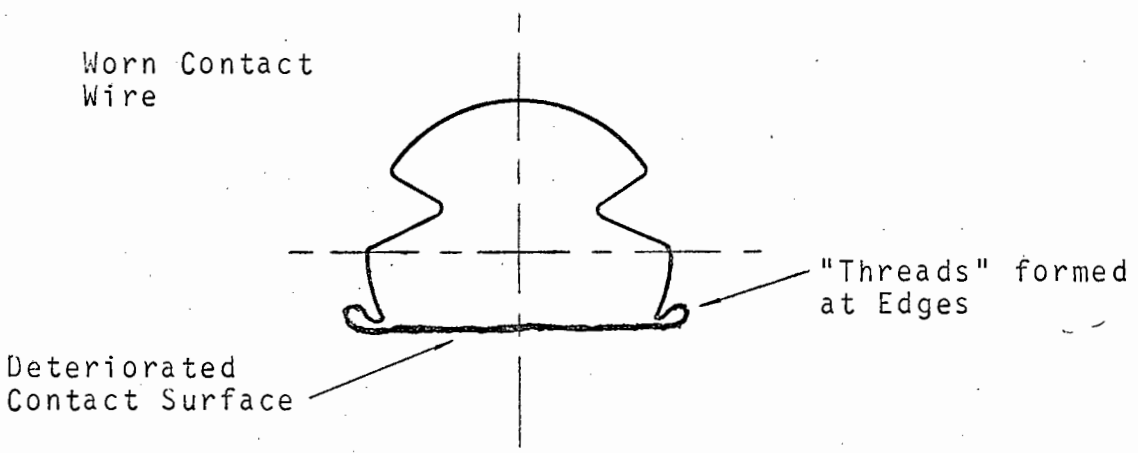

Fig 1-14: Example of Anomolous Wear occurring on Japanese New Jocaido Line.

speed, more frequent contact breaks between pantograph and overhead wire, contact pressure and contact strip materials.

(c) They also speak of a unique type of wear peculiar to this line, which was characterised by a deterioration of the contact surface, and the formation of what they termed "string sized wear pieces"[18] at the edges. Figure 1-14 better describes the situation, which was evidently confined only to sections of line where the train speeds were low. It was very dangerous however, since these metal "threads", which often reached lengths of over 50 cm, were easily stripped off, and so became insulation hazards.

The phenomenon was attributed to a large frictional force existing between pantograph and contact wire - which implied poor lubrication. Originally this had been achieved by the inclusion of a low melting point metal in the contact strip material, so that the contact wire could be protected at its expense. The spaces between the contact strips were also filled up with grease.

The "current lubrication" method proved satisfactory, especially at high speeds, but the effectiveness of the grease did not measure up to expectations. This was because of the high temperatures involved which, on the low speed sections, actually burned away the grease on the contact surfaces.

The measures proposed to counter this were improved lubrication, a reduction in contact force and the use of contact materials with better wear resisting properties.

1-44 Permissible Wear

The permissible wear of the contact wire is dependent on the shape and dimension of its cross-section. If allowed to go too far, the current collectors are liable to catch on the dropper clamps, causing a severe mechanical shock on the overhead system, and possibly pulling the contact wire out of its mountings. Figure 1-15 shows some of the types used in America.

The type used by the S.A.R. is shown in Fig 1-16. When new it has a diameter of 15 mm, and it is considered critically worn when this has been reduced to 9 mm in the vertical direction.

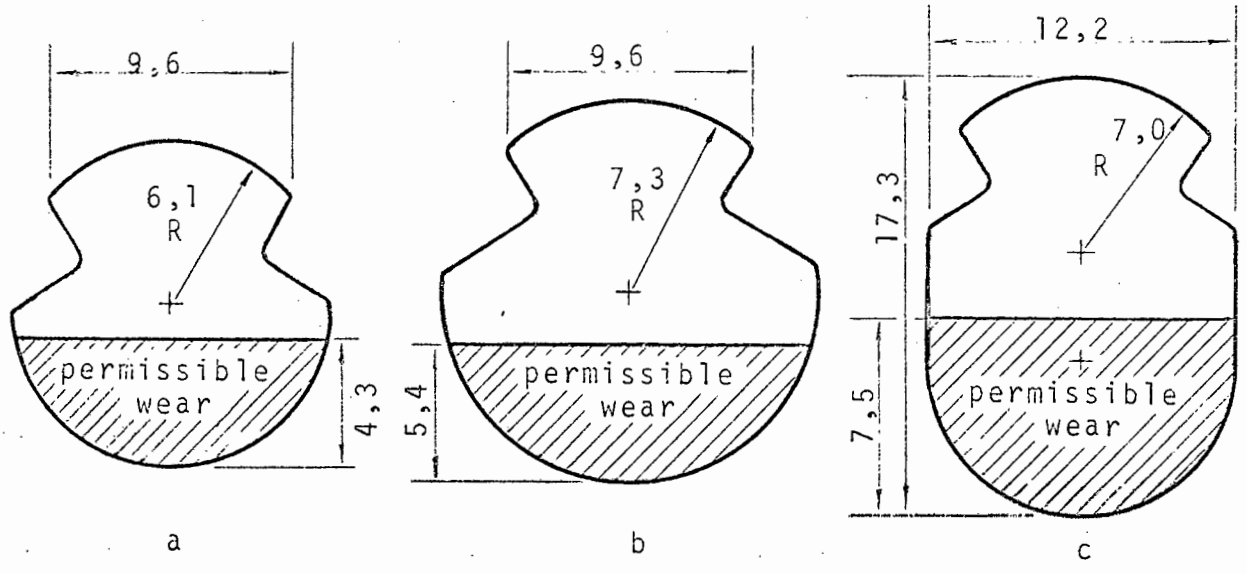

Fig 1-15: Different Types of Contact Wire used in America
(All Dimensions in mm)

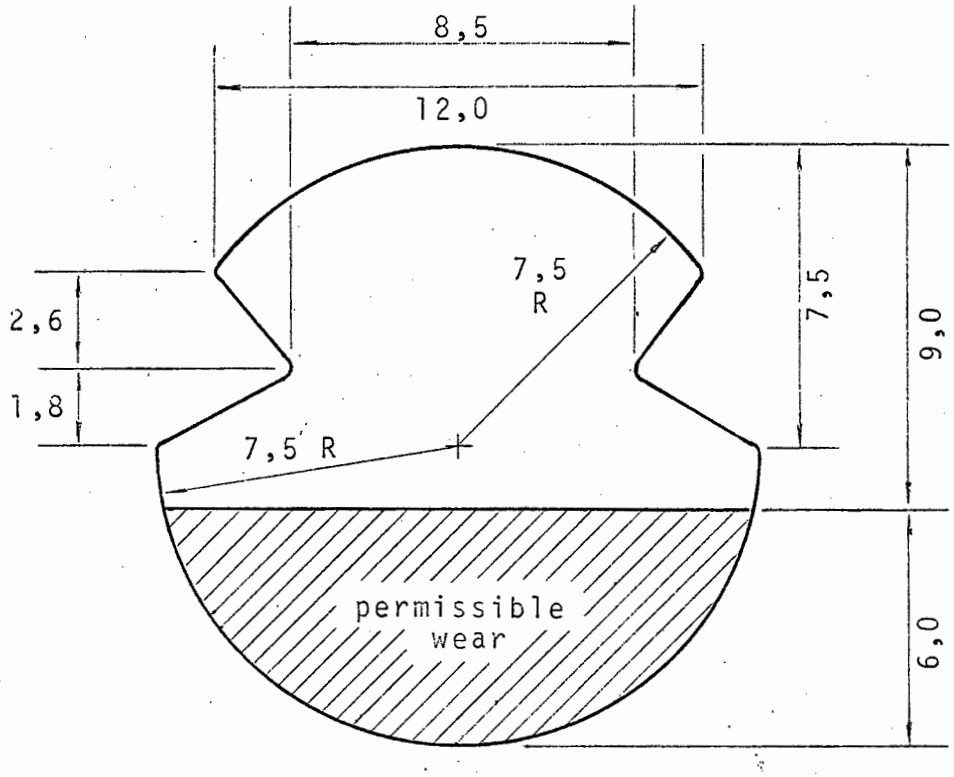

Fig 1-16: Permissible Wear of Contact Wire used by the South African Railways.
(All Dimensions in mm)

At a hard spot the thickness can vary almost from the one limit to the other over as little as 2 cm.

In the absence of such wear, the life of the contact wire can be expressed in terms of "thousands of pantograph passes". Fortunately when hard spots do occur, it is possible to replace the small section involved, rather than the whole tension length. This is done by means of clamps, and the ends of the new piece are filed down so as to ensure a smooth transition for the pantograph.

REFERENCES

1. KENJI HORIKIand MATSUTARO ICHIKAWA: "ITV Technique for Measurement of Trolley Wire Wear", J.R.T.R.I. Quarterly Reports, 1971, Vol 12, No 2, p 34.

2. H.P. CALLWELL: "The Overhead Equipment of the Melbourne Suburban Electrified Railways", IEE Convention on Electric Railway Traction, 20 - 23rd March, 1950.

3. "Specifications for Hard Drawn, Grooved, Copper Contact Wire for Electrical Traction Purposes", S.A.R. Electrical Dept, Dec. 1966, Specification Number CEE-C1A-1. (All dimensions have been converted to Metric Units in the script.)

4. F.B. KITCHIN B.C.E. and J. HOLLAND: "Railway Electrifi= cation: Design of Overhead Equipement." IEE Convention on Electric Railway Traction, 20-23rd March 1950, Paper No 979.

   (a) P1 (b) P1 (c) P8 (d) P10 (e) P1 (f) P5 (g) P1 (h) P6 (i) P10 (j) P10.

5. J.G. BRUMMER and A.v.W. SCHOEMAN: "Regenerative Braking Equipment on the Cape Western System of the South African Railways", S.A.I.E.E. Trans., Dec. 1960, Vol. 51, Part 12 p 269.

6. T.A. WILLETS B.Sc. and A.D. SUDDARDS B.Sc., C.Eng., M.I.C.E., M.I.Mech.E.: "Dynamic Model Studies of Overhead Equipment for Electric Railway Traction", Proc: I.E.E., Sept. 1970, Vol 117, No 9, pp 1819-1828.

7. G. GILBERT, B.Sc. and H.E.H. DAVIES B.Sc.: "Pantograph Motion on a Nearly Uniform Railway Overhead Line", Proc. IEE, March 1966, Vol 113, No 3.

8. KEIICH TSUCHIYA: "The Dynamic Behaviour of Overhead Catenary Wire Systems", J.R.T.R.I., Quarterly Reports, March 1969, Vol 10, No 4.

9. "Contact Wire Tension Chart - HANS SCHMIDT GAUGE", S.A.R. Elec= trical Department, Reference No ET 1/500/12.

10. (Author not known): "Development of the Pantograph for High Speed Collection", Journal of the I. Mech. E. Railway Div.

    (a) p424 (b) p423 (c) p419 (d) p420 (e) p418 (f) p430 (g) p425 (h) p430

11. O. KASPEROWSKI (Munich): "Contact Materials for Current Collec= tors of Electric Motive Power Units", Monthly Bulletin of the I.R.C.A., Electric Traction on the Railways, Feb., 1964, Vol XV, No 2.

(a) p59/

(a) p59
(b) p53
(c) p48
(d) p48
(e) p54
(f) p51
(g) p53
(h) p50
(i) p50

12. OSAMU ODA: "Mid-Span Vibration of Catenary Overhead Wire", J.R.T.R.I. Quarterly Reports, 1967, Vol 8, No 3.

13. D.S. FARR, Associate Member, H.C. HALL, M.Sc., A.L. WILLIAMS, Ph.D.,M.Sc., Member: "A Dynamic Model for Studying the Behaviour of the Overhead Equipment used in Electrical Railway Traction", I.E.E., March 1961, Paper No 3530.

14. MASUHARU KUNIEDA, Dr Eng., CHIDORI HAMAKAWA, EISAKU YASUMATSU, MATSUTARU ICHIKAWA and OSAMU MURASHIMA: "Performance Tests of Tentatively Manufactured Pantographs for High Speed Railcar", J.R.T.R.I., Quarterly Reports, 1969, Vol 10, No 2.

15. MASARU IWASE: "Current Collection by Pantograph and its Wear", J.R.T.R.I. Tokyo, Quarterly Reports, 1960, Vol 4, No 3.

16. MASARU IWASE, Dr Eng.: "Wear of Pantograph Contact Strip (1); Effects of Arc Generation", J.R.T.R.I., Tokyo, Quarterly Reports, 1963, Vol 4, No 2.

17. MASARU IWASE, Dr Eng., TOSHIO SAITO, Dr Eng., KOZUO YOKOI and MASAMI MAEDA: "Wear of Trolley Wire on the New Tokaido Line, (Report 1)", J.R.T.R.I., Quarterly Report, 1965, Vol 6.

18. MASARU IWASE, DrEng., KINJI KOBUBU, TOSHIO SAITO, Dr Eng., KAZUO YOKOI, MASAHIRO KUMAZAI and MASAMI MAEDA: "Pre= vention from Abnormal Wear of Trolley Wire", J.R.T.R.I., Quarterly Reports, 1969, Vol 10, No 1.

19. MASARU IWASE, Dr Eng.: "Wear in High Speed Pantograph Current Collection", J.R.T.R.I., Tokyo, Quarterly Reports, 1969, Vol 10, No 4, p206.

CHAPTER 2
THE SYSTEM

2-10 GENERAL

Many problems are associated with contact wire wear measurement. These must be studied carefully before a decision can be made regarding the best method of approach.

For instance the presence of droppers makes the use of any type of mechanical feeler running along the top of the wire impossible. In fact, anything at all mounted on top of the pantograph is dangerous, since it will be struck by the cable at forks and at cross-overs.

Whatever method is used must be affected neither by stagger nor by the varying height of the contact wire. It must be able to operate in the hostile environment of the overhead system among large electric and magnetic fields, obtain information from a point at a potential of 3 kV and then transmit this down to ground where it can be recorded. It must also be robust enough to withstand the vibrations and shocks associated with pantograph motion, and must not be affected by grease, water, copper dust etc.

Information regarding the extent of wear can be obtained by measuring one of three basic parameters. These are listed in the table below, together with some of the associated methods of approach.

Parameter	Method
1) Cross-Sectional Area	(a) Resistance Measurement. (b) Deflection due to Bending.
2) Width of Sliding Surface	(a) Closed Circuit Television.
3) Vertical Thickness	(a) Ultrasonic Means (b) Optical Scanning of Profile.

THE METHOD/

The method eventually selected as being most likely to succeed was the last one.* One of the main reasons for this choice was the recent rapid advance in optical semi-conductor technology.

2-20 WEAR MEASUREMENT BY OPTICAL SCANNING OF CONTACT WIRE PROFILE

(a) Method

The principle entails shining a parallel beam of light across the pantograph shoe, as shown in figure 2-1, and measuring the light quantity reaching the other side. It has the major advantage of being a direct measurement, and does not require having to infer the result from any other parameter.

Though the dimensions of Fig 2-1 are somewhat out of perspective, another advantage does make itself apparent. This is that a limited amount of contact loss can be tolerated. Even if the contact wire does bounce right out of the beam at various places, the wear there can be considered potentially bad. Also, to allow for wear in the contact strips, a slot can be cut along the length of the pan and the level of the lens dropped slightly.

(b) Protective Ramps

As for the problem of having the optical equipment swept off at points and at cross-overs, protective ramps could be built at each end of the pan, as shown in Fig 2-2. Consider the orders of magnitude involved in the ramp dimensions.

Distance extended by horns below contact strips	= 36 cm
Diameter of New Cable	= 1,5 cm
Diameter of Lens	= 4 cm
Hence height of ramps above contact strips	= 6 cm

Regarding wear on the contact wire due to the ramps, it must be remembered that contact will only be made with them at places where the stagger is particularly large, and also at points and at cross-overs. Then too this particular pantograph will not be required to draw any current, so the only type of wear that can occur will be due to simple mechanical friction.

* Appendix I explains why the other methods were rejected.

THIS IS/

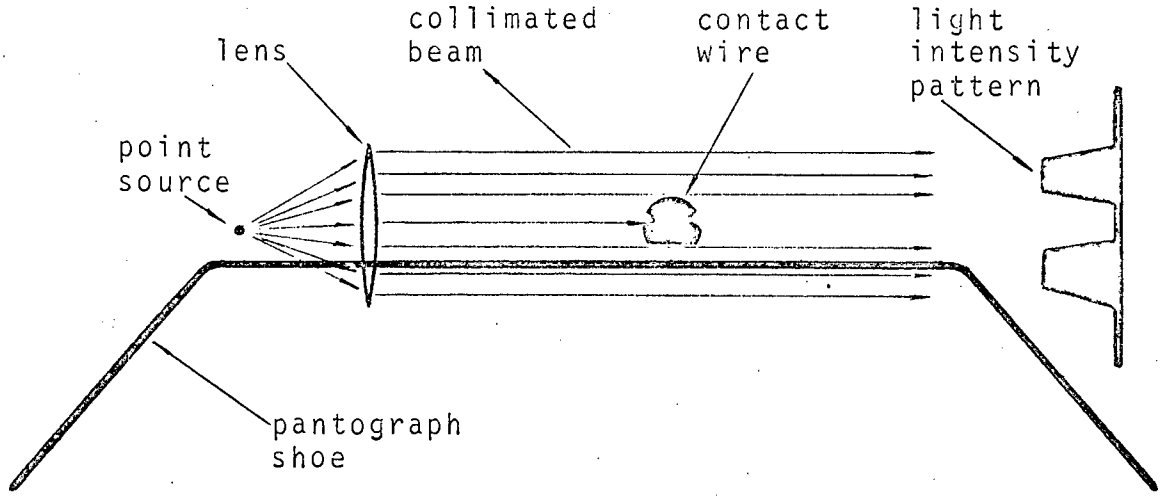

Fig 2-1: Principle of Contact Wire Measurement using Optics.

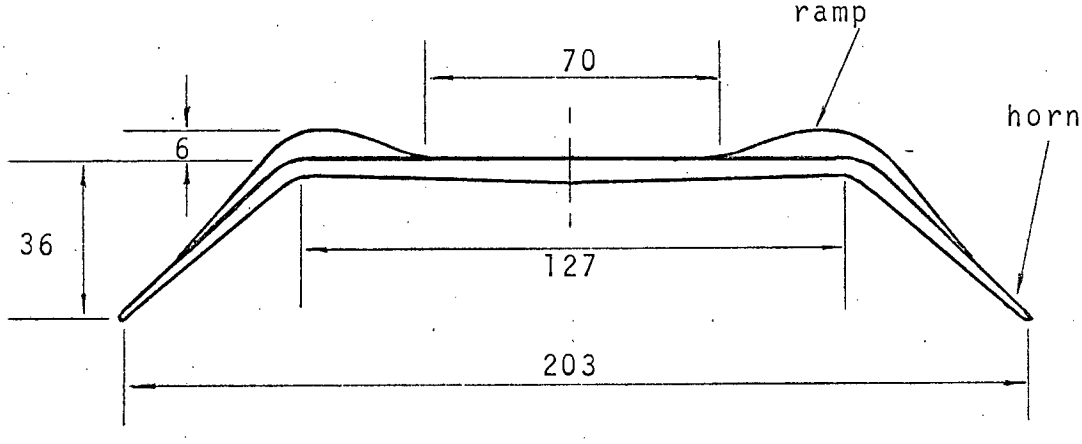

Fig 2-2: Scale Drawing of Pan with Protective Ramps. (All Dimensions in cm)

This is generally much less than that due to arcing, especially on well lubricated contact wires.

What warrants more attention though, is the impact of the contact wire on the ramps. On any normal pantograph, this is born by the horns so the addition of ramps merely means that the possible contact length extends over a vertical range of 42 cm instead of 36 cm.

So severe are these collisions on the horns however, that after a while they buckle and must be repaired. The ramps will be even more vulnerable, so they will have to be made out of a very strong material (steel), and be smoothly sloped and tapered to deflect, rather than absorb the blows. Even then they will have to be continually checked to see if repairs are necessary.

(c) Analogue or Digital Measurement?

The next question that arose was whether to use an analogue or a digital measuring technique.

The former was attractive because of its simplicity, and entailed the use of a second lens at the receiving end to focus the light on to a single photodetector. The contact wire thickness could then have been related to the intensity of the light. However this method was doomed to failure since any dust or dirt on the lenses would cause variations in the light intensity which would be misinterpreted by the receiver.

Consequently the digital approach was pursued. This re= quired a vertical array of detectors spaced at equal intervals apart at the receiving end of the pantograph head, so that the number of them in shadow at any instant of time would be proportional to the thickness of the contact wire. Unlike the analogue method, it is immune to minor intensity variations, because the amplifying circuit of each photodetector would be either in a "high" state or a "low" state. Also a comparator triggered at the midpoint between the two limits could be used to make the final decision. However the lenses would still have to be cleaned at frequent intervals in order for accuracy to be assured.

(d) PROBLEM/

(d) Problem of Dirty Lens

It is possible that dirt and grease could be thrown on to the lens and the photodetector faces by virtue of the sideways movement of the cable. (The Japanese with their ITV method, also experienced difficulty with their lenses misting up*)

A possible solution which could be tested in the proto= type, would be to recess the lens behind a protective"pop-out"glass window, (also recessed), inside a cylinder as shown in Fig 2-3.

This would protect the system from grease approaching from obligue angles, and in the event of the glass window becoming dirty, it would be relatively simple to pull it out and clean it.

(e) Overall System

A block diagram of the envisaged system is shown in Fig 2-4.

Briefly it entails using a light-emitting diode to con= tinuously pulse a parallel beam of light across the pantograph head. Between each pulse, the detecting circuit counts the number of detectors that were in shadow, and transmits this information down to ground via a fibre-optic light guide (to provide the necessary isolation), where it is decoded and re= corded.

The reasons for this choice of approach are given in the succeeding chapters, together with a feasibility study of the proposed method.

* See Appendix I (c)

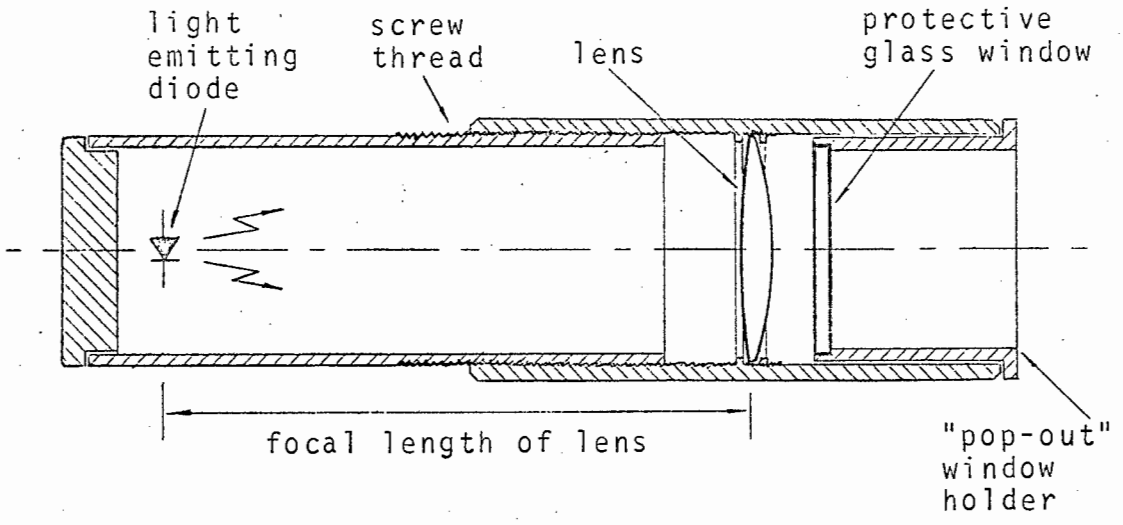

Fig 2-3: Section View of LED and Lens Housing.

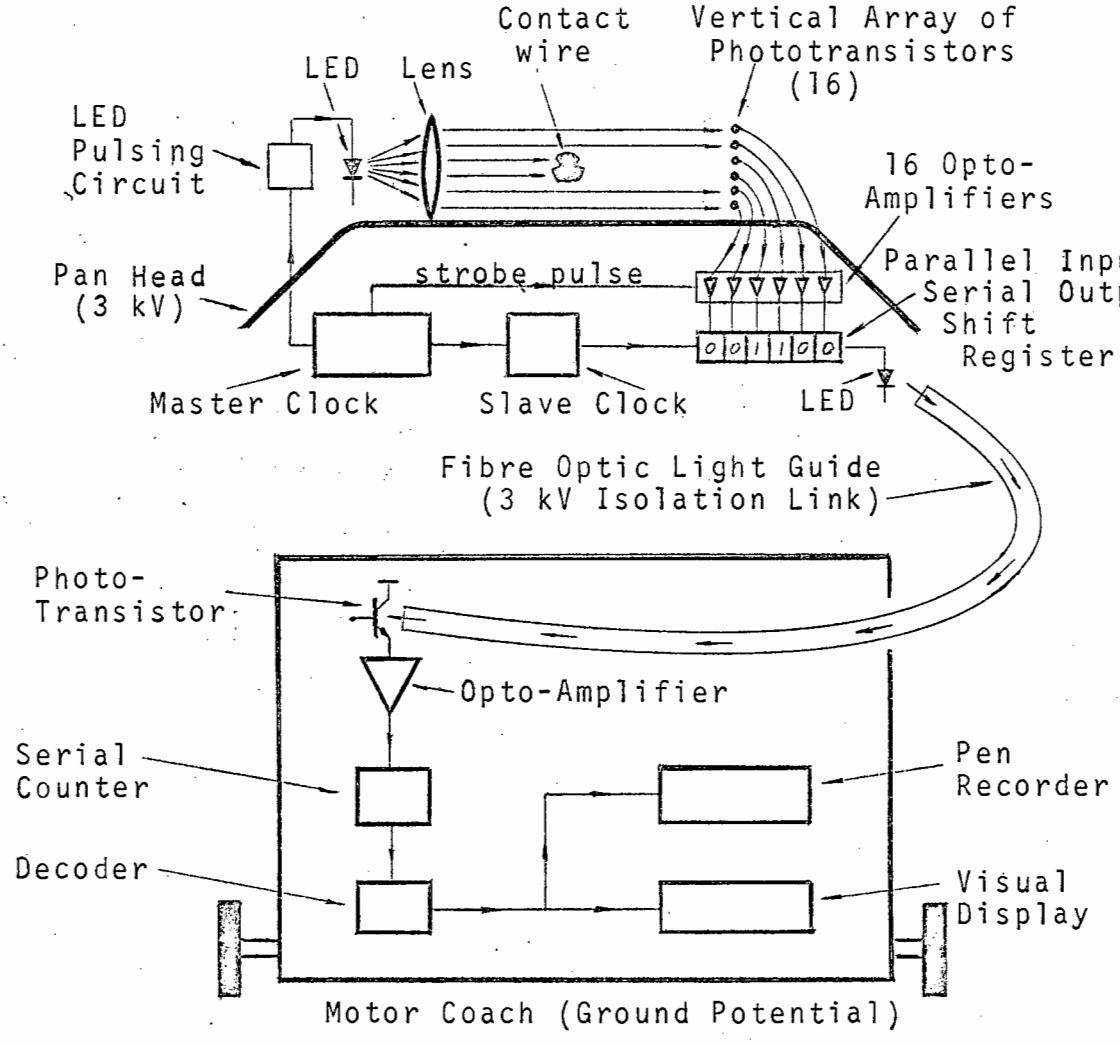

Fig 2-4: Block Diagram of Contact Wire Wear Measurement System.

C H A P T E R 3

FEASIBILITY STUDY

3-10 COMPONENTS

3-11 Choice of Light Source

To obtain a parallel beam of light, a point source must be placed at the focal point of a lens. The choice of source lies between a filament bulb placed behind a pin hole, and one of the semiconductor (Gallium Arsenide) light emitting devices.

(a) Filament Bulb

Though an order of magnitude less efficient in its conversion of electrical power to light, this is compensated by the greater powers it can dissipate in comparison to the semiconductors. Even under d.c. conditions it can emit light intensities of the same order of magnitude as certain semiconductors do only under pulsed conditions. However it also has many disadvantages.

(i) Modulation Capabilities:- Because of the filament afterglow, it can respond only to d.c. and slow a.c. signals. Hence its advantages of greater emitted intensity is offset by its poor modulation capabilities.

(ii) Pin Hole:- To obtain a point source, it would have to be placed behind a pin hole, so most of the emitted light would be wasted anyway.

(iii) Lack of Robustness:- Filament devices housed in glass, and operating at high temperatures are not suited to the vibrations and impacts associated with pantograph motion.

(iv) Effect of Ageing:- Filament sag due to ageing results in a deterioration of light emitting qualities.

(v) Reliability:- Compared to semiconductors, filament devices are notoriously unreliable and prone to fusing - especially if subjected to rough treatment.

(b) Gallium Arsenide Infra-Red Emitters

In almost every respect these are better suited to the task.

The semidonductors capable of being used for signalling emit in the near infra-red region around 900 nanometres. They have long since proved their worth in such devices as burglar alarms, computor card readers, optical "walkie talkies", tellurometers (capable of distance measurement up to almost 10 km), and many others.

Some of their more advantageous features are listed below.

(i) Small size:- This facilitates easy mounting.

(ii) Small Emitting Area:- Diameters of the order of half-a-millimetre and less are typical, which is of the same order of magnitude as the circle of least confusion of the required lens. See Section 3-13. Hence no light need be wasted by placing the device behind a pin hole.

(iii) Robust:- The devices are light and robust, and unlike filament bulbs, can withstand a great deal of vibration and shock.

(iv) Lifetime:- This is an order of magnitude longer than filament devices.

(v) Modulation Capabilities:- The radiation turn-on and turn-off times range from some tens of nanoseconds for the ordinary light-emitting diode to less than 0,1 nanosecond for the laser light-emitting diode, giving them excellent modulation capabilities. This is essential considering the varying ambient light conditions (one cannot compete with the sun) - so the light detecting circuits must not be d.c. coupled. The noise rejection capabilities of the receiver can therefore also be enhanced by using some signal extraction technique such as synchronous detection.

(vi) Power Requirements:- Though instantaneous values of up to 50 watts can be tolerated under pulsed conditions (very low duty cycles), their maximum average dissipation is of the order of half-a-watt. This eliminates the power supply problems associ= ated with filament bulbs, which can consume hundreds of watts continuously.

(vii) Quantum Efficiency:- This is defined as [1]

$$\eta = \frac{\text{Light emitted in photons/sec}}{\text{Forward current in electrons/sec}} \qquad (3\text{-}1)$$

$$\text{Light Current} = \frac{\Phi\lambda}{hc} \quad \text{photons/sec}$$

$$\text{Forward Current} = \frac{I}{e} \quad \text{electrons/sec}$$

Where:

Φ = radiant power in watts.

I = current in amperes.

λ = output wavelength in microns.

e = electronic charge = $1{,}6 \times 10^{-19}$ Amp-sec

h = Planck's constant = $6{,}63 \times 10^{-34}$ Joule-sec

c = velocity of light = $3{,}00 \times 10^{14}$ microns/sec

$$\text{Hence } \eta = \frac{\Phi\lambda e}{hcI} \qquad (3,2)$$

For most gallium arsenide devices, η is between 1% and 5%, but it decreases with increasing junction temperature, and hence with increasing forward current. No filament bulb can match this figure, though it is difficult to compare the two, since the bulb radiates over a broad spectrum extending from the visible to deep into the infrared, whereas the semiconductor concentrates all its energy in a narrow band no more than 50 nm wide centred in the vicinity of 900 nm. Fortunately this happens to be very close to the region where most silicon detectors have their spectral response peak, so all the radiant energy is used with almost maximum efficiency. The converse applies to the filament bulbs, where a great deal of the radiant energy is hardly "seen" by the detector. See Graph 3-1.

(viii) Lens Aberrations:- Since the emission spectrum of the semiconductors covers such a narrow band, it would not need an expensive chromatically corrected lens to create a parallel beam, as would be the case with a filament bulb.

The choice is therefore narrowed to either the ordinary L.E.D. of the laser L.E.D. The important differences between them are listed in Table 3-1, where for the sake of convenience a comparison is made between specific devices which are typical of their respective families.

At this stage it is also useful to consider the different types of detectors available (which are described in Table 3-2), so that the optimum emitter-detector pair can be chosen. Again

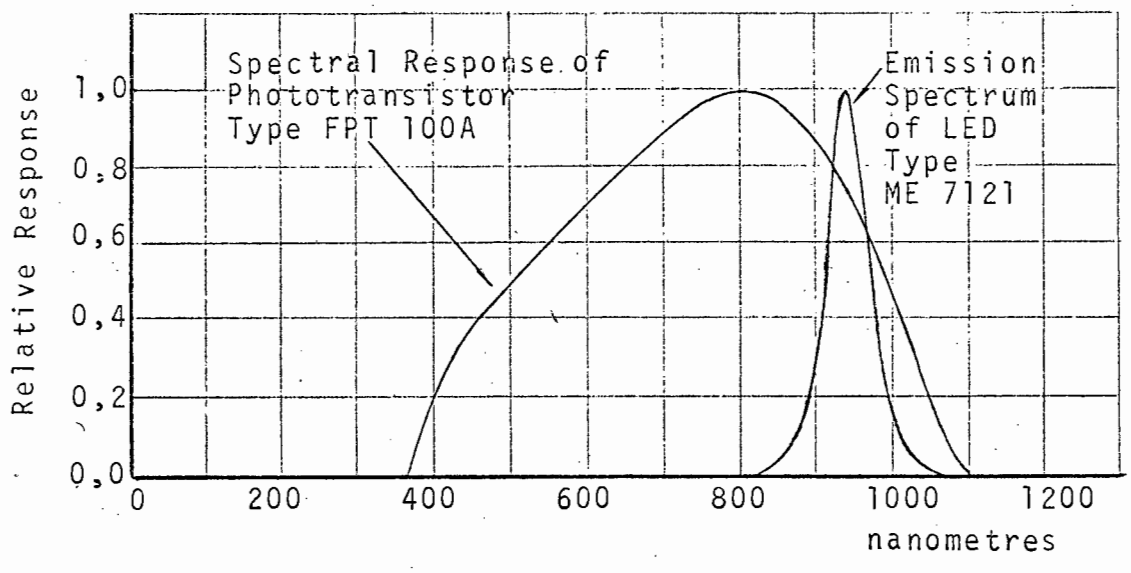

Graph 3-1: Spectral Curves of Optical Devices.

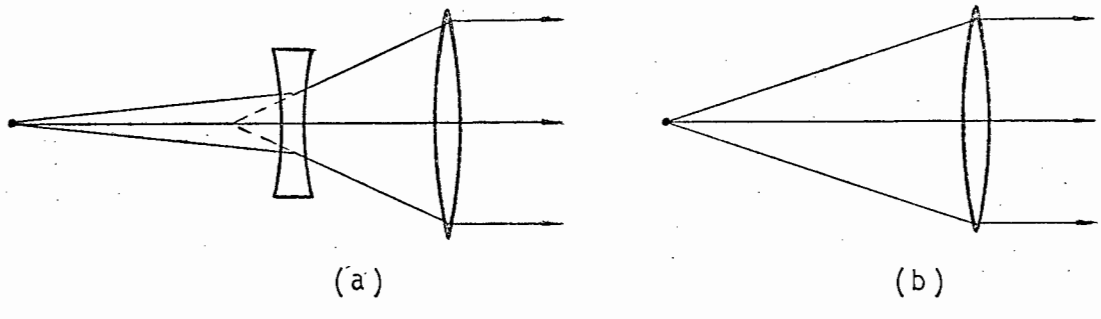

Fig 3-1: (a) Lens System for Laser Diode.
(b) Lens System for Ordinary LED.

a comparison is made between specific devices.

The laser diode, though much more efficient and emitting a great deal more light, does have certain disadvantages.

(i) Mode of Operation:- It can only remain on for about 200 ns at a time, (and that at a 0,1% duty cycle), which means that its detector is restricted to the PIN photodiode. As shown in Table 3-2, these are far less sensitive than phototransistors (especially the FPT 100A). Hence, if the relatively slower rise times can be tolerated, it would be far easier to use an ordinary LED-phototransistor pair, where simpler and cheaper driver and amplifier circuits could be used.

(ii) Radiation Beamwidth:- For the laser diode, this is of the order of 16^{o}. So, with the limited space on the pantograph shoe, a more complicated lens system would be required in order to obtain a parallel beam, as shown in Fig 3-1.

Hence, provided the ordinary LED's emit sufficient light, it would be far simpler to use them instead of lasers.

The following analysis is therefore made in order to estimate the order of magnitude of the irradiance H at the detectors.

Since the light emerges from the lens in a parallel beam, the irradiance at the detectors will be equal to that at the lens surface. Also the light from the LED obeys an inverse square law. (The following calculations are based on the characteristics of the LED type TIXL 27.)

θ = Angle between half-power points and central axis of LED.
= $67\frac{1}{2}^{o}$

f = Focal length of lens (See Section 3-13.)
= 12 cm

A = Area illuminated by LED at a distance f of 12 cm. (or area of spherical cap of radius f.)

$$A = \int_0^{\theta}\int_0^{2\pi} f^2 \sin\theta \, d\phi \, d\theta \qquad (3\text{-}3)$$

$$= 2\pi f^2(1-\cos\theta)$$

$$= 2\pi(12)^2(1-\cos 67\tfrac{1}{2}^{o})$$

$$= 559 \text{ cm}^2$$

IF Φ/

If Φ is the radiant intensity of the LED, then the irradiance H at the lens 12 cm away will be:

$$H = \frac{\Phi}{A} \qquad (3\text{-}4a)$$

Since the TIXL 27 can either run continuously at a maximum average current of 300 mA, or pulsed at a low duty cycle at a maximum peak current of 4 amps, the respective values of irradiance will be:

$$H_c = \frac{20}{559} = 0{,}036 \text{ mW/cm}^2 \text{ (max. cont. irradiance)}$$

$$H_p = \frac{250}{559} = 0{,}448 \text{ mW/cm}^2 \text{ (max. peak irradiance)}$$

However the infrared light will attenuate as it passes through the glass lens and the "pop out" protective windows in front of the lens and the detectors. Measurements indicate transmission factors of the order of 0,85 for glass, so the resultant transmission factor will be the product of the three.

$$t_R = t_1 t_2 t_3 = 0{,}61 \qquad (3\text{-}5)$$

Hence the irradiance at the detectors will be of the order of:

$$H'_c = t_R H_c = 0{,}022 \text{ mW/cm}^2 \text{ (max. cont. irradiance)}$$

$$H'_P = t_R H_P = 0{,}275 \text{ mW/cm}^2 \text{ (max. peak irradiance)}$$

From Table 3-2 both these values are well within the useful operating levels of the detecting devices. The next step is therefore to choose the photo-sensor.

3-12 Choice of Detector.

There are many different types of photo-detectors, including phototransistors, darlington phototransistors, photodiodes, photo S.C.R.'s, photo F.E.T.'s and also photovoltaic, photoconductive and photoemissive devices.

The last three are automatically excluded because of their size, since a primary requisite is that the detectors be

SUFFICIENTLY/

Table 3-1: CHARACTERISTICS OF CERTAIN SEMICONDUCTOR LIGHT EMITTING DEVICES.[2]

	ORDINARY L.E.D.		LASER L.E.D.	
	Type ME 7121	Type TIXL 27	Type RCA 40856	Type RCA 40857
Peak Emission Wavelength (nm)	940	940	904	904
Linewidth at Half Intensity Points (nm)	50	45	3,5	3,5
Radiation Turn-On Time (ns)	500	A Few Tens of ns	< 0,1	< 0,1
Radiation Turn-Off Time (ns)	500	A Few Tens of ns	< 0,1	< 0,1
Minimum Operating Current (A)	-	-	4 (Threshold Current at which Lasing starts)	6
Average Rated Current (mA)	100	300	-	-
Maximum Allowed Current (Pulsed) (A)	6	4	10	10
Radiant Output at Rated Current (mW)	3	20	-	-
Approximate Radiant Output at Peak Current (mW)	160	250	1000 (min)	2000 (min)
Radiation Beamwidth Between Half Power Points	15^{o}	135^{o}	16^{o}	16^{o}
Quantum Efficiency at I_{PK}	4,5%	4,7%	7,3%	14,5%
Forward Voltage at 50 mA (V)	1,3	1,3	1,2	1,2
Dynamic Resistance (Ω)	2	2	0,33	0,33
Max. Allowed Reverse Volt. (V)	3	2	2	2
Mode of Operation	Continuous or Pulsed		Only Pulsed. (Max. Allowance Pulse Width at 10 A, 0,1% Duty Cycle is 200 ns)	

CHARACTERISTICS OF CERTAIN
SEMICONDUCTOR LIGHT DETECTING DEVICES

TABLE 3-2

	PHOTOTRANSISTORS		PIN PHOTODIODES	
	MRD 100	FPT 100A	MD 2	HP 5082-4200
Sensitivity $\mu A/(mW/cm^2)$	90	1 300	4	4
Light Current Rise Time	2,5 (max) µs	2,8 µs	< 1 ns	0,5 ns
Light Current Fall Time	4,0 µs (max)	2,8 µs	< 1 ns	0,5 ns
Max Current Capability (mA)	-	25	20	-
Max Voltage (V)	80	80	20	50
Max Power Dissipation (mW)	50	100	100	300
Spectral Response	400 to 1 100 nm Peaking at 800 nm		400 to 1 100 nm Peaking at 800 nm	900 nm
Useful Operating Light Level Range (mW/cm^2)	0,001-20	0,001-20	0,001-200	0,001-200
Long Term Stability	Good	Good	Excellent	Excellent
Diameter of Light Sensitive Area (mm)	0,4	0,5	1	0,8
Dark Current (µA)	0,1	0,025	0,002	0,003

sufficiently small for high density stacking.

A further requisite is that enough bandwidth is available at the detector for every centimetre of the overhead cable to be inspected, when travelling at a velocity of about 50 km/hr.

Time taken to travel 1 cm at 50 km/hr

$$t = 0{,}7 \text{ ms} \qquad (3\text{-}6)$$

Assuming the LED to be operating in the pulsed mode, it must be switched at least once every 0,7 milliseconds. Since better signal to noise ratios can be obtained by pulsing large forward currents through the LED at low duty cycles, the frequency capabilities of the detector must be considerably better than the pulse frequency of about 1 400 cycles/sec.

With a duty cycle of 1% the "on" time of the LED will be:

$$t_{ON} = \frac{t}{100} = 7 \text{ µs} \qquad (3{,}7)$$

To register such a pulse the detector must be able to respond in at least 3 µs, which eliminates the use of the darlington phototransistor despite its greater sensitivity, since its rise time is typically 100 µs.

Also the speed of the P.I.N. photodiode (< 1 ns) is not required. In fact a greater bandwidth than necessary is a liability since it is accompanied by more noise. The fact that its sensitivity is about two orders of magnitude less than the phototransistor also counts against it.

Hence the obvious choice is the phototransistor, which also happens to be the more readily available. It was therefore decided to use the F.P.T. 100 A, (described in Table 3-2), because of its superior sensitivity.

3-13 Design of Lens

To obtain a perfectly parallel beam of light an ideal point source is required, together with an accurately ground lens corrected for all the important aberrations, (save perhaps chromatic, since LED's only emit in a very narrow region of the spectrum). However, since all available LED's have emitting

areas with diameters of the order of ½ mm, it is pointless to use a lens that has been absolutely corrected for spherical aberrations. Instead it is merely necessary to ensure that the diameter of the circle of least confusion of the lens is of the same order of magnitude as the emitting area of the LED.

This is obtained from[4]

$$b = \frac{0,07f}{N^3} \qquad (3\text{-}8)$$

where b is the diameter of the circle of least confusion.
f is the focal length
N is the F/No of the lens

Since $N = \frac{f}{d}$, where d is the diameter of the lens, it is apparent that the greater N is, the smaller b will be, and hence the better will be the lens.

From the point of view of signal strength however, the focal length must be as short as possible, since the irradiance of the light emitted from the LED obeys an inverse square law. Then too, space on the pantograph shoe is limited so the focal length can not be too long.

The irradiance at the lens surface for a LED situated at its focal point can be obtained by substituting A of Equation 3-3 into Equation 3-4.

Hence

$$H = \frac{\Phi}{2\pi f^2(1 - \cos\theta)} \qquad (3\text{-}4b)$$

Figure 3-2 gives a scaled down indication of the dimensions involved on the shoe.

L = Length of upper flat surface of Pantograph shoe
≃ 127 cm.

S = Allowable Stagger (Peak to peak).
≃ 70 cm.

Since space must be allowed for the protective ramps, the following absolute maximum limit on the focal length can be stipulated.

f_{max}/

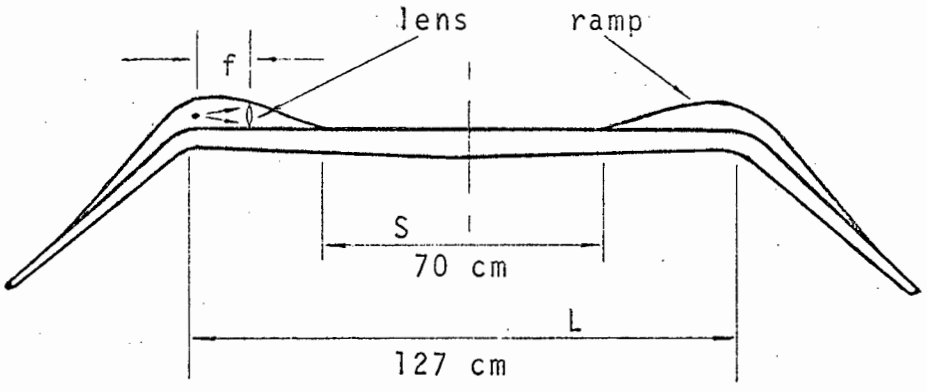

Fig 3-2: Profile of Pantograph Shoe with Protective Ramps and Lens System.

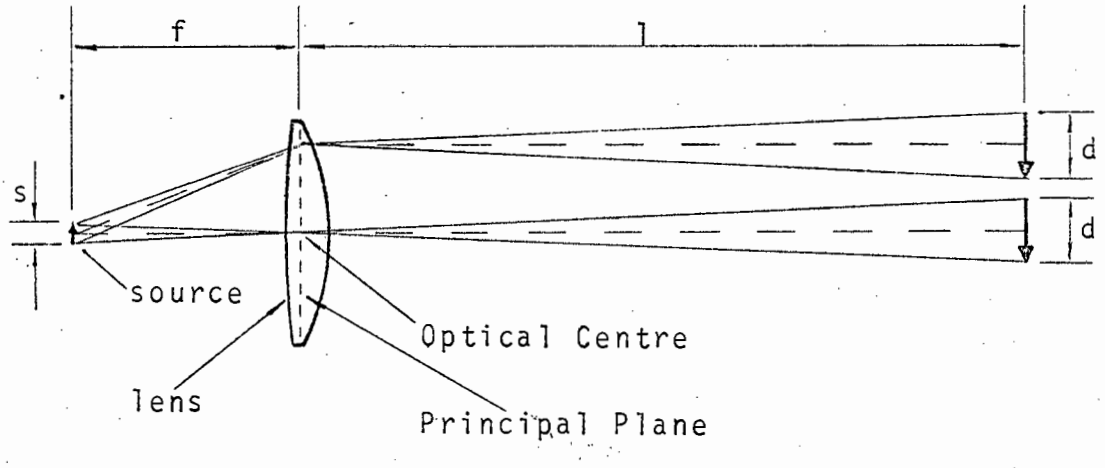

Fig 3-3: Divergence of Light Beam due to Finite Size of Source.

$$f_{max} = (\tfrac{1}{2})\frac{L - S}{2} \qquad (3\text{-}9)$$

$$\simeq 14,3 \text{ cm}$$

However, allowing a depth of about 2 cm for the protective "pop-out" window, the focal length eventually chosen was

$$f = 12 \text{ cm}$$

The diameter of the lens also has certain limitations. If it protrudes too high above the level of the pantograph head, the slope of the ramps may be too great to allow a smooth transition of the overhead cable. Also the larger the diameter, the worse the lens.

Allowing a maximum diameter of ½ mm for the circle of least confusion, we get from Equation 3-8.

$$N = \left(\frac{0,07\ f}{b} \right)^{1/3} \qquad (3\text{-}10)$$

$$= \left(\frac{0,07 \times 120}{0,5} \right)^{1/3}$$

$$= 2,56$$

This gives a maximum allowable lens diameter of

$$d = \frac{f}{N} \qquad (3\text{-}11)$$

$$= \frac{12,0}{2,56}$$

$$= 4,7 \text{ cm}$$

Since the thickness of the overhead cable when new is only 1,5 cm, it was decided that a 4 cm lens would suffice, for which the circle of least confusion has a diameter

$$b = \frac{0,07\ f}{N^3} \qquad (3\text{-}12)$$

$$= 0,31 \text{ mm}$$

Of the different kinds of lens aberrations, probably one of the most serious for this application is spherical aber= ration. It can be reduced to a minimum however, by the

PROPER/

proper choice of the radii of curvature.

The following analysis calculates the radii (without any proof of the formulae used), to give minimum spherical aberration for parallel incident light.[5]

Define

r_1, r_2 = radii of curvature of the lens surfaces.

f = focal length of lens
= 12 cm.

n = refractive index of glass
= 1,5.

s = distance of object from lens
= ∞ (for parallel light).

s' = distance of image to lens
= 12 cm (in this case equal to f).

P = position factor of lens

$$= \frac{s' - s}{s' + s} \qquad (3\text{-}13)$$

$$= \frac{12 - \infty}{12 + \infty}$$

$$= -1 \longrightarrow$$

q = shape factor of lens

$$= \frac{r_2 + r_1}{r_2 - r_1} \qquad (3\text{-}14)$$

$$= -\frac{2(n^2 - 1)P}{n + 2} \qquad (3\text{-}15)$$

$$= \frac{-2(1,5^2 - 1)(-1)}{1,5 + 2}$$

$$= 0,714 \longrightarrow$$

$$r_1 = \frac{2f(n - 1)}{q + 1} \qquad (3\text{-}16)$$

$$= \frac{2(12)(1,5 - 1)}{1,714}$$

$$= 7,00 \text{ cm} \longrightarrow$$

$$r_2 = \frac{2f(n - 1)}{q - 1} \qquad (3\text{-}17)$$

$$= \frac{2(12)(1,5 - 1)}{0,714 - 1}$$

$$= -42,00 \text{ cm} \longrightarrow$$

The negative sign means that the surface curves in the opposite direction.

Note that the side of the lens with the greater curvature should point toward the parallel light rays. If the flatter side was to face the parallel rays, the spherical aberation

would increase by a factor of 4.

It is also fortunate that the above shape factor (q = 0,714) comes very close to that for which there is no coma.

The characteristics of the required lens are listed below.

Type	——	Bi-convex	
Focal Length	: f =	12 cm	
Diameter	: d =	4 cm	
Circle of Least Confusion	: b =	0,31	mm
Radius 1	: r_1 =	7 cm	
Radius 2	: r_2 =	42 cm	

3-20 ACCURACY

A very important question - in fact one on which the feasibility of the whole project hinges - lies in the degree of accuracy that can be expected. The object of this section is therefore to isolate the different factors that affect the accuracy in so far as the optics are concerned, and to analyse them.

3-21 Lens Limitations

One of the biggest drawbacks in trying to create a perfectly parallel beam, is the fact that all the available light sources are not the hypothetically ideal "points" at all, and do have a finite size.

The result is that even if the LED is placed at the focal point of the lens, the light passing through it will diverge, with each point on the principal plane of the lens acting as a type of "fulcrum" as shown in Fig 3-3. It is a fundamental law of optics that light passing through the optical centre of a lens continues in the same straight line. The extent of divergence from any other point on the principal plane will be of the same order of magnitude, and can be gauged from the following relation.

$$\frac{d}{l} = \frac{s}{f} \qquad (3\text{-}18)$$

Hence

$$d = \left(\frac{l}{f}\right)s \qquad (3\text{-}19)$$

Where

d = divergence of beam

f = focal length of lens (In this case, distance from LED to lens)

l = distance from lens to detectors

s = source diameter.

In consequence, the sides of the intensity pattern will have a finite slope, and the parallelness of the beam will

DETERIORATE/

deteriorate as the ratio $\frac{l}{f}$ increases.

An experiment was therefore conducted to determine the intensity distribution of the beam at the appropriate distance from the lens, and to study the effect of placing a cylin= drical rod in the middle of the beam. A schematic diagram of the apparatus is shown in Fig 3-4.

The sketch is almost self-explanatory. A pulse generator of which the mark-space ratio could be varied, was used to provide a train of pulses about 10 μs long and 1 ms apart. These were sent into the "LED pulsing circuit", (which was triggered by the negative-going edges), to be converted into current pulses for exciting the LED. The light emitted was then formed into a parallel beam by a lens.

The photodetector was mounted on a sliding structure which was constrained to move only in the x-direction. This was connected via string and pulleys to a potentiometer which produced a d.c. voltage proportional to the displace= ment of the detector in the x-direction. The voltage pro= duced was fed into the x-input of an X-Y recorder.

(The above construction was rather a "Heath-Robinson" affair, consisting of a small bench vice mounted onto a wooden platform. The photodetector was attached to the sliding part of the vice, while the pulleys and potentiometer were mounted onto the fixed part or onto the platform.)

Measurements of displacement were taken with a sliding vernier gauge and, provided "backlash" of the moving part was avoided, accuracies of the order of 0,05 mm could be achieved.

By adjusting the position of the LED till the width of the shadow cast by the rod differed by < 0,1 mm from its actual diameter, it was possible to obtain a parallel beam of light, (or a very close approximation to one).

The operation of the electrical circuits is explained by Fig 3-5. The LED was excited with large current pulses to obtain sufficient irradiance at the photodetector. To remain within its power dissipating capabilities however, it had to be operated at a very low duty cycle (about 1%).

The photodetector converted the light into a current, from which the current-to-voltage converter-amplifier produced

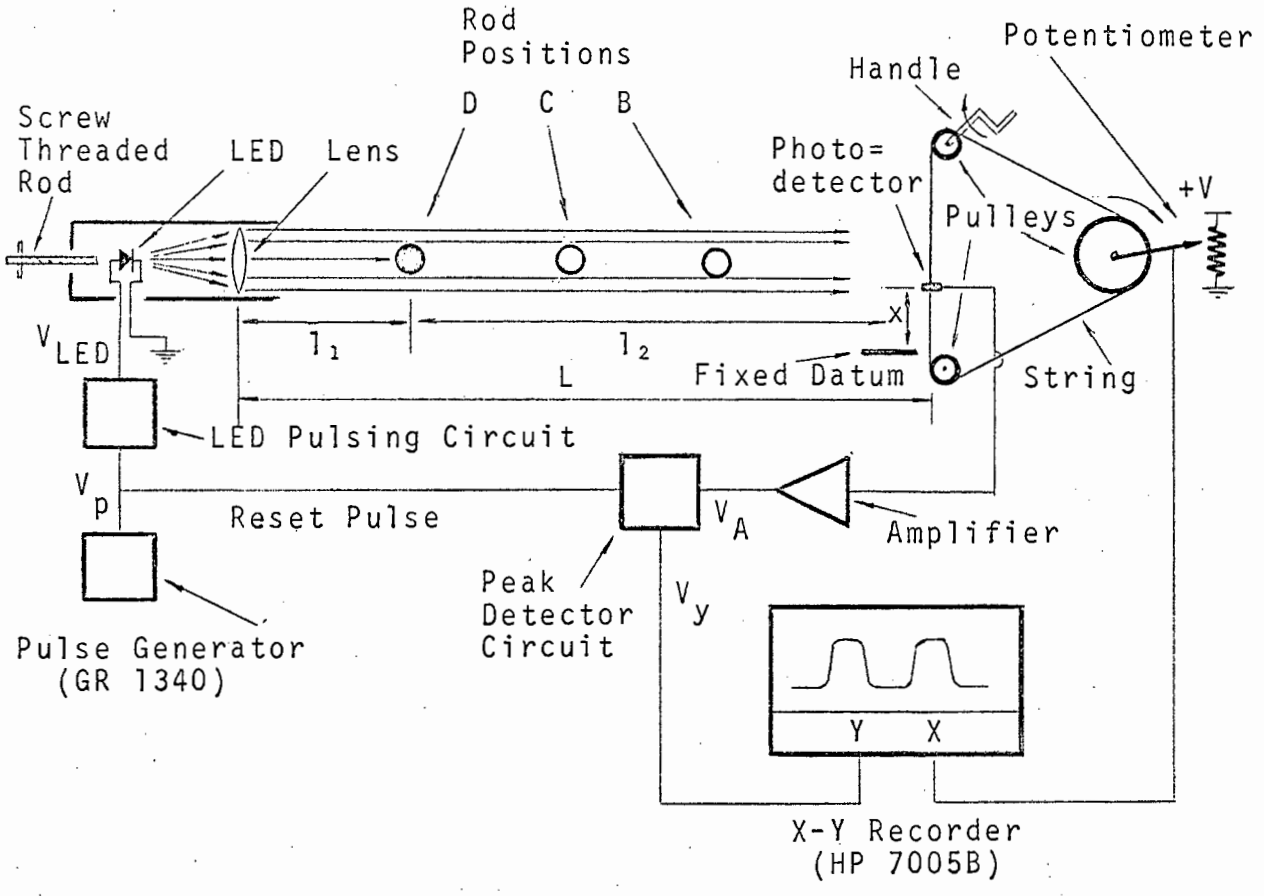

Fig 3-4: Schematic Diagram of Apparatus used to Determine Intensity Pattern of Collimated Light Beam.

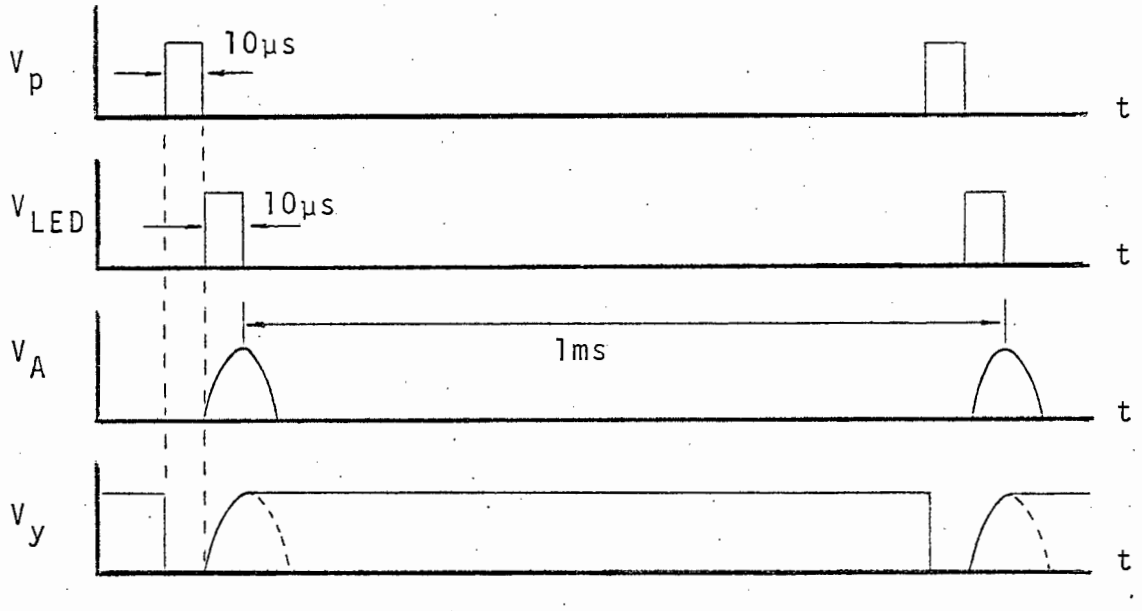

Fig 3-5: Associated Waveforms of the Circuitry Shown in Fig 3-4.

the voltage V_A, which was directly proportional to the irradiance at the detector.

The peak detector sampled the voltage V_A at each pulse, holding the maximum value until it was again reset to zero, just before the advent of the next pulse. The output of the peak detector was then fed into the Y-input of the X-Y re= corder, which, being a mechanical device, could not respond to the rapid voltage changes, but instead traced out the average value of V_y. This was about 99% of its maximum.

Hence by moving the photodetector across the beam, the intensity pattern could be recorded.

The results of this can be seen in Fig 3-6 and Fig 3-7. Graph A of each figure shows the shape of the light beam as "seen" by the detector with nothing obscuring its view, while B, C and D show the results of a rod being placed at the corresponding positions. (See Fig 3-4).

If l_1 is the distance between lens and rod, and l_2 the distance between rod and detector, while the distance between lens and detector L is kept constant, then the three positions can be defined as follows:

B at $l_1 = \frac{3}{4}L$, $l_2 = \frac{1}{4}L$
C at $l_1 = \frac{1}{2}L$, $l_2 = \frac{1}{2}L$
D at $l_1 = \frac{1}{4}L$, $l_2 = \frac{3}{4}L$

(These three cases correspond to the centre or average position of the overhead cable on the pantograph shoe, and the two extreme positions due to stagger.)

For Fig 3-6 the diameter of the rod used was 8 mm, corresponding very closely to the thickness of the critically worn cable, while for Fig 3-7 it was 16 mm, which is 1 mm greater than that of the new cable. Hence these tests catered for a slightly greater range than is actually required.

The effect of the finite size of the emitting source is clearly discernible. As would be expected, condition D (rod closest to lens) is the worst in each case. This too can be explained by the lever analogy, with the rod being the fulcrum.

From Equation 3-19, the region illuminated by any

Fig 3-6: Intensity Distribution of Parallel Light Beam with 8 mm Rod in Beam.

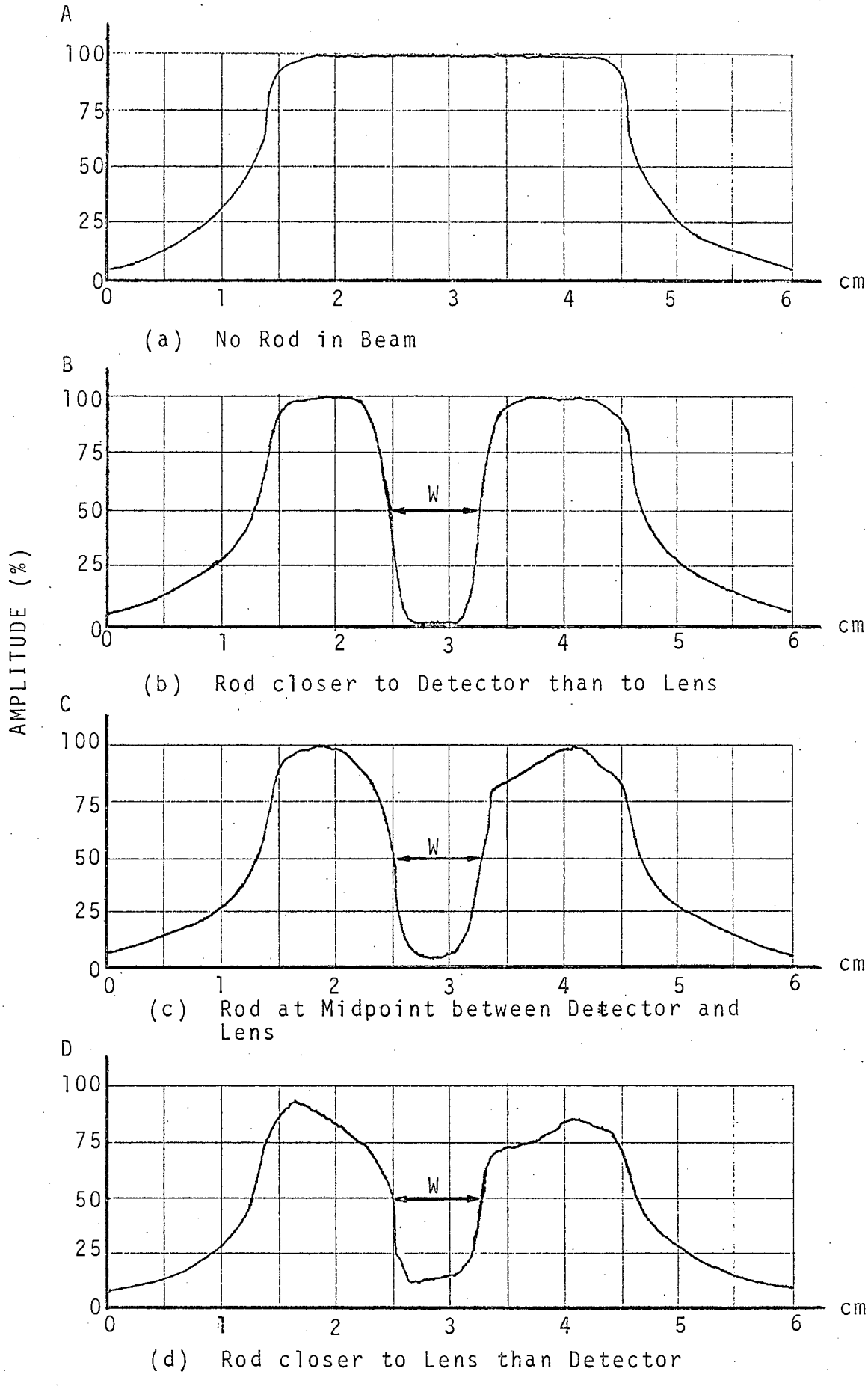

Fig 3-7: Intensity Distribution of Parallel Light Beam with 16 mm Diameter Rod in Beam.

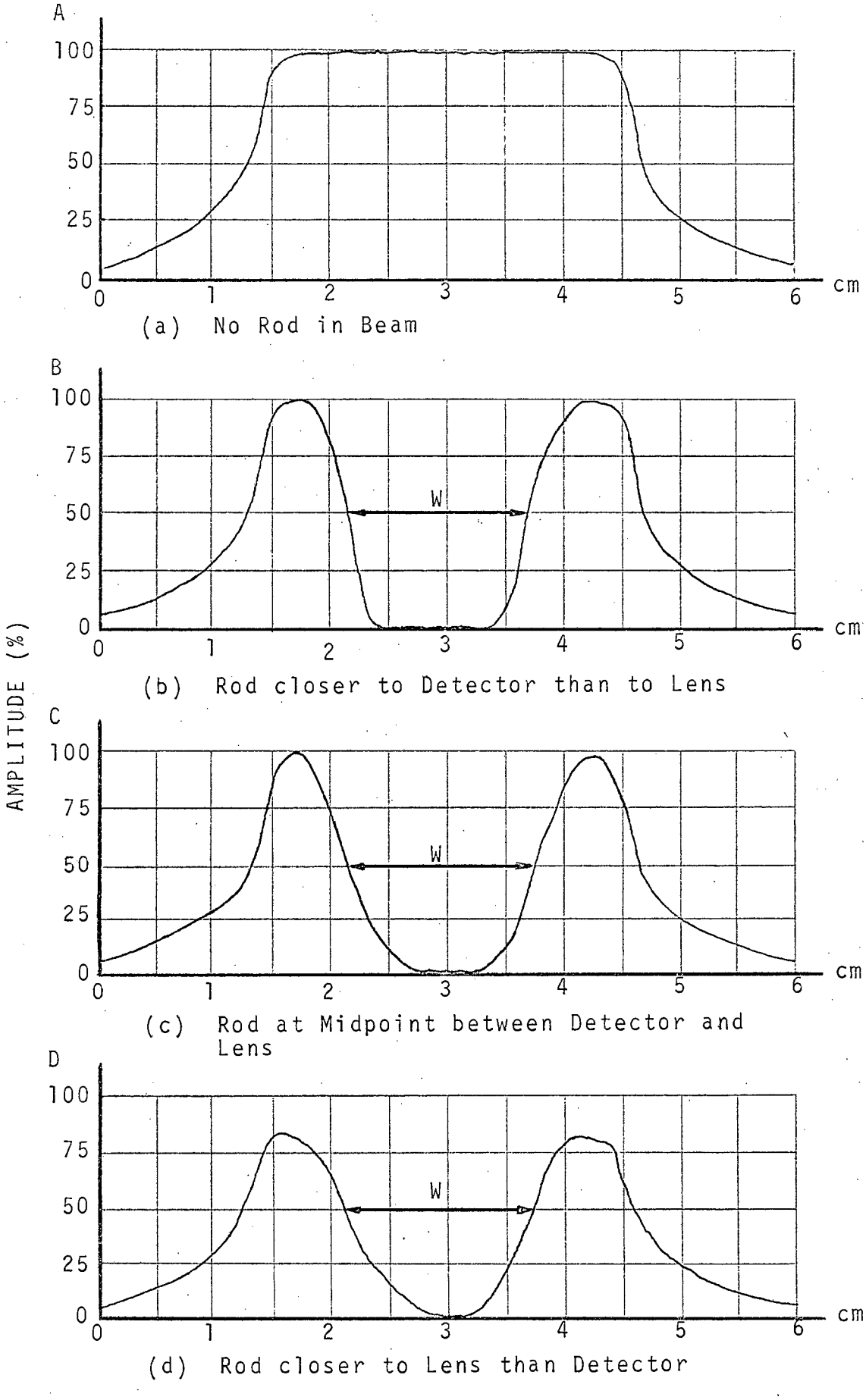

(a) No Rod in Beam

(b) Rod closer to Detector than to Lens

(c) Rod at Midpoint between Detector and Lens

(d) Rod closer to Lens than Detector

individual point of the lens has the diameter

$$d = \left(\frac{l}{f}\right)s$$

With reference then to Fig 3-8, if the rod is placed in the beam a distance l_1 from the lens and a distance l_2 from the detector, then all points on the detector path below x_1 will not be illuminated at all. All points between x_1 and x_2 will be increasingly illuminated as x increases from x_1 to x_2 until a maximum is reached at x_2. Thereafter the illumination will be uniform along x until the edge of the beam is reached. The difference $(x_2 - x_1)$ gives the distance over which the shoulder slopes. This can be calcu= lated by simple geometrical means to be:

$$x_2 - x_1 = \frac{d l_2}{l_1 + l_2} \qquad (3\text{-}20)$$

Since $l_1 + l_2 = L$ (a constant), $(x_2 - x_1)$ is seen to be be directly proportional to l_2, partially confirming the results of the experiment. ("Partially" because the experi= mental and theoretical values do not agree with each other exactly. Nonetheless they are of the same order of magnitude.)

For $f = 120$ mm
$L = 1\,000$ mm
$s = 0{,}5$ mm

From Equation 3-19,

$$d = \left(\frac{L}{f}\right)s = 4{,}2 \text{ mm}$$

Hence for $l_1 = 750$ mm, $l_2 = 250$ mm

$x_2 - x_1 = 1{,}0$ mm (theoretical value)

Compare this with the experimental values:

From Fig 3-6 B:— $x_2 - x_1 \simeq 3{,}3$ mm
From Fig 3-7 B:— $x_2 - x_1 \simeq 4{,}4$ mm

As can be seen they differ by factors of three and four from the theoretical result.

This, as well as the fact that the intensity of the side

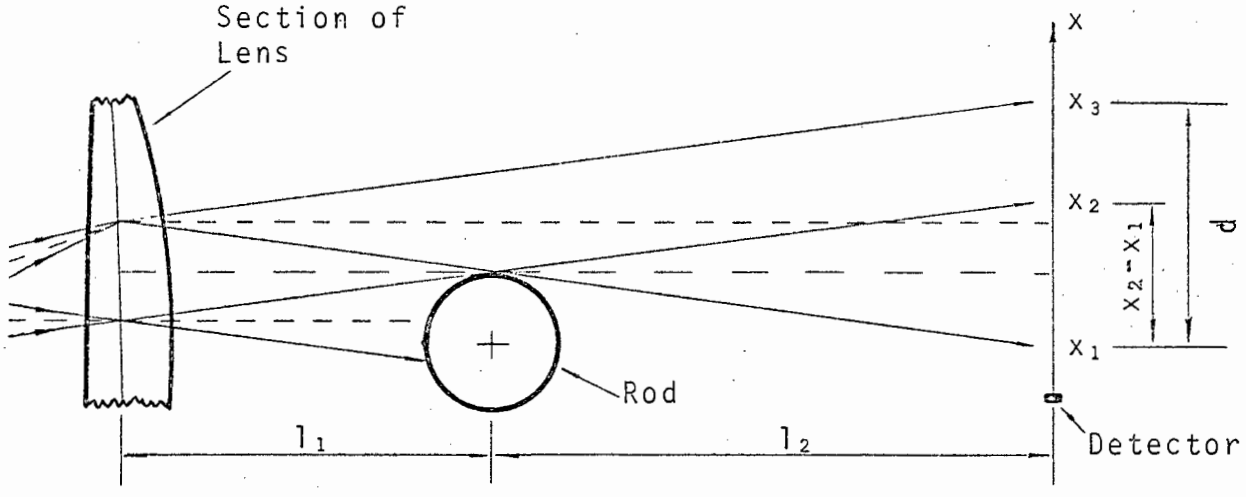

Fig 3-8: Effect of the Finite Size of the Source on the Light Beam when a Rod is placed in the Beam.

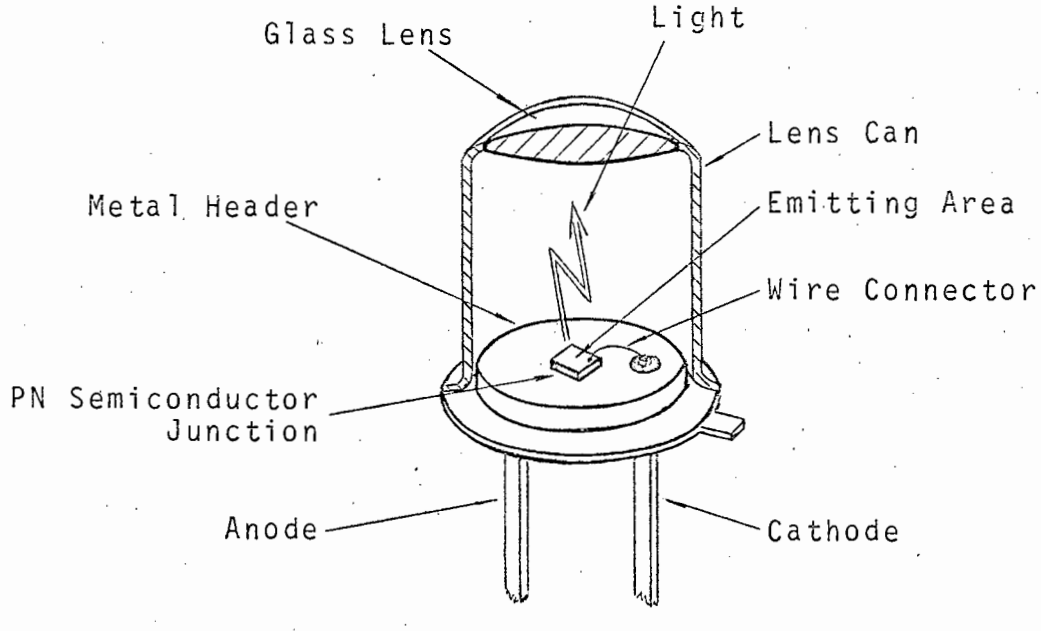

Fig 3-9: Typical Light Emitting Diode

lobes drops as the rod is moved closer to the lens can possibly be explained by assuming that a certain percentage of the light passing through the lens is in fact scattered over a wider area than is suggested by Equation 3-19. This may possibly be the result of microscopic discontinuities in the glass which cause a random scattering of all the photons striking them. This could also account for the gradual "tailing off" of the intensity distribution on either side of the beam.

This is a diffractive phenomena, so it is conceivable that it should be accompanied by interference fringes, especially since LED's emit quasic-coherent light. Optical theory* does in fact predict the existance of interference fringes on the intensity pattern, but fortunately the degree of coherence is sufficiently small to ensure that the amplitude of these fringes is negligible. Also the inter-fringe spacing is small in comparison to the detector diameter ($\frac{1}{2}$ mm), so it can only register the average intensity over its surface.

Consequently no sign of fringes of any description is noticeable on the intensity patterns of Fig 3-6 and Fig 3-7.

3-22 Deciding at what Intensity Level to Recognise Presence of Light

(a) Having seen how the sides of the intensity pattern slope, and how the slope varies with rod position and size, a problem presents itself. At what intensity level must the detector make its decision as to whether the light beam is obscured or not?

The following is a mathematical study of the situation.

Equation 3-19 indicates that the area illuminated by any point of the lens has the diameter d. However the emitting area of the source is not circular, but rather square in shape, so it is really a square of side d that is illuminated by each point. (See Fig 3-9 — It was merely considered circular for convenience before, and no results were affected.)

* Further information on quasi—coherent interference can be obtained from the book "Introduction to Modern Optics", by Grant R. Fowles.

FROM/

From the viewpoint of the detector the same thing would apply. Each point on it would "see" a square source of light of side d on the lens surface. (The receptive area of each detector is also square of side length say δ.)

With reference then to Fig 3-10, the inner unshaded section of the emitting square corresponds to those points on the lens surface which illuminate every individual point of the detec= tor.

It seems reasonable therefore to assume that there exists a square within the total emitting area (the dotted one in the diagram), which directs as much light to the detector as the other, but every point of which can be "seen" by every point of the detector. Let this equivalent square have side D. (This step simplifies the mathematics tremendously, while not really affecting the result.)

The current created in the photodetector is proportional to the number of photons striking it. This in turn is pro= portional to the visibility of each point on the emitter to each point on the detector, as each point on the former emits light to each point of the latter. In other words the current is proportional to the product of the two areas visible to one another.

If a screen now partially obscures the one from the other, the situation becomes slightly more complicated. (See Fig 3-11). Assume it projects a height "a" above the x-axis. The emitter can now be divided into three zones.

(i) $o \leqslant y \leqslant y_1$

None of the light emitted in this region reaches the detector, hence its contribution to the current is zero.

(ii) $y_1 \leqslant y \leqslant y_2$

The light emitted from the elemental strip at height y above the x-axis will be able to illuminate a section of the detector of width z. Two cases now occur - $y_1 < y < a$ and $a < y < y_2$.

(a) For $y_1 \leqslant y \leqslant a$,

$$y = a - b \qquad (3\text{-}21)$$

$$z = h - a - c \qquad (3\text{-}22)$$

$$c = b\left(\frac{l_2}{l_1}\right) \qquad (3\text{-}23)$$

../

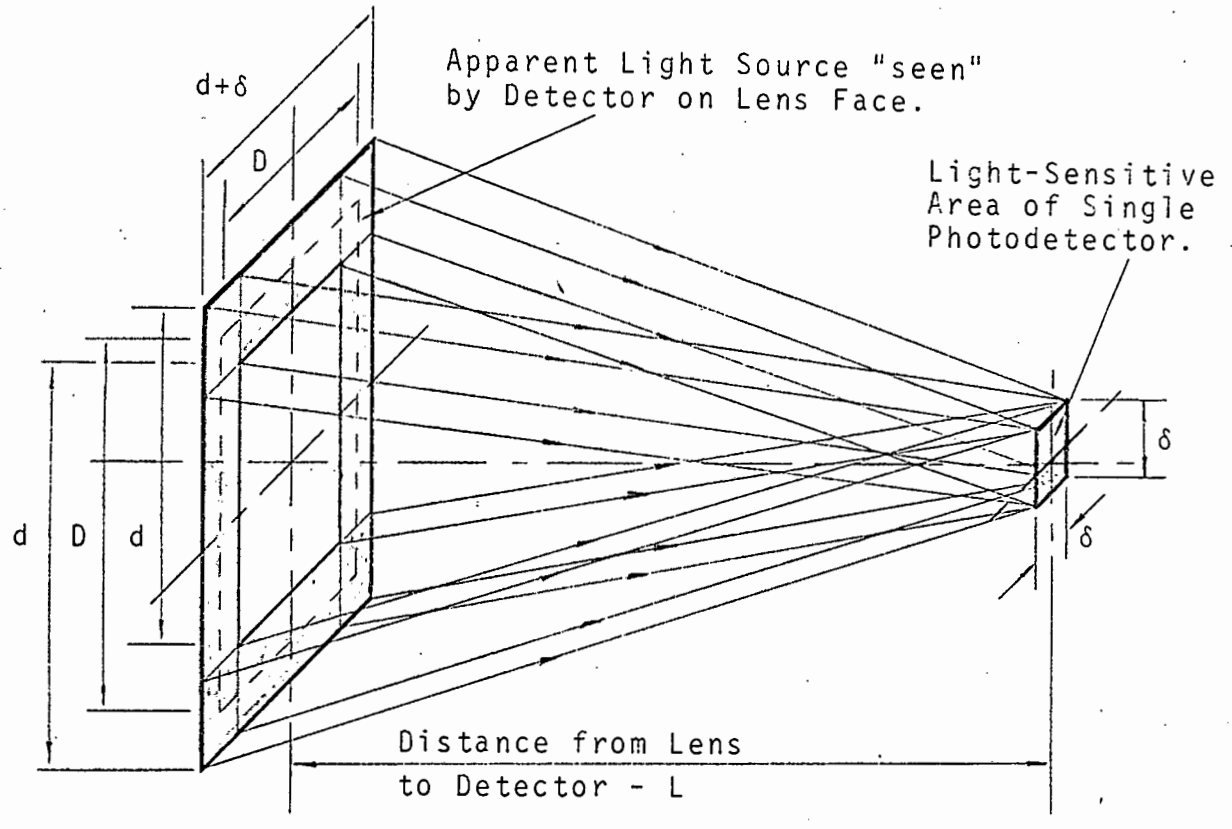

Fig 3-10: Geometry of Light Rays Emerging from Lens and striking a Single Photodetector.

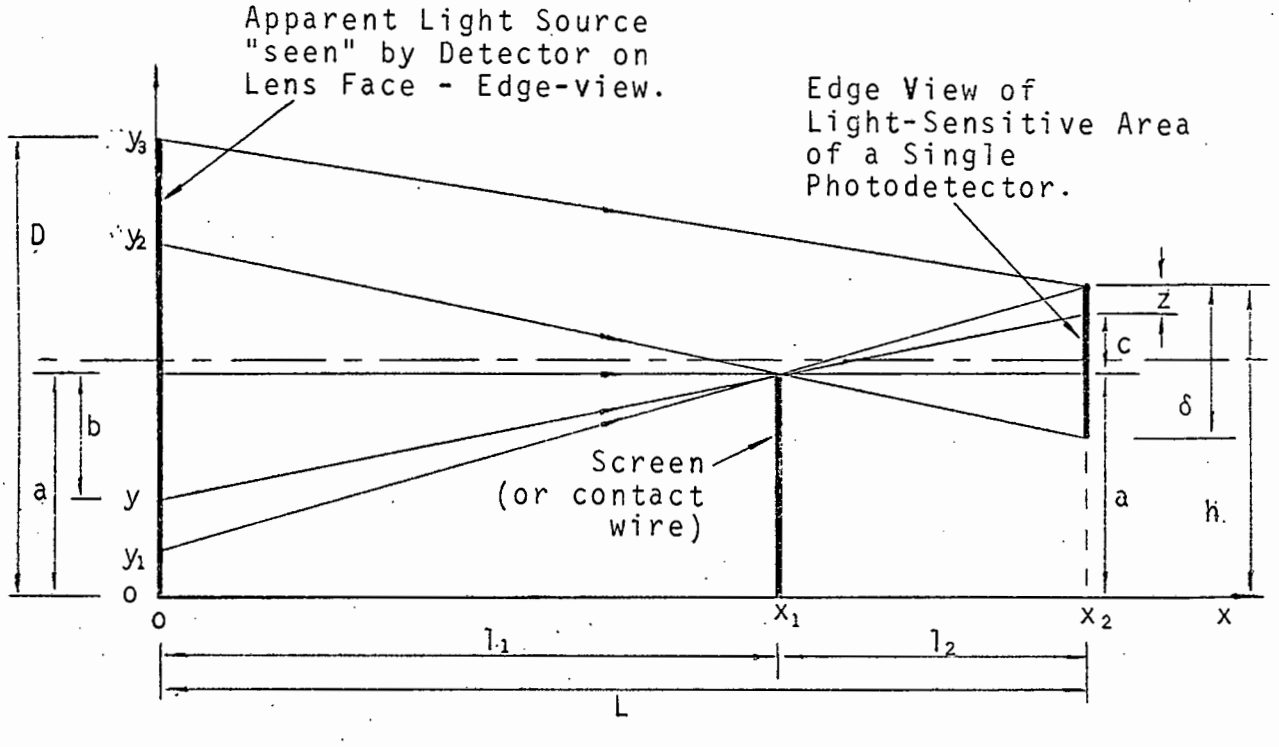

Fig 3-4: Geometry of Light Rays Emerging from Lens and Striking Single Photodetector shown in 2 Dimensions.

$$\therefore \quad z = h-y-b-b(l_2/l_1)$$
$$= h-y-b(x_2/x_1)$$
$$= h-y-(a-y)(x_2/x_1)$$
$$= h+y\{(x_2-x_1)/x_1\}-a(x_2/x_1) \qquad (3\text{-}24)$$

(b) For $a \leqslant y \leqslant y_2$,

$$y = a+b \qquad (3\text{-}25)$$
$$z = h-a+c \qquad (3\text{-}26)$$
$$c = b(l_2/l_1)$$

$$\therefore \quad z = h-a+(y-a)\{(x_2-x_1)/x_1\}$$
$$= h+y\{(x_2-x_1)/x_1\}-a(x_2/x_1) \qquad (3\text{-}27)$$

Fortunately these two expressions for z are identical. Hence for each elemental strip of the emitter between y_1 and y_2, the receptive area is

$$A_r = z\delta \qquad (3\text{-}28)$$

while the area of each elemental emitter is

$$dA_e = D\,dy \qquad (3\text{-}29)$$

The current created by one such element is therefore

$$dI_2 = k.A_r.dA_e \qquad (k = \text{proportionality constant})$$
$$= kz\delta D.dy \qquad (\text{Let } k\delta D = K)$$
$$= Kzdy. \qquad (3\text{-}30)$$

The current created by all the elements between y_1 and y_2 then becomes

$$I_1 = \int_{y_1}^{y_2} Kzdy \qquad (3\text{-}31)$$

$$I_1 = K\int_{y_1}^{y_2}\left\{h+y\{(x_2-x_1)/x_1\}-a(x_2/x_1)\right\}dy \qquad (3\text{-}32)$$
$$= K\left[y\{h-a(x_2/x_1)\} + \tfrac{1}{2}y^2\{(x_2-x_1)/x_1\}\right]_{y_1}^{y_2}$$
$$= K\left[(y_2-y_1)\{h-a(x_2/x_1)\} + \tfrac{1}{2}(y_2^2-y_1^2)\{(x_2-x_1)/x_1\}\right]$$
$$= \tfrac{1}{2}K\{(y_2-y_1)/x_1\}\left[2(hx_1-ax_2) + (y_2+y_1)(x_2-x_1)\right]$$

But $y_1 = (ax_2-hx_1)/(x_2-x_1) \qquad (0 \leqslant y_1 \leqslant y_3) \qquad (3\text{-}33)$

And $y_2 = \{ax_2-(h-\delta)x_1\}/(x_2-x_1) \qquad (0 \leqslant y_2 \leqslant y_3) \qquad (3\text{-}34)$

Hence keeping the above conditions in mind,

$I_1 =/$

$$I_1 = (K\delta^2 x_1)/\{2(x_2-x_1)\} \qquad (3\text{-}35)$$

(iii) $y_2 \leqslant y \leqslant y_3$

All the light emitted from this region in the direction of the receiver reaches its target. The associated current is therefore

$$\begin{aligned} I_2 &= kA_eA_r \\ &= k(y_3-y_2)D\delta^2 \\ &= K(y_3-y_2)\delta \qquad \text{(Since } K = kD\delta\text{)} \end{aligned} \qquad (3\text{-}36)$$

The total current developed by the photodetector is simply the sum of the various contributions.

$$I_T = I_1+I_2 \qquad (3\text{-}37)$$

With further manipulation the expression becomes very unwieldy, so it is more instructive at this point to substitute typical values for the various parameters.

From Equation 3-19, d = 4,2mm, so a reasonable and convenient estimation of D would be about 4 mm.

With reference then to Fig 3-10 and Fig 3-11:

$D = 4$ mm $(=y_3)$
$\delta = 0{,}5$ mm
$h = \frac{1}{2}(D+\delta) = 2{,}25$ mm
$x_2 = 1000$ mm

$0 \leqslant a \leqslant D$
$0 \leqslant x_1 \leqslant x_2$

It was discovered that if K was chosen to be 0,5 , then the total current I_T became normalised to unity when nothing obscured the light beam.

The expressions for I_1, I_2, y_1 and y_2 then become:

$$I_1 = \{16(1000/x_1 - 1)\}^{-1} \qquad (3\text{-}38)$$

$$I_2 = (1 - y_2/4) \qquad (3\text{-}39)$$

$$y_1 = (1\,000a - 2{,}25x_1)/(1000 - x_1) \qquad (3\text{-}40)$$

$$y_2 = (1\,000a - 1{,}75x_1)/(1000 - x_1) \qquad (3\text{-}41)$$

Note:- Equation 3-38 holds only if

$(0 \leqslant y_1 \leqslant D)$, and
$(0 \leqslant y_2 \leqslant D)$.

IF y_1/

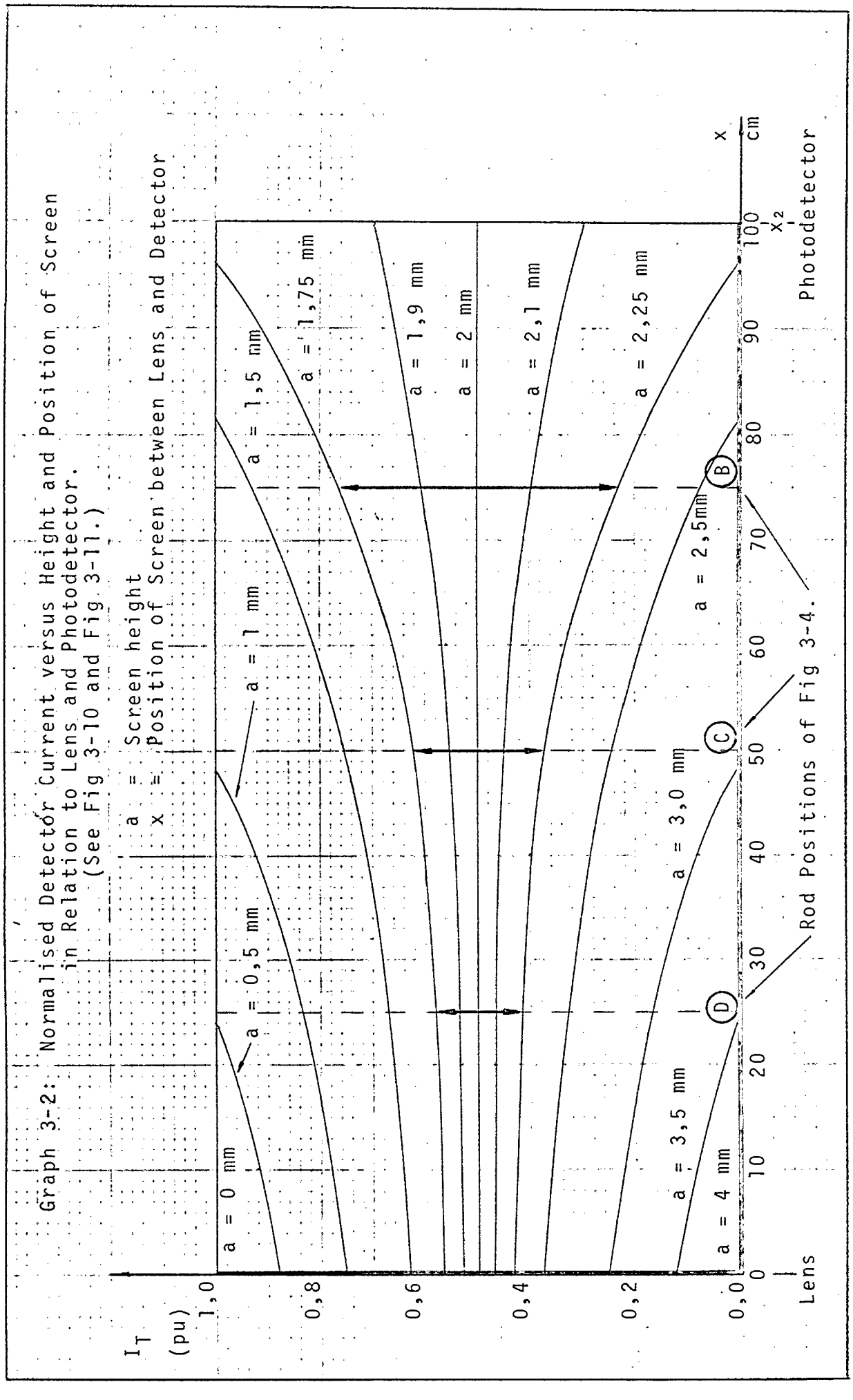
Graph 3-2: Normalised Detector Current versus Height and Position of Screen in Relation to Lens and Photodetector. (See Fig 3-10 and Fig 3-11.)
a = Screen height
x = Position of Screen between Lens and Detector
I_T (pu)
1,0
0,8
0,6
0,4
0,2
0,0
a = 0 mm
a = 0,5 mm
a = 1 mm
a = 1,5 mm
a = 1,75 mm
a = 1,9 mm
a = 2 mm
a = 2,1 mm
a = 2,25 mm
a = 2,5mm
a = 3,0 mm
a = 3,5 mm
a = 4 mm
Lens
0
10
20
30
40
50
60
70
80
90
100
x
cm
x_2
Photodetector
Rod Positions of Fig 3-4.
B
C
D

If y_1 or y_2 fall outside this range, then they must be put equal to 0 or to D depending on whether the calculated value was negative or positive respectively. In this event, Equation 3-42 should be used for I_2.

$$I_2 = \{(y_2-y_1)/4x_1\}\{4,5x_1-2000a+(y_2+y_1)(1000-x_1)\} \quad (3-42)$$

The results for various values of a and x_1 are plotted in Graph 3-2.

In Graph 3-2 the total per unit current is plotted on the vertical axis, while the horizontal axis refers to the length of the pantograph shoe. Each curve plotted corresponds to a different height of the screen (or overhead cable). The point B and D on the x—axis denote the limits of contact wire stagger. (When the wire moves outside these points it starts moving up the protective ramps, so these readings would be discarded anyhow.)

Also if the height of the screen, "a", falls outside the range (1,75 mm < a < 2,25 mm), then if a truly parallel light beam were used, the detector would not be obscured at all. The double arrows at B and D show the confines of this range, which, for the assumed values used is

$$(0,44 \leqslant I_{T(PU)} \leqslant 0,56).$$

This is only 12% of the total current range.

As the symmetry of the situation suggests, the only time the detector current is invariant with screen position, is when the top of the screen is at the same height as the mid=point of the detector. Also, as expected, the associated current is exactly half of its maximum possible value.

This suggests that the detector should make its "decision" at exactly half the maximum intensity level.

This would indeed be the case if the railway environment were both dust- and moisture free, but unfortunately it is neither. Clearly a dust layer on the lens would reduce the intensity at the detector. (The "pop-out" protective windows to facilitate easy cleaning have already been discussed.)

It follows therefore that a value slightly less than half

should be chosen, to ensure a better average accuracy over a prolonged period.

(Note:- The actual numerical values should not be believed implicitly here, because of the probable errors involved in the estimations of the various parameters - especially D. They can however, be used as a rough guide.

The value of the exercise is mainly the prediction of the shape of the family of curves shown in Graph 3-2.)

(b) Section 3-22 (a) concentrated on the theoretical approach to the problem. However it is also necessary to determine in practice the optimum fraction of the received pulses' amplitude at which to make the decision.

The same apparatus as described in Fig 3-4 was used for the experiment, except for the peak detector and X-Y recorder. These were replaced by a comparator and digital counter, as shown in Fig 3-12.

Again a parallel beam of light was obtained by adjusting the position of the LED until the width of the shadow cast by a rod was approximately the same as the rod's diameter. (The width was measured between 50% intensity levels.)

The rod was then removed from the beam, the maximum amplifier voltage noted, and the comparator set to trigger at exactly half this figure. The number of pulses per second displayed by the digital counter was also noted.

The rod was then replaced in the beam and the detector made to do a slow traverse. Whenever the counter reading was exactly half the maximum value, measurements of photodetector displacement were taken.

The argument was that when the amplifier output voltage V_A was just below the trigger voltage, spurious noise spikes would sometimes trigger the comparator and sometimes not. The hysteresis ensured that no multiple triggering could occur per light pulse.

However, since the comparator did not take an instantaneous sample of the signal voltage synchronously with each pulse, but instead remained on continuously, there was a certain margin for error. This was minimal though, and could be neglected, as the the peak-signal-to-r.m.s.-noise ratio was

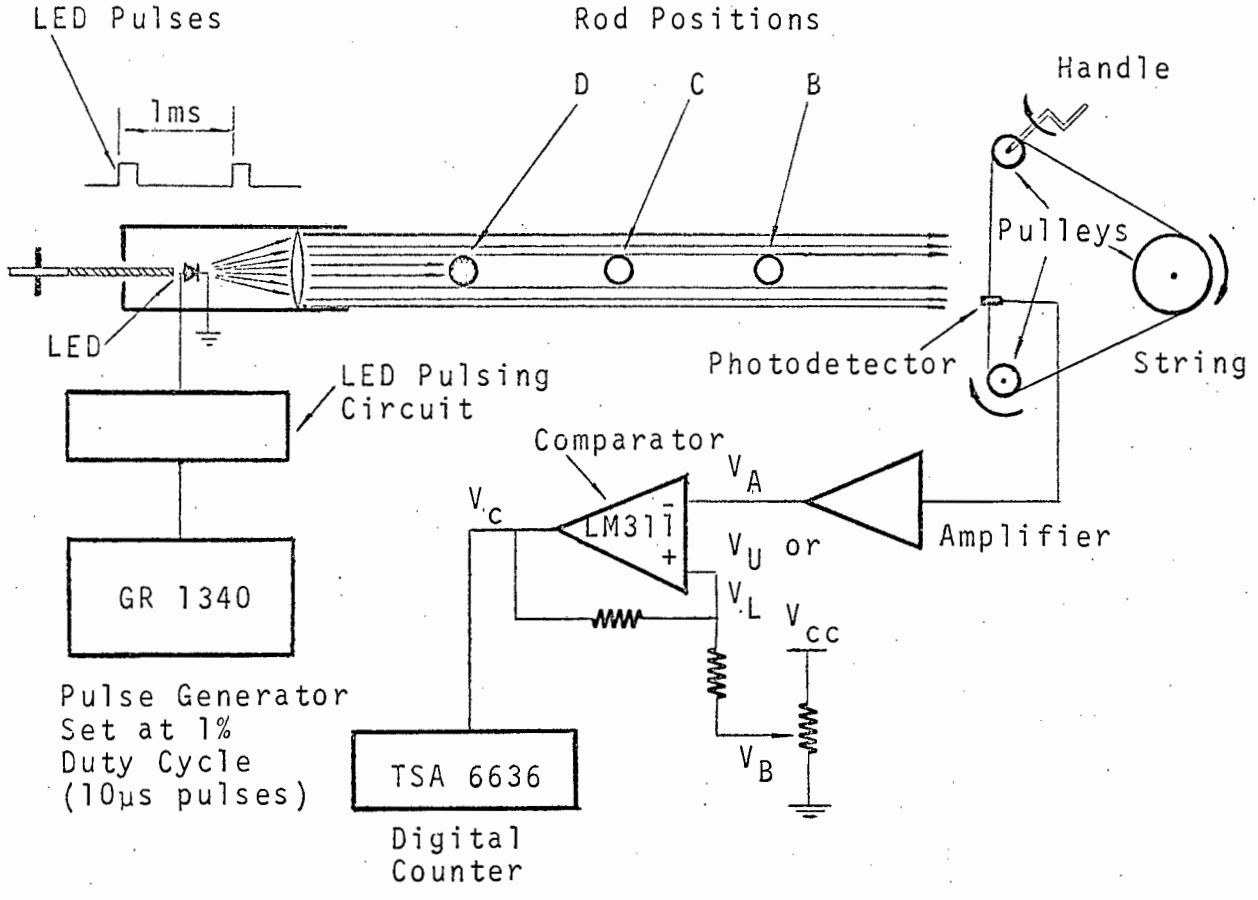

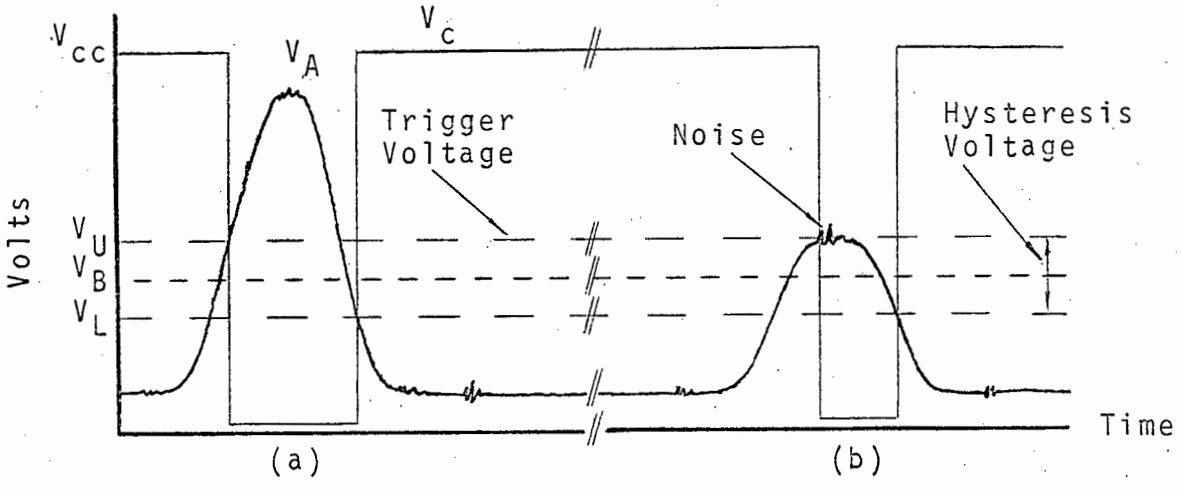

Pulse (a) - Photodetector not obscured by rod
Pulse (b) - Photodetector half-obscured by rod

Fig 3-12: Determination of Optimum Trigger Voltage of Comparators which follow optical amplifiers.

very large, (of the order of 200 to 1).

The thickness of the rod was then obtained by taking the difference of the two displacement readings. This was repeated with the LED at various positions along the principal axis, and also for rods of different diameter, and at different positions in the beam.

The trigger voltage of V_U was then set at 30% of V_A (max), and then at 40%, and the whole procedure repeated each time.

The results are displayed in Graphs 3-3, and 3-4, 3-5 and 3-6. Note that for each case the focal point of the lens corresponds to the zero of the horizontal axis.

Table 3-3 compares the errors predicted by theory to those measured, for various rod positions and trigger voltages. The readings have been corrected to one decimal place.

TABLE 3-3		THEORETICAL ERRORS (mm)			EXPERIMENTAL ERRORS (mm)		
Trigger Voltage V_U (PU)	Rod Diam (mm)	Rod Position B	C	D	Rod Position B	C	D
0,5 V_A(max)	16	0,0	0,0	0,0	0,0	0,0	0,1
	8	0,0	0,0	0,0	0,0	0,0	0,1
0,4 V_A(max)	16	0,1	0,2	0,3	0,3	0,3	0,6
	8	0,1	0,2	0,3	0,3	0,4	0,6
0,3 V_A(max)	16	0,2	0,4	0,6	0,4	0,6	0,8
	8	0,2	0,4	0,6	0,4	0,5	1,9

Errors, theoretical and experimental, for rod thickness measurements. (All error readings are in millimetres.)

More than eighty per cent of the measured values fall within a factor of two of what was predicted, and the remainder fall within a factor of three. The worst case is that of the 8 mm rod at position D (closest to the lens) for a trigger voltage of 30% of V_A (max). This, together with the curve for the 3 mm rod in Graph 3-6, tends to support the theory that a certain proportion of the light passing through the lens

Graph 3-3: Measured Thickness of Rod Versus Position of LED on Lens Principal Axis. (Trigger Voltage at 50% of Max. Pulse Amplitude).

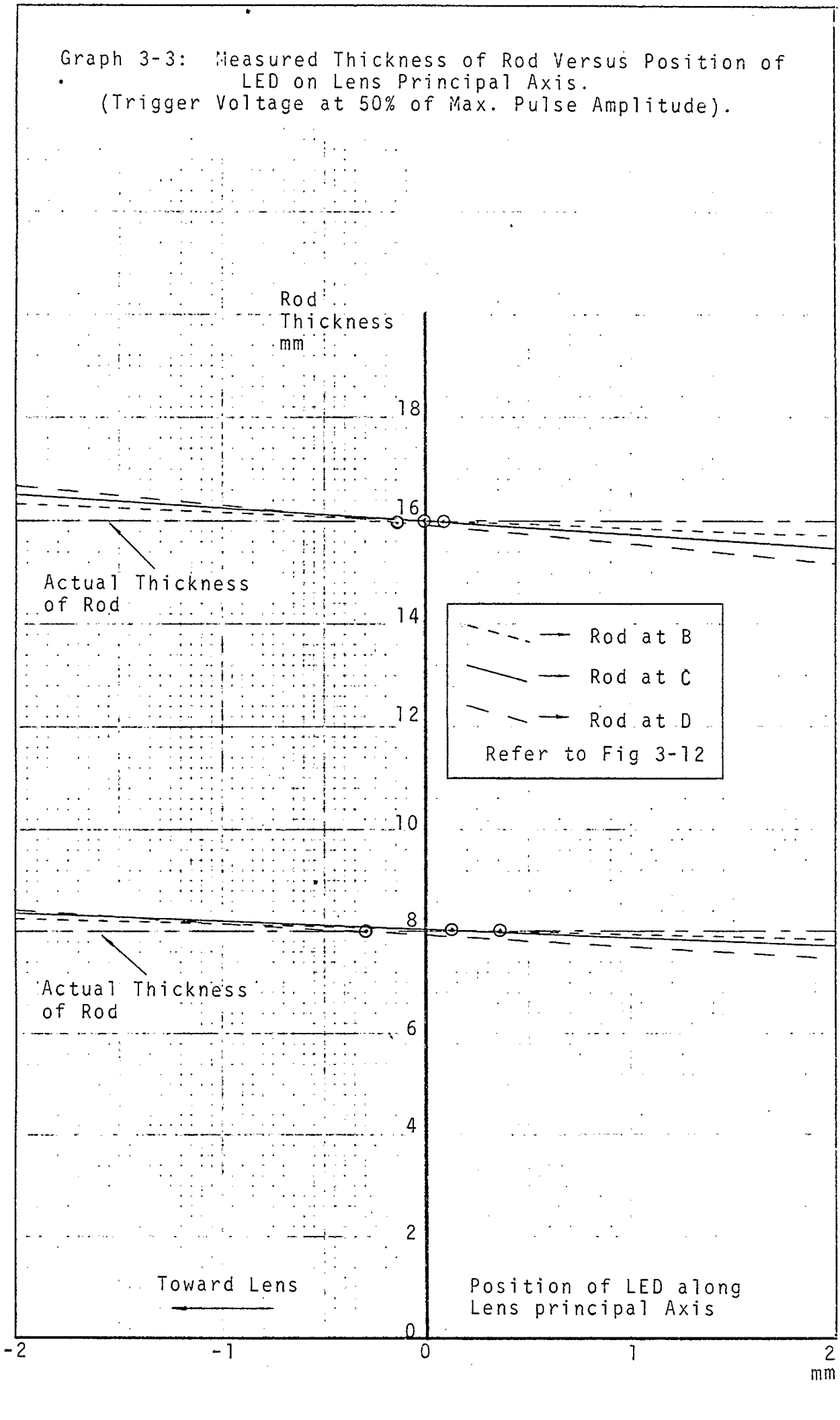

Graph 3-4: Measured Thickness of Rod Versus Position of LED on Lens Principal Axis.
(Trigger Voltage at 40% of Max. Pulse Amplitude).

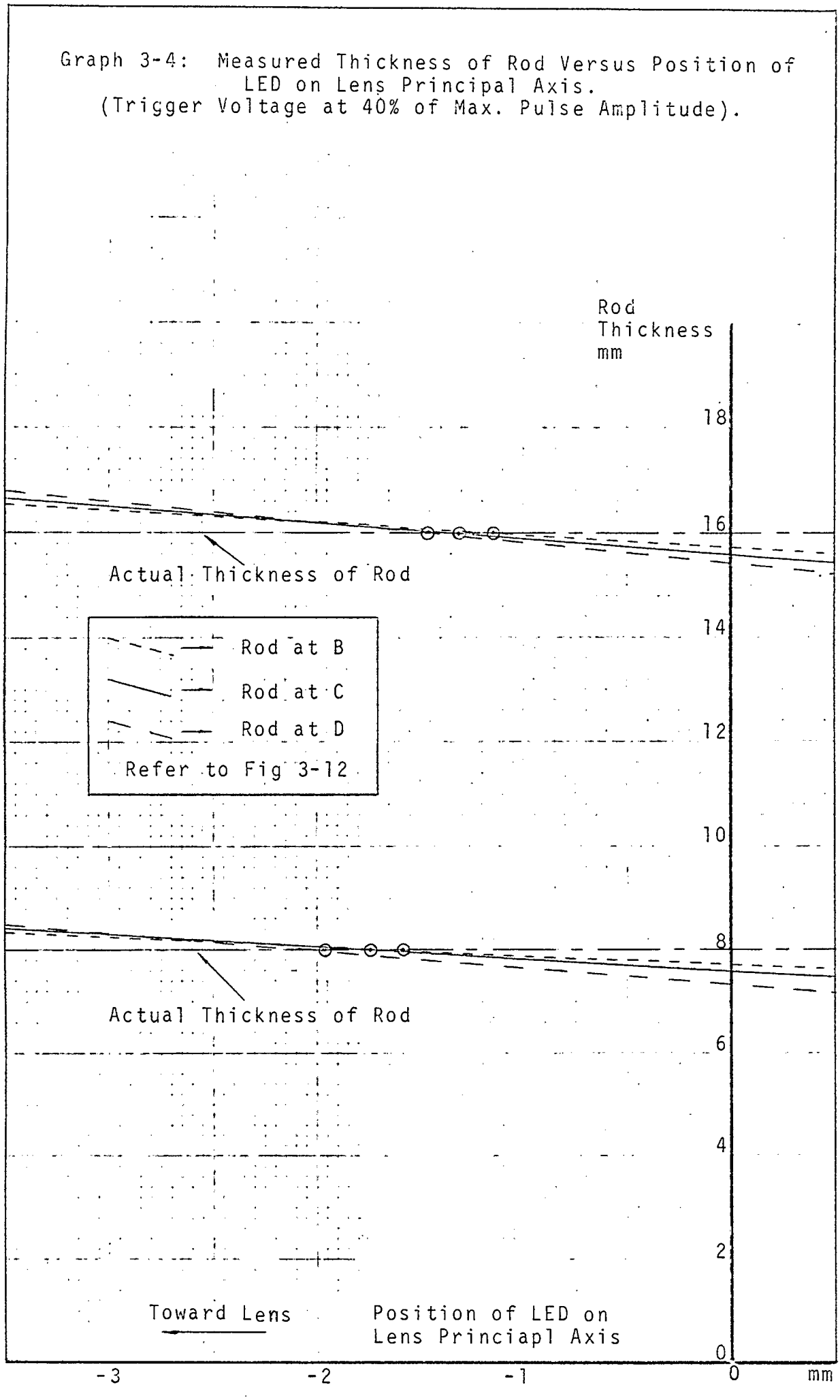

Graph 3-5: Measured Thickness of Rod Versus Position of LED on Lens Principal Axis. (Trigger Voltage at 30% of Max. Pulse Amplitude).

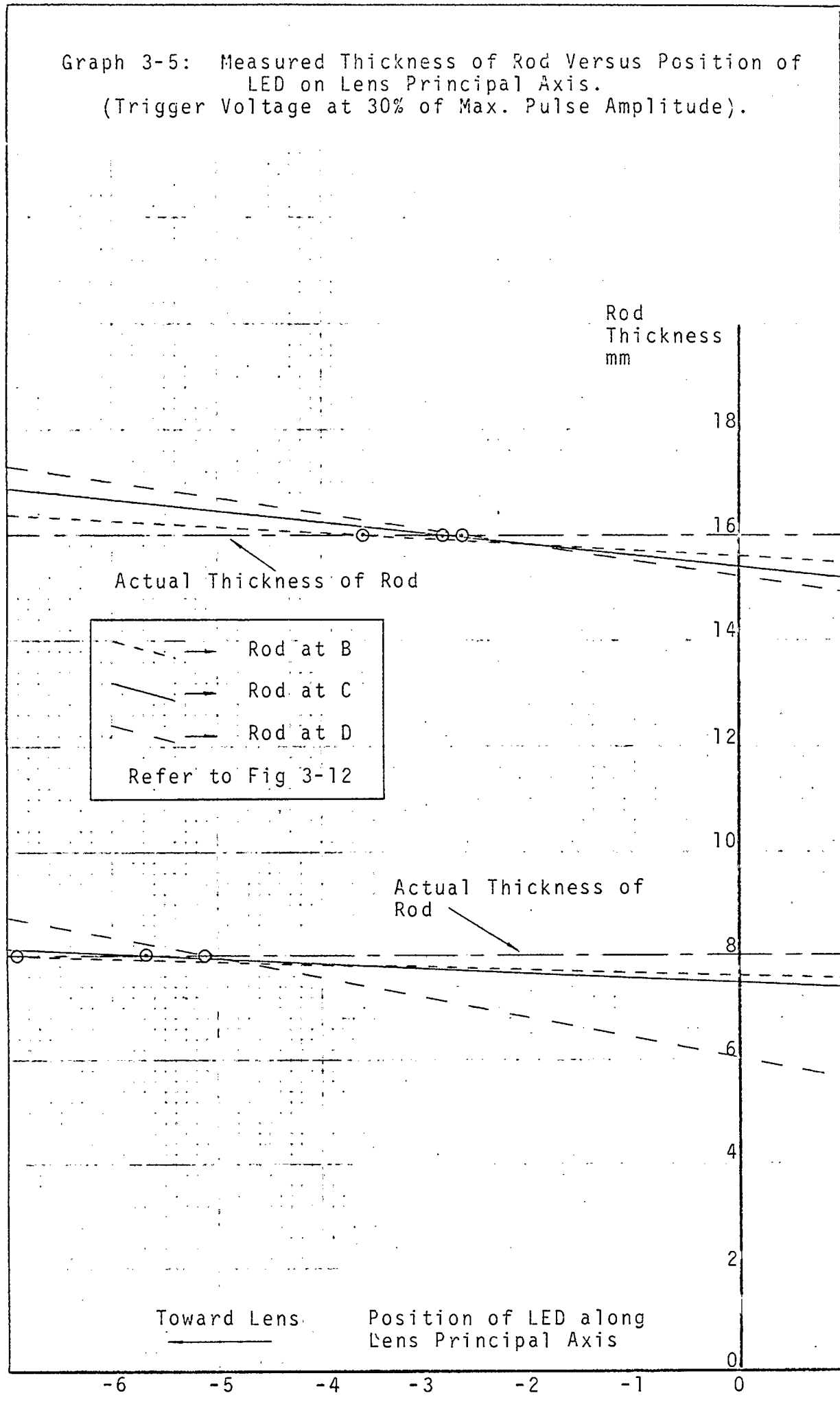

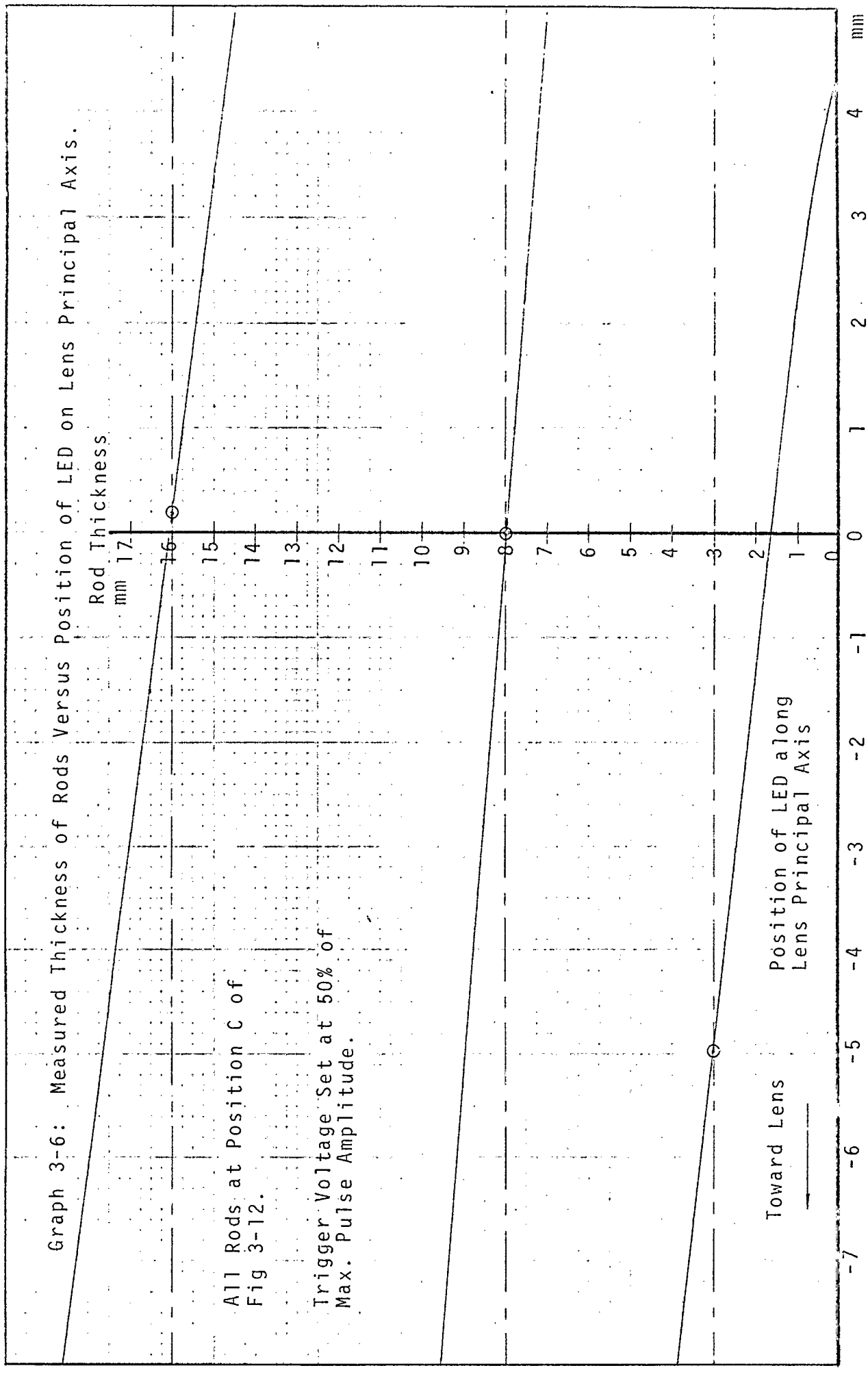
Graph 3-6: Measured Thickness of Rods Versus Position of LED on Lens Principal Axis.
All Rods at Position C of Fig 3-12.
Trigger Voltage Set at 50% of Max. Pulse Amplitude.
Rod Thickness
mm
17
16
15
14
13
12
11
10
9
8
7
6
5
4
3
2
1
0
-7
-6
-5
-4
-3
-2
-1
0
1
2
3
4
mm
Toward Lens
Position of LED along Lens Principal Axis

is scattered more than is predicted by simple geometry.

Otherwise the results are favourable, and indicate that provided the trigger voltage V_U is set no lower than 40% of V_A (max), the best resolution that can be obtained is of the order of 0,6 mm. Compared to the new cable of 15 mm diameter, this implies a worst case inaccuracy of 4%; while compared to the critically worn cable (9 mm), the worst case is only 7%.

3-23 Setting Light Source at Focal Point of LED.

It may happen that while in use, vibration or impact may dislodge the LED from its position at the focal point of the lens. Because of the infra-red nature of the light, (in= visible to the human eye), certain difficulties were envisaged in resetting the LED to its required position - especially under field conditions.

It is important that the operators be able to do this "on the spot", and by a method which is not time-consuming and is easy to perform.

After some research, it was decided that the best solution to the problem was to use the simple process of trial and error. (The mathematical approaches attempted did not prove very successful, and can be found in Appendix II.)

The chosen method entails placing a rod of known diameter in the light beam, and adjusting the position of the LED until the correct thickness is indicated by the photodetec= tor array. Finer adjustments can be made by repeating the performance with the rod at other positions in the beam, and even further accuracy can be obtained by repeating with a second rod of different diameter.

In practice the duration of the exercise seldom exceeds three or four minutes, and the resultant accuracy is such that all subsequent readings are true – that is to within the resolution imposed by the centre-to-centre spacings of the detectors.

3-24 Resolution

If the centre-to-centre spacing of the detectors were smaller than the inherent uncertainty that has already been discussed, the uncertainty of the overall system would be

dominated by the lens's aberrations alone. However if the reverse were true, then the uncertainty would be set by the inter-detector spacing.

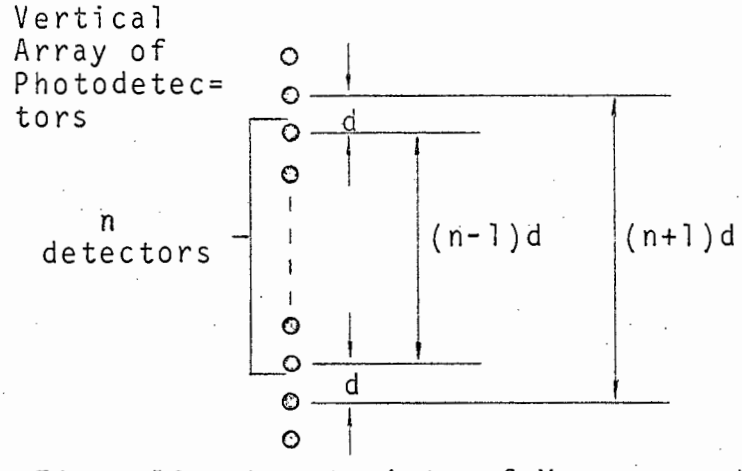

Fig 3-13: Uncertainty of Measurement due to Vertical Spacing of Elements in Detector Array.

Consider first the contribution of the detector spacing alone. With reference to Fig 3-13 where they are a distance d apart, it is clear that if n of the detectors are in shadow, the thickness of the cable T will lie between two limits.

Hence

$$(n-1)d < T < (n+1)d \qquad (3\text{-}42)$$

ie. $$T = nd \pm d \qquad (3\text{-}43)$$

The overall uncertainty of the system would then be

$$E = d+e \qquad (3\text{-}44)$$

where E = overall uncertainty
e = error due to limitations of lens system.

To return then to the spacing of the detectors, the argument proceeds as follows:

The diameter of the new cable is 15 mm. Bearing in mind that the thickness of the contact strips is about 6 mm, and that they should be replaced when they have worn down to about 1 mm, the absolute minimum length of the array could be set at

$l_{(min)}$/

$$l_{(min)} = 15 + 5 = 20 \text{ mm.}$$

This however would mean that information would be lost whenever the contact wire bounced, unless of course either the wire or the strips had already suffered a little wear.

Then too the array should not protrude too high above the contact strips, since space in that direction is limited. (It must be mounted inside a type of cylindrical housing, the diameter of which should be large enough to accomodate the protective "pop-out" window; while the overall height would be that of the ramp, which should protrude sufficiently above the housing to protect it from being swept off the shoe.)

Consequently an array length of 24 mm was chosen as being a reasonable compromise. This would accommodate minor bouncing and vibrations of the new cable when there is no real concern about it. At the other extreme with worn con= tact strips too, the maximum bounce that could be accommodated would be of the order of 14 mm.

Regarding the spacing between the detectors, Equation 3-44 indicates that a reasonable limit would be

$$d < \frac{e}{5} \approx 0{,}12 \text{ mm} \qquad (3\text{-}45)$$

which unfortunately cannot be achieved with discrete components. (At the time of construction, photodetector arrays with inter-element spacings of this order of magnitude, had already come onto the market. However one could not be found which had both an acceptable spacing and the required length, so it would have meant stacking two together. This however was deemed unacceptable, mainly because of their prohibitive cost, as it was not considered wise to spend too much on a device which might not be able to stand up to the harsh over= head environment.)

For the prototype therefore, d was eventually determined by the diameter of the photodetector housing. For the FPT 100 A, this was 5 mm, but by staggering them it was possible

to locate them at vertical intervals of 1,5 mm resulting in a total of 16 detectors in the array. Fig 3-14 shows how this was achieved.

The absolute maximum error that could occur would then be

$$E = 2,1 \text{ mm}$$

but the probability of it ever being this large would be very small.

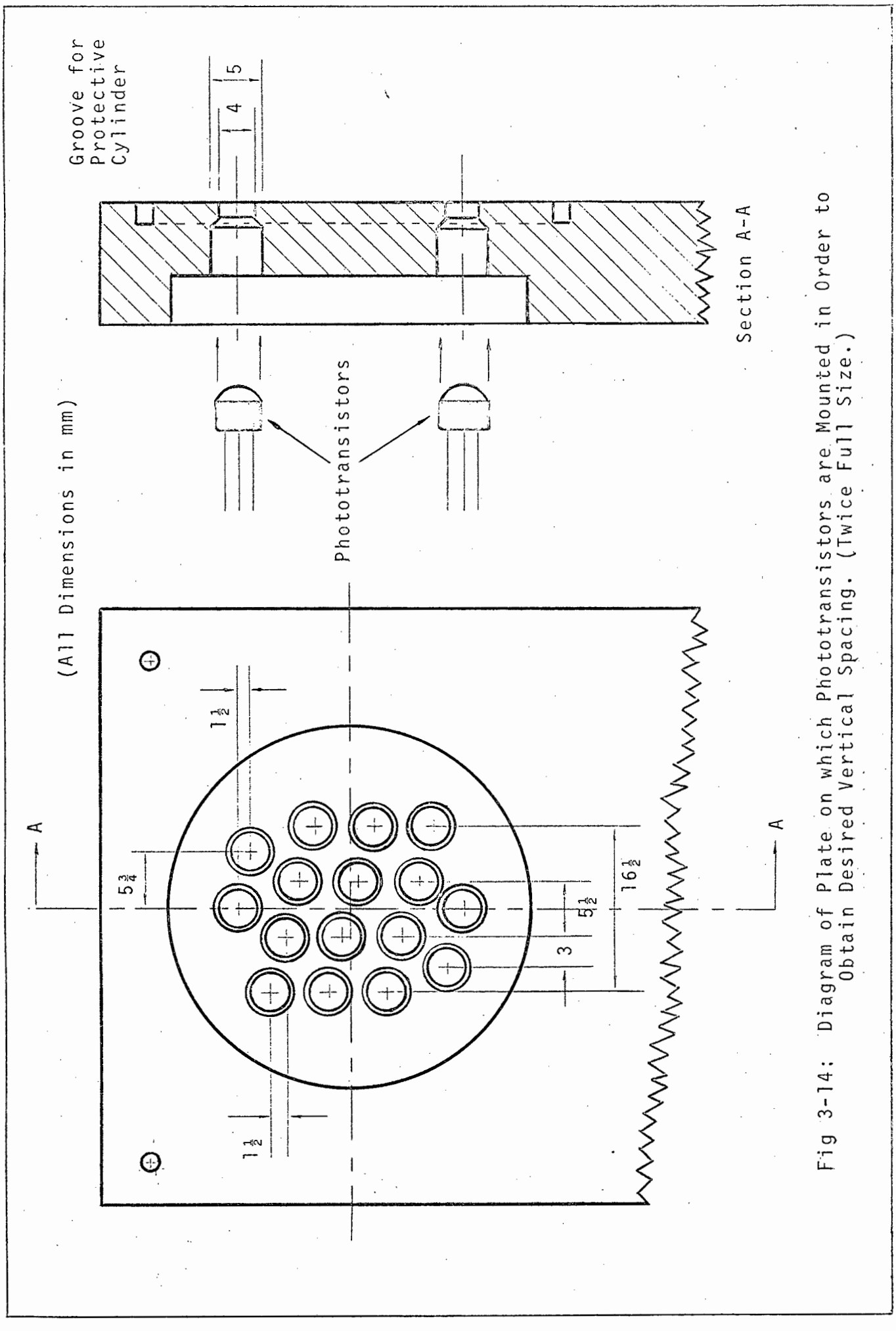

Fig 3-14: Diagram of Plate on which Phototransistors are Mounted in Order to Obtain Desired Vertical Spacing. (Twice Full Size.)

3-30 ELECTRICAL CONSIDERATIONS.

3-31 Mode of Operation.

The uncertainty due to the optical limitations will not be the only type of error in the system. Other sources of error will include such things as the ever changing ambient light conditions, and even electrical noise - especially in the sensitive amplifiers used to convert the optical signal into a usable voltage.

Because of the large error resulting from the optics alone, these other types of error will have to be rendered negligible in comparison. It is therefore important to choose the method for signal transmission and extraction for which errors are least likely to occur.

This immediately rules out the d.c. mode of light transmission, because of the changing light conditions at different times of the day. The detector will also have to differentiate between the more rapid ambient light changes, (for instance when the locomotive suddenly passes into the shadow of a bridge, building or tree etc.) and the signal proper. Hence some type of synchronous detection and/or matched filter technique will have to be applied.

The alternative methods fall into two main categories - continuous wave or pulsed - each of which can be made to have very good noise rejection capabilities.

(a) Continuous Wave Method

(i) Using a Matched Filter:- The LED should be excited by an extremely stable oscillator (eg. crystal), and each detector output fed into a very narrow band filter centred at the oscillator frequency.

Each filter's output should then be rectified, and fed via a low pass filter to a comparator, set to trigger at a predetermined voltage. The outputs of the comparators should then be instantaneously interrogated at fixed intervals of time, (corresponding, say, to 1 cm of locomotive travel at its average speed), and the number of "untriggered"

ONES/

ones would be proportinal to the thickness of the overhead cable.

If this method were to be used, it would be expe= dient to combine the bandpass filtering and ampli= fying actions into an active device - since this would save space and avoid the use of undesirable inductors.

A disadvantage of using a high Q device however, is that a wave passing through it suffers a group delay which increases with increasing Q according to the relation:[6]

$$\tau(\omega) = \frac{2Q\cos^2\{\phi(\omega)\}}{\omega_0} + \frac{\sin\{2\phi(\omega)\}}{2\omega} \text{ seconds} \qquad (3\text{-}46)$$

where ω_0 is the centre-frequency of the filter,
ω is the frequency under consideration,
$\phi(\omega)$ is the phase change of the wave, and
Q is the quality factor of the device.

$$\phi(\omega) = \tfrac{1}{2}\pi - \arctan\{(2Q\omega/\omega_0)+\sqrt{4Q^2-1}\} - \arctan\{(2Q\omega/\omega_0)-\sqrt{4Q^2-1}\} \text{ radians} \qquad (3\text{-}47)$$

Note:- $\tau(\omega) = \frac{d\phi(\omega)}{d\omega}$ = Group Delay

It is interesting at this stage to substitute a few typical values into Equation 3-46 to see what delays can be expected.

Since the transmission frequency ω should be as close as possible to the centre frequency ω_0, and assuming $Q>>1$, Equation 3-47 can be reduced to:

$$\phi(\omega) \simeq \tfrac{1}{2}\pi - \arctan(4Q) \text{ radians} \qquad (3\text{-}48)$$

Assuming the detector is a phototransistor, the frequency response of the system will be of the order of 50 kc/s. Hence let

$$\omega_0 = 10^5\pi \text{ radians/sec.}$$

Table 3-4 shows the delays that can be expected for various values of Q.

Quality Factor Q	Group Delay $\tau(\omega_0)$
10	64 μs
20	130 μs
50	320 μs
100	640 μs
200	1300 μs

Table 3-4: Relationship of Group Delay $\tau(\omega_0)$ to Quality Factor Q.

If, at 50 km/hr, the contact wire is to be inter=rogated once every cm, it means the detectors should be scanned once every 720 μs.
It is apparent then, that good accuracy could be obtained for Q's of up to 50 or 60, while Q's of even up to 100 might be tolerated. However, for Q's greater than 100, the group delays would be so long that they would cause the more rapid fluctuations in the contact wire condition to be missed.
Hence the "disadvantage" does not really present a problem. Even with a Q of 50 the only active noise energy would be concentrated in a frequency band 1000 c/s wide, whereas all the signal energy would be concentrated at the centre of that band where the gain is highest.

(ii) Using Synchronous Detection:- This method would not require such a stable oscillator as the other, unless of course, the two methods were used in conjunction with each other.
This time the detected signal should be "chopped" in synchronism with the transmitted signal. The out=put from each detector should then be rectified, low-pass filtered and fed into a comparator as before. Thereafter the procedure remains the same.

It is common practice to combine the principles of matched filtering and synchronous detection into one circuit, hence obtaining the best of both worlds.

(b) PULSING/

(b) Pulsing

This method entails "blasting" as much light as possible from the LED in a short burst, and then switching it off for a while to allow it to cool down. The time between pulses should be about 0,7 ms, as before, to ensure that every centimetre of the contact wire is scanned.

The bandwidth of the detector circuit need not be so great as to reproduce the pulse shape with any fidelity, since this would only allow more noise through without increasing the signal amplitude very much. After all, only the presence of the pulse needs to be detected. The optimum bandwidth can be obtained by applying the principles of matched filtering to the detection of binary signals.

The principle of operation of the detector circuits then is as follows. The amplified signal is fed directly into a comparator which has been set to trigger at a predetermined voltage. Synchronous detection can then be applied in the extraction of the signal, by instantaneously sampling the outputs of the comparators at that point during each light pulse when the output signal from the detector is maximum.

This method was finally chosen in preference to the other, for the following reasons.

(i) More Light

Since at a 1% duty cycle the LED can be pulsed at currents at almost two orders of magnitude greater than its rated d.c. value, the corresponding emitted light intensity will also be at almost two orders of magnitude greater. This means that the amplifier gains need not be as large as when using the continuous wave method. Since space is also a limiting factor, this is important, as the amplifiers could operate with one stage less than they would otherwise require.

(ii) Simplicity

Another important factor is that whereas the detectors for the continuous wave method would require an amplifier, a band-pass filter and a low-pass filter, the pulse technique requires only an amplifier. In addition

precision components would be required for the band-pass filters, because of the high Q's involved.

(iii) Noise Rejection Capabilities

Since both synchronous detection and matched filtering would be applied in both methods, their noise rejection capabilities should be of the same order of magnitude. Hence the simpler of the two techniques is the obvious choice.

3-32 Noise Statistics

It is now necessary to assess the minimum signal to noise ratio allowable in the detectors, to ensure satisfactory operation of the system.

Assuming that the electrical noise in the system is white and Gaussian in nature, the analysis proceeds as follows.[7a]

With reference to Fig 3-15 which shows the Gaussian probability density distribution, the following quantities are defined.

v = noise voltage.

$$f(v) = \frac{e^{-(v^2/2\sigma^2)}}{\sqrt{2\pi\sigma^2}} \quad \text{(probability density function)}$$

σ = standard deviation of probability function, or rms noise voltage.

The probability that the noise voltage will be less than some prescribed value, $K\sigma$ (where k is a constant), can then be written as follows:

$$\text{Prob } (-K\sigma < v < K\sigma) = \int_{-K\sigma}^{K\sigma} f(v)dv \qquad (3\text{-}49)$$

Putting $y = \frac{v}{\sqrt{2}\sigma}$ and using the symmetry of f(v), Equation 3-49 becomes

$$\text{Prob } (-K\sigma < v < K\sigma) = \frac{2}{\sqrt{\pi}} \int_{0}^{K/\sqrt{2}} e^{-y^2} dy \qquad (3\text{-}50)$$

This integral is more commonly known as the "error function",

AND/

and abbreviated erf $\left(\frac{K}{\sqrt{2}}\right)$.

Erf(x) cannot be integrated in closed form, but solutions have been developed for it in terms of infinite series.

$$\text{(i)}\quad \operatorname{erf}(x) = (2/\sqrt{\pi})\left\{\frac{x^1}{1} - \frac{x^3}{3.1!} + \frac{x^5}{5.2!} - \frac{x^7}{7.3!} + \ldots\right\} \tag{3-51}$$

$$\text{(ii)}\quad \operatorname{erf}(x) \simeq 1-(e^{-x^2}/x\sqrt{\pi})\left\{1 - \frac{1}{2x^2} + \frac{1.3}{(2x^2)^2} - \frac{1.3.5}{(2x^2)^3} + \ldots\right\} \tag{3-52}$$

Clearly (i) will converge faster for small values of x, while (ii) will converge faster for large values.

In applying the above to the problem in hand, the distinction is drawn between two cases:

(a) Synchronous Pulse Detection.
(b) Non-Synchronous Pulse Detection.

Of the two, synchronous detection is the superior technique. Also, for the detectors mounted on the pan, it is relatively simple and expedient to implement - as further analysis will show.

However, with regard to the digital transmission of data across the 3 kV potential difference to the inside of the motor-coach, non-synchronous detection must be used. This is because it is impossible to bridge this potential barrier with a conductor which could "tell" the receiver when to expect a signal pulse.

The problem is not insurmountable though. If the peak-signal-to-rms-noise ratio was small, M-ARY[7b] orthogonal signals* could be used in the transmission. Since it is large, it is possible to transmit the information directly without first encoding it. The limiting S/N ratio is calculated in section (b) below.

* This is a particular class of encoded signals that has been utilized successfully in approaching the Shannon limit on capacity.

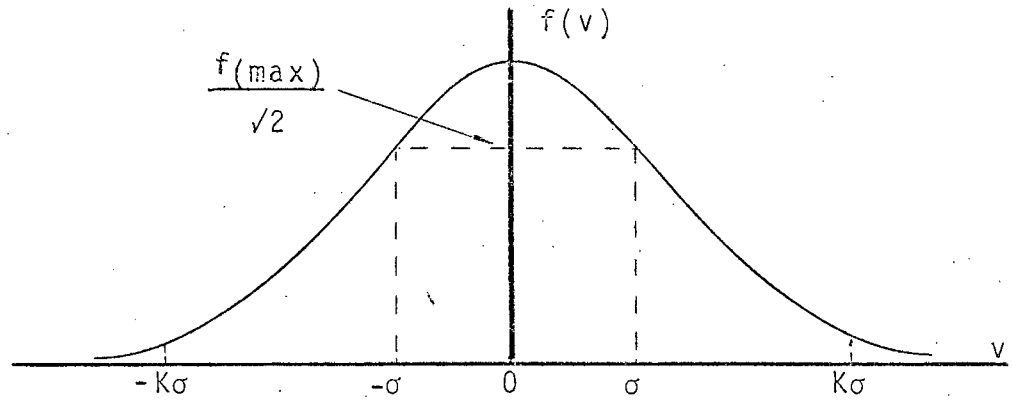

Fig 3-15: Gaussian Probability Density Distribution.

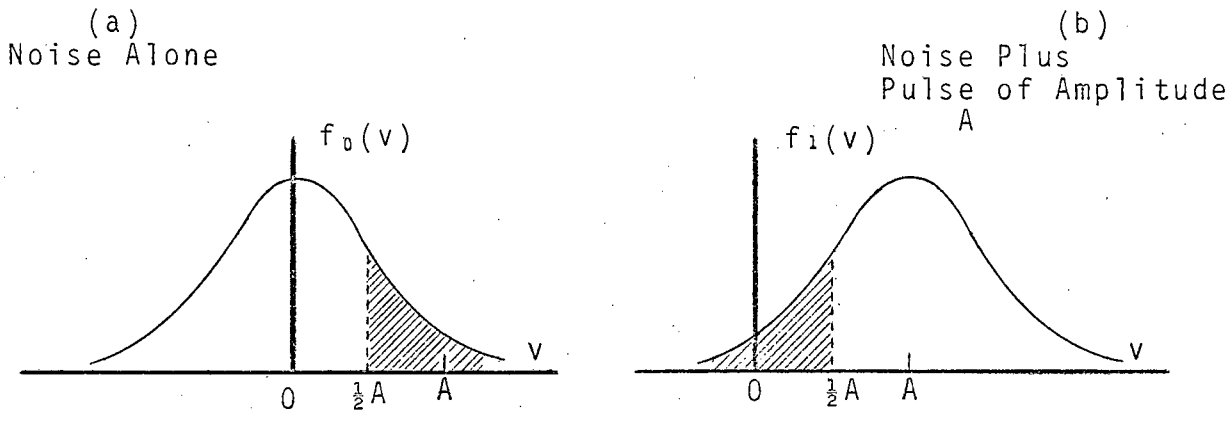

Fig 3-16: Probability Densities in the Transmission of Binary Pulses where the Trigger Level of the Comparator is set at $K\sigma = \frac{1}{2}A$.

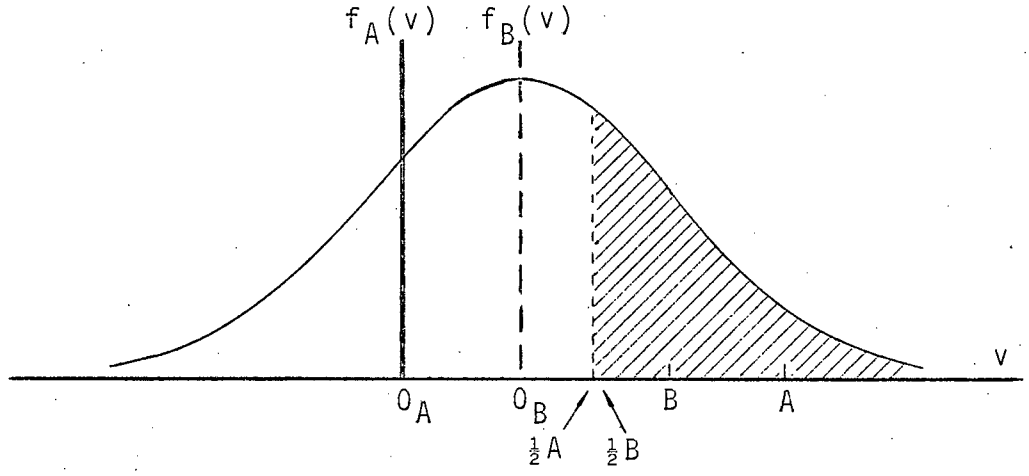

Fig 3-17: Noise Situtation for Partially Obscured Detectors at Edges of Shadow.

(a) Synchronous Detection.

With synchronous detection, an instantaneous decision is made per light pulse as to whether light is present or not. ("Instantaneous" because the decision is made on the edge of a TTL pulse, which is instantaneous in comparison to the bandwidth of the system). The problem therefore reduces to finding the probability of any one pulse being read incorrectly.

If A is the peak amplitude of the received pulses, and the trigger voltage of the comparator is set at $K\sigma = A/2$, what is the probability of the noise being mistaken for a pulse - or if the pulse is already there, the noise subtracting from it to register the absence of a pulse? The situation is shown graphically in Fig 3-16.

The probability of a 1 being registered instead of a 0 is simply the shaded area of Fig 3-16(a). Let this be called P_{e_1}. Similarly P_{e_0} is the probability of a 0 being registered instead of a 1, which is the shaded area of Fig 3-16(b).

The total probability of an error being registered by any single detector is then

$$P_e = P_0 P_{e_0} + P_1 P_{e_1} \qquad (3\text{-}53)$$

where P_0 is the probability of the signal being a 0 and P_1 the probability of it being a 1.

By the symmetry of the two Gaussean curves in Fig 3-15 it is clear that for a threshold voltage A/2, $P_{e_0} = P_{e_1}$. Also if it is assumed that there is an equal probability of a 1 as a 0 being registered,

$$P_0 = P_1 = \tfrac{1}{2}$$

The probability of an error occurring in any one detector is then

$$P_e = \tfrac{1}{2}\left(1 - \operatorname{erf}\frac{A}{2\sqrt{2}\sigma}\right) \qquad (3\text{-}54)$$

and the reliability of each individual detector is

R_e/

$$R_e = 1 - P_e \tag{3-55}$$

For n such detectors, the resultant reliability is

$$R_{R_1} = R_e^n = (1-P_e)^n \tag{3-56}$$

This can be expanded using Taylor's Theorem

$$R_{R_1} = 1 - \frac{nPe}{1!} + \frac{n(n-1)P_e^2}{2!} - \frac{n(n-1)(n-2)P_e^3}{3!} + \ldots \tag{3-56}$$

If P_e is small, then the second order and higher terms can be neglected. Hence the resultant probability of an error occurring in any one of the n detectors is

$$\begin{aligned} P_{R_1} &= 1 - R_{R_1} \\ &= nP_e \end{aligned} \tag{3-57}$$

The relationship between P_e and the peak-signal-to-rms-noise ratio can be seen in Graph 3-6.

The above analysis is strictly true only for signal pulses of constant amplitude. This criterion holds for 14 of the 16 detectors, but for the one at each edge of the shadow, the amplitude may be at some intermediate value.

Equation 3-57 will therefore have to be modified to take into account the probability P_E of an error occurring in one of these.

Since the expressions for erf(x)in Equations 3-51 and 3-52 give the area under the curve in the range $[-x, x]$, it follows that the shaded area of Fig 3-15(a) is

$$\begin{aligned} \text{Prob } (v \geq A/2) &= \int_{\frac{1}{2}A}^{\infty} f(v)dv \\ &= \tfrac{1}{2}\left\{1 - \text{erf}\frac{A}{2\sqrt{2}\sigma}\right\} \end{aligned} \tag{3-58}$$

The new situation is shown in Fig 3-17, where a second ccordinate system is defined at the "centre of gravity" of the

GAUSSEAN/

Gaussean function. O_A and O_B are the respective origins of the two systems.

For the B-coordinate system, Equation 3-58 becomes

$$\text{Prob } (v \geq B/2) = \tfrac{1}{2}\left\{1 - \text{erf}\frac{B}{2\sqrt{2}\sigma}\right\} \tag{3-59}$$

Since O_B has a uniform probability of being anywhere in the range $[O_A, A]$, the average probability of an error can be determined by integrating over this range and dividing by the interval between the limits of integration.

Hence the average probability of a 1 being recorded in error is

$$\bar{P}_e(O_A \leq O_B \leq A/2) = (1/\tfrac{1}{2}A)\int_0^{\frac{1}{2}A} \tfrac{1}{2}\left\{1 - \text{erf}\frac{B}{2\sqrt{2}\sigma}\right\}dB \tag{3-60}$$

and the average probability of a 0 being recorded in error is

$$\bar{P}_e(A/2 \leq O_B \leq A) = (1/\tfrac{1}{2}A)\int_{\frac{1}{2}A}^{A} \tfrac{1}{2}\left\{1 - \text{erf}\frac{B}{2\sqrt{2}\sigma}\right\}dB \tag{3-61}$$

By symmetry,

$$\bar{P}_e(O_A \leq O_B \leq A/2) = \bar{P}_e(A/2 \leq O_B \leq A) \tag{3-62}$$

Define

$$P_< = \text{Prob } (O_A \leq O_B \leq A/2) \tag{3-63}$$

$$P_> = \text{Prob } (A/2 \leq O_B \leq A) \tag{3-64}$$

Because of the uniform probability of O_B being anywhere between O_A and A,

$$P_< = P_> = \tfrac{1}{2} \tag{3-65}$$

The probability of an error from a partially obscured detector is then

P_E'/

$$P_E' = P_{<}.\bar{P}_e(0_A \leq 0_B \leq A/2) + P_{>}.\bar{P}_e(A/2 \leq 0_B \leq A)$$
$$= \tfrac{1}{2}\left[\bar{P}_e(0_A \leq 0_B \leq A/2) \times 2\right]$$
$$= \bar{P}_e(0_A \leq 0_B \leq A/2)$$
$$= 2/A\int_0^{A/2} \tfrac{1}{2}\left(1 - \operatorname{erf}\frac{B}{2\sqrt{2}\sigma}\right)dB \qquad (3\text{-}66)$$

Equation 3-66 would suffice if the light-sensitive surfaces of adjacent detectors were actually touching each other. However there is a gap between them which must be accounted for.

Let

c = centre-to-centre spacing of detectors in the vertical direction ($1\frac{1}{2}$ mm)

d = diameter of light-sensitive area ($\frac{1}{2}$ mm)

Then g = c-d = gap width between adjacent detectors

If the edge of the shadow falls in the gap between two detectors, then the probability of an error in either of them is simply P_e as given in Equation 3-54. If one of the detectors is partically obscured though, then the probability of an error is P_E' as in Equation 3-66.

Combining the above two conditions,

$$P_E = (g/c)P_e + (d/c)P_E' \qquad (3\text{-}67)$$
$$= (2/3)P_e + (1/3)P_E'$$

The "reliability" of a detector at the edge of the shadow is therefore

$$R_E = 1 - P_E \qquad (3\text{-}68)$$

while the resultant "reliability" for 2 such detectors is

$$R_{R2} = R_E^2 \qquad (3\text{-}69)$$
$$= 1 - 2P_E + P_E^2$$

IF/

If $P_E << 1$, this reduces to

$$R_{R2} \simeq 1 - 2P_E \qquad (3\text{-}70)$$

The resultant uncertainty for the two detectors at the edges of the shadow is then

$$P_{R2} = 1 - R_{R2} \qquad (3\text{-}71)$$
$$\simeq 2P_E$$

The TOTAL PROBABILITY for the whole system which comprises n detectors with constant peak-signal-to-rms-noise ratio, and 2 detectors with variable ratios,is then

$$P_T = P_1P_{R1} + P_2P_{R2} \qquad (3\text{-}72)$$

where

P_1 = probability of a detector being one with a constant S/N ratio, and

P_2 = probability of a detector being one with a variable S/N ratio.

Since there are a total of 16 detectors in the system,

$$P_1 = (14/16) \qquad (3\text{-}73)$$
$$P_2 = (2/16) \qquad (3\text{-}74)$$

Hence Equation 3-72 reduces to

$$P_T = (14/16)(14P_e) + (2/16)(2P_E) \qquad (3\text{-}75)$$
$$= 12{,}25\ P_e + 0{,}25\ P_E$$

ORDER OF MAGNITUDE OF P_T:

To find the order of magnitude of P_T for the actual system, it is first necessary to evaluate the integral in Equation 3-66. This can best be performed numerically.

FOR/

For each of the 16 detectors, the peak-signal-to-rms-noise ratio was a minimum of 200:1.

Hence

$$(A/\sigma)_{min} = 200 \qquad (3\text{-}76)$$

and the limits of integration are B = 0 and B = 100σ

Table 3-5 lists the values of Prob (v > B/2) for various values of v. Using Simpson's Rule for numerical integration, P_E' can be found to be

$$P_E' = 4{,}0 \times 10^{-3} \qquad (3\text{-}77)$$

Graph 3-6 shows that

$$A/\sigma = 20 \Longrightarrow P_e = 7{,}6 \times 10^{-24}$$

and

$$A/\sigma = 22 \Longrightarrow P_e = 1{,}9 \times 10^{-28}$$

Hence for $A/\sigma = 200$, P_e will be negligibly small and can be regarded as zero.

Hence

$$\begin{aligned} P_E &= (2/3)P_e + (1/3)P_E' \\ &\simeq (1/3)P_E' \\ &= 1{,}3 \times 10^{-3} \end{aligned} \qquad (3\text{-}78)$$

while the probability of an error occurring in any of the 16 detectors is given by Equation 3-75 as

$$\begin{aligned} P_T &= 12{,}25\ P_e + 0{,}25\ P_E \\ &\simeq 0{,}25\ P_E \\ &= 3{,}3 \times 10^{-4} \end{aligned} \qquad (3\text{-}79)$$

The fact that P_T is very large in comparison to P_e should not be viewed in too serious a light, since P_T receives the major contribution to its magnitude when the edge of the shadow is close to the centre of a detector. Under such cirum=stances that detector has "every right" to register either a "0"

OR/

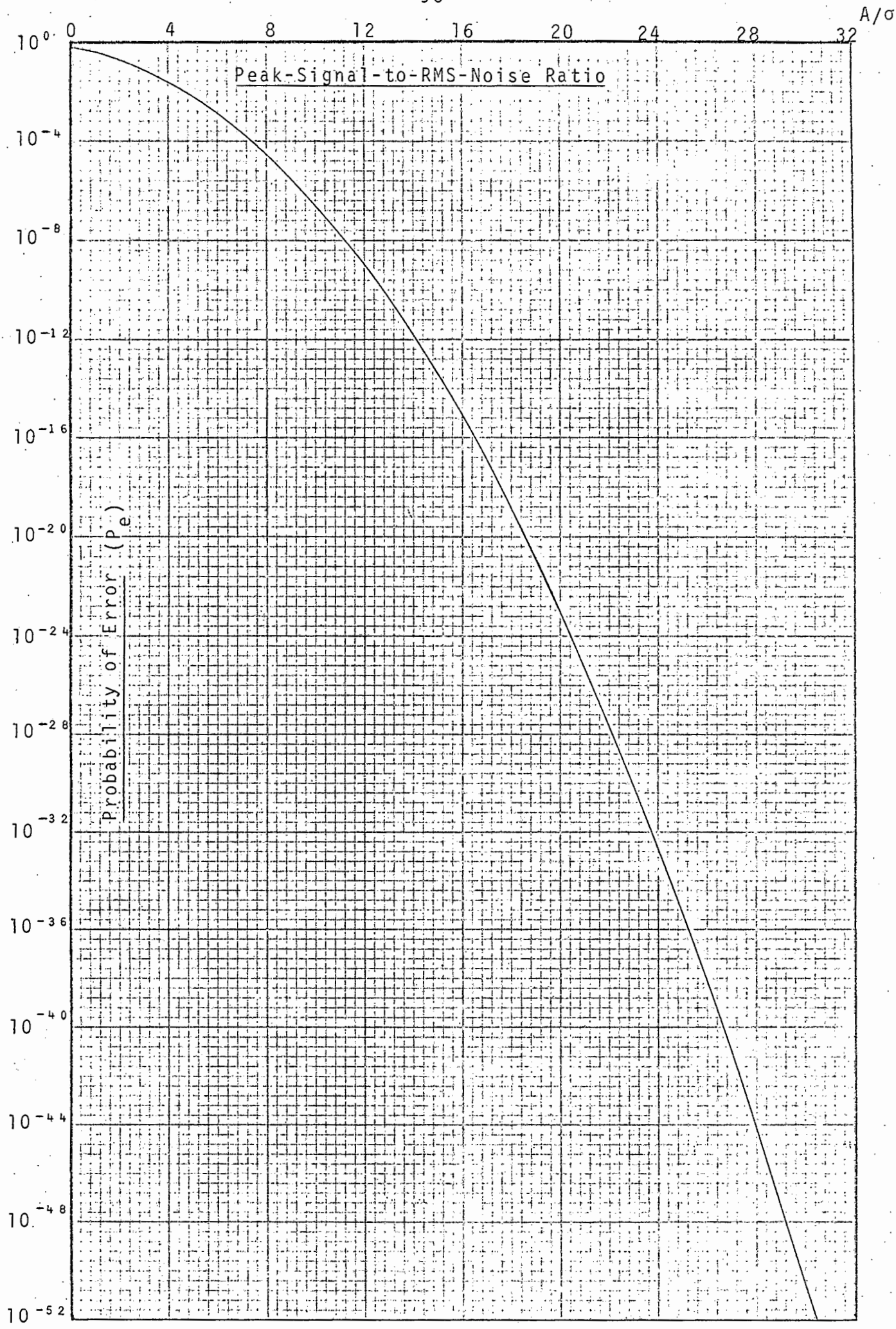

Graph 3-6: Probability of Error in Detection of Binary Signals in Gaussian Noise.

or a "1", since it will be at the limits of its resolving capa= bilities.

Table 3-5

B/σ	Prob ($v > B/2$)
0	$5{,}0 \times 10^{1}$
1	$3{,}1 \times 10^{1}$
2	$1{,}6 \times 10^{1}$
3	$6{,}7 \times 10^{2}$
4	$2{,}3 \times 10^{2}$
5	$6{,}2 \times 10^{3}$
6	$1{,}4 \times 10^{3}$
7	$2{,}3 \times 10^{4}$
8	$3{,}2 \times 10^{5}$
9	$3{,}4 \times 10^{6}$
10	$2{,}9 \times 10^{7}$
11	$1{,}9 \times 10^{8}$
12	$9{,}9 \times 10^{10}$
13	0
14	0
⋮	⋮
100	0

(b) Non-Synchronous Detection.

In this case, the same analysis can be applied as before up to Equation 3-54, which states

$$P_e = \tfrac{1}{2}\left(1 - \operatorname{erf}\frac{A}{2\sqrt{2}\sigma}\right)$$

Translated into words this means that Gaussian electrical noise of σ volts rms has a probability P_e of exceeding a voltage A/2.

Unlike the previous case however, where this equation was only applied for an instant in time when the received pulse was

MAXIMUM/

maximum, it now applies continuously, so more errors can be expected than before. Clearly too, the number of errors will somehow be related to the system bandwidth.

Let the bandwidth of the detector circuit therefore be B. Then let

$\tau = (1/B)$ = minimum possible time between two successive noise peaks at the output of the detector circuit, and

T = average time between noise peaks that exceed the critical voltage A/2.

See Fig 3-18.

Clearly the probability of any individual noise peak exceeding the critical voltage is simply

$$P_e = (\tau/T) \tag{3-80}$$

Hence an error can be expected to occur every T seconds, where

$$T = (\tau/P_e) = (1/BP_e) \tag{3-81}$$

The following experiment was then performed to check the validity of Equation 3-81.

A pseudo-random Gaussian noise generator was connected via a filter to a comparator. Each time the noise voltage exceeded the trigger voltage of the comparator (the output of which was being monitored by a digital counter), this would be registered by the counter. A stopwatch was used to record the time of each run. See Fig 3-19.

Note:- The noise generator was pseudo-random in that it generated a repetitive sequence of noise. This did not affect matters for trigger voltages close to the rms noise voltage σ, but led to poor correlation for larger trigger voltages.

This is because if a large noise spike was present in the sequence, it would be registered every time the sequence was repeated. However if no spike in the sequence was large enough, the comparator would never trigger.

The results can be seen in Table 3-6, where the following

SYMBOLS/

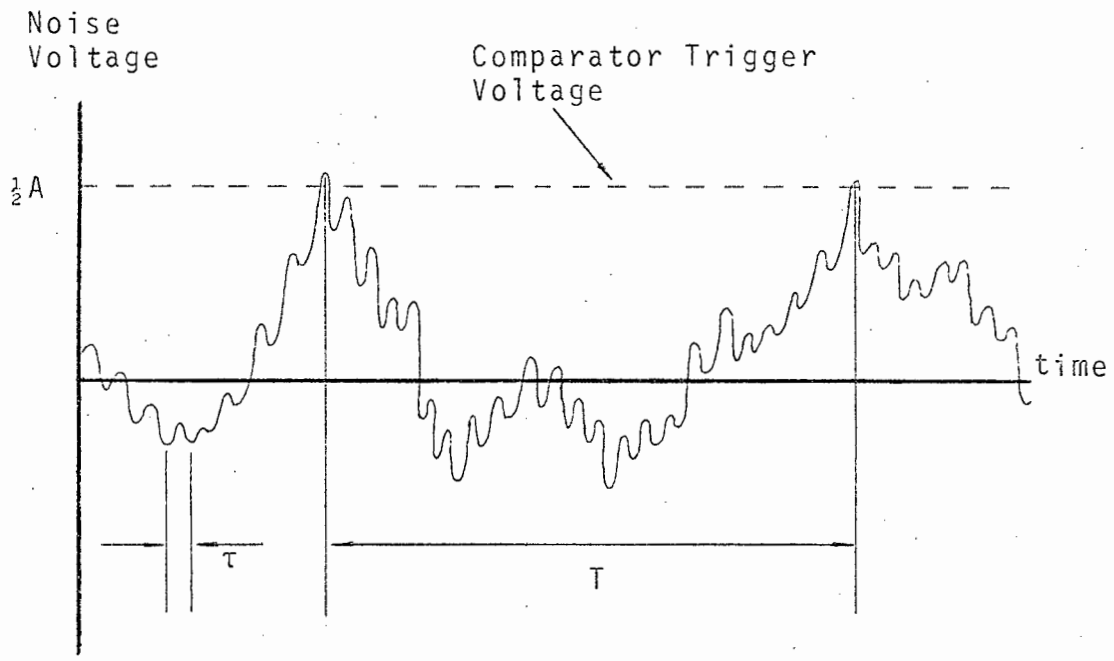

Fig 3-18: Random Noise Voltage Appearing at Output of Detector Circuit of Bandwidth B = (1/τ).

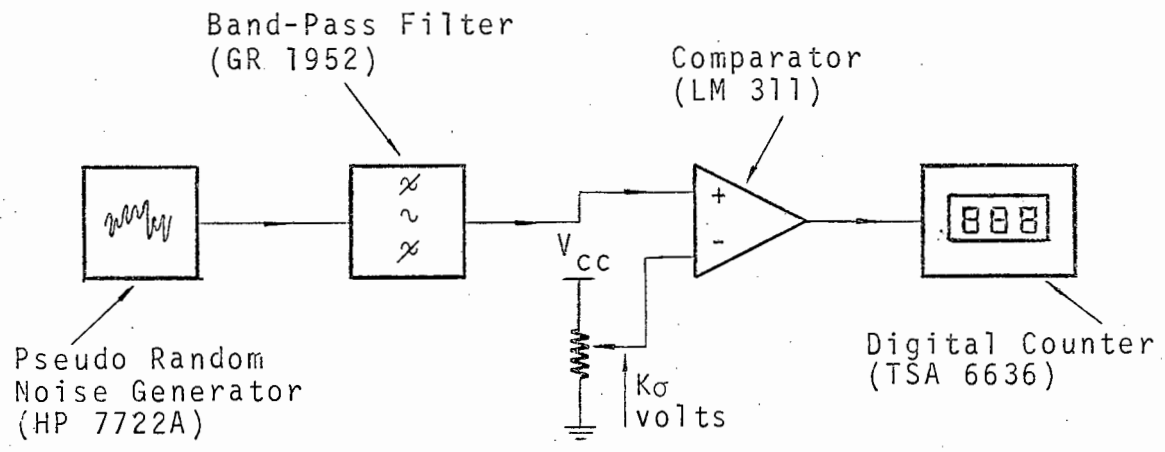

Fig 3-19: Apparatus for Verification of Noise Statistics for Non-Synchronous Pulse Detection.

symbols apply.

K = ratio of trigger voltage of comparator to rms noise voltage σ.

P_e = theoretical probability that the noise voltage exceeds $K\sigma$ volts.

f_L = lower limit of filter bandwidth

f_u = upper limit of filter bandwidth

N = number of pulses registered by digital counter per run

t = length of run in seconds

T_E = average time interval between noise peaks exceeding $K\sigma$ volts obtained by experiment.

T_T = average time interval between noise peaks exceeding $K\sigma$ volts predicted by theory.

TABLE 3-6

K	f_L (Hz)	f_u (Hz)	P_e	t (sec)	N (Pulses)	T_E (ms)	T_T (ms)
1,25	30	3K	$1,1 \times 10^{-1}$	30	20654	1,5	3,0
1,43	300	3K	$7,6 \times 10^{-2}$	30	20029	1,5	4,4
1,67	0	1K	$4,7 \times 10^{-2}$	60	3301	18,0	21,0
2,17	0	5K	$1,5 \times 10^{-2}$	58	4399	13,0	13,0
2,50	30	3K	$6,5 \times 10^{-3}$	30	1006	30,0	51,0
2,50	30	3K	$6,5 \times 10^{-3}$	60	2627	23,0	51,0
2,70	0	2K	$3,4 \times 10^{-3}$	120	3934	30,0	147,0
2,70	300	3K	$3,4 \times 10^{-3}$	100	1016	9,8	98,0
2,86	300	3K	$2,1 \times 10^{-3}$	60	2435	25,0	159,0
3,33	0	1K	$4,3 \times 10^{-4}$	60	1326	45,0	2326,0
3,75	30	3K	$8,8 \times 10^{-5}$	30	219	140,0	3787,0
4,00	300	3K	$3,2 \times 10^{-5}$	200	0	∞	10470,0

As can be seen the results correlate acceptably for $K < 2,5$, but thereafter they differ by orders of magnitude. This can also be attributed to the fact that the response of the noise generator was not flat over its various frequency ranges. Rather, the pseudo-random nature of its output is the

DOMINANT/

dominant factor. It seems reasonable therefore to assume that the theory has been vindicated.

Returning to the problem, it remains merely to calculate the minimum acceptable signal to noise ratio. In practice 1 error in 10^5 is often used as a design standard for binary communication.[7c]

Assuming then, that the main LED on the pantograph shoe is pulsed once every 700 μs, and that about 10 detectors will be in shadow each time, the number of bits that must be transmitted down to ground per second is about $1,4 \times 10^4$.

The minimum allowable time between error pulses is then

$$T = (1,4 \times 10^4 \times 10^{-5})^{-1} \simeq 7 \text{ seconds} \qquad (3\text{-}82)$$

Assuming the bandwidth of the system to be about 40 KHz, and using Equation (3-81)

$$P_e = (1/TB) = 3,6 \times 10^{-6} \qquad (3\text{-}83)$$

From Graph 3-6

$$P_e = 3,6 \times 10^{-6} \Longrightarrow (A/\sigma) \simeq 9,0 \qquad (3\text{-}84)$$

(Note that the same criterion applied to synchronous detection gives $A/\sigma \simeq 8,2$. The difference in P_e becomes more marked at lower signal-to-noise ratios.)

REFERENCES

1. "Solid State Lamp Manual - Theory, Characteristics and Applications", General Electric Miniature Lamp Department. (3-8270). p 29

2. Information on LED's obtained from:
   Monsanto Directory of GaAsLite Products (Type ME 7121)
   Texas Data Book (Type TIXL 27)
   RCA Data Book (Types RCA 40856 and 40857)

3. Information on Photodetectors obtained from:
   Motorolla Data Book (Type MRD 100)
   Fairchild Data Book (Type FPT 100A)
   Monsanto Directory of GaAsLite Products (Type MD 2)
   Hewlett Packard Data Book (HP 5082 - 4200 Series)
   Electronics Today International, (Oct 1972): "Operating Characteristics of Light-Sensitive Devices".

4. "The Facts of Light", I.P.L. Information Sheet, No 201, July 1971.

5. FRANCIS A. JENKINS and HARVEY E. WHITE: "Fundamentals of Optics", Second Edition, pp 127 - 136.

6. TOBEY, GRAEME and HUELSMAN: "Operational Amplifiers - Design and Applications", Burr-Brown, p 286.

7. MISCHA SCHWARTZ: "Information Transmission, Modulation and Noise", McGraw-Hill, Kogakusha.
   (a) p 330
   (b) p 612
   (c) p 335

CHAPTER 4

ELECTRICAL DESIGN DETAIL

A block diagram of the system is shown in Fig 4-0.

The Master block controls the timing of the entire system. It activates the LED via the LED Pulsing Circuit, and then strobes the outputs of the receiving opto-amplifiers for optimum signal extraction. Once the information from the 16 receivers has been fed into the shift registers (parallel input), it activates the slave clock which serially clocks the information down to ground via the isolatory light-guide. It then waits until the information has been processed and recorded before repeating the whole process about 0,7 ms later.

On the ground the pulses are detected, amplified, and fed into a serial counter. From there the information is decoded and then fed into a pen recorder. (A visual numerical display facility is also provided.) The serial counter is then reset to zero to await the next train of pulses.

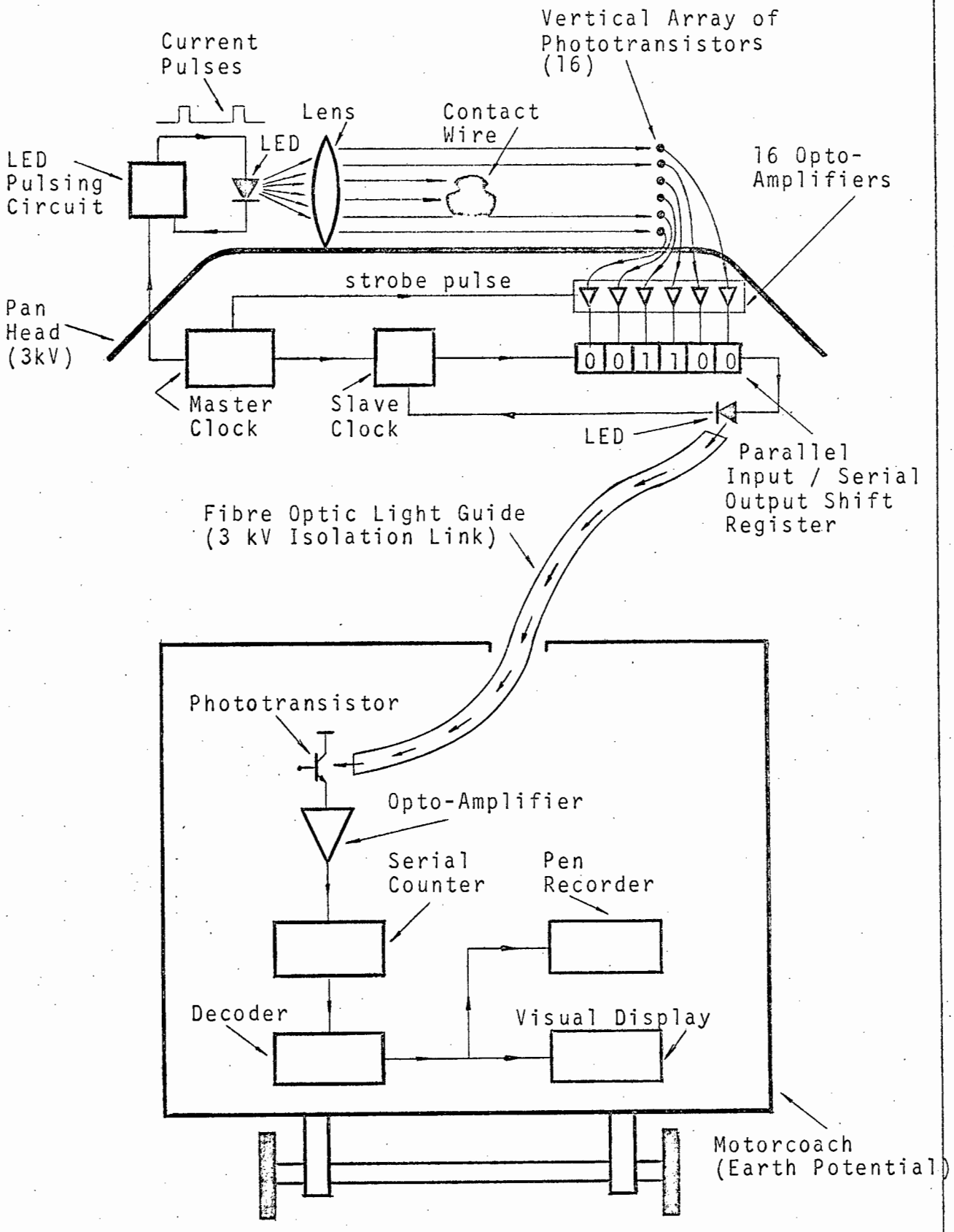

Fig 4-0: Block Diagram of Contact Wire Wear Measurement System.

4-10 DESIGN OF LED PULSING CIRCUIT

The objective is to design a circuit that will convert voltage pulses to current pulses for exciting the LED. The current pulses should be as large as possible to achieve maximum signal-to-noise ratio at the detector but not so large as to damage the LED an any way.

Several different circuits were considered before settling on the one described in Fig 4-1. (Brief descriptions of the others can be found in Appendix III-1). Its principle of operation is as follows.

When the input voltage, V_{in} is high, the circuit is in its "off" state. Transistors T_2 and T_4 are turned off, but T_1 is hard on, forcing T_3 to generate a constant current into capacitor C_2. The voltage across C_2 then increases linearly with time until the collector voltage of T_3 equals its emitter voltage, after which the current entering through R_{10} escapes across the forward biased P-N collector-base junction. This ensures that T_5 and T_6 are kept off, so no current passes through the LED.

When the input voltage drops to zero, T_1 is suddenly turned off, and hence T_3 is too. T_2 however, is turned on, forcing T_4 to extract a constant current from capacitor C_2. The voltage across C_2 therefore starts decreasing linearly with time, turning T_5 and T_6 harder and harder on, until it reaches a value dic= tated by the zener diode. At this stage the current passing through T_6, and hence through the LED, is at its maximum, and remains constant until the input voltage again goes high. It then decreases to zero as described before and awaits the next negative pulse at the input.

If for some reason the input becomes shorted to ground, for instance during testing or because of some electrical failure, the large current through the LED will not continue flowing indefinitely, but will be turned off automatically. This is brought about by capacitor C_1 charging up via R_2 and the parallel combination of R_3 and the emitter-base junction of T_2, until T_2 is switched off. T_4 then also turns off, and the capacitor C_1 is charged up via R_2 , (since T_3 would also be off). When the

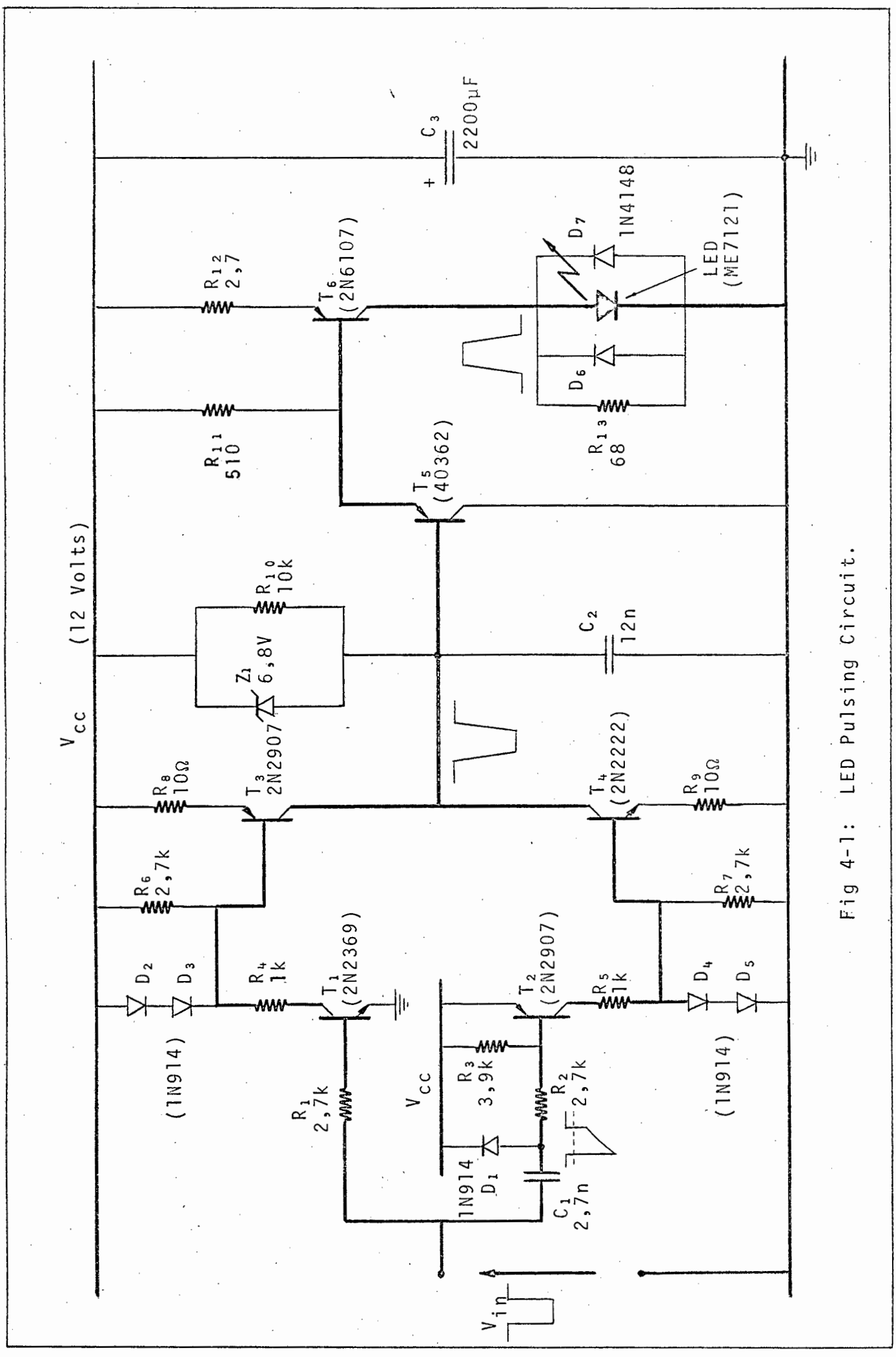

Fig 4-1: LED Pulsing Circuit.

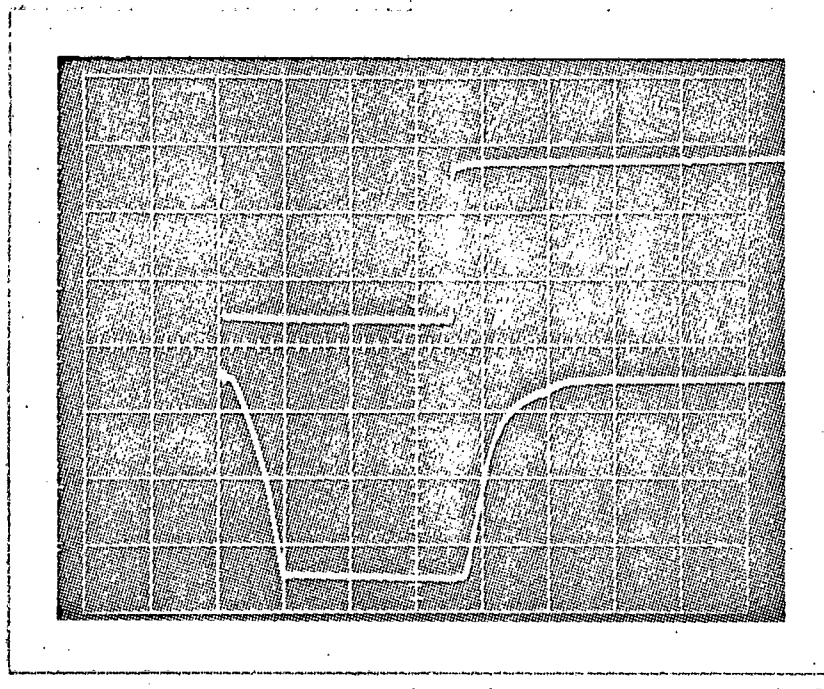

Top Trace: TTL Input Pulse Applied to LED Pulsing Circuit. (LP of Fig 4-5 & Fig 4-6)

Bottom Trace: Voltage Across 6,8 Volt Zener Diode (Z_1) of LED Pulsing Circuit.

(Time Scale: 2 μs/div.)

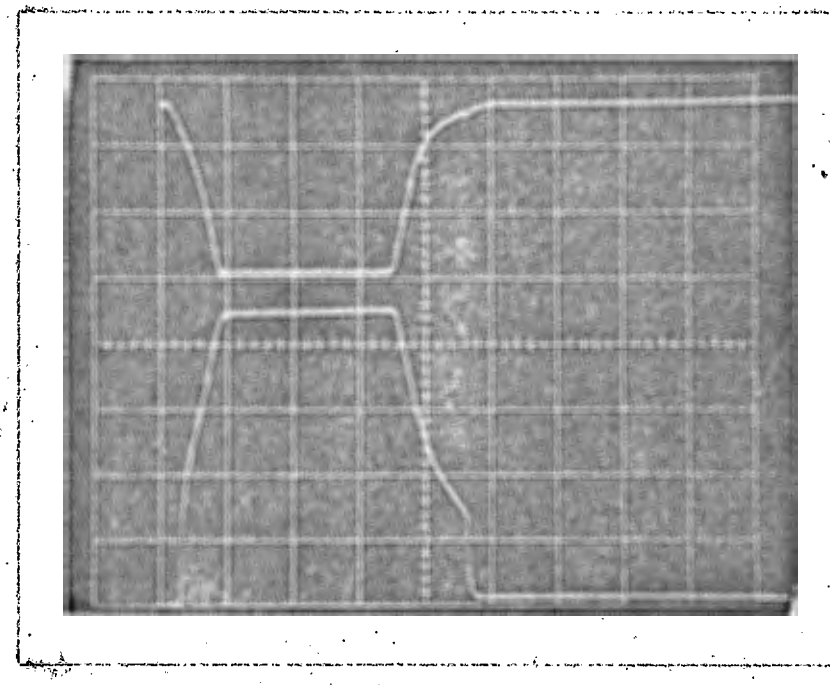

Top Trace: Voltage Across 6,8 Volt Zener Diode (Z_1) of LED Pulsing Circuit.

Bottom Trace: Voltage Across LED. (Scale: 1 V/div.)

(Time Scale: 2 μs/div.)

voltage across it becomes large enough, T_5 and T_6 turn off, hence protecting the LED from destruction.

The inclusion of capacitor C_2 is to ensure that the current through the LED increases and decreases slowly. This prevents large voltage spikes from occurring across it, especially in the reverse direction. (From the specifications the reverse voltage across the LED used should not exceed 3 volts). Provided the leads joining the LED to the collector of T_6 and to ground are kept short however, and the reverse voltage is not allowed to exceed 0,7 volts by the inclusion of diodes D_6 and D_7, the advantages of using C_2 are small.

Originally the pulsing circuit was situated about 0,3 metres away from the LED, so interconnecting wires had to be used.* At this stage the pulsing transistors were operating at their maximum possible speed too, which proved disastrous for the LED; until it was discovered that using a trapezoidal pulse rather than a square one provided a certain measure of safety.

It was therefore decided to mount the circuit shown in Fig 4-1 within a few cm of the LED, and to mount transistor T_6 right next to it. This solved the problem.

The circuit was tested without C_2, and it was discovered that there was a noticeable increase in the size of the voltage spike in the forward direction only. This in itself is not really serious, but it was decided to retain the integrator in the circuit as an added safety feature. Clearly it is undesirable to be forever replacing the LED, and since only one light pulsing circuit is required, it would not be inexpedient to use extra safety features.

The transistors used are listed in Table 4-1 together with some of their ratings and characteristics. For the sake of reliability they were chosen so that their maximum ratings were well above the values at which they were to operate.

Detailed Analysis of LED Pulsing Circuit.

Accumulators will be used to power the device. The supply voltage of the circuit, V_{CC} was therefore set at 12 volts, this being a standard value of accumulator voltage.

* Appendix III-1.

THE INPUT/

The input voltage pulse, V_{in}, comes from a TTL output, so when high, it will be at about 3,5 volts, and when low, at about 0,2 volts.

TABLE 4-1			P_c	I_c	V_{cbo}	h_{fe}	f_t
Transistor	Type	Polarity	Watts	Amps	Volts		MHz
T_1	2N2369	NPN	0,36	0,2	40	40	500
T_2 γ T_3	2N2907	PNP	0,4	0,6	40	100	200
T_4	2N2222	NPN	0,5	0,8	30	35	250
T_5	40362	PNP	5,0	0,7	70	35	100
T_6	2N6107	PNP	40,0	7,0	80	30	4

(a) Transistor T_1.

I_c required ≃ 10 mA (<< 200 mA)

$$\text{Hence} \quad R_4 = \frac{V_{cc} - V_{D3} - V_{CE(sat)} - V_{D2}}{I_c} \qquad (4\text{-}1)$$

$$= \frac{(12 - 0,7 - 0,7 - 0,2)V}{10\ mA}$$

$$\simeq 1\ k\Omega$$

I_b required > (I_c/h_{fe}) = 0,25 mA

$$\text{Hence} \quad R_1 < \frac{V_{in} - V_{BE}}{I_b} \qquad (4\text{-}2)$$

$$< \frac{(3,5 - 0,7)V}{0,25\ mA}$$

$$< 11,2\ k\Omega$$

Say R_1 = 2,7 kΩ

(b) Transistor T_2.

I_c required ≃ 10 mA (<< 600 mA)

Hence R_5 = 1 kΩ (as for T_1)

I_{b2}/

$$I_{b2}\ (\text{required}) > \frac{I_{c2}}{h_{fe}} = 0{,}1\ \text{mA}$$

Since the voltage across a capacitor cannot change instantaneously, when the input voltage drops suddenly, the voltage on the right hand side of C_1 must fall an equal amount. However it will immediately start charging up again via R_2.

Under normal circumstances, the input pulse will remain low for 7 µs. At the end of this time T_2 must still be getting enough base current to ensure saturation. Also, in the event of the input pulse remaining low for longer than 7 µs, the decay of C_1 must cause T_2 to switch off within about 5 times the normal pulse duration.

Hence choosing a decay ratio of 1/3 over the pulse duration as being a convenient value, the initial base current of T_2 must be at least 3 times its limiting saturation requirement.

R_2 may then be calculated as follows:

$$R_2 < (-V_{BE} - V_{in})\left(\frac{1}{3I_b}\right) \qquad (4\text{-}3)$$

$$< \frac{(-0{,}7 + 3{,}5)\text{V}}{3(0{,}1\ \text{mA})}$$

$$< 9{,}3\ \text{k}\Omega$$

$$\text{Say } R_2 = 2{,}7\ \text{k}\Omega$$

(This ensures saturation over the pulse duration with a factor of safety of about 3. The increased base current is well within the transistor limitations.)

C_1 can now be calculated from

$$V_{R5}(7\ \mu\text{s}) = V_{R5}(0\ \mu\text{s})e^{-(t/R_2C_1)} \qquad (4\text{-}4)$$

$$1/3 = e^{-\left(\frac{7 \times 10^{-6}}{2700\ C_1}\right)}$$

$$C_1 = 2{,}36 \times 10^{-9}\text{F}$$

$$\text{Say } C_1 = 2\ 700\ \text{PF}$$

The resistance R_3 will play little part in the proceedings

UNTIL/

until the base voltage of T_2 rises above its turn-off value, since until then R_2 will be fed from a constant voltage source.
At the instant of cut-off, V_{R2} can be obtained from

$$\left(\frac{R_3}{(R_2 + R_3)}\right)(V_{BE(on)} + V_{R2}) = V_{R3} \qquad (4\text{-}5)$$

Since after 7 µs the voltage across R_2 will have dropped from 3,5 volts to 0,9 volts, this new value of V_{R2} should be chosen to be say 0,5 volts to ensure it is reached only after 7 µs have passed.
This gives

$$R_3(0{,}7V + 0{,}5V) = (2{,}7\ k\Omega + R_3)(0{,}7\ V)$$

$$R_3 = 3{,}8\ k\Omega$$

$$\text{say } R_3 = 3{,}9\ k\Omega$$

The effect of R_3 will therefore only be felt in the event of V_{in} remaining low and endangering the LED, when it will ensure that C_1 charges right up to the positive voltage rail, keeping T_2 "hard off".

The time taken for T_2 to switch off in this event can be calculated from

$$V_{R2}(t_1) = V_{R2}(0)e^{\left(\frac{-t_1}{R_2C_1}\right)} \qquad (4\text{-}6)$$

$$\ln\frac{(0{,}5V)}{(2{,}8V)} = \frac{-t_1}{(2{,}7\ k\Omega)(2{,}7\ nF)}$$

$$t_1 = 13\ \mu s$$

The function of the diode D_1 is to ensure that each time the input voltage goes high, the right hand terminal of C_1 is prevented from rising more than 0,7 volts above the positive rail. As well as immediately re-setting the network for the next pulse, it also protects the base-emitter junction of T_2 from having a reverse bias of greater than 0,7 volts applied to it.

WITH/

With regard to diodes D_1, D_2, D_3, D_4 and D_5 any low powered silicon switching diodes will suffice provided they are capable of handling at least 10 mA continuously. In this case, the type IN914 was used, which has a maximum continuous current rating of 75 mA.

(c) Transistors T_3 and T_4:

As has already been explained, the constant current generators T_3 and T_4 are included to ensure that the LED's current pulse does not turn on or off too fast, causing large reverse voltages across it. Since the signal pulse lasts only for about 10 µs, the integrating capacitor C_2 should be chosen to ensure rise and fall times of between 1 and 2 µs, which is some orders of magnitude slower than the 10 ns response time of a TTL gate.

Choosing R_8 and R_9 both to be 10Ω sets the collector currents of T_3 and T_4 at

$$I_c = \frac{V_{D1} + V_{D2} - V_{BE}}{R_e} \qquad (4\text{-}7)$$

$$= \frac{0,7V}{0,01\ k\Omega}$$

$$= 70\ mA \quad (<<\ 600\ mA \text{ or } 800\ mA)$$

Using the minimum rated value of h_{fe} for the two transistors sets the maximum required base current at

$$I_b = \frac{I_c}{h_{fe}} = \frac{70\ mA}{35} \qquad (4\text{-}8)$$

$$= 2\ mA$$

This is small enough to be absorbed by the collector current of T_1 and T_2 without affecting the voltage across the diodes D_2 and D_3 or D_4 and D_5.

Resistors R_6 and R_7 are included to tie the base connections of T_3 and T_4 to ground. This is a protective measure to guard against the leakage currents which exist in semiconductor devices. Under certain conditions these currents might otherwise become large enough to provide enough base current to transistors T_3 and T_4 to momentarily turn them on.

It is merely necessary to ensure that the currents through

R_6 and R_7 under operating conditions are less than 10% of the collector currents of T_1 or T_2.

Hence

$$I_{R6} < \frac{I_{R4}}{10} = 1 \text{ mA}$$

$$R_6 > \frac{V_{D2} + V_{D3}}{I_{R6}} \qquad (4\text{-}9)$$

$$> \frac{1,4 \text{ V}}{1 \text{ mA}}$$

$$> 1,4 \text{ k}\Omega$$

Say $R_6 = 2,7 \text{ k}\Omega$

Then $R_7 = 2,7 \text{ k}\Omega$ (by the symmetry of the situation)

While T_4 is in the off state, the voltage at the positive terminal of C_2, is approximately V_{cc}. When T_4 turns on, charge is extracted from C_2, causing this voltage to drop until the breakdown voltage of the Zener diode Z_1 is reached. The amplitude of the trapezoidal voltage across C_2 is hence equal to the Zener breakdown voltage.

If this is set at 6,8 volts to allow a reasonable voltage across R_{12}, then C_2 can be calculated as follows.

$$C_2 = \frac{It}{V_{Z1}} \qquad (4\text{-}10)$$

(Where I is the constant current from either T_3 or T_4.

Hence

$$C_2 = \frac{(70 \text{ mA})(1 \text{ µs})}{(6,8 \text{ V})}$$

$$= 1,03 \times 10^{-8} \text{F}$$

Say $C_2 = 12\,000 \text{ pF}$

The peak power dissipation of Z_1 is then

$$P_{peak} = V_{Z1} I_{C4} = 0,48 \text{ watts} \qquad (4\text{-}11)$$

Since this is only for 1% of the time, the average Zener dissipation is 4,8 mW, which is negligible.

R_{10} FULFILLS/

R_{10} fulfills a similar function to R_6 and R_7 — that of providing a leakage current path to ground. Its main purpose however is to ensure that C_2 charges up to the positive rail in the event of the drive voltage staying low, and hence saving the LED from destruction.

Its contribution of current to C_2 must be small in comparison to I_{C4}. This condition is fulfilled if it is of the order of a mA.

$$\text{Hence} \quad R_{10} > \frac{V_{Z1}}{I_{R10}} \qquad (4\text{-}12)$$

$$> \frac{6{,}8\ V}{1\ mA}$$

$$> 6{,}8\ k\Omega$$

$$\text{Say} \quad R_{10} = 10\ k\Omega$$

The total time it will take for C_2 to charge up and turn off T_5 can only be calculated once R_{11} and R_{12} have been determined.

(d) Transistors T_5 and T_6:

In the design of the components surrounding these transistors, it is first necessary to determine the LED to be used together with its characteristics.

The ME 7121 was eventually chosen, being the only cheap, locally available one which had a quantum efficiency as high as 4,5%. Its chief competitor, the TIXL 27 (which was not locally available), has recently been discontinued; and superior types such as the TIXL 12, cost about 50 times as much and are also not locally available. Other locally available LED's have quantum efficiencies seldom exceeding 1%, and are not rated at such high currents as the one chosen.

A disadvantage of the ME 7121 however, is that its emitting junction is encased behind a directional clear plastic lens which gives a total beam spread of 30^{o} between half-power points. This problem was overcome by filing the lens down with fine water paper (a not-too-delicate operation), and then polishing it with an abrasive mixture (Brasso), to restore its light transmission properties.

THE RESULT/

The result was that it radiated over a much larger solid angle, and hence uniformly over the lens surface, so that a parallel beam of uniform intensity could be obtained.

The phototransistor chosen was the FPT 100A, which has rated rise and fall times of typically 2,8 µs. Since the pulse repetition rate of the LED has already been decided at about once every 0,7 ms, a 1% duty cycle would require a pulse width of 7 µs, which is within its capabilities.

From the specifications of the ME7121,

Maximum continuous power rating	P_{av}	= 150 mW
Hence theoretical instantaneous power capability at 1% duty cycle	P_{peak}	= 15 W
Junction forward voltage	V_j	≃ 1,3 V
Dynamic resistance	R_D	≃ 2 Ω

Since the ME7121 is housed in a plastic case, its heat sinking qualities are not very encouraging, so an arbitrary 50% safety factor was used.

Hence

$$\tfrac{1}{2}P_{peak} = IV_j + I^2R_D \qquad (4\text{-}13)$$

$$7{,}5\ W = 1{,}3\ I + 2\ I^2$$

$$I = 1{,}6 \text{ amps or } -2{,}3 \text{ amps.}$$

where I is the current through the LED. Since current cannot flow through the LED in the reverse direction, the only acceptable solution is I_{peak} = 1,6 amps.

(This gives an average power dissipation of 75 mW, which is reasonable considering that the device has an absolute maximum current rating of 6 amps, giving a peak power of 80 watts. This however is at a 0,1% duty cycle, with 1 µs pulses, giving an average dissipation of 80 mW.)

R_{13} provides a path to ground for the charge that builds up on the LED's junction capacitance with each pulse. A process of trial and error showed that R_{13} = 68Ω was a reasonable choice.

The total collector current of T_6 can now be determined.

$$V_{LED} = V_j + I_{LED}R_D \quad (4\text{-}14)$$
$$= 1{,}3V + (1{,}6\ A)(2\ \Omega)$$
$$= 4{,}5 \text{ volts.}$$

Hence $$I_{R_{13}} = \frac{V_{LED}}{R_{13}} \simeq 0{,}1 \text{ amp.} \quad (4\text{-}15)$$

Hence $$I_{C6} = I_{LED} + I_{R_{13}} = 1{,}7 \text{ amps} \quad (4\text{-}16)$$

The emitter resistance of T_6,T_{12} can now be determined.

$$R_{12} = \frac{V_{Z1} - V_{BE5} - V_{be6}}{I_{C6}} \quad (4\text{-}17)$$
$$= \frac{(6{,}8 - 0{,}7 - 1{,}0)V}{1{,}7A}$$
$$= 3\ \Omega$$

Say $$R_{12} = 2{,}7\ \Omega$$

Finally R_{11}, the resistance tying the base of T_6 to the positive rail, can be determined. (It fulfills the same protec= tive function as R_6, R_7 and R_{10}.) Its contribution to the emitter current of T_5 is not critical provided the transistor is running well within its limits. A value of $I_{R_{11}}$ of 20% of the base current of T_6 is a reasonable choice.
Hence

$$I_{R_{11}} = \frac{V_{Z1} - V_{BE5}}{R_{11}} < \frac{I_{C6}}{(5)(h_{fe})} \quad (4\text{-}18)$$
$$\therefore \quad R_{11} > \frac{(5)(6{,}8\ V - 0{,}7\ V)(30)}{(1{,}9\ A)}$$
$$> 480\ \Omega$$
Say $$R_{11} = 510\ \Omega$$

The collector current of T_5 can now be calculated

$$I_{C5} = I_{R_{11}} + \frac{I_{C6}}{h_{fe}} \quad (4\text{-}19)$$
$$= \frac{(6{,}8 - 0{,}7)V}{510\ \Omega} + \frac{(1{,}9\ A)}{30}$$
$$= 0{,}075\ A$$
$$= 75\ mA \quad (<< 700\ mA)$$

THIS/

This is well within the limitations of the transistor.

Regarding D_6 and D_7, there should be very fast switching diodes capable of suppressing any reverse voltage spikes across the LED. In practice type IN4148 diodes were used. They are rated at 400 mA continuous, have a p.i.v. of 75 volts and have a switching time of 4 ns.

To allow for a failure, two of these were placed in parallel across the LED. Their leads were also cut as short as possible to limit their inductance.

It is now possible to calculate the total time C_2 will take to charge up after T_2 and T_4 have been turned off by C_1.

For this it is necessary to determine the base current of T_5.

$$I_{b5} = \frac{I_{C5}}{h_{fe5}} = \frac{75\ mA}{35} = 2,1\ mA \qquad (4\text{-}20)$$

The total charging current of C_2 will then be

$$\begin{aligned} I_{cap2} &= I_{R10} + I_{b5} \qquad (4\text{-}21) \\ &= 2,1\ mA + 0,68\ mA \\ &\simeq 2,8\ mA \end{aligned}$$

Since the impedance "seen" looking into the base of T_5 is resis= tive in nature, the total charging current of C_2 can be thought of as coming from an equivalent resistance of magnitude

$$R_{eq} = \frac{V_{Z1}}{I_{cap2}} = \frac{6,8\ V}{2,8\ mA} = 2,4\ k\Omega \qquad (4\text{-}22)$$

The LED current will turn off once the base voltage of T_5 is within 1,5 volts of V_{cc}.

Hence a reasonable estimate of the time it will take for T_5 to switch off is,

$$V_{off} = V_{Z1} e^{-\left(\frac{t_2}{R_{eq} C_2}\right)} \qquad (4\text{-}23)$$

SO t_2/

so $$t_2 = R_{eq}C_2 \ln\frac{(V_{Z1})}{(V_{off})} \quad (4\text{-}24)$$

$$= (2\ 400\ \Omega)(12 \times 10^{-9}F)\ln\frac{(6{,}8\ V)}{(1{,}5\ V)}$$

$$\simeq 44\ \mu s.$$

The LED current will therefore only flow for about 51 μs longer than it would under normal conditions. Its total "on-time" will be

$$T = t_1 + t_2 \quad (4\text{-}25)$$

$$= (13 + 44)\mu s$$

$$= 57\ \mu s.$$

which is far less than that required to destroy it - especially since the current would be decaying exponentially over this period.

It now remains only to determine the value of the power supply decoupling capacitor, C_3. This is an essential component considering that the accumulator will have to be mounted on the base of the pantograph frame, and that the large current pulses will therefore have to be carried by long inductive wires.

A 2200μF, 16 volt electrolytic capacitor was used, since it had the largest capacity-to-physical size ratio that could be found locally. This proved quite adequate for the task. Hence

$$C_3 = 2\ 200\ \mu F.$$

A 10 μF, 16 volt Tantulam Capacitor was placed in parallel with it to cater for the high frequencies.

(e) Circuit Response Time

When saturation occurs in a transistor, its total rise time for a step input can be written

$$T_R = t_d + t_r \quad (4\text{-}26)$$

where t_d = delay time

t_r = rise time

AND/

and its total fall time can be written

$$T_F = t_s + t_f \qquad (4\text{-}27)$$

where t_s = storage time
t_f = fall time

Since for silicon transistor, t_r, t_f and t_d are usually of the order of a few tens of nanoseconds, while t_s is sometimes of the order of 100 ns, the rise and fall time of the circuit will be determined solely by C_2.

Although the f_t of T_5 and especially that of T_6, is much lower than that of the other transistors, these two are never saturated. Also their bases "look" into low impedances, so they are quite capable of switching at the required frequencies.

4-20 DESIGN OF OPTO-AMPLIFIER CIRCUIT.

In the design of the opto-amplifier or photodetector circuit it is necessary to ensure that:

(i) the amplifying circuitry is ac coupled to the detector to prevent the randomly varying ambient light from affecting the output;

(ii) in the event of the phototransistor ever pointing directly at the sun, the first stage of each amplifier will not saturate;

(iii) the device is match-filtered to the incoming light pulses to achieve a maximum signal-to-noise ratio.

A few different circuits were tried, (see Appendix III-2 and Chapter 4-50) in an attempt to find one that was optimum. The final choice was that shown in Fig 4-3.

The circuit design proceeded as follows.

4-21 Circuit Sensitivity

(a) To infra-red light:-

The phototransistor chosen was the FPT 100A, mainly because of its large sensitivity and its availability. (See Table 3-2). From its specification sheet[1], a radiant intensity of 5,0 mW/cm^2 from a 2 870^{o}K Tungsten source causes a collector current of typically 2,0 mA.

Hence for a Tungsten source, its sensitivity is

$$S_T = 0,4\ mA/(mW/cm^2)$$

Since the radiation from such a source is only about 25% effective on the transistor, while the LED, radiating almost entirely monochromatically at a wavelength near that at which the device sensitivity is maximum is about 80% effective[2], the phototransistor sensitivity to the LED is*

$$S_{LED} = \frac{(0,80)}{(0,25)} S_T = 1,3\ mA/(mW/cm^2) \qquad (4\text{-}28)$$

(b) To Sunlight:-

This is more complicated since the solar radiant energy

* See Graph 3-1.

EXTENDS/

extends from the ultra-violet to well into the infra-red part of the spectrum. If the expression for the solar radiation intensity curve is $P(\lambda)$ $mW^1cm^{-2}nm^{-1}$, and that of the photo= transistor spectral response curve is $R(\lambda)$, (dimensionless), then the effectiveness of the sunlight on the phototransistor will be[†]

$$\text{p.u. Effectiveness} = \frac{\int_{\lambda_0}^{\lambda_1} P(\lambda) \cdot R(\lambda) d\lambda}{\int_0^{\infty} P(\lambda) d\lambda} \qquad (4\text{-}29)$$

A very good approximation for $P(\lambda)$ can be obtained from the Planck Equation for black body radiation at 6 000^oK,[3a] which is

$$P(\lambda) = \frac{C_1 \lambda^{-5}}{e^{C_2/\lambda T} - 1} \; mW^1cm^{-2}nm^{-1} \qquad (4\text{-}30)$$

where C_1 and C_2 are constants, T is the temperature in degrees Kelven, and λ is the wavelength of radiation.

Since no simple expression exists for $r(\lambda)$, it is easier to evaluate Equation 4-29 by graphical means, using Simpson's Rule. With reference to Fig 4-2 this states that the area under a curve is

$$A = \frac{d}{6}(h_1 + 4h_2 + 2h_3 + 4h_4 + \ldots\ldots + 4h_{n-1} + h_n) \qquad (4\text{-}31)$$

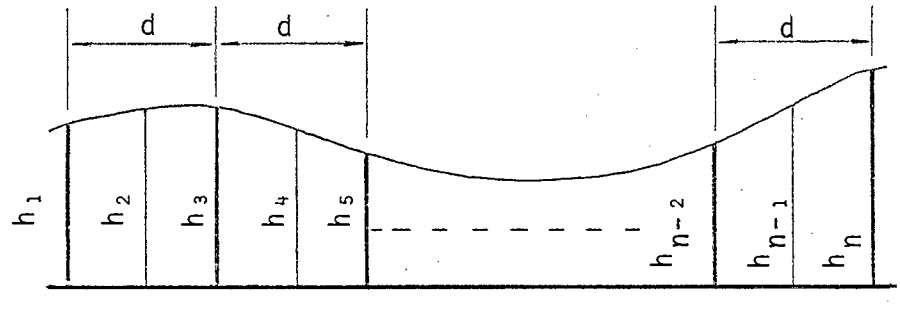

Fig 4-2: Evaluation of Area under a Curve of Simpson's Rule.

[†]See Graph 4-1.

APPLYING/

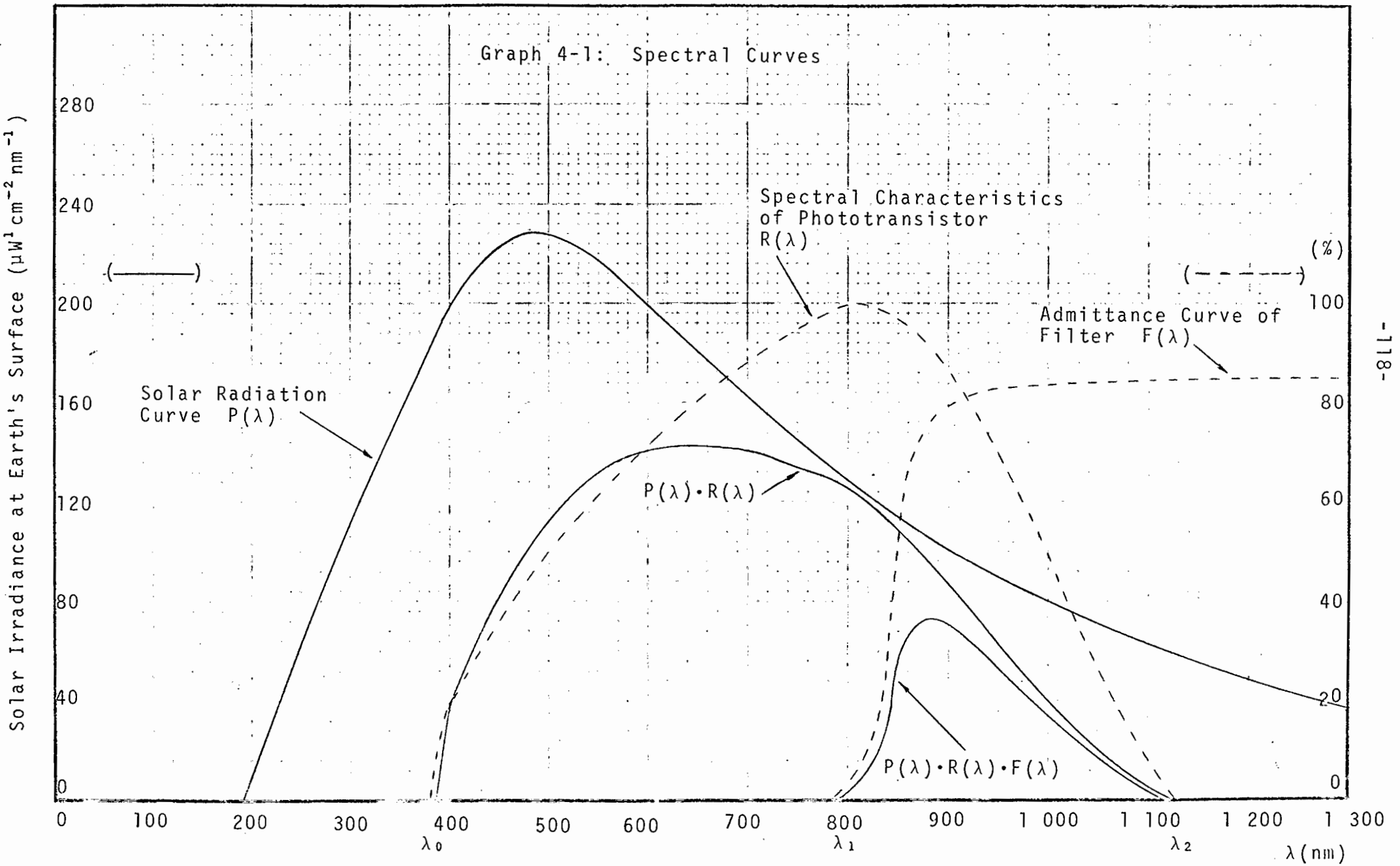
Graph 4-1: Spectral Curves
Solar Irradiance at Earth's Surface ($\mu W^1 cm^{-2} nm^{-1}$)
280
240
200
160
120
80
40
0
(%)
100
80
60
40
20
0
Spectral Characteristics of Phototransistor R(λ)
Admittance Curve of Filter F(λ)
Solar Radiation Curve P(λ)
P(λ)·R(λ)
P(λ)·R(λ)·F(λ)
0
100
200
300
400
500
600
700
800
900
1 000
1 100
1 200
1 300
λ0
λ1
λ2
λ(nm)

Applying Equation 4-31 to the Effective Solar Radiation Curve, and using d intervals of 50 nm between λ_0 = 350 nm and λ_2 = 1 150 nm gives:

$h_1 = 0$	$h_7 = 144$	$h_{13} = 63$
$h_2 = 40$	$h_8 = 142$	$h_{14} = 40$
$h_3 = 82$	$h_9 = 134$	$h_{15} = 20$
$h_4 = 112$	$h_{10} = 126$	$h_{16} = 6$
$h_5 = 132$	$h_{11} = 108$	$h_{17} = 0$
$h_6 = 141$	$h_{12} = 87$	

(all dimensions in $\mu W \cdot cm^{-2} \cdot nm^{-1}$)

Hence

$$A = \int_{\lambda_1}^{\lambda_2} P(\lambda) \cdot R(\lambda) d\lambda \qquad (4\text{-}32)$$

$$= \frac{(50)(4\ 142)}{6}$$

$$= 34\ 500\ \mu W/cm^2$$

$$= 34{,}5\ mW/cm^2.$$

It is unnecessary to evaluate $\int_0^{\infty} P(\lambda) d\lambda$ since this is the solar constant, or average solar radiant intensity reaching the earth, which is given in any text book as H_s = 1 390 w/m^2, or H_s = 139 mW/cm^2.[3b]

The per unit effectiveness of the suns's radiation on the phototransistor is then

$$\text{p.u. Effectiveness} = \frac{34{,}5\ mW/cm^2}{139\ mW/cm^2}$$

$$= 0{,}25$$

which is the same as for a tungsten source. Hence the sensitivity of the transistor for sunlight is

$$S_s = 0{,}4\ mA/(mW/cm^2) \qquad (4\text{-}33)$$

It is interesting at this stage to compare the expected dc

CURRENT/

current due to sunlight with the peak pulsed current due to the LED.

Assuming then that the LED radiates over 2π steradians once its lens has been filed down, the area it will illuminate at a distance of 12 cm (focal length of lens) is, from Equation 3-3.

$$A = 2\pi f^2 = 905 \text{ cm}^2 \quad (4\text{-}34)$$

At 50 mA the LED (ME 7121) radiates typically 3 mW of light power. Hence at 1,6 amps it should radiate

$$P \simeq \frac{(3 \text{ mW})(1\,600 \text{ mA})}{(50 \text{ mA})} \simeq 96 \text{ mW} \quad (4\text{-}35)$$

At a distance of 12 cm from the LED, the irradiance will therefore be

$$H = \frac{P}{A} = 0{,}11 \text{ mW/cm}^2 \quad (4\text{-}36)$$

However this will be attenuated when it passes through the lens and the perspex "pop-out" windows, so according to Equation 3-5 the transmission factor will be

$$t_R \simeq 0{,}61$$

The resultant current at the detector will then be

$$I_{C(L)} = S_{LED} H t_R = \{1{,}3 \text{ mA/(mW/cm}^2)\}\{0{,}11 \text{ mW/cm}^2\}\{0{,}61\} = 0{,}09 \text{ mA} \quad (4\text{-}37)$$

The sunlight on the other hand, will only have to pass through one window. Assuming it has a transmission factor of 85%, the maximum dc current due to the sunlight will be

$I_{C(S)}$/

$$I_{C(S)} = S_s H_s t \qquad (4\text{-}38)$$
$$= \{0,4\ mA/(mW/cm^2)\}\{139\ mW/cm^2\}\{0,85\}$$
$$= 47\ mA$$

Clearly if the phototransistor ever does point towards the sun it will saturate. The matter can be remedied however, by placing an infra-red filter in front of the detectors. A Kodac gelatin filter (type 87C) was found to have the desired admittance characteristic (shown by the $F(\lambda)$ curve in Graph 4-1).

The per unit effectiveness of the solar radiation then becomes

$$\text{Per Unit Effectiveness} = \frac{\int_{\lambda_1}^{\lambda_2} P(\lambda)R(\lambda)F(\lambda)d\lambda}{\int_0^{\infty} P(\lambda)d\lambda} \qquad (4\text{-}39)$$

The numerator of the above expression will also be evaluated using Simpson's Rule. Again using intervals of d = 50 nm, but this time between λ_1 = 750 nm and λ_2 = 1 150 nm we get,

h_1	= 0	h_6	= 33
h_2	= 2	h_7	= 16
h_3	= 58	h_8	= 4
h_4	= 70	h_9	= 0
h_5	= 52		

(all dimensions in $\mu W \cdot cm^{-2} \cdot nm^{-1}$)

Hence

$$A = \int_{\lambda_1}^{\lambda_2} P(\lambda) \cdot R(\lambda) \cdot F(\lambda)d\lambda \qquad (4\text{-}40)$$
$$\simeq \frac{(50)(688)}{6}$$
$$= 5\ 730\ \mu W/cm^2$$
$$= 5,73\ mW/cm^2$$

The per unit effectiveness of the sunlight is therefore:

$$\text{p.u. Effectiveness} = \frac{5,73 \text{ mW/cm}^2}{139 \text{ mW/cm}^2} \simeq 0,04 \qquad (4\text{-}41)$$

and the final sensitivity of the phototransistor for sunlight becomes

$$S_{F(S)} = S_T \frac{(0,04)}{(0,25)} \qquad (4\text{-}42)$$
$$= 0,06 \text{ mA/(mW/cm}^2\text{)}$$

The maximum dc contribution of the sunlight is then

$$I_{C(S)} = S_{F(S)} H_s t \qquad (4\text{-}43)$$
$$= \{0,06 \text{ mA/(mW/cm}^2\text{)}\}\{139 \text{ mW/cm}^2\}\{0,85\}$$
$$= 7,1 \text{ mA}$$

Since at 900 nm the transmission factor of the filter is about 80%, the sensitivity for the LED will be accordingly decreased.

Hence $S_{F(L)} = 0,8\, S_{LED} \simeq 1,0 \text{ mA/(mW/cm}^2\text{)}$

and $I_{C(L)} = S_{F(L)} H t_r \qquad (4\text{-}44)$
$= 0,07 \text{ mA}$

This is only 100 times less than for the sunlight, (compared to the 520 times less without the filter), which is acceptable.

4-22 Circuit Design

(a) Supply Voltage:-

The system used digital techniques to process its information (TTL). Hence a 5 volt supply was required. This was obtained from a dry rechargeable 12 volt battery via an LM 309 voltage regulator. (This is an integrated circuit made specifically for powering TTL).

It was therefore considered expedient to run the other circuits* from the same voltage rail, ensuring however that the voltage spikes created in the TTL supply were prevented from

*A notable exception is the LED Pulsing Circuit (Fig 4-1), which for regulation purposes was run directly off the battery.

reaching that of the sensitive optical amplifiers.

With reference to Fig 4-3, this was achieved by using the series transistor T_1 in the supply line, and decoupling its base very heavily with capacitors C_1 and C_2 via resistor R_1. The effective capacitance "seen" looking into the emitter of T_1 will then be

$$C_{eff} = h_{fe1}(C_1 + C_2) \qquad (4\text{-}45)$$
$$\simeq (40)(230\ \mu F)$$
$$\simeq 9\ 200\ \mu F$$

where h_{fe} is the current gain of the transistor.

This proved adequate to the task. (Note that C_1 is a 10 µF Tantulum capacitor to cater for the high frequency noise spikes, while C_2 is a 220 µF electrolytic to cater for the lower frequencies.)

DC-wise the base voltage of T_1will be held at

$$V_{b1} = \frac{V_{cc}}{1 + R_1/R'} \qquad (4\text{-}46)$$

where $$R' = R_2//R_{b1} \qquad (4\text{-}47)$$

where R_{b1} is the dc resistance "seen" looking into the base of T_1.

The supply voltage of the 16 optical amplifiers is therefore

$$V'_{cc} = V_{b1} - V_{BE1} \qquad (4\text{-}48)$$

For $V_{cc} = 5$ volts, $V_{BE} = 0{,}65$ volts, $R_1 = 100\ \Omega$, $R_2 = 10\ k\Omega$,
$3{,}5\ k\Omega < R_{b1} < 15\ k\Omega$

V_{b1} and V'_{cc} will lie in the following ranges

$$4{,}8\ v < V_{b1} < 4{,}9\ v$$
$$4{,}2\ v < V'_{cc} < 4{,}3\ v.$$

This part of the circuit, together with other standard

techniques such as earthing the negative rail of each circuit board directly to the metal box with short leads, and taking the positive rail of each board directly to one common point at the voltage source with longer leads, proved very effective in keeping the supply free of noise.

(b) Amplifier:-

This is required to generate an output of the order of 3 volts for an input irradiance of about 0,07 mW/cm .

(i) The collector current of a phototransistor is related to both its base current and the ambient irradiance according to the relation

$$I_C = h_{FE} I_B + SHt \qquad (4\text{-}49)$$

where S = phototransistor sensitivity in $mA/(mW/cm^2)$
H = irradiance in mW/cm^2
t = transmission factor of lens and "pop out" protective windows to infra-red light
I_B = quiescent base current of phototransistor
h_{FE} = dc current gain of phototransistor.

The dc current gains of the 16 phototransistors were measured with their photo-sensitive areas masked, and found to be of the order of 100.

It was also found that at very low collector currents, the sensitivity of the device dropped off dramatically, until in the absence of base drive and in complete darkness, it did not respond to the LED pulses at all. The phototransistor base resistor, R_3, was therefore inserted to ensure a minimum quiescent operating current. This was chosen to be about 5% of the maximum solar contribution of 7,1 mA.

Hence $I_{C(min)} \simeq 0,4$ mA

But $$I_B = \frac{V'_{cc} - V_{BE2}}{R_3} = \frac{I_{C(min)}}{h_{FE}} \qquad (4\text{-}50)$$

Therefore $$R_3 = \frac{100(4,3 - 0,6)V}{0,4\ mA}$$

$$= 925\ k\Omega$$

$$\simeq 1\ M\Omega$$

THE QUOTED/

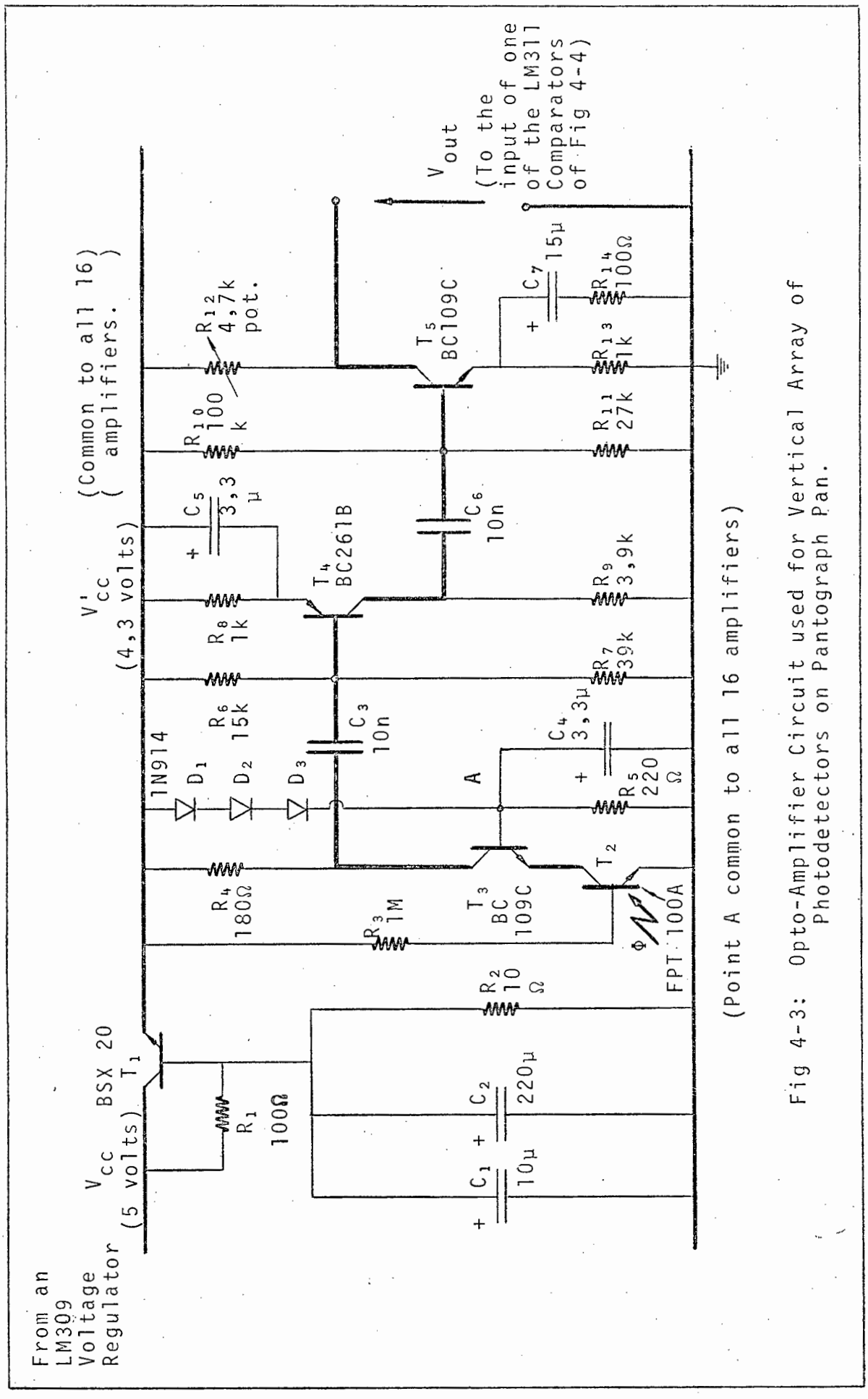

Fig 4-3: Opto-Amplifier Circuit used for Vertical Array of Photodetectors on Pantograph Pan.

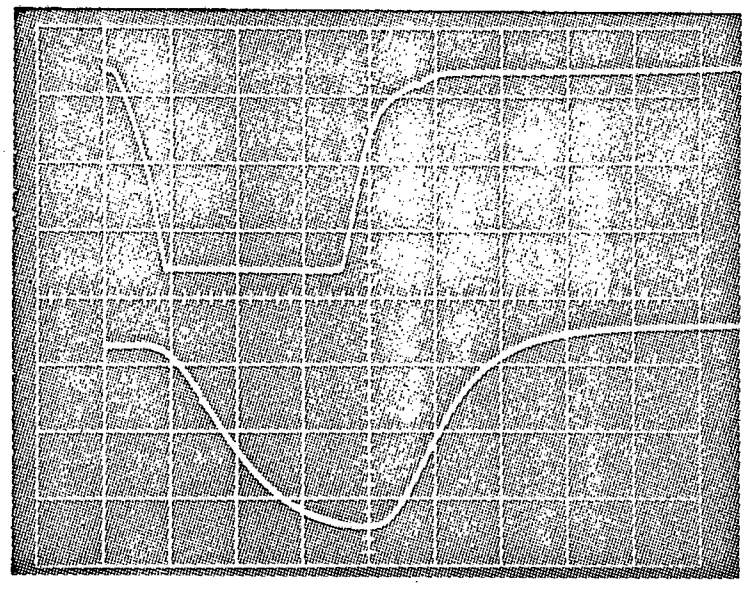

Top Trace: Voltage Across 6,8 V Zener Diode (Z_1) of LED Pulsing Circuit. (Fig 4-1)

Bottom Trace: Output Voltage of Opto-Amplifier Shown in Fig 4-3. (Scale: 1 V/div.)

(Time Scale: 2 μs/div.)

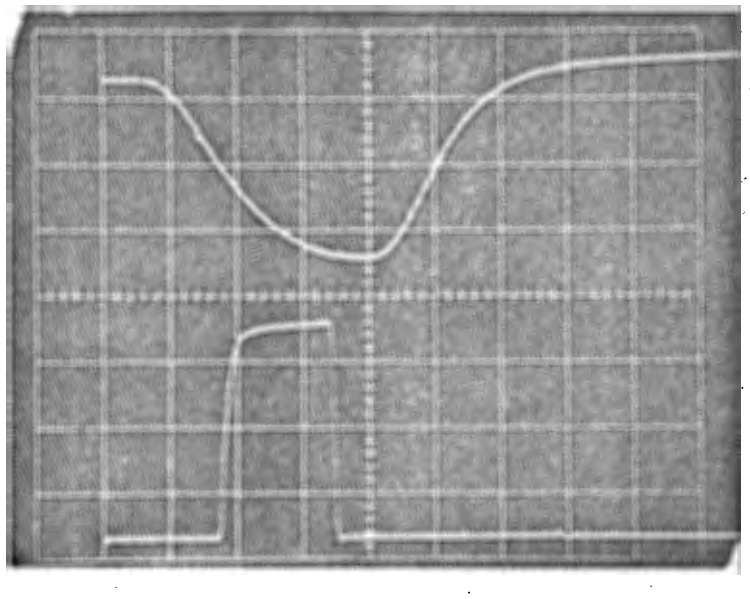

Top Trace: Output Voltage of Opto-Amplifier of Fig 4-3.

Bottom Trace: TTL Pulse (CL2) Described in Figs 4-5 & 4-6.
Leading Edge Slowed Down for Better Opto-Amplifier Noise Immunity.
Falling Edge Interrogates Output of Opto-Amplifier. (Synchronous Detection)

(Time Scale: 2 μs/div.)

The quoted rise and fall times of the FPT 100A when operating at a 4 mA collector current into a 100Ω emitter load are both 2,8 µs. When the collector current drops to 0,5 mA, this rises to about 5 µs. (See the Specification Sheet at the end of this book.)

Putting the load resistance into the collector will increase the rise time even more.This however can be compensated for by using a cascode transistor (T_3 of Fig 4-3), so that the actual load can be greater than the above 100Ω while the effective collector resistance "seen" by the phototransistor (T_2) is much less. In this way sufficient gain can be extrac=ted from the phototransistor stage without unduly derating its response time.

The incremental load resistance of T_2 is therefore

$$R_{L2} = 1/g_{m3} \qquad (4\text{-}51)$$

where g_{m_3} is the transconductance of T_3.

$$g_{m3} = 40\ I_{C3} \qquad (4\text{-}52)$$

Hence for

$$0{,}4\ \text{mA} < I_{C2} < 7{,}5\ \text{mA},$$
$$63\Omega < R_{L2} < 3\Omega$$

This arrangement gave turn-on delays of the order of 0,5 µs. Since the collector current of the phototransistor never drops to zero between pulses, this can mainly be ascribed to the sloping nature of the input pulse's leading edge. Rise times of the order of 4 µs were measured at the amplifier output, which implies an upper frequency break point of about 40 kHz. This was satisfactory.(Hence $f_{u_1} \simeq 40$kHz.)

The next task was to ensure that the first stage would not saturate in the event of the phototransistor pointing direct=ly at the sun. This was achieved by making R_4 so small that the maximum possible collector voltage excursion of T_3 was only about 60% of that required for saturation.

Hence

$$V_{R4(max)} \simeq (0{,}6)\{V_{D1} + V_{D2} + V_{D3}\} \qquad (4\text{-}53)$$
$$\simeq I_{C(max)}R_4$$

THEREFORE/

Therefore

$$R_4 = (0,6)\frac{(3 \times 0,7 \text{ volts})}{(7,5 \text{ mA})}$$
$$\simeq 0,17 \text{ k}\Omega$$
$$\simeq 180 \ \Omega$$

The diodes D_1 to D_3* are used to set the base voltages of the cascode transistor of each of the 16 amplifiers. Their forward current was chosen to be about 10 mA. Hence

$$R_5 = (1/I_F)(V'_{cc} - 3V_D) \qquad (4\text{-}54)$$
$$= \frac{4,3 \text{ V} - 2,1 \text{ V}}{10 \text{ mA}}$$
$$= 0,22 \text{ k}\Omega$$
$$= 220 \ \Omega$$

Since BC 109's ($h_{FE} \simeq 500$) were used for the cascode transistors, their combined base currents for collector currents of 7,5 mA would be less than 0,3 mA and therefore negligible.

C_4 consists of about five 3,3 µF Tantulum capacitors distributed over the board, to counter the effects of any fluctuations in V'_{cc}.

The GAIN of the first stage can be expressed in terms of "output voltage per incident irradiance". In terms of incremental values, the output swing is

$$v_{out} = i_c R_L \qquad (4\text{-}55)$$

where

$$R_L = R_4 // r_{be4} // R_6 // R_7$$

and r_{be4} is the incremental resistance "seen" looking into the base of T_4.

Since $r_{be4} \simeq 14 \text{ k}\Omega$, (see section on "Stage 2"), $R_6 \simeq 15 \text{ k}\Omega$, $R_7 = 39 \text{ k}\Omega$ and $R_4 = 180\Omega$,

$$R_L \simeq R_4$$

However

$$i_c = S_{F(L)} H_L t_R$$

and the gain is

---

* Better noise immunity could be obtained by interchanging R_5 and the diodes D_1, D_2 and D_3, since the base of T_3 should really be fixed relative to ground and not to V'_{cc}.

$$G_1 = -\left(\frac{V_{out}}{H_L}\right) \qquad (4\text{-}56)$$

$$= -S_{FL} t_R R_L$$

$$= -0{,}12 \text{ V}/(\text{mW/cm}^2)$$

The signal voltage at the collector of T_3 is then

$$V_{out} = G_1 H_L \qquad (4\text{-}57)$$

$$= -13 \text{ mV}$$

Since an output voltage of about 3 volts is required from the final stage of each amplifier, the combined gains of stage 2 and 3 must be about 230. For optimum noise considerations, stage 2 should be designed for as much gain as possible, with stage 3 merely making up the balance.

(ii) Stage 2:-

For this stage to have a large gain, the voltage across the emitter resistor R_8, must be made as small as possible (without rendering the calculation of the collector current unreliable), in order to give the collector a large enough voltage range.

A nominal value of $V_{R_8} = 0{,}5$ volts was chosen, with $R_8 = 1\ k\Omega$, setting the collector current at about 0,5 mA. (Since speed is not a limiting factor for stages 2 and 3, there is no point in using larger currents.)

The base voltage of T_4 relative to V'_{cc} is then

$$V_{B4} = V_{R8} + V_{BE4} \qquad (4\text{-}58)$$

$$= (0{,}50 + 0{,}65)\text{volts}$$

$$= 1{,}15 \text{ volts}$$

But

$$V_{B4} = \frac{R_6 V'_{cc}}{R_6 + R_7} \qquad (4\text{-}59)$$

Hence

$$R_7 \simeq 2{,}7\ R_6 \qquad (4\text{-}60)$$

Transistor T_4 (type BC 261B) has a current gain between 200

AND/

and 300, implying that its base current should be of the order of 3 μA. Hence R_6 and R_7 should conduct at least 10 times this value.

$$R_6 + R_7 < \frac{V'_{cc}}{10\ I_{B4}} = 140\ k\Omega \qquad (4\text{-}61)$$

The values finally chosen were

$$R_6 = 15\ k\Omega$$
$$R_7 = 39\ k\Omega$$

C_5 is a 3,3 μF Tantulum Capacitor which breaks with R_8 at about 50 Hz. (This only gives an indication of the order of magnitude of the break frequency, and a more rigorous treatment will follow.)

The dc voltage across R_9 was set at roughly half that required to saturate T_4. This was done to obtain as much gain as possible without causing saturation.

$$V_{R9} \simeq \tfrac{1}{2}(V'_{cc} - V_{R8} - V_{CE(sat)}) \qquad (4\text{-}62)$$
$$= \tfrac{1}{2}(4,3 - 0,5 - 0,2)\text{volts}$$
$$= 1,8\ \text{volts}.$$

$$R_9 = \frac{V_{R9}}{I_C} = 3,6\ k\Omega \qquad (4\text{-}63)$$

say $R_9 = 3,9\ k\Omega$.

The transconductance of T_4 is

$$g_m = 40\ I_C = 20\ mA/v \qquad (4\text{-}64)$$

and the gain is therefore

$$G_2 = -g_m\{R_9 // R_{10} // R_{11} // \beta(\frac{1}{g_m} + R_{14})\} \qquad (4\text{-}65)$$
$$= -67$$

The expected signal voltage across R_9 is therefore about

1 VOLT/

1 volt, causing a maximum collector voltage of about 3 volts, which leaves over half a volt before saturation occurs.

It is now possible to calculate the limiting rise time of this stage. Assuming worst case values, the maximum possible parasitic capacitance that can exist between the base of T_4 and ground is

$$C_T = C_{be4} + (1 - G_2)C_{bc4} \qquad (4\text{-}66)$$
$$= (9 + 67 \times 4{,}5)\ pF$$
$$= 310\ pF$$

This is fed from a source resistance of

$$R_s = R_4 // R_6 // R_7 // r_{be4} \qquad (4\text{-}67)$$
$$= 175\ \Omega$$

giving an associated time constant of

$$\tau_2 = R_s C_T \qquad (4\text{-}68)$$
$$= 54\ ns$$

which implies an upper break frequency

$$f_{u3} = 2{,}9\ MHz$$

In determining C_3 it must be remembered that although the overhead line is at 3 kV dc, this is actually created from a rectified 50 Hz 3-phase supply. Consequently there will be certain low frequency harmonics in the surrounding electric and magnetic fields - the most dominant of which occuring at about 300 Hz.
Then too all the street lights, though excited at 50 Hz, actually flicker at 100 Hz; and there will be many higher frequency components of optical interference by virtue of the speed at which the locomotive moves into and out of shadows.
The latter can be taken care of by synchronously detecting the output of each amplifier. The low frequencies however must be suppressed by choosing C_3, C_5, C_6 and C_7 so that

BREAK/

break points are created well above these danger points.

Inspection of Graph 4-2, which shows a Fourier analysis of a trapezoidal wave such as the one used to excite the phototransistor, indicates that a low frequency break point of about 2 KHz will result in very little signal energy being lost, while greatly attenuating the noise frequencies.

The section of the amplifier circuit common to C_3 and C_5 is shown in Fig 4-3(a) (i). The equivalent circuit of this as "seen" from the emitter of T_4 is shown in (ii), while (iii) shows a simplified version of this equivalent circuit. The frequency response of this circuit can be determined by finding the expression for the series current through the network. Since the voltage across R_a will be in phase with this current, the same information can be obtained by solving for V_{Ra}.
The analysis proceeds as follows.

Series impedance of network

$$Z(s) = R_a + \frac{1}{sC_a} + \frac{R_b}{1 + sC_b} \qquad (4\text{-}69)$$

$$= \frac{s^2 C_a R_a C_b R_b + s(C_a R_a + C_b R_b + C_a R_b) + 1}{sC_a(1 + sC_b R_b)}$$

where s is the Laplace variable ($s = j\omega$), and C_a, C_b, R_a and R_b are as defined in (iii) of Fig 4-3(a).
The transfer function relating the voltage across R to the input voltage is therefore:

$$\frac{V_{Ra}(s)}{V_{in}(s)} = \frac{R_a}{Z(s)} \qquad (4\text{-}70)$$

$$= \frac{sC_a R_a(1 + sC_b R_b)}{s^2 C_a R_a C_b R_b + s(C_a R_a + C_b R_b + C_a R_b) + 1}$$

$$= \frac{s(s + 1/\tau_b)}{s^2 + s(1/\tau_a + 1/\tau_b + 1/\tau_{ba}) + 1/\tau_a \tau_b}$$

WHERE/

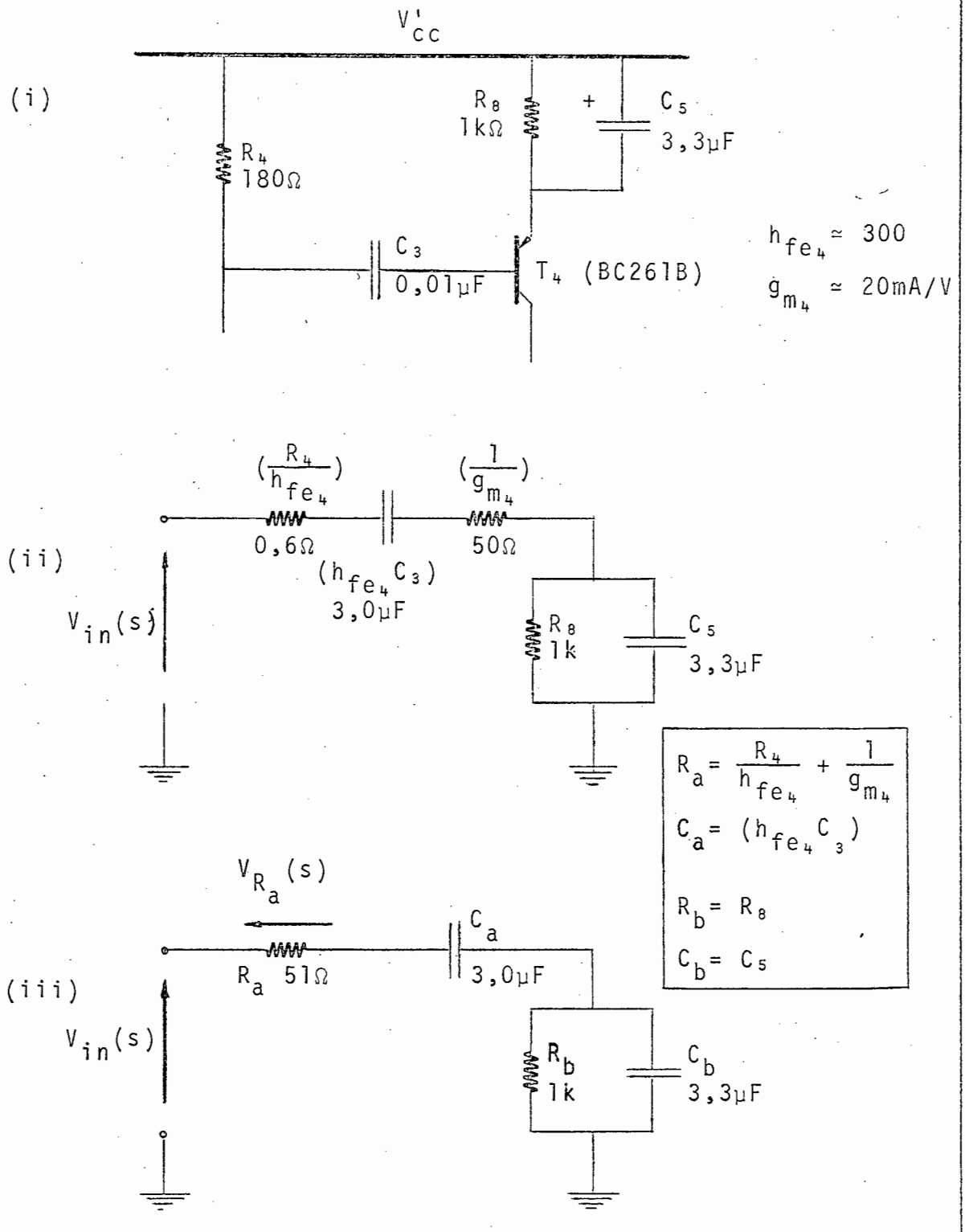

Fig 4-3(a)

(i) Low Frequency Circuit of Stage 2 of Amplifier shown in Fig 4-3.

(ii) Small Signal Equivalent Circuit of (i) as "seen" from the Emitter of T_4

(iii) Simplified Version of (ii).

where

$$\tau_a = C_a R_a$$

$$\tau_b = C_b R_b$$

$$\tau_{ba} = C_b R_a$$

In an equation of this complexity it is easier to substitute a few trial values for the one unknown (C_3) and select one that gives a favourable result.

Hence

C_3 = 10 nF R_4 = 180 Ω

C_5 = 3,3 µF R_8 = 1 kΩ

Reflecting these into the emitter of T_4, and taking into account the emitter-base incremental resistance ($1/g_{m_4}$), we get

$$R_a = \frac{R_4}{h_{fe4}} + \frac{1}{g_{m4}} = (\frac{180}{300} + \frac{1}{0,02})\Omega = 51\ \Omega$$

$$C_a = h_{fe4}C_{13} = (300 \times 0,01\ \mu F) = 3\ \mu F$$

R_b = 1 kΩ

C_b = 3,3 µF {See Circuit (iii) of Fig 4-3(a)}

Hence

$\tau_a = 1,53 \times 10^{-4}$sec

$\tau_b = 3,30 \times 10^{-3}$sec

$\tau_{ba} = 1,68 \times 10^{-4}$sec

Equation 4-70 therefore reduces to

$$\frac{V_{Ra}(s)}{V_{in}(s)} \simeq \frac{s(s + 303)}{s^2 + 1,28 \times 10^4 s + 1,98 \times 10^6}$$

$$= \frac{s(s + 303)}{(s + 157)(s + 1,26 \times 10^4)}$$

This circuit has two poles and one zero.

$$f_{p2} = \frac{157}{2\pi}\ Hz = 25\ Hz$$

$$f_{p4} = \frac{1,26 \times 10^4}{2\pi} Hz = 2\ kHz$$

f_{z2}/

$$f_{z2} = \frac{303}{2\pi} \text{ Hz} = 48 \text{ Hz}$$

(See Graph 4-3)

(iii) Stage 3:-

The dc requirements of T_5 are similar to those of T_4.

$$V_{B5} = \frac{R_{11}V'_{cc}}{R_{10} + R_{11}} = 1{,}15 \text{ volts} \qquad (4\text{-}71)$$

Hence

$$R_{10} = 2{,}7\ R_{11}$$

Since transistor T_5 (type BC109C) has a typical current gain of 500, slightly larger resistors can be used for R_{10} and R_{11}.

$$R_{10} = 100 \text{ k}\Omega$$
$$R_{11} = 27 \text{ k}\Omega$$

The emitter resistor R_{13} was also made 1 kΩ to ensure a collector current of 0,5 mA.
The decoupling capacitor C_7 was made 15 μF, giving a breakpoint of 11 Hz with R_{13}. (A more rigorous analysis of its effect will follow however, as this gives only an indication of the order of magnitude involved.)
Since stage 3 is a large signal amplifier requiring a small gain of between 3 and 5, and the transconductance varies from transistor to transistor, R_{14} was included to introduce a measure of predictability in the gain calcula= tions, and also to "soften the blow" of the input voltage step.
The gain of this stage is

$$G_3 = \frac{-g'_m R_{12}}{1 + g'_m R_{14}} \qquad (4\text{-}72)$$

where g'_m is the approximate average transconductance over

the pulse duration.

For Equation 4-72 to hold, R_{14} must be about 10 times less than R_{13}, hence

$$R_{14} = 100\ \Omega$$

If the average transconductance $g_m' = 120$ mA/v (see Equation 4-73), the collector resistance can be calculated.

$$R_{12} \simeq 500\ \Omega$$

(In practice it was found necessary to use 4,7 kΩ "trim-pot" for R_{12}, since variations in the g_m of T_4 caused G_2 to drop as low as 50 in some cases, and the emitter voltages of T_4 and T_5 turned out to be only 0,4 volts from their respective rails. Each potentiometer was individually set, and glued in position with nail varnish.)
To obtain an estimate of the high frequency break point of stage 3, it is necessary to consult Fig 4-3(b). This shows the section of the circuit containing T_5 and the parasitic junction capacitors of T_5 (i), as well as a small signal model of T_5.
(The reason that the following calculations should not be believed implicitly is that they pertain only to the small signal analysis of transistors, whereas the voltage excursions of T_5 are large. T_5 however does not saturate, so they may be used to obtain the expected order of magnitude of the break point. This is acceptable since the upper break point of the whole circuit is set by the phototransistor, and this exercise is merely to verify that the breakpoint of T_5 is some decades above this value.)
The collector voltage swing of T_5 is of the order of 3 volts. For a collector resistor of about 500 Ω, this implies a peak collector current of about 6 mA. For the purpose of this analysis, the average collector current over the pulse duration shall be used, which is approximately 3 mA.

The approximate average transconductance of T_5 is then

g_m'/

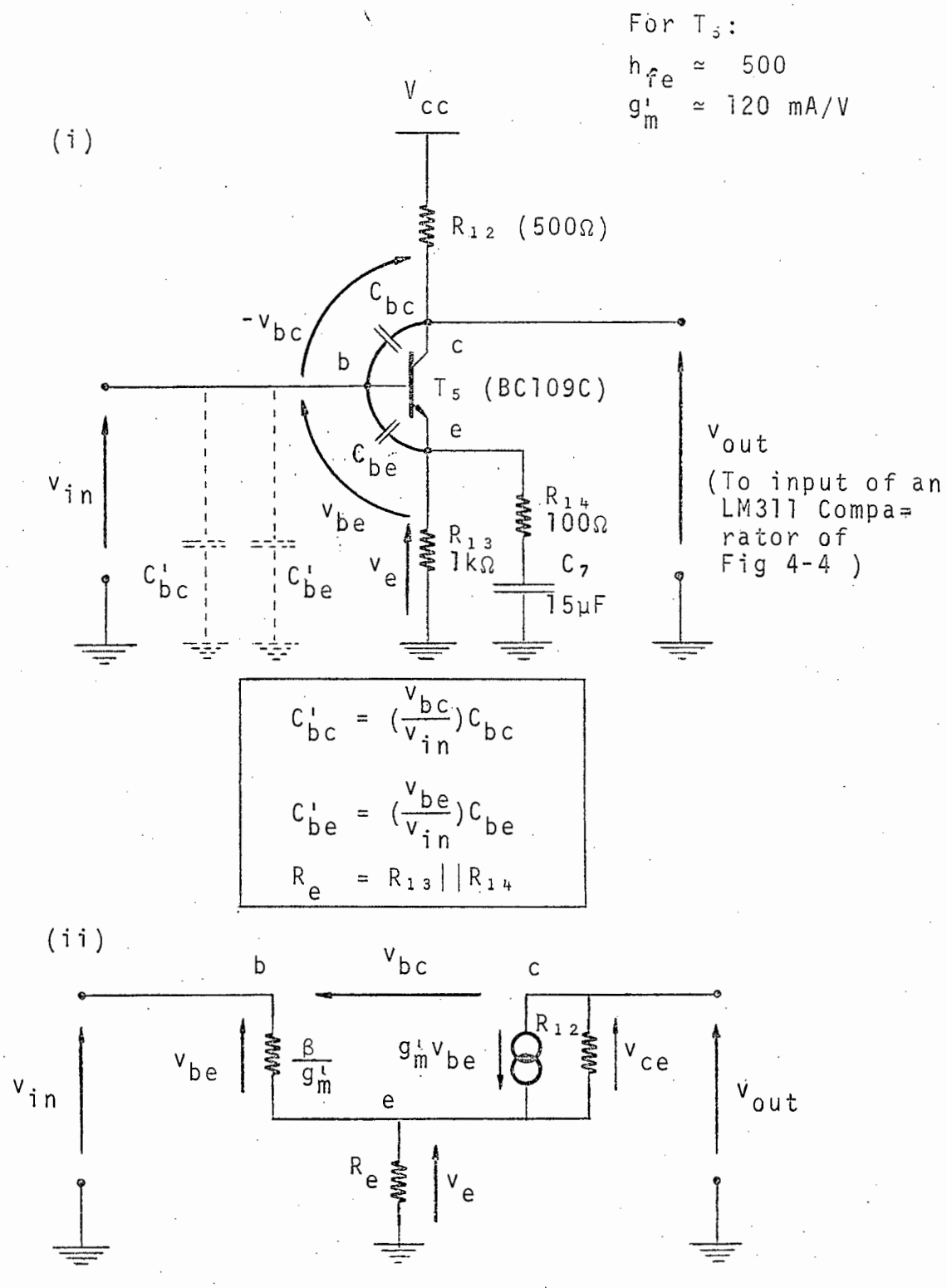

Fig 4-3(b):

(i) Stage 3 of Opto-Amplifier of Fig 4-3 (showing parasitic junction capacitors).

(ii) Small signal model of T_5.

$$g'_m \simeq 3 \times 40 \text{ mA/V} \simeq 120 \text{ mA/V} \simeq 0{,}12 \text{ A/V} \quad (4\text{-}73)$$

The parasitic junction capacitors of T_5, C_{bc} and C_{be} must be reflected down to ground to become C'_{be} & C'_{bc} to find their effective value as "seen" by the circuit.
Hence

$$C'_{bc} = \left(\frac{V_{bc}}{V_{in}}\right)C_{bc} \quad (4\text{-}73a)$$

$$C'_{be} = \left(\frac{V_{be}}{V_{in}}\right)C_{be} \quad (4\text{-}73b)$$

where V_{bc}, V_{be} and V_{in} are described in Fig 4-3(b).
Then

$$\frac{V_{be}}{V_{in}} \simeq \frac{\beta/g'_m}{\beta/g'_m + \beta R_e} \simeq \frac{1}{1 + g'_m R_e} \quad (4\text{-}74a)$$

$$\simeq \frac{1}{1 + (0{,}12 \text{ A/V})(91\ \Omega)} \simeq 8{,}4 \times 10^{-2}$$

where R_e is the parallel combination of R_{13} and R_{14}, C_7 being a short circuit at high frequencies.
(R_e = 1 000 Ω//100 Ω ≃ 91 Ω)

Also, from (ii) of Fig 4-3(b),

$$V_{bc} = V_{be} - V_{ce}$$

$$\simeq V_{be}(1 + g'_m R_{12}) \quad (\text{Since } V_{ce} \simeq -g'_m V_{be} R_{12})$$

$$\frac{V_{bc}}{V_{in}} \simeq \frac{V_b(1 + g'_m R_{12})}{V_{in}} \simeq \frac{1 + g'_m R_{12}}{1 + g'_m R_e} \simeq 5{,}1 \quad (4\text{-}74b)$$

In general the base-emitter capacitance of a transistor is given by

$$C_{be} \simeq \frac{g_m}{2\pi f_t}$$

where g_m is the transconductance and f_t is the transition frequency. (For the BC109C this is about 300 MHz).

HENCE/

Hence

$$C_{be} \simeq \frac{0,12\ A/V}{(2\pi)(300 \times 10^{6}Hz)}$$
$$\simeq 64 \times 10^{-12}F$$
$$\simeq 64\ pF.$$

From the specification sheet of the BC109, its collector-base junction capacitance is of the order of 5 pF.

The total effective capacitance "seen" by the circuit is

$$C_T = C'_{be} + C'_{bc}$$
$$\simeq (64\ pF)(8,4 \times 10^{-2}) + (5\ pF)(5,1)$$
$$\simeq 31\ pF$$

This is driven from a source resistance of

$$R_s \simeq R_9//R_{10}//R_{11}//\beta(1/g'_m + R_{13}//R_{14})$$
$$\simeq 3,1\ k\Omega$$

Hence the order of magnitude of the high frequency break point is

$$f_{u2} \simeq \frac{1}{2\pi R_s C_T} \qquad (4\text{-}75)$$
$$\simeq 1,7\ MHz$$

This is nearly two decades higher than that of the photo-transistor.
To determine the low frequency break point of this stage, it is necessary to consult Fig 4-3(c). This shows the relevant section of Stage 3 (i), the equivalent circuit as "seen" from the emitter of T_5 (ii), and a simplified equivalent circuit as "seen" from the emitter of T_5 (iii).
The following analysis applies to (iii).
As for Stage 2, the low frequency response of the network is given by the voltage across the series resistive element R_a.
The total series impedance of (iii) is

Z(s)/

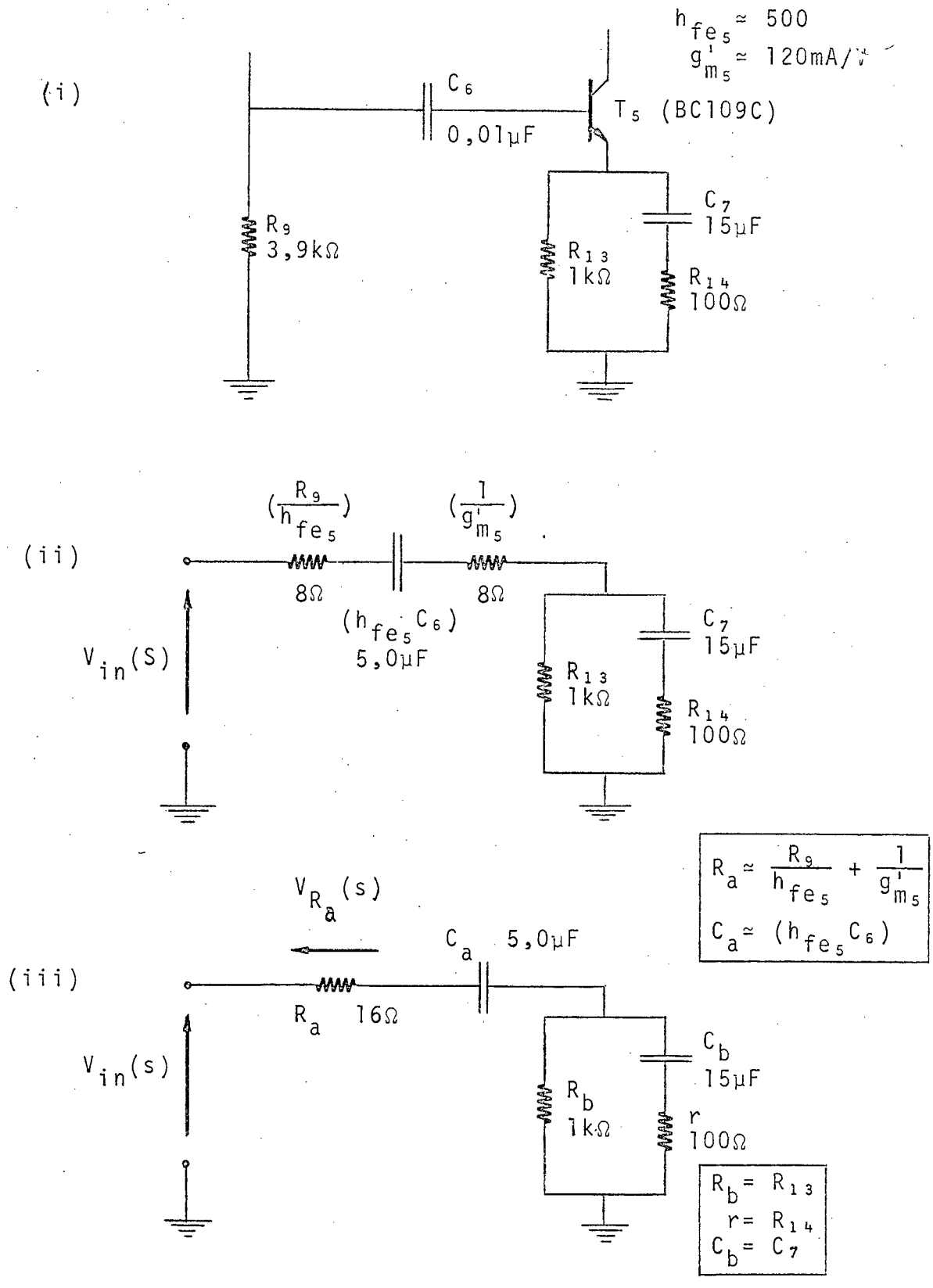

Fig 4-3(c):

(i) Low Frequency Circuit of Stage 3 of Amplifier shown in Fig 4-3.

(ii) Approximate Equivalent Circuit of (i) as "seen" from the Emitter of T_5.

(iii) Simplified Version of (ii).

$$Z(s) = R_a + \frac{1}{sC_a} + \frac{R_b(1 + srC_b)}{1 + s(rC_b + R_bC_b)} \qquad (4\text{-}76)$$

$$Z(s) = \frac{s^2(R_aC_arC_b + R_aC_aR_bC_b + R_bC_brC_a) + s(R_aC_a + rC_b + R_bC_b + R_bC_a) + 1}{sC_a\{1 + s(rC_b + R_bC_b)\}}$$

where s is the Laplace variable ($s = j\omega$), and C_a, C_b, R_a, R_b and r are as defined in (iii) of Fig 4-3(c).

The transfer function relating the voltage across R_a to the input voltage is therefore:

$$\frac{V_{Ra}(s)}{V_{in}(s)} = \frac{R_a}{Z(s)} \qquad (4\text{-}77)$$

$$= \frac{sC_aR_a\{1 + s(rC_b + R_bC_b)\}}{s^2(R_aC_arC_b + R_aC_aR_bC_b + R_bC_brC_a) + s(R_aC_a + rC_b + R_bC_b + R_bC_a) + 1}$$

At this stage it is more useful to substitute the respective values of the various parameters into the equation. As for Stage 2, a value for the series capacitor C_6 must be assumed, and its effect checked. Taking C_6 as 0,01 µF, we have

$C_a = h_{fe5}C_6 = (500 \times 0{,}01\ \mu F) = 5\ \mu F$

$R_a = \frac{R_9}{h_{fe5}} + \frac{1}{g'_{m5}} = \frac{3\,900}{500}\Omega + \frac{1}{0{,}12}\Omega \simeq 16\Omega$

$C_b = 15\ \mu F$

$R_b = 1\ k\Omega$

$r = 100\ \Omega$

Then Equation 4-77 becomes

$$\frac{V_{Ra}(s)}{V_{in}(s)} = \frac{8{,}0 \times 10^{-5}s(1 + 1{,}65 \times 10^{-2}s)}{8{,}82 \times 10^{-6}s^2 + 2{,}16 \times 10^{-2}s + 1}$$

$$= \frac{0{,}15s(s + 60{,}6)}{s^2 + 2\,447s + 1{,}134 \times 10^5}$$

=/

$$= \frac{0,15s(s + 60,6)}{(s + 47,3)(s + 2\ 399)}$$

This shows two poles at

$$f_{p1} \simeq \frac{47,3}{2\pi} \text{ Hz} \simeq 8 \text{ Hz}$$

$$f_{p3} \simeq \frac{2\ 399}{2\pi} \text{ Hz} \simeq 380 \text{ Hz}$$

and a zero at

$$f_{z1} \simeq \frac{60,6}{2\pi} \text{ Hz} \simeq 10 \text{ Hz}$$

It must be borne in mind that f_{p_1}, f_{p_3} and f_{z_1} are only approximations because g_{m_5} varies from about 20 mA/V to about 240 mA/v over the pulse duration. This does not effect the bandwidth of the system to any significant extent though, as the dominant low frequency break point f_{p_4}, is set by Stage 2. Hence the minor perturbations of f_{p_3} will only have a second order effect.
(See the Bode Plot in Graph 4-3.)
Hence C_6 = 0,01 µF is a reasonable choice.

The resultant gain of the whole circuit over its pass band is then

$$G_{pb} = G_1G_2G_3 \qquad (4\text{-}78)$$
$$\simeq -28 \text{ volts}/(\text{mW/cm}^2)$$

Defining -1 volt/(mW/cm²) as 0dB, then G_{pb} expressed in logarithmic terms, is 29 dB. The approximate theoretical frequency response of the circuit is shown in Graph 4-3. Its validity is borne out by the fact that the rise time at the output for a (light) pulse excitation at the input, is of the right order of magnitude for the circuit's predicted bandwidth.[4]

Compare this with Graph 4-2, which shows the Fourier Components of the symmetrical trapezoidal wave train shown in Fig 4-3(d). (It is a pulse train of this nature that is generated by the LED

Pulsing Circuit.) Clearly the trapezoidal pulses' spectrum fits into the Opto-Amplifier's active band with very little loss of harmonic energy.

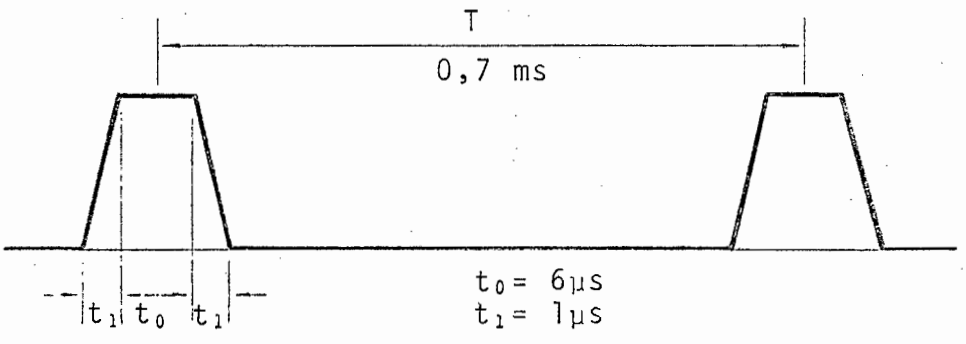

Fig 4-3(d): Trapezoidal Signal Pulse Train Emi= nating from LED. (A Fourier Analysis of this Waveform can be found in Graph 4-2.)

This proved a perfectly adequate foil against a 200 Watt light bulb held within 10 cm of the detectors, with only an intervening infra-red filter for protection. Admittedly the frequency of the optical interference was only 100 Hz, but then its intensity was many orders of magnitude greater than anything that would be encountered under normal working conditions. (In any event any excessive low frequency interference could easily be countered by reducing C_5, C_6 and C_7 to obtain an 80 dB per decade drop-off below 2 KHz.)

The dominant high frequency break-point of about 40 KHz is due only to the limitations of the phototransistor itself, as stages 2 and 3 break at 2,9 MHz and 1,3 MHz respectively. In other words the drop-off characteristic is that of a one-stage RC filter which has a time constant of about 4 µs.

This is indeed fortunate from the point of view of noise rejection, since the criterion for match-filtering a square wave of duration T by a single-stage RC network is that

$$BT = 0,25 \qquad (4\text{-}79)$$

where B is the receiver bandwidth.

FOR THE/

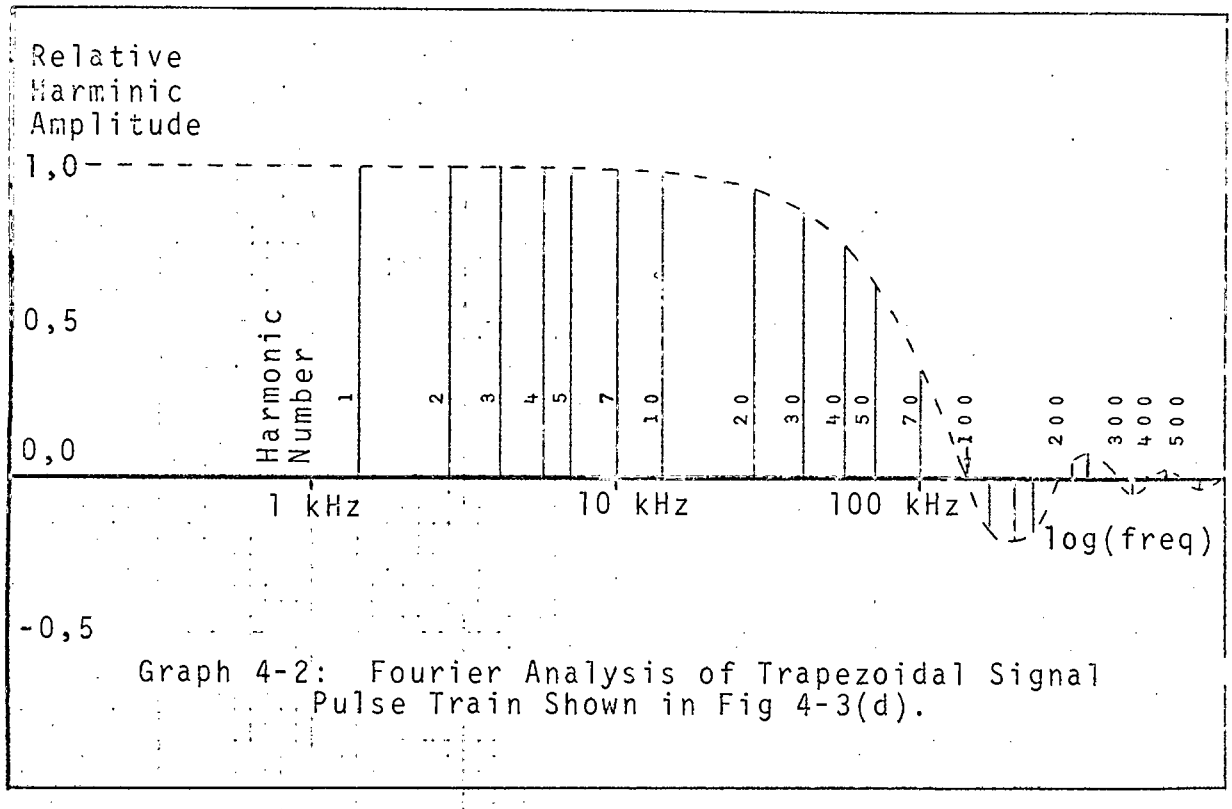

Graph 4-2: Fourier Analysis of Trapezoidal Signal Pulse Train Shown in Fig 4-3(d).

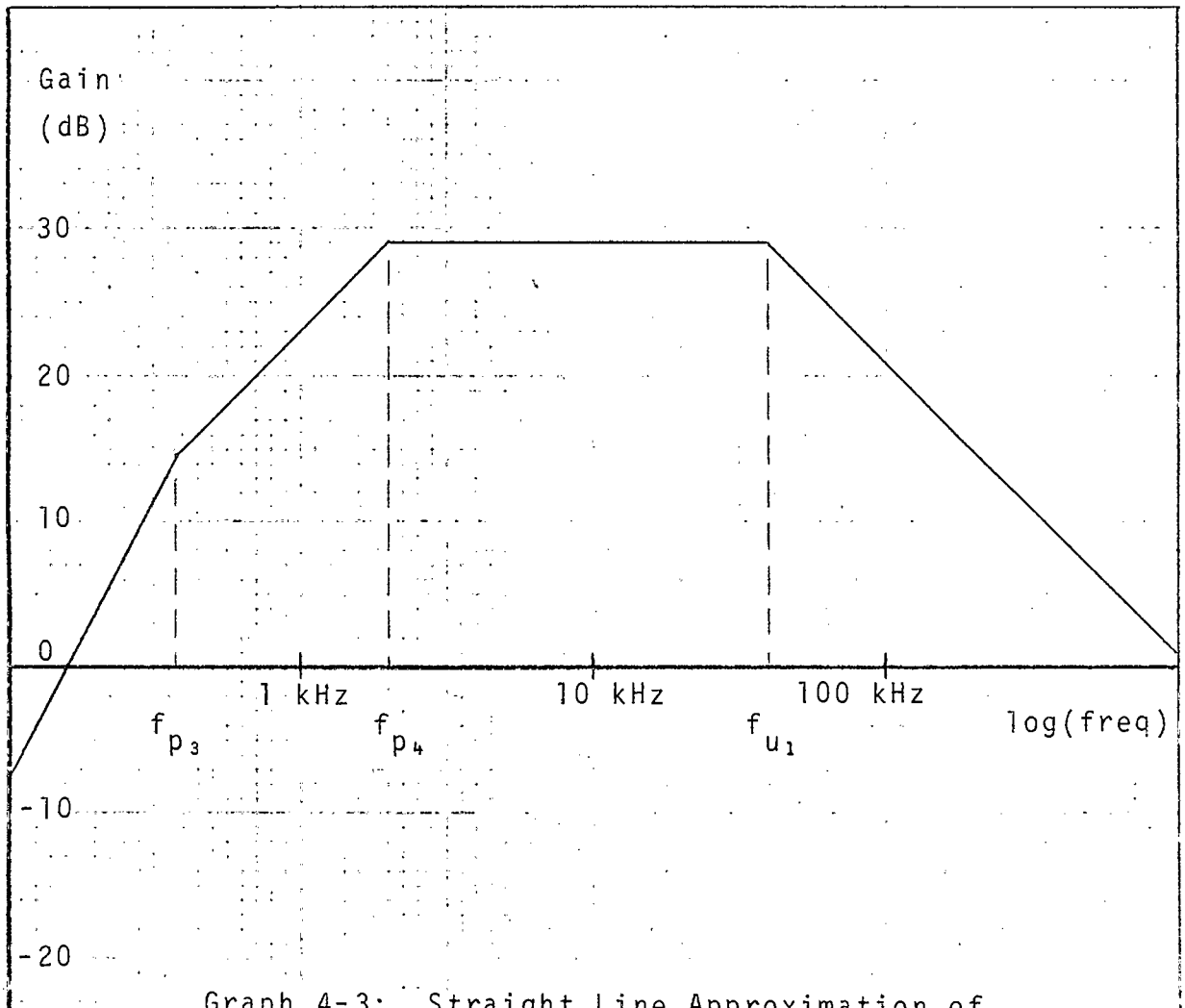

Graph 4-3: Straight Line Approximation of Opto-Amplifier Frequency Response Curve.

For the case in question,

$$BT = (f_3 - f_2)T \qquad (4\text{-}80)$$
$$= (4\ kHz - 2\ kHz)(7\ \mu s)$$
$$= (38 \times 10^3 Hz)(7 \times 10^{-6}\ sec)$$
$$= 0,27$$

which is almost optimum. This means that the amplifier output will reach its maximum amplitude when the input pulse turns off, so any synchronous detection must be performed at this instant in time.

The peak-signal-to-rms-noise ratio of each of the 16 amplifiers was measured. They were all approximately equal, and the lowest one was of the order of 200:1. (This is a conservative figure.)

The probability of an error occurring in any one of the detectors was calculated in Section 3-32 to be

$$P_T = 3,3 \times 10^{-4} \qquad \text{(See Equation 3-79)}$$

This is a perfectly acceptable figure.

(iv) Output Buffering for TTL Application.

The next step was to find a device which could monitor the output of each amplifier, triggering each time the output pulse reached the correct level; and also to buffer this signal for TTL application.

All these requirements were met in the LM 311 Comparator, a TTL-compatible device which can operate from a single 5 volt supply. It has an open-collector output, and also features typical response times of 200 ns, maximum input currents of 250 nA and typical input offset voltages of 2 mV.

Its recommended output resistance for TTL operation is 1 kΩ, but this proved to be too low since current conservation is an important factor, whereas speed is not. Consequently 10 kΩ resistors were used which reduced the current ten-fold, while only increasing the response time to 3 μs, which is quite acceptable.

4-30 DIGITAL MANIPULATION OF DATA AT 3 kV.

4-31 Data Decoding.

It was decided to transmit the data down to ground in serial digital form, and that a "count-initiating pulse", (CIP) would precede each data train to ground. Hence a maximum of 17 pulses could be transmitted each cycle. Bearing in mind that the maximum number of detectors which can be obscured from the light by the new cable is 10, then the deciphered data can be broken up into the following categories.

(i) One pulse sent down per cycle, (condition A):
this would occur if the contact wire had bounced right out of the beam, so that only the C.I.P. would be de= tected. This would indicate that either the driver had been travelling too fast, that the rails in that vicinity were in need of repair, that there was something wrong with the overhead system itself, or that the contact wire had slid up one of the protective ramps.

(ii) Two pulses sent down per cycle, (condition B):
since it is impossible for the contact wire to be "one detector" thick, this was used to indicate that it had undergone a small amplitude bounce, and was partially in and partially out of the beam. It is important to be able to recognise this condition as otherwise the contact wire might appear thinner than it actually is.

If the top detector is in shadow and the eleventh is not, then clearly condition B will apply. Fig 4-4 shows how it is recognised electrically. If the 16 optical amplifiers are numbered I to XVI starting at the topmost one, then in Boolean notation

$$B = \frac{(I)\cdot\overline{(XI)}}{\overline{(I)}+(XI)} \qquad (4\text{-}81)$$

WHERE/

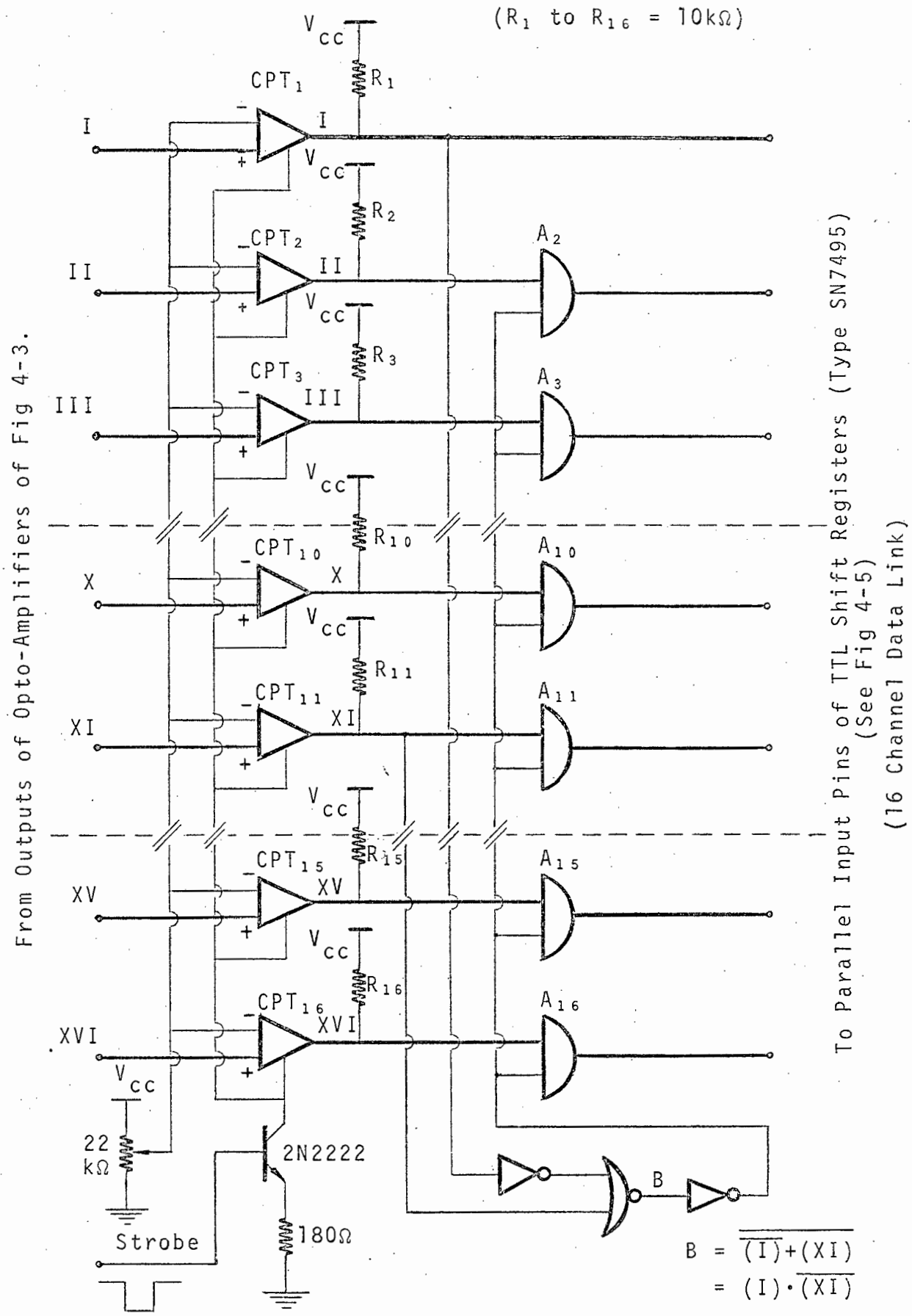

Fig 4-4: Comparator Buffers for Outputs of Opto-Amplifiers, and TTL Circuitry for Digital Recognition of Small Amplitude Bounce Condition of Contact Wire.

where (I) means that detector I is in shadow, and ($\overline{XI}$) means that detector XI is not.
By means of the "and-gates", A_2 to A_{16}, the outputs of all the detectors save I are inhibited so that only one "1" is fed into the shift register to be "clocked" down to ground. Since this will be preceded by the C.I.P., this state will be represented by two pulses.

(iii) Three to Eleven Pulses sent down per cycle, (conditions "-, 0, 1, 2, 3, 4".):
if neither the top nor the bottom detector is in shadow, then the number of intermediate ones that are, is clearly proportional to the contact wire thickness. As will be explained later, for display purposes this was further subdivided into the following categories:

"-" ==> 3, 4, 5 or 6 pulses transmitted ==> sub-critical wear,
"0" ==> 7 pulses ==> critically worn,
"1" ==> 8 pulses ==> three-quarters worn,
"2" ==> 9 pulses ==> half worn,
"3" ==> 10 pulses ==> one-quarter worn,
"4" ==> 11 pulses ==> new contact wire.

(iv) Twelve to Sixteen pulses sent down per cycle, (condition C):
If both the top detector and the eleventh one are in shadow, then the contact wire will appear to be thicker than is possible, so some foreign body must be on it. This could either be a lump of grease, or more likely a dropper clamp.

(v) Seventeen pulses sent down per cycle, (condition D):
if the bottom detector falls in shadow, then either that detector's light has been blocked off by grease splattering onto the "pop-out" window, or more serious, the contact strips are excessively worn and need to be replaced. In either event it will not be long before a dropper clamp obscures all the detectors. This would mean that all fur= ther readings should not be trusted, and that the panto= graph should be lowered as soon as possible to check the optical equipment and contact strips.

4-32 Circuit Realisation.

Fig 4-5 shows the technical details of the rest of the circuitry mounted under the pantograph shoe.

Block A contains the master clock of the system which consists of a free-running square-wave generator and two TTL decade counters (Type SN 7490), to achieve the required 1% duty cycle for pulsing the LED. This is followed by various TTL logic elements which select certain pulses during each cycle to control the rest of the circuit.

The square-wave generator exploits the hysteresis in a TTL "nand" gate (Type SN 7413) to achieve oscillation. Provided R_1 is made small enough so that it can carry sufficient current to render the gate input current negligible, the values of the timing components can be calculated from

$$t = R_1 C_1 \{\ln(\frac{V_{max} - V_L}{V_{max} - V_u}) + \ln(\frac{V_u - V_{min}}{V_L - V_{min}})\} \qquad (4\text{-}82)$$

where t is the period, (7 µs),
V_{max} is the gate high level output voltage (3,3 v)
V_{min} is the gate low level output voltage (0,2 v)
V_u is the upper input threshold voltage (typ 1,7 v)
V_L is the lower input threshold voltage (typ 0,9 v)

These figures give

$$R_1 C_1 \simeq \frac{7 \times 10^{-6}\ s}{1,2} \simeq 6,0 \times 10^{-6}\ sec \qquad (4\text{-}83)$$

Let $R_1 = 100\Omega$

Hence $C_1 \simeq 60$ nF (Say 56 nF)

Block B contains four 4-bit shift registers (type SN 7495) which are mounted in series and operate in the "parallel-input, serial-output" mode. They feed the incoming data from the optical amplifiers through to a light-emitting diode which froms part of an isolatory optical link down to ground.

Also in Block B is a slave clock which is activated by the master clock and designed to count off exactly 16 pulses per cycle.

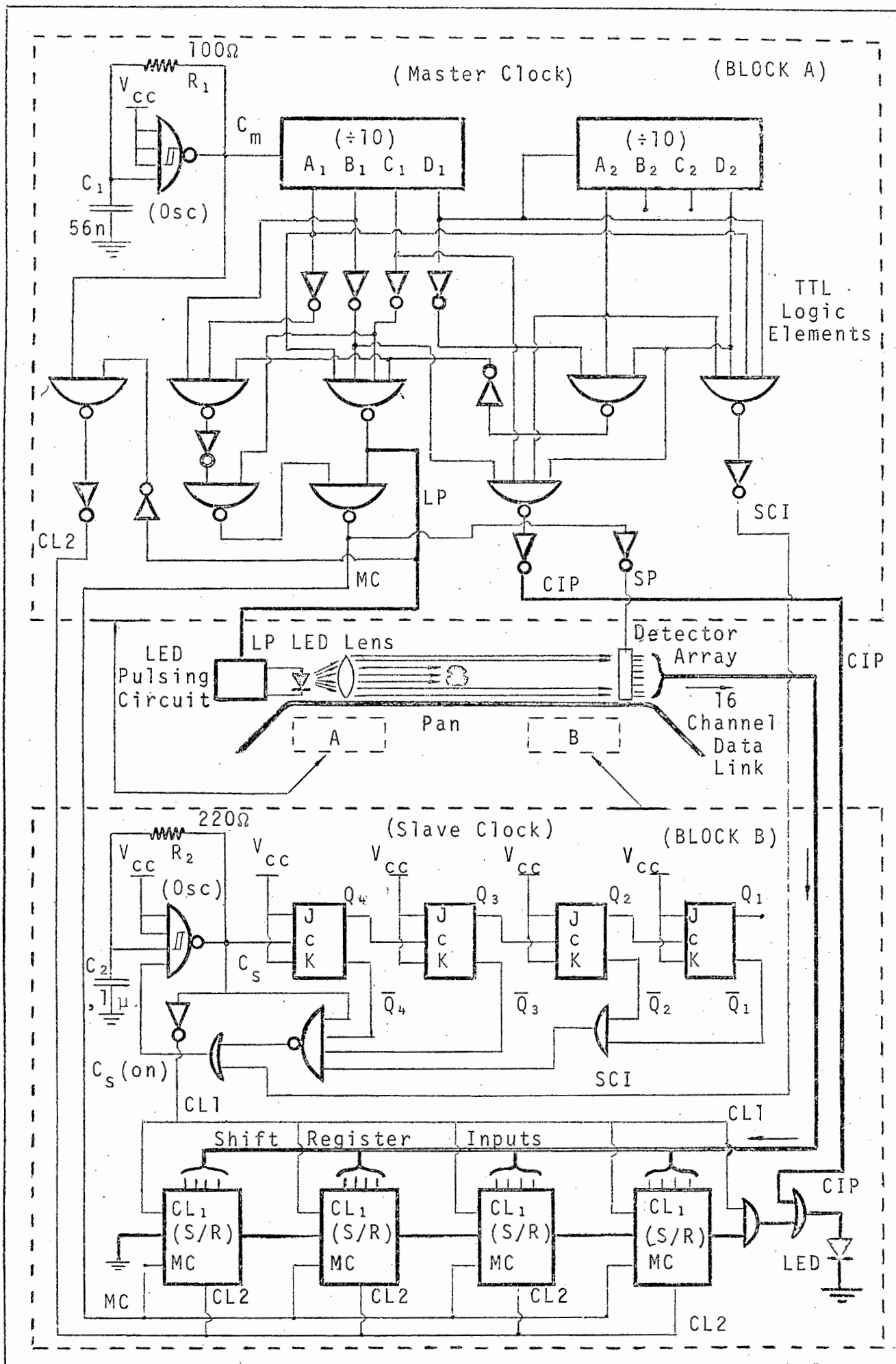

Fig 4-5: Block diagram of Circuitry Mounted on Pantograph Pan.
Block A - Master Clock of System and Associated Logic.
Block B - Reception of Optical Information and Transmission of Data to Ground.

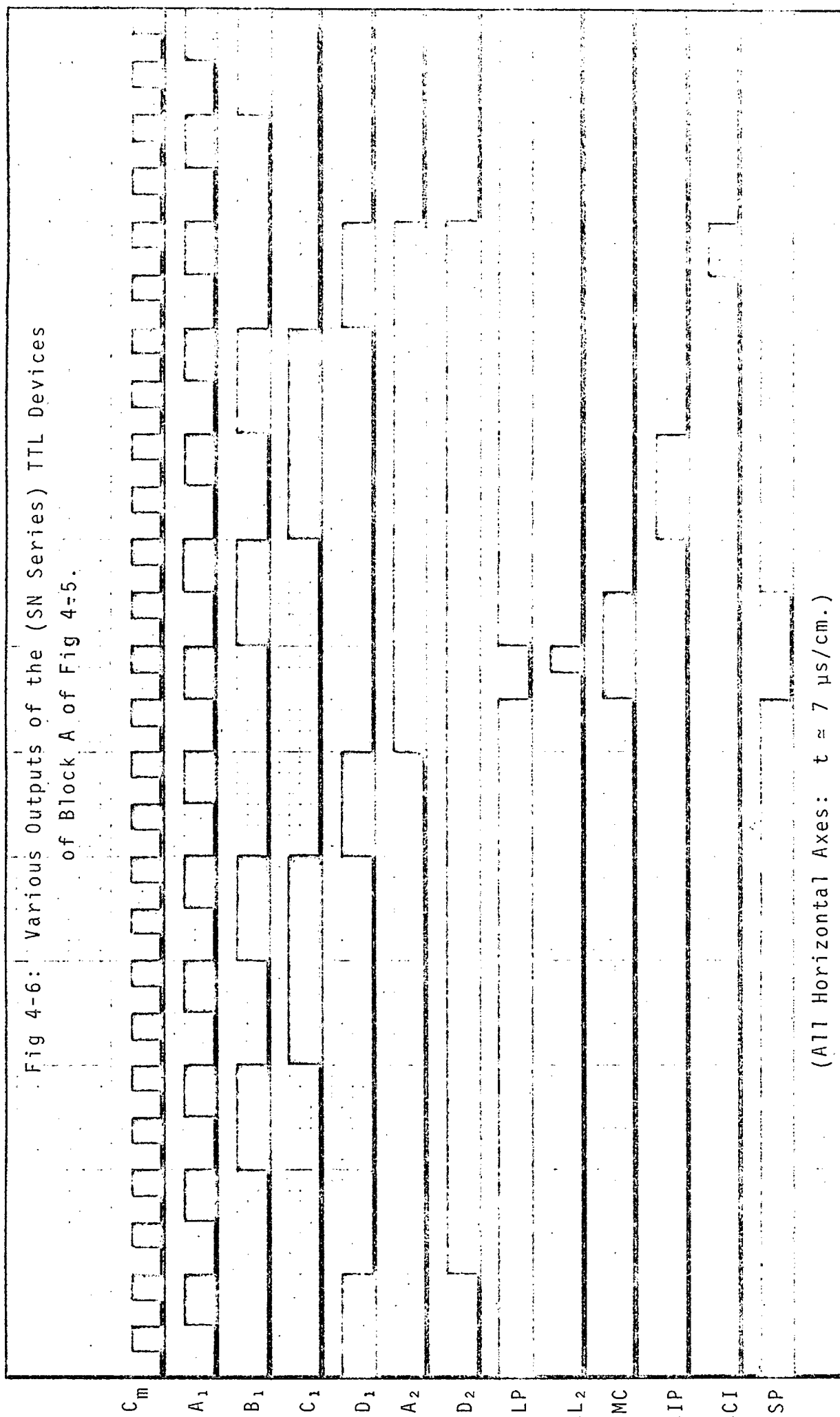

Fig 4-6: Various Outputs of the (SN Series) TTL Devices of Block A of Fig 4-5.

(All Horizontal Axes: t ≈ 7 μs/cm.)

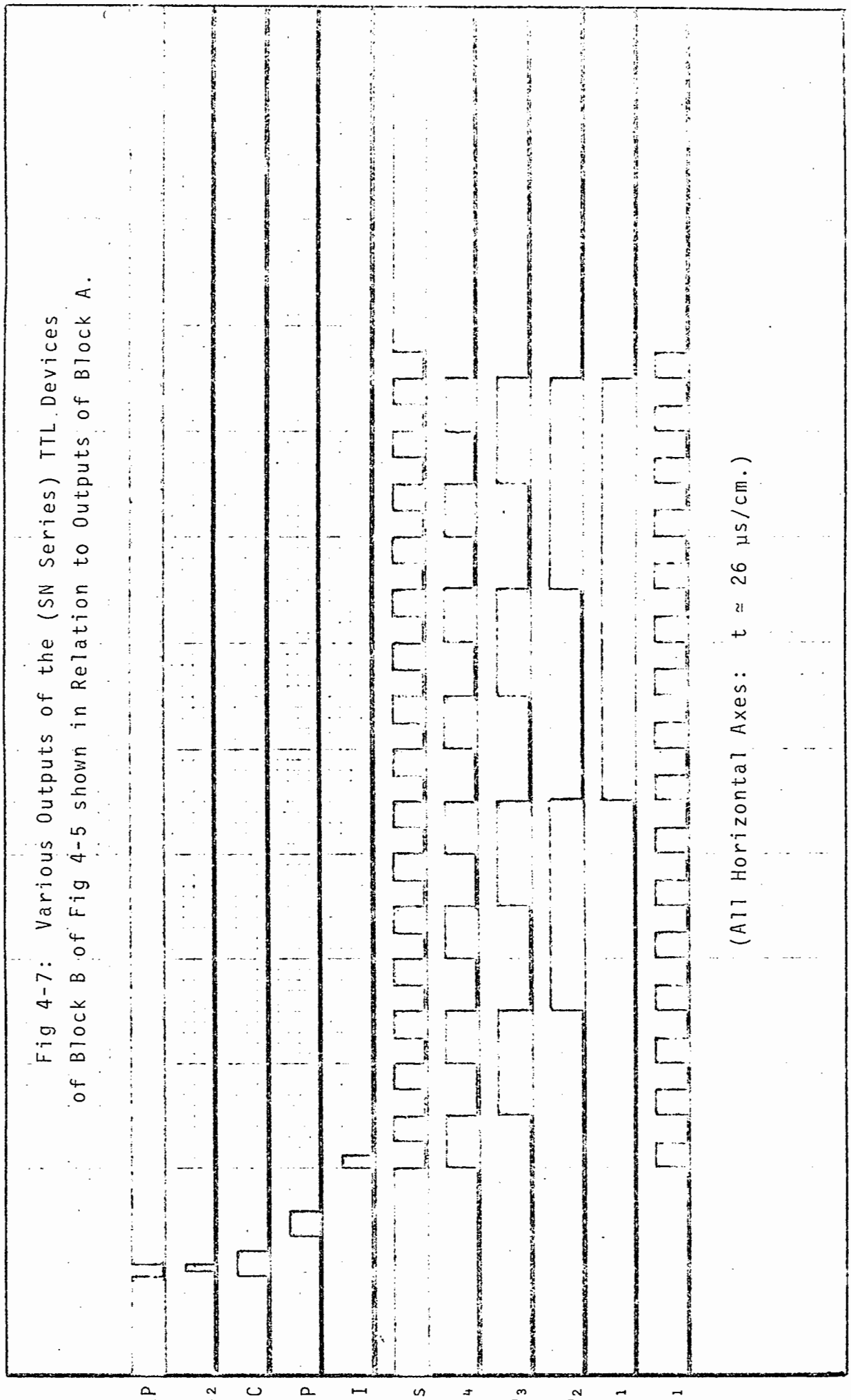

Fig 4-7: Various Outputs of the (SN Series) TTL Devices of Block B of Fig 4-5 shown in Relation to Outputs of Block A.

These are used to empty the shift registers of their 16 data bits per cycle. Four J-K Flip-Flops (type SN 7476) are used as the counting elements, and these are driven by the same type of square-wave generator as is used to drive the master clock. This time however, one of the inputs is used to turn it on at the correct time each cycle, and to turn it off again once it has clocked all the information out of the shift registers. The Boolean expression for the slave clock to be on is

$$C_s(on) = (SCI) + \overline{C_s \cdot \bar{Q}_1 \cdot \bar{Q}_2 \cdot \bar{Q}_3 \cdot \bar{Q}_4} \qquad (4\text{-}84)$$

where SCI - slave clock initiating pulse
C_s - slave clock output, and
Q_i - output of i th J-K Flip-Flop.

As shown in Fig 4-5 and 4-7, C_s must first be inverted before the 16 shift register clock pulses are obtained.

The operational time of the slave clock should be approxi= mately 60% of the master clock cycle, so that the remaining 40% may be used as a synchronising gap for the data reception on the ground. Hence one period of C_s should be

$$t = (0,6)\{\frac{700 \times 10^{-6}s}{16}\} \simeq 26 \times 10^{-6}sec \qquad (4\text{-}85)$$

Using Equation 4-83

$$R_2C_2 = \frac{26 \times 10^{-6}s}{1,2} = 22 \times 10^{-6}sec \qquad (4\text{-}86)$$

Hence if $R_2 = 220\ \Omega$

then $C_2 \simeq 0,1\ \mu F$

The operation of the SN 7495 shift registers is controlled by three of its inputs, which in the TTL handbook are called the "Clock 1", "Clock 2" and "Mode Control" inputs ... (CL 1, CL 2 and MC).

When a logical 0 is applied to the MC input, and CL2 ex= periences a transition from the 1 to the 0 state, then any

information present at the data inputs will be entered into the register. Right-shift operation can then be performed by applying a 1 to the MC and clocking the CL 1 input.

Inspection of Figures 4-6 and 4-7 shows the order in which these inputs are pulsed.

Formally

$$(CL\ 1) = \overline{C_s} \tag{4-87}$$

$$(CL\ 2) = (\overline{LP}) \cdot C_m \tag{4-88}$$

$$(MC) = (\overline{LP}) + \{\overline{A}_1 \cdot B_1 \cdot \overline{C}_1 \cdot D_1 \cdot A_2 \cdot D_2\} \tag{4-89}$$

As has already been mentioned, each data sequence is preceded down to ground by the "Count-initiating-pulse", (CIP), which can be expressed as

$$(CIP) = \overline{B}_1 \cdot C_1 \cdot A_2 \cdot D_2 \tag{4-90}$$

In the above equations LP denotes the negative going pulse which activates the LED pulsing circuit described in Section 4-10.

$$(LP) = \overline{A_1 \cdot \overline{B}_1 \cdot \overline{C}_1 \cdot \overline{D}_1 \cdot A_2 \cdot D_2} \tag{4-91}$$

The Slave Clock Initiating Pulse (CIP) mentioned in Equation 4-84 can be expressed as

$$(SCI) = A_1 \cdot D_1 \cdot A_2 \cdot D_2 \tag{4-92}$$

(Note: A_1, B_1, C_1, and D_1 refer to the outputs of the first decade counter, while A_2 and D_2 refer to those of the second.)

Finally there is the Strobe Pulse (SP) which is used to switch on the LM 311 Comparitors only when a light pulse is anticipated. (See circuit in Fig 4-4).

This was originally necessary to prevent any switching transients from being reflected into the amplifiers and causing instability during the LED's "off" time. However the optical semiconductors used then, have since been outmoded and it has been possible to significantly reduce the gains of the ampli= fiers with the advent of more efficient emitters. However

IT WAS/

it was still decided to keep the strobe facility as an added safety feature, since the full extent of the overhead electrical noise can probably never be ascertained.

$$(SP) = (\overline{MC}) \qquad (4\text{-}93)$$

A problem was encountered in that switching transients from the TTL pulses which occurred during the amplifier operational period, were injected into the amplifier output. The most important offender in this regard was CL 2 itself - the pulse used to coherently detect the incoming signals. To overcome this a simple RC integrator circuit was inserted in series with the CL 2 line, and also with the other offender, the strobe pulse (SP).

The integrators, which had time constants of the order of $\frac{1}{2}$ μs, successfully eliminated all the previously induced noise in the amplifier outputs.

4-40 POWER SUPPLY.

The total current drawn by the circuits described in Section 4-10, 4-20 & 4-30 was of the order of 650 mA.

For a power source it was therefore decided to use an "El= power Rechargeable Solid-Gel Battery" which has a 12 volt, 8 amp-hour rating. This proved ideal because of its small size (21 cm x 14 cm x 7 cm), and also because, being "solid gel", it required no servicing save periodic recharging. With its capacity, it was able to operate the circuit for at least 10 hours, which is a full working day, and it can be recharged overnight.

It was mounted on the base of the pantograph and leads were run up the frame members to the circuit. This was necessary because it weighed about 3,5 kg, and there was al= ready too much weight on the pantograph in the form of the heavy steel box which provided the necessary electromagnetic screening.

Since all the circuitry save the LED pulsing circuit operated off 5 volts, two LM309 voltage regulators were used to step down the voltage. (The current demanded was too much for one to handle.) All the standard techniques were employed to reduce noise in the power supply, such as using the box itself as the "earth", and running a lead from the positive outputs of the 5 volt regulators to each individual circuit. Heavy decoupling was applied at every circuit and also at the inputs and outputs of the two regulators. For the TTL circuits, a fast capacitor (Ceramic or Tantulum) was used to decouple the supply at every third IC.

These measures achieved the desired aim, and the supply was relatively noise free. The wiring diagram is shown below.

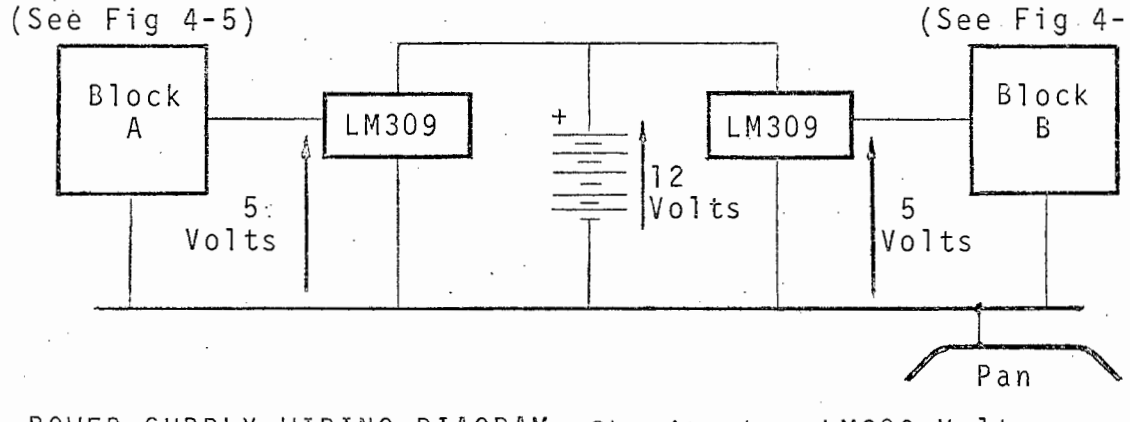

POWER SUPPLY WIRING DIAGRAM: Showing how LM309 Voltage Regulators feed Block A and Block B. (Opto-Amplifiers included in Block B.) Pan connected to Negative Rail.

4-50 DATA TRANSMISSION ACROSS 3kV

This was achieved by an optical link via an eight-metre length of fibre-optic light guide.

The guide used was of the Fort "2G" variety which is ex= tremely flexible and tough. For added protection it was placed inside an equal length of ½ inch PVC hose pipe.

Its electrical isolation capability is quoted at 100 kV/metre. However the actual gap between the 3 kV panto= graph base and the grounded locomotive roof is only about 1/3 metre. The maximum voltage that can safely be borne by the same length of guide is therefore 33 kV, which gives a factor of safety of about 11.

A Monsanto LED (type ME 7124) was used as the light emitter. This is ideally suited to light guide applications as it concen= trates all its radiant energy into a narrow cone of half-angle 4^{o}, hence there is very little wastage.

The device has an absolute maximum continuous current ra= ting of 100 mA. Therefore with a 30% duty cycle and a 66% safety factor, a peak current of 220 mA should not cause any damage. Since this is so low in comparison with the previous LED, it was possible to use a single driver transistor coupled directly to the relevant TTL output. See Fig 4-8.

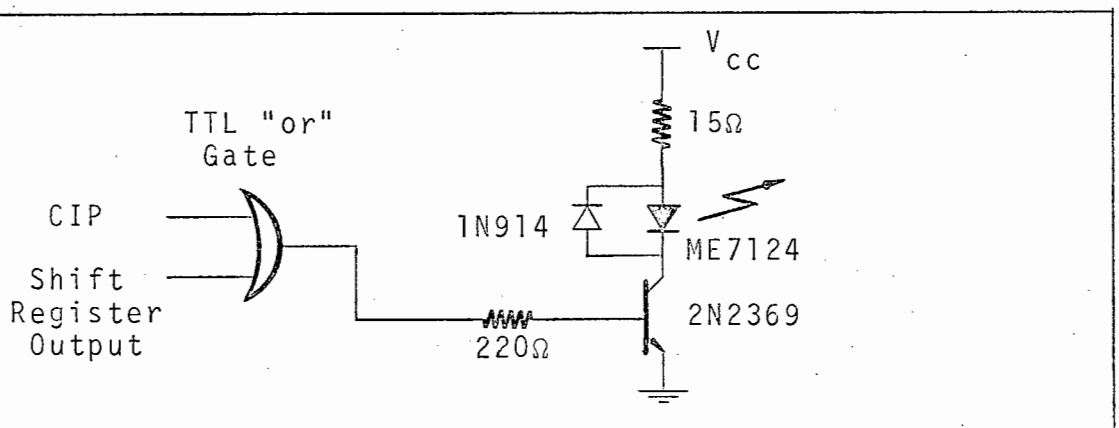

Fig 4-8: Driver Circuit for Light Guide LED.

At 50 mA the LED's total radiant power is quoted at 3 mW, hence at 220 mA it is about 13 mW. However the signal collector current of the phototransistor at the other end of the guide, (also type FPT 100A), was measured at 25 µA.

(From Equation 4-28, this implies an irradiance of 0,02 mW/cm^2;

AND/

and with the emitting area of the guide being 0,13 cm , there is an emergent radiant power of about 2,6 μW. Hence the intensity is attenuated at least 5 000 times along the guide.)

Fig 4-9 shows the detector amplifier circuit which features a front end wired in the series-cascode mode. It has no real advantage or disadvantage over the one described in Section 4-22, and also has the desirable quality of being slower than the one described in Appendix III, 2.

Since this detector will always operate in complete darkness it is not necessary to compensate for varying ambient light levels, so more gain may be obtained from the first stage.

The design follows.
With V'_{cc} set at 4,6 volts and R_2 and R_3 being 39 kΩ and 56 kΩ respectively, the base voltage of T_2 is

$$V_{b2} = \frac{R_3 V'_{cc}}{R_2+R_3} = 2,7 \text{ volts} \qquad (4\text{-}94)$$

The base voltage of the phototransistor is then 1,2 volts higher, hence V_{b_1} = 3,9 volts.

If a collector current of about 0,3 mA is desired in T_1, then the base current of T_1 should be h_{FE} times less, which is about 3 μA.
Hence

$$R_4 = \frac{V'_{cc} - V_{b1}}{I_{b1}} = 230 \text{ kΩ (Say 220 kΩ)} \qquad (4\text{-}95)$$

With R_5 = 2,7 kΩ, the collector voltage of T_2 is about 0,8 volts, which is well below the saturation value.

If R_6 = 100 kΩ, and R_7 = 27 kΩ, then the base voltage of T_3 is

$$V_{b3} = \frac{R_7 V'_{cc}}{R_6+R_7} \simeq 1 \text{ volt} \qquad (4\text{-}96)$$

With R_9 = 1 kΩ, the collector current of T_3 is therefore

I_{c3}/

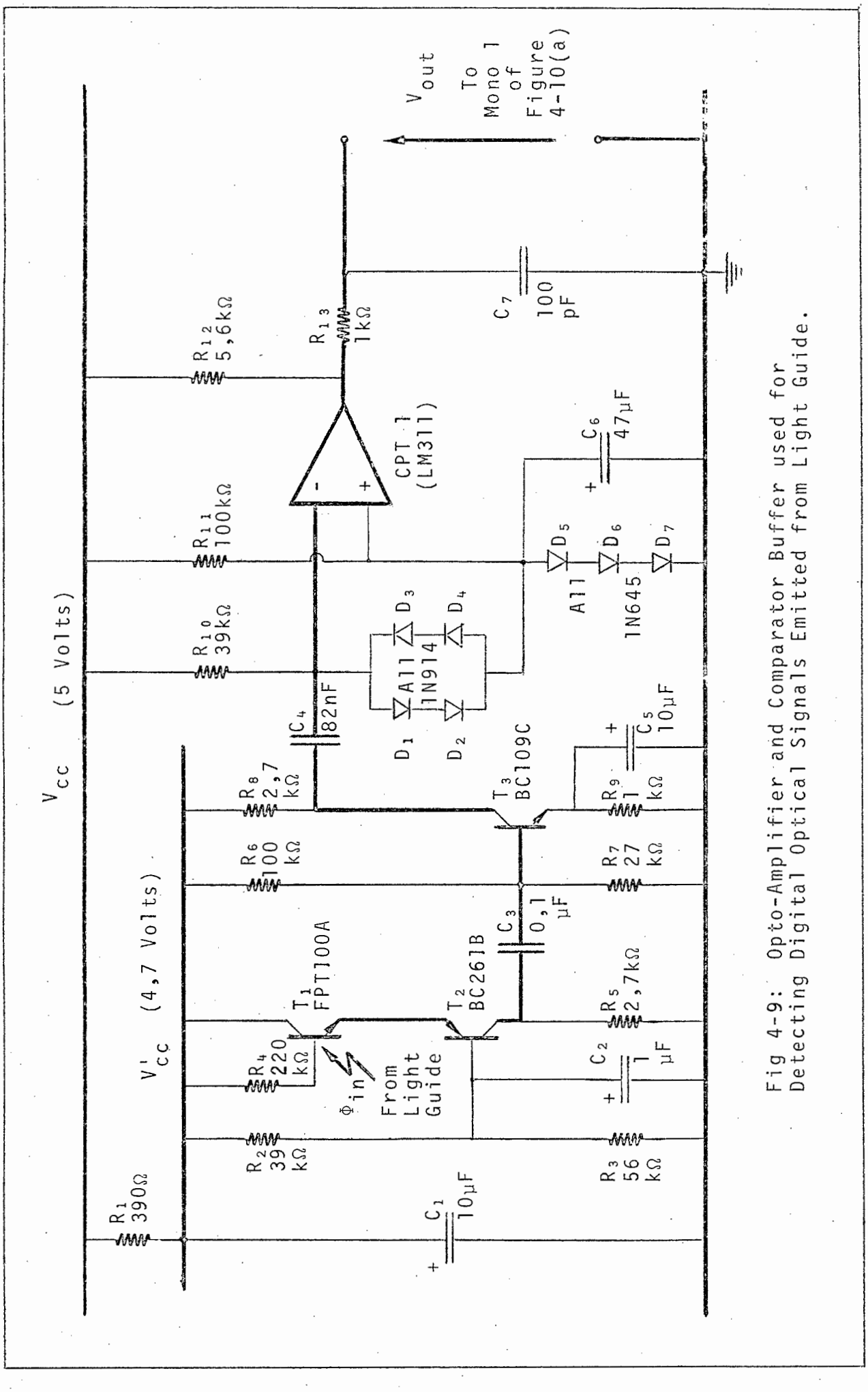

Fig 4-9: Opto-Amplifier and Comparator Buffer used for Detecting Digital Optical Signals Emitted from Light Guide.

$$I_{c3} = \frac{V_{b2} - V_{be(on)}}{R_9} \simeq 0,4 \text{ mA.} \quad (4\text{-}97)$$

The dynamic load resistance of T_2 is then

$$R_{L2} = R_5//R_6//R_7//(\frac{h_{fe}}{g_{m3}}) \simeq 2,2 \text{ k}\Omega \quad (4\text{-}98)$$

If an output signal of about -2 volts is required from the collector of T_3, and the signal collector current of T_1 is 25 µA, then R_9 can be calculated from

$$v_o = (-g_{m3}R_9)(i_{c1}R_{L2}) \quad (4\text{-}99)$$

Hence

$$R_9 = \frac{-v_o}{(40\ I_{c3})(i_{c1}R_{L2})} \simeq 2,4 \text{ k}\Omega.$$

(Say R_9 = 2,7 kΩ, since it appears in parallel with R_{10}, which is 39 kΩ.)
The total supply current drawn by the amplifier was of the order of 1 mA, hence

$$R_1 = \frac{V_{cc} - V'_{cc}}{I} \simeq 390\ \Omega \quad (4\text{-}100)$$

The peak-signal-to-rms-noise ratio of the amplifier was found to be of the order of 70 to 1, which is about 8 times better than the minimum acceptable value derived in Equation 3-84. Inspection of Graph 3-6 shows the resultant error probability to be so small as to be incalculable.

The output signals from the amplifier were fed into a comparator (type LM 311) for TTL buffering. The self-biasing resistor-capacitor-diode network at the comparator front end,

ensures that the non-inverting input remains fixed at the midpoint of the upper and lower voltage extremities of the inverting input.

To slow down the output of the comparator to prevent noise from being injected back into the sensitive amplifier via the supply, an RC integrator circuit was added in series with the output. This comprises R_{13} and C_7 in the diagram which are 1 kΩ and 100 pF respectively. This together with standard supply decoupling proved sufficient.

Because only 8 meters of light guide were obtained, which was too short to reach to every point inside the locomotive, it was necessary to mount the circuit shown in Fig 4-9 inside a separate little box with an extension chord leading to the main decoding circuit and display.

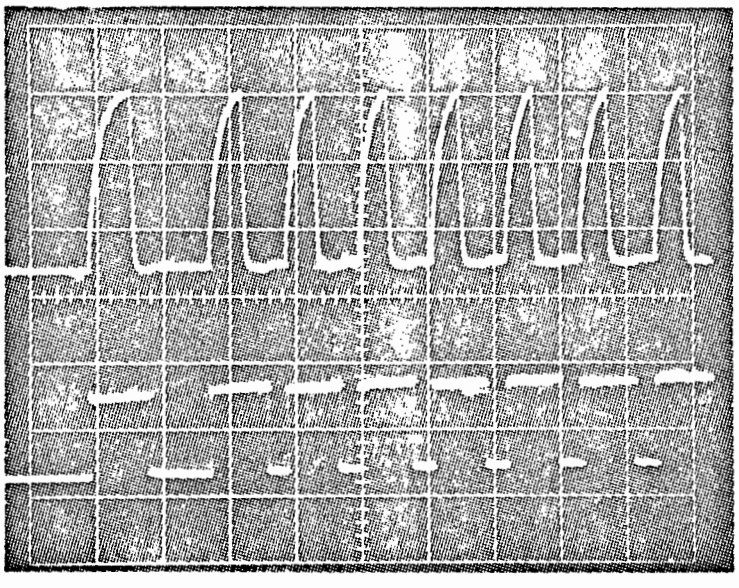

Top Trace: CIP Followed by Data Pulses at Output of Comparator CPT 1 of Fig 4-9.
(Scale: 1 V/div)

Bottom Trace: Output of Mono 1 (M1) of Fig 4-10(a) Showing Time-Lengthening of Data Pulses for Added Noise Immunity.
(Scale: 2 V/div)

(Time Scale: 20 μs/div)

4-60 DATA DECODING AND DISPLAY.

4-61 Data Reception.

Although the peak-signal-to-rms-noise ratio was very high, and the probability of any spurious noise spikes causing the comparator to trigger was negligible, the comparator sensitivity was such that the noise present on the slowly rising amplifier output, was capable of causing multiple triggering as it passed the triggering point.

Slowing down of the comparator output by means of the RC integrating circuit was a partial solution to the problem. To make absolutely sure however, the output was then fed into a non-retriggerable TTL monostable multivibrator (Type SN 74121) which time-lengthened each pulse by a factor of $1\frac{1}{2}$. Hence when the comparator output goes high, the monostable {Mono 1 in Fig 4-10(a)} will trigger and remain on regardless of any oscillations at the crossing point, until the middle of the time interval dividing that pulse's downstroke and next one's upstroke. In this way the large noise immunity was preserved.

Equation 4-82 gives the period of the data pulses t, as about 26 μs. The "on" time of Mono 1 should therefore be

$$t_{M1} = (\tfrac{1}{2}t)(1\tfrac{1}{2}) \simeq 19{,}5\ \mu s \qquad (4\text{-}101)$$

According to the TTL Handbook the pulse width of the SN 74121 monostable can be adjusted by the addition of an external resistor and capacitor. The time is then given by

$$t_M = (RC)\ln 2 \qquad (4\text{-}102)$$

Hence with R_1 arbitrarily set at 3,9 kΩ, C_1 becomes 7,2 nF - (say 6,8 nF)

The output of Mono 1 then divides into two — one path going to a 5-bit serial binary counter comprising 5 J-K Flip-Flops (Type SN 7476), and the other going to a second SN 74121 Monostable Multivibrator (Mono 2).

The operation of the circuit is explained in Fig 4-10(b).

THE LEADING/

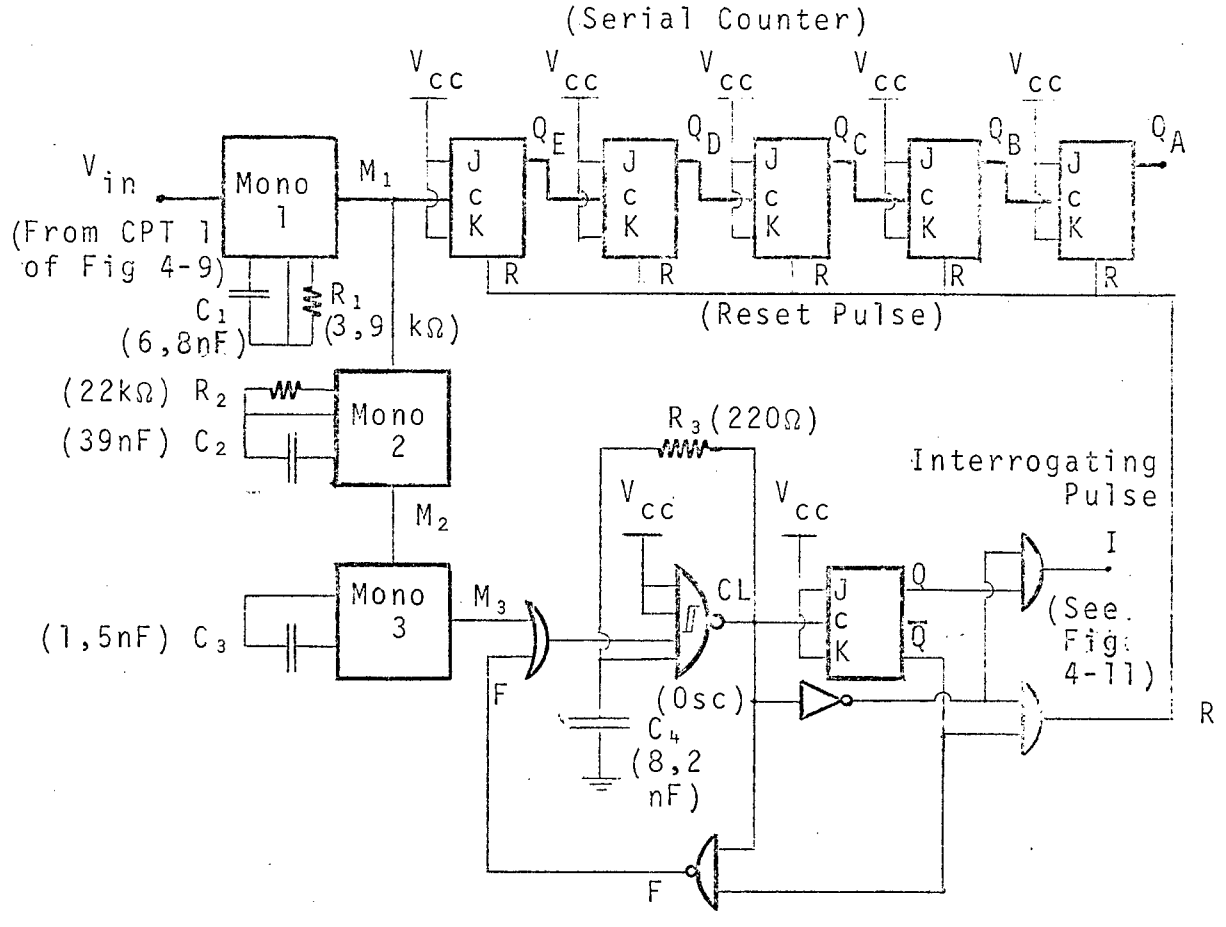

Fig 4-10(a): Serial Counter for Counting Number of Light Pulses Received via Light Guide, and Associated Synchronising Circuitry.

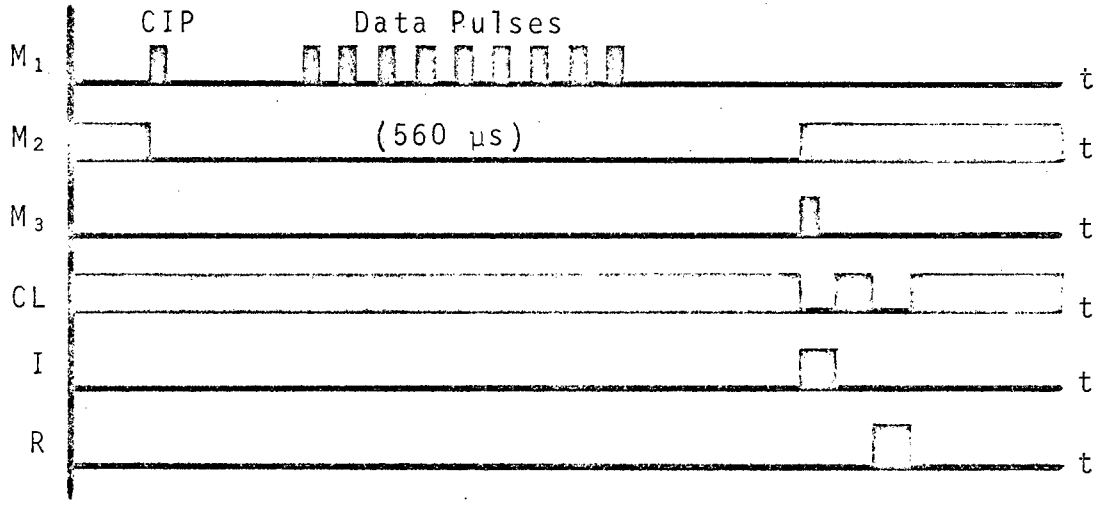

Fig 4-10(b): Associated Waveforms of Circuitry Shown in Fig 4-10(a). Data Pulses Arrive During On-Time of Mono 2.

The leading edge of the first pulse of each cycle (the CIP) triggers Mono 2, while the falling edge registers a count of 1 in the serial counter. The following data pulses are then also clocked up.

Mono 2, which is really the main time-keeper of the circuit, utilises the 40% synchronising gap to extract the data from the binary counter and then to reset it to zero in readiness for the next train of pulses. It remains on until a point in the cycle midway between the last possible data pulse and the beginning of the next cycle - in other words for about 80% of the cycle. From Equation 4-102

$$R_2C_2\ln 2 = (0,8)(0,7\times10^{-3}\text{sec}) \qquad (4\text{-}103)$$

Hence

$$T_{M2} = R_2C_2 \simeq 8,1\times10^{-4}\text{sec.}$$

Hence if R_2 is set at 22 kΩ, then C_2 should be 37 nF - (say 39 nF).

The rising edge of Mono 2 is used to trigger Mono 3 (also type SN 74121). This activates a divide-by-two counter comprising a "quad-input nand gate with hysteresis" (type SN 7413) which is used in the oscillating mode, and a J-K Flip-Flop (type SN 7476). This link passes via a two-input "nor" gate, the other input of which is used in a feedback loop which stops the oscillator (CL) after a count of 2.

The first of these pulses is used as an interrogating pulse "I", which interrogates the 5-bit counter to see how many data pulses have been sent down that cycle. The second "R" resets the counter outputs to zero in readiness for the next series of pulses.

The time available for this operation is of the order of 140 μs, but by exploiting TTL speeds it is possible to complete it in very much less time. Setting C_3 to 1,5 nF and using the internal timing resistor of Mono 3 (nominally 2 kΩ), a pulse width is obtained of approximately

$$T_{M3} = R_iC_3\ln 2 = 2\ \mu\text{s.} \qquad (4\text{-}104)$$

For the following counter to stop after a count of 2, Mono 3's

OUTPUT/

output must already have returned to zero before the count is over. Using Equation 4-82 this is assured by setting

$$R_3C_4\{\ln(\frac{V_{max} - V_L}{V_{max} - V_U}) + \ln(\frac{V_U - V_{min}}{V_L - V_{min}})\} \doteq 2T_{M3} \qquad (4\text{-}105)$$

Hence

$$R_3C_4 \simeq 1{,}7\times10^{-6} \text{ sec} \qquad (4\text{-}106)$$

Setting $R_3 = 220\Omega$ implies that C_4 should be about 7,8 nF (say 8,2 nF), and the total counting operation will be completed in about 6 μs.

To stop the oscillator at the required time, the feedback voltage F should be made to go low when both CL and $\overline{Q}$ are in the "1" state.

Formally

$$F = \overline{(CL)\cdot\overline{Q}} \qquad (4\text{-}107)$$

In Boolean notation, the expressions for the Interrogating and Reset pulses are:

$$I = (\overline{CL})\cdot Q \qquad (4\text{-}108)$$

$$R = (\overline{CL})\cdot\overline{Q} \qquad (4\text{-}109)$$

4-62 Data Interrogation.

The data interrogation circuitry is shown in Fig 4-11. For maximum efficiency in TTL gate usage, a Karnaugh Map was used in the analysis which follows below. The logic conditions derived are those explained in Section 4-31.

$$A = \overline{Q}_A \cdot \overline{Q}_B \cdot \overline{Q}_C \cdot \overline{Q}_D \cdot I \quad (4\text{-}110)$$

$$B = \overline{Q}_A \cdot \overline{Q}_B \cdot \overline{Q}_C \cdot \overline{Q}_E \cdot I \quad (4\text{-}111)$$

$$C = \{Q_B \cdot Q_C + Q_A \cdot \overline{Q}_E\} \cdot I \quad (4\text{-}112)$$

$$D = Q_A \cdot Q_E \cdot I \quad (4\text{-}113)$$

$$\text{"-"} = Q_B \cdot \{Q_C \cdot \overline{Q}_D + Q_C \cdot \overline{Q}_E + \overline{Q}_C \cdot Q_D \cdot Q_E\} \cdot I \quad (4\text{-}114)$$

$$\text{"0"} = \overline{Q}_B \cdot Q_C \cdot Q_D \cdot Q_E \cdot I \quad (4\text{-}115)$$

$$\text{"1"} = \overline{Q}_C \cdot \overline{Q}_D \cdot \overline{Q}_E \cdot I \quad (4\text{-}116)$$

$$\text{"2"} = Q_B \cdot \overline{Q}_C \cdot \overline{Q}_D \cdot Q_E \cdot I \quad (4\text{-}117)$$

$$\text{"3"} = Q_B \cdot \overline{Q}_C \cdot Q_D \cdot \overline{Q}_E \cdot I \quad (4\text{-}118)$$

$$\text{"4"} = Q_B \cdot \overline{Q}_C \cdot Q_D \cdot Q_E \cdot I \quad (4\text{-}119)$$

Number of Pulses					
Decimal	Binary				
	Q_A	Q_B	Q_C	Q_D	Q_E
0	0	0	0	0	0
1	0	0	0	0	1
2	0	0	0	1	0
3	0	0	0	1	1
4	0	0	1	0	0
5	0	0	1	0	1
6	0	0	1	1	0
7	0	0	1	1	1
8	0	1	0	0	0
9	0	1	0	0	1
10	0	1	0	1	0
11	0	1	0	1	1
12	0	1	1	0	0
13	0	1	1	0	1
14	0	1	1	1	0
15	0	1	1	1	1
16	1	0	0	0	0
17	1	0	0	0	1

Karnaugh Map

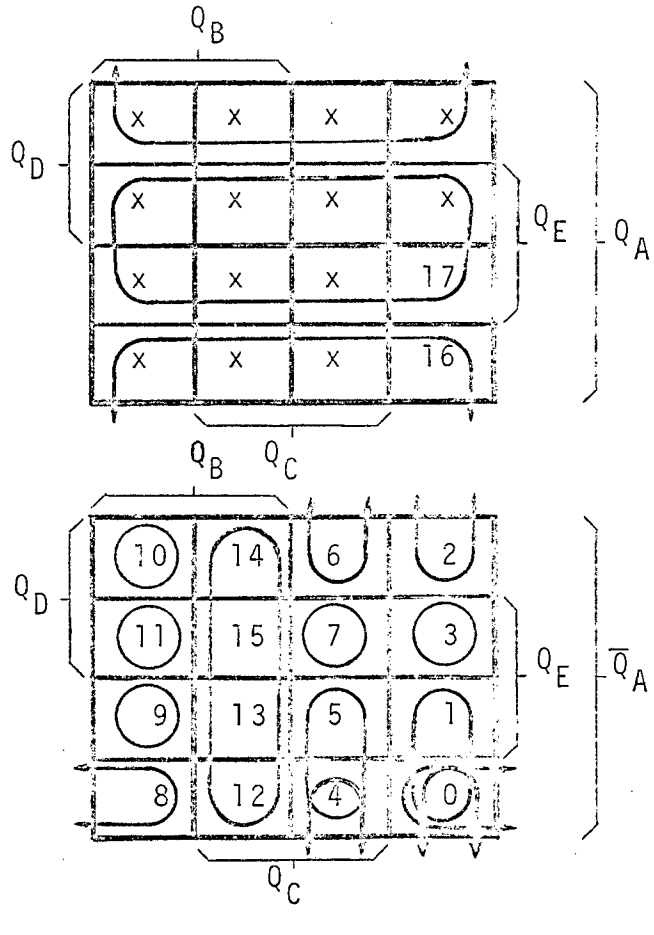

The Various Signal Outputs go to the Corresponding Monostable Inputs of Fig 4-13 to be Time-Lengthened for Recording and Display Purposes.

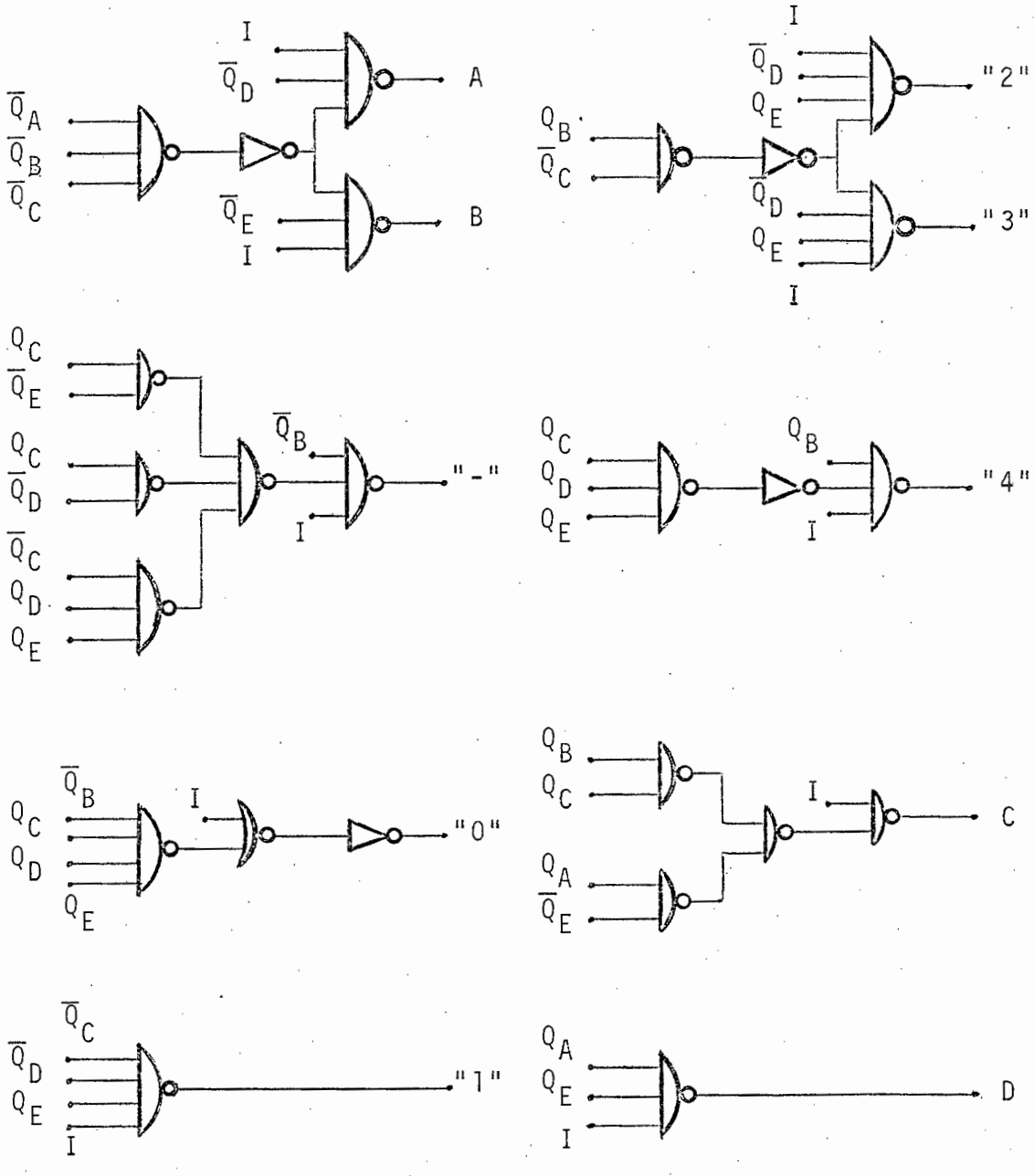

Fig 4-11: Digital Circuitry for Interrogation of Serial Counter Shown in Fig 4-10(a). (TTL Realisation of Boolean Equations 4-110 through to 4-119.)

The outputs of the individual circuits of Fig 4-11 are fed into retriggerable TTL monostable multivibrators (type SN 74123), which time lengthen the pulses for display and re= cording purposes. The on-times of these monostables are there= fore of the order of seconds.

Clearly if n different states of the overhead contact wire are detected in n successive 700 μs cycles, then these n states will be displayed immediately in terms of human response times. However since it is more important to know "how bad" the contact wire condition is rather than "how good" it is, the operator need only record the worst condition displayed.

Also if the state of the contact wire remains unchanged for any length of time, then the retriggerable facility of the mono= stables will cause that state to be registered for as long as it endures, plus of course the on-time of that particular mono= stable.

4-63 Data Display and Recording.

(a) The lay-out of the display panel is shown and explained in Fig 4-12. For the symbols "-" through to "4", Monsanto seven segment displays (type MAN7) were used, which were pre-wired to display only the relevant number, and driven by transistors which were in turn activated by the above-mentioned monostables.

For the conditions A, B, C and D, Monsanto visible infra- red emitters were used, (type MV5020), which are specifically made for panel mounting.

The construction of the seven segment displays are such that the segment anodes are commoned internally in the following groups:

(i) Segments "a" and "b" anodes common,
(ii) Segments "c" and "d" anodes common, and
(iii) Segments "e", "f", "g" and "p" anodes common.

The maximum permissible continuous current through a segment is 30 mA, while that of the panel mounted LED's is 70 mA. For safe operation and maximum visability, they were therefore designed to run at 25 mA and 50 mA respectively. The circuit diagram of the display is shown in Fig 4-13.

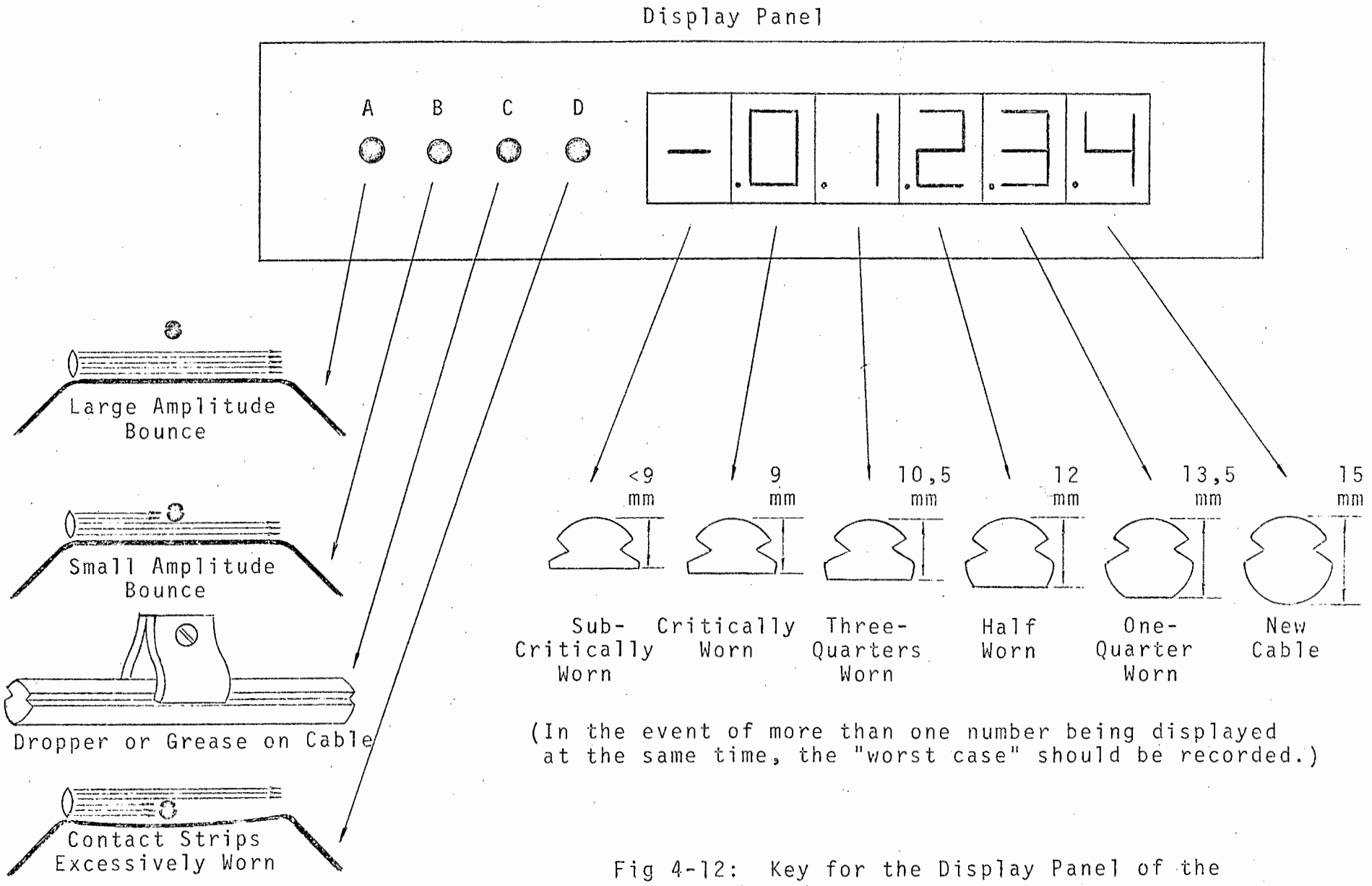

(In the event of more than one number being displayed at the same time, the "worst case" should be recorded.)

Fig 4-12: Key for the Display Panel of the Contact Wire Thickness Gauge.

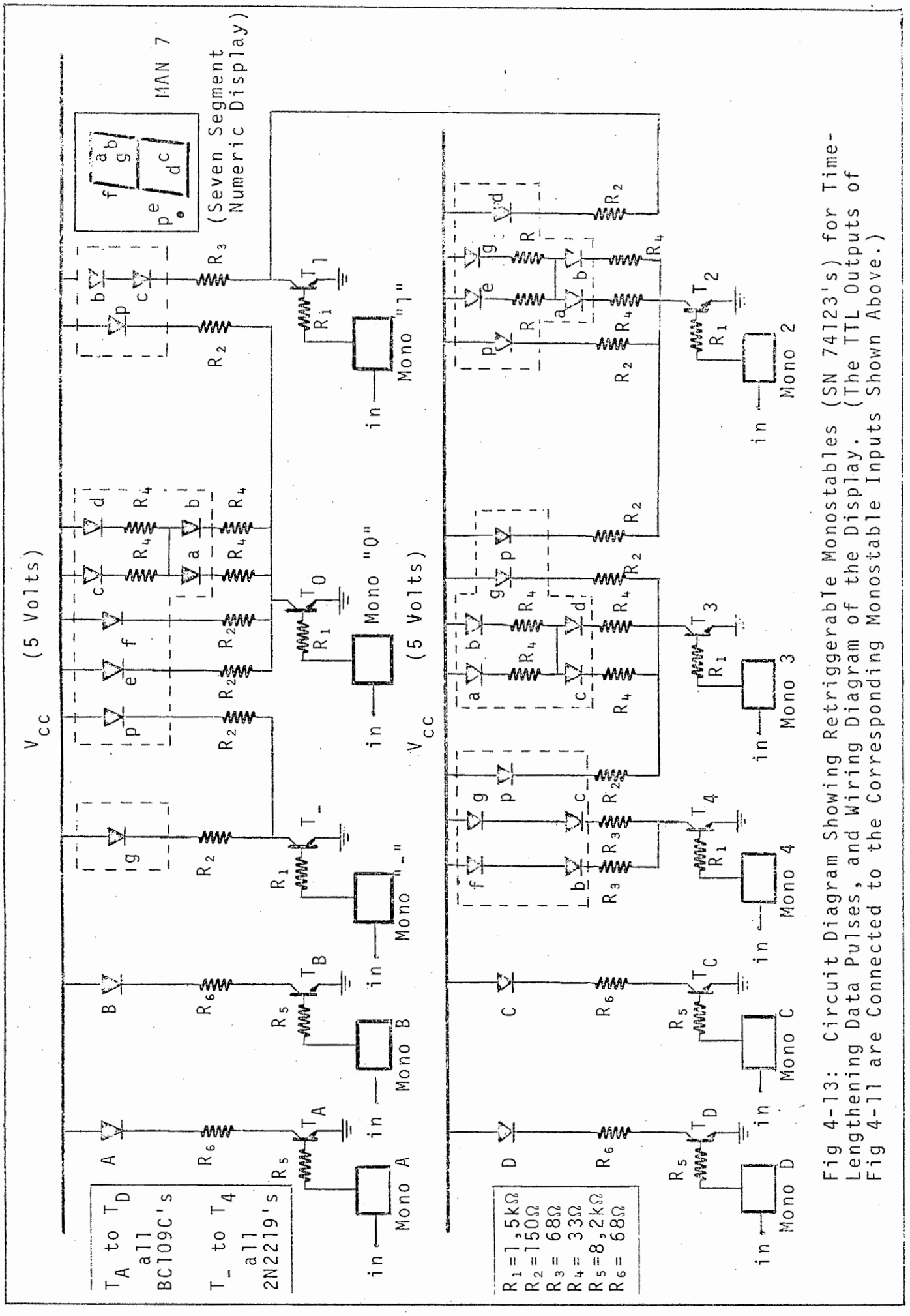

Fig 4-13: Circuit Diagram Showing Retriggerable Monostables (SN 74123's) for Time-Lengthening Data Pulses, and Wiring Diagram of the Display. (The TTL Outputs of Fig 4-11 are Connected to the Corresponding Monostable Inputs Shown Above.)

Because of the geometry of the phototransistor detecting array (see Fig 3-14), clearly each time a dropper clamp goes past, successive detectors on the upper section of the array will be cast into shadow until all are blanked out, save those which receive light from below the contact wire.

Since droppers are spaced at intervals of about 5 metres along the line, if the contact wire were for instance half-worn, then conditions "2", "3" and "4" would be continuously dis= played, together with "C", and the operator would therefore take condition "2" as being indicative of the state of the wire.

The pulse widths of the SN 74123 Monostables were weighted according to the seriousness of their respective conditions. According to the TTL Data Book, these could be set by the addition of an external resistor and capacitor, the values of which could be derived from the following equation.

$$t = 0{,}28\ RC\left(1 + \frac{700}{R}\right) \text{ seconds} \qquad (4\text{-}120)$$

Hence:

Mono "-", Mono "0": R = 22 kΩ, C = 1 000 µF ⟹ t = 6,4 seconds

Mono "1": R = 15 kΩ, C = 1 000 µF ⟹ t = 4,4 seconds

Mono "2", Mono "3", Mono "4": R = 22 kΩ, C = 470 µF ⟹ t = 3,0 seconds

Mono "A", Mono "B": R = 22 kΩ, C = 470 µF ⟹ t = 3,0 seconds

Mono "C": R = 2,2 kΩ, C = 470 µF ⟹ t = 0,4 seconds

Mono "D": R = 22 kΩ, C = 1 000 µF ⟹ t = 6,4 seconds

(b) The recording of the data posed more of a problem because of the high information density of the incoming signals.

With a maximum of 17 pulses capable of being transmitted to ground every 700 µs, the information density is about 24 Kilo-Bits per second. Even after being clocked into the serial counter, which has 5 separate outputs, it is still over 7 Kilo-Bits per second, so recording of every binary word is

STILL OUT/

out of the question.

Eventually it was decided to use a circuit which would reject all irrelevant information in much the same way as would a human operator, and only select the worst case at any particular time. Furthermore, instead of being recorded digitally, a pen recorder would plot out the profile of the contact wire. No accuracy would be lost in this digital-to-analog conversion because the signal would be in large, well-defined steps.

Since the response times of pen recorders are of the same order of magnitude as humans, the information would also first have to be time-lengthened, so the same monostable outputs could be utilised as are used to drive the display lights.

Fig 4-15 shows the circuit developed to achieve this. The dotted rectangle represents a TTL open-collector hex-inverter (type SN 7405) - one inverter being used for each of the conditions "-" through to "4". Each inverter output is fed via a resistor-divider network to what is basically a "selective or function" device, comprising diodes D_- through to D_4 and resistor R_3.

Starting with the "-" state, the voltages created by each divider at the output at each diode's cathode, increases with each successive state by approximately equal intervals. Only one diode can conduct at any one instant of time, viz. that with the lowest cathode voltage, since the others will all be reverse biased. The darlington arrangement of T_1 and T_2 then forms a buffer capable of supplying the required current to drive a pen recorder. Resistor R_4 is included to limit the current in case of a short circuit.

The emitter voltage of T_2 for each state can be calculated as follows:

$$V_1 = \frac{(V_{cc} - V_{sat})R_2}{R_1 + R_2} + V_{sat} \qquad (4\text{-}121)$$

where V_{cc} = 5 volts (Supply voltage)

V_{sat} = 0,2 volts (Saturation voltage of the inverters.)

THEN/

Then

$$V_{b1} = V_1 + \frac{(V_{cc} - V_1 - V_D)R_2}{R_3} \qquad (4\text{-}122)$$

where V_D = 0,6 volts (Diode forward bias voltage).

and V_{b1} = base voltage of T_1.

The emitter voltage is then

$$V_{out} = V_{b1} - V_{be_1(on)} - V_{be_2(on)} \qquad (4\text{-}123)$$

where $V_{be_1(on)}$ and $V_{be_2(on)}$ are the forward bias base-emitter voltages of T_1 and T_2 respectively, and approximately equal to 0,6 volts each.

The following table shows the various values of R_1 and R_2, together with the corresponding output voltage, as well as the voltage interval between states at the output. R_3 was chosen to be 68 kΩ.

State	R_1	R_2	V_{out}	ΔV
"4"	3,9 kΩ	6,8 kΩ	2,67 v	
"3"	4,7 kΩ	5,6 kΩ	2,23 v	} 0,44 v
"2"	2,7 kΩ	2,2 kΩ	1,79 v	} 0,44 v
"1"	3,3 kΩ	1,8 kΩ	1,33 v	} 0,46 v
"0"	3,3 kΩ	1,2 kΩ	0,92 v	} 0,41 v
"-"	3,3 kΩ	0,68 kΩ	0,47 v	} 0,45 v

R_5 and R_6 are "bleeder" resistances which maintain small quiescent currents in T_1 and T_2 when there is no load at the output. They were chosen to be 560 kΩ and 5,6 kΩ respectively.

In the event of information involving contact wire bounce and the state of the contact strips also being required, a similar circuit was built which had only two inputs - B and D. Since case D was the least likely to occur, and also the more

SERIOUS/

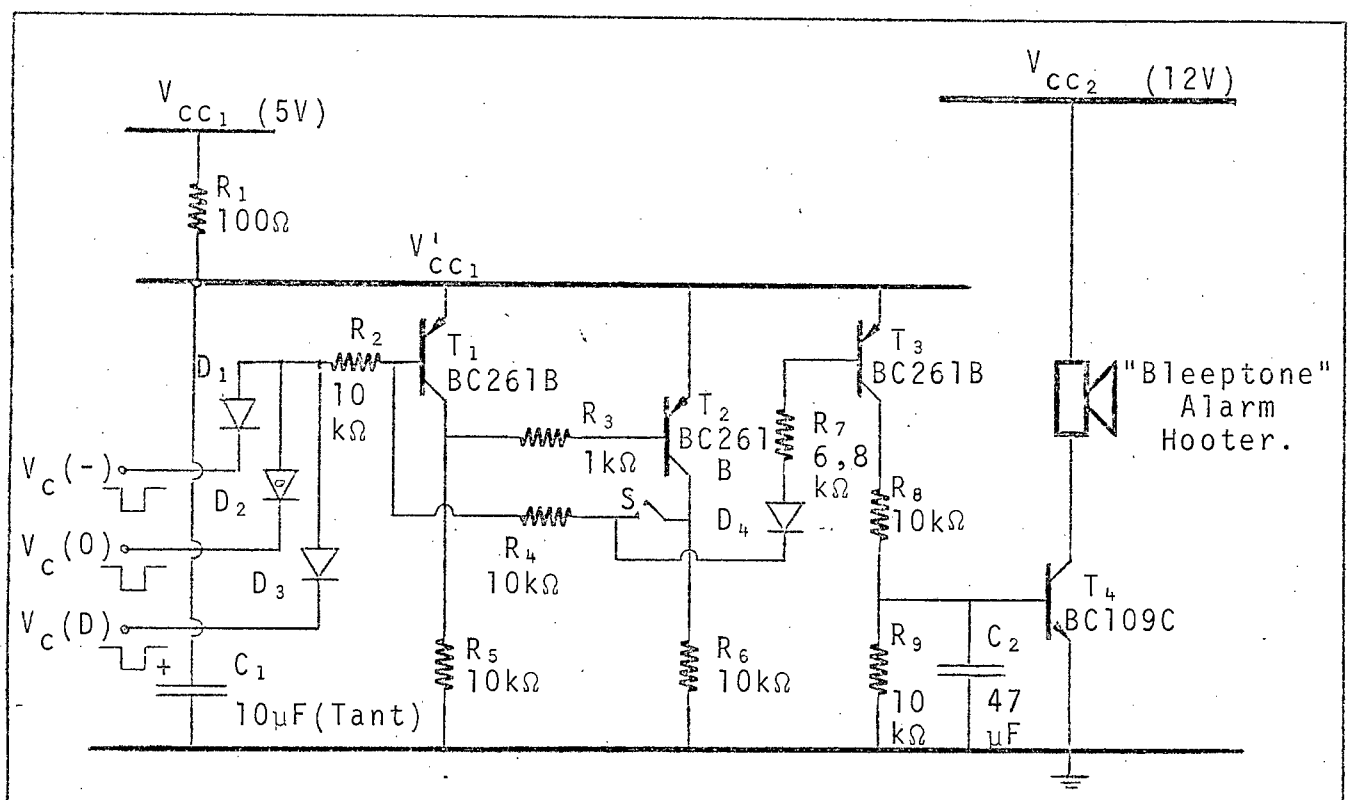

Fig 4-14: Alarm Circuit. T_3 & T_4 Form a Latch Circuit which, once Triggered, Keeps the Hooter on as Long as the Switch S is Closed.

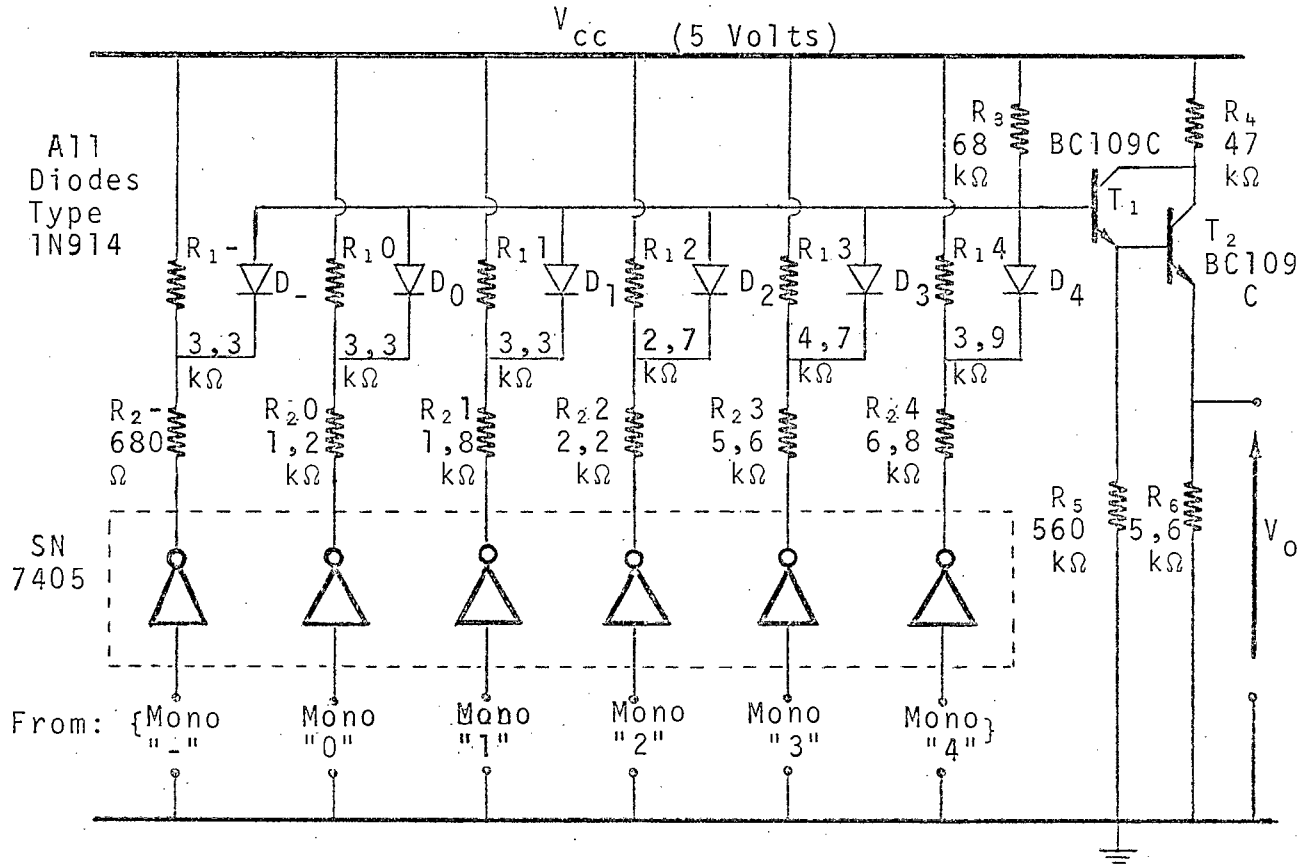

Fig 4-15: Circuit used for Selecting "Worst Condition of Contact Wire. The Output is fed via a Darlington Buffer (T_1 & T_2) to a Pen Recorder.

serious of the two, it was designed to overide the bounce signal.

4-64 Alarm Circuit.

It was decided to incorporate an alarm into the circuit, to sound whenever one of the more serious overhead conditions is detected, (the "-" and the "0" states), and also when the shoe contact strips are excessively worn (state D).

This would warn the operator if he did not happen to be watching the display panel at that particular moment, allowing him to note the position along the track where the contact wire needed attention.

The circuit used for this is shown in Fig 4-14, where the three inputs are taken directly from the collectors of T_-, T_0 and T_D of Fig 4-13. These usually rest in the high state, but when any of them goes low, the diodes D_1, D_2 and D_3 perform an "or" function, and T_1 is turned on.

T_1 and T_2 combine to form a latch circuit, which, once triggered, remains on for as long as the switch S is closed. When T_2 is turned off, base current from T_3 is allowed to flow via R_7, D_4 and R_6, hence T_4 is also turned on and the "Bleep= tone" alarm hooter activated.

The hooter operates from a 12 volt supply, and draws 15 mA of current. It emits a shrill tone which can be heard quite clear= ly inside a locomotive.

It was found necessary to decouple at the base of T_4, since otherwise the hooter emitted short "blips" of sound whenever any noise spikes were injected into supply V_{cc1} (5volts). For this reason V_{cc1} was also decoupled with the resistor and capacitor combination R_1 and C_2. These measures proved satisfactory.

4-70 POWER SUPPLY FOR SYSTEM ON GROUND.

As in the case of the circuit on the pantograph, an Elpower 12 volt, 8 amp-hour solid-gel rechargeable battery was used as the energising source. It supplied current both to this circuit, and to the receiver circuit described in Section 4-50.

When all the display lights were on, about 1,1 amps were required, and when all were off, about 0,6 amps. The average operating current was about 0,8 amps, so this circuit was also capable of running for about 10 hours, (or one working day) before requiring recharging.

As before, two LM309 voltage regulators were used to share the current, and to step down the voltage to the required 5 volts; and standard decoupling rules were applied. The Power Supply Wiring Diagram is shown below.

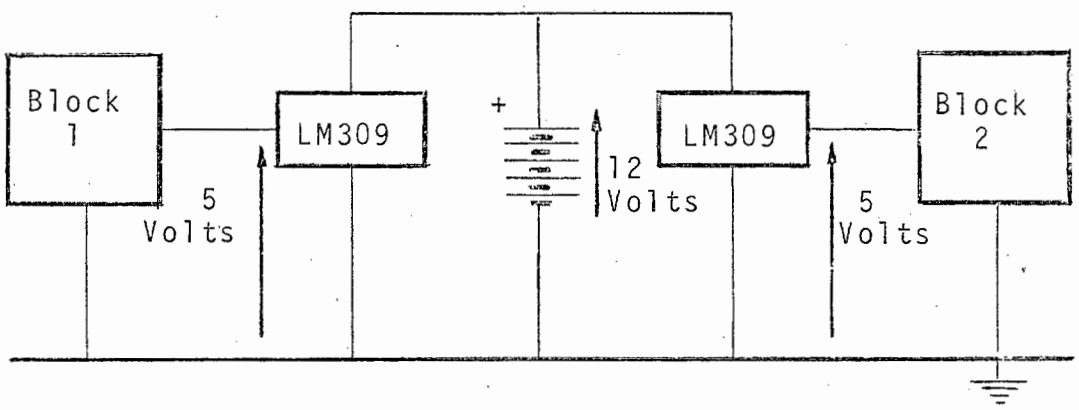

POWER SUPPLY WIRING DIAGRAM: Showing how LM309 Voltage Regulators are used to Supply Current to Circuitry inside Motorcoach.

(Block 1 contains circuitry of Figs 4-9, 4-10 & 4-11.)
(Block 2 contains circuitry of Figs 4-13, 4-14 & 4-15.)

REFERENCES.

1. "NPN Planar Phototransistors: FPT 100/100A/100B, FPF 110/110A/110B", Fairchild microwave and Optoelectronics Division, August 1971.

2. JOHN BLISS: "Build Reliable Optoelectronic Circuits by knowing how to use data on photosensors and light sources, both incandescent and solid-state", Electronic Design 3, Feb 3, 1972, pp 52 - 56.

3. ALEX G. SMITH: "Radio Exploration of the Sun",
   (a) p 63
   (b) p 69.

4. MISCHA SCHWARTZ: "Information Transmission, Modulation and Noise - Second Edition", Mc Graw Hill, Kogakusha. p 419.

C H A P T E R 5

RESULTS.

5-10 PERFORMANCE IN THE LABORATORY.

5-11 Accuracy.

To check the device's accuracy of measurement tests were conducted with rods of different but accurately known diameters. At least 20 readings were taken for each rod, each one in a different position relative to the detectors, and also relative to the contact strips of the pantograph shoe. The measured probability* of a rod of given diameter being correctly or incorrectly classified is recorded in Table 5-1.

TABLE 1-5	Probability of a Condition being Displayed.						
Rod Diameter	"-" (< 9 mm)	"0" (9 mm)	"1" (10,5 mm)	"2" (12 mm)	"3" (13,5 mm)	"4" (15 mm)	"C" (> 15 mm)
7,0 mm	100%	-	-	-	-	-	-
8,0 mm	65%	35%	-	-	-	-	-
9,0 mm	5%	85%	10%	-	-	-	-
9,7 mm	-	50%	50%	-	-	-	-
11,0 mm	-	5%	70%	25%	-	-	-
12,0 mm	-	-	15%	75%	10%	-	-
13,0 mm	-	-	-	30%	65%	5%	-
14,3 mm	-	-	-	-	50%	50%	-
15,0 mm	-	-	-	-	-	70%	30%
16,0 mm	-	-	-	-	-	25%	75%
17,0 mm	-	-	-	-	-	-	100%

As can be seen the errors are of the order of magnitude predicted in Section 3-20; in other words a reading is never out by more than one inter-detector spacing, and that for only a relatively small portion of the time. When the rod diameter

*These results apply to the new lens.
See Section 5-20.

IS EXACTLY/

is exactly midway between two successive resolution conditions, then each condition is registered for 50% of the time.

Also the effect of the spherical aberration of the lens is clearly apparent in that the accuracy of measurement is different for different zones of the lens. The distance between lens and emitter was therefore set to ensure maximum accuracy for the smaller diameter rods.

The readings in Table 5-1 are valid only if the contact surface of the contact wire is parallel to the plane of the upper surface of the pantograph shoe. As was expected, the staggering of the phototransistors in their "vertical" array resulted in the system not tolerating any tilting of the shoe relative to the wire. Inspection of Fig 3-14 shows that even as little as a 5^{o} tilt is sometimes sufficient to cause a detector to receive, or not to receive, the optical signal. (It is true that a one-dimensional vertical array would be subject to a cosine law, but this effect would be negligible in comparison to a whole row of detectors suddenly being cast into or out of shadow by virtue of a tilt.)

By lifting the sample rods out of the beam, the circuit's ability to recognise the large and small amplitude bounce con= ditions, ("A" and "B") was also verified; while casting 11 to 15 detectors in shadow at any instant caused a "C" to be dis= played. When all the detectors were occluded, a "D" was registered.

5-12 Noise Immunity.

(a) Optical:

Two tests were performed to ascertain the circuit's immunity to optical interference. In the first a mirror was used to re= flect the light from a bright, midsummer morning sun, directly onto the detectors.

As predicted, in the absence of the infra-red filter, the phototransistors became saturated. However, with the filter in place, the circuit functioned as normal.

Such an extreme condition is not likely to occur in practice though, since the detectors are housed at the back end of a

protective cylinder.

In the second test, optical noise was injected into the system by means of a 200 Watt, 220 volt light bulb. With the infra-red filter in position, the circuit proved immune to this provided the source was not within 10 cm of the detectors.

The reason for the bulb upsetting the circuit and not the sunlight, is that its 100 Hz fluctuation is an infinitude of decades higher up the frequency scale, than the solar dc contribution; and the optical amplifiers have a series of low frequency break points, the dominant one of which is at about 2 kHz. (See Graph 4-3).

Since the irradiance of the light bulb at such close range is many orders of magnitude greater than anything likely to be encountered in practice (eg. streetlamps), the problem of optical interference becomes non-existent.

(b) Electromagnetic:

Much concern was felt initially, about the effects of the large overhead magnetic fields on the delicate electronic circuitry to be mounted in such close proximity to it. Hence for screening purposes, the possibility of a multi-layered box was considered, but this was not feasible because of the limited weight allowed on the pantograph, especially since the outer layer would have to consist of a strong metal capable of withstanding any reasonable mechanical impact.

Eventually a single-layer box was constructed out of 1 mm steel, which also features the high permeability necessary for magnetic screening. An overlapping layer was fixed around the perimeter of the box opening, making a slot for the lid to fit into, as shown in Fig 5-1. This makes it more difficult for a magnetic field to penetrate.

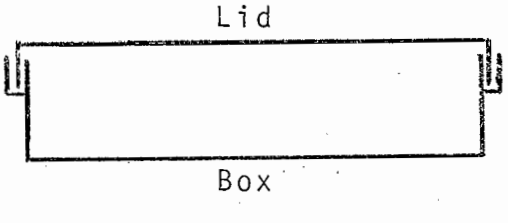

Fig 5-1: Cross-Section of Box used to Screen Circuitry from Large Overhead Magnetic Fields.

The screening capabilities of the box were then tested by wrapping a few turns of heavy duty cable around the primary of a power transformer, looping it around the box, and then joining it back on itself. When the primary was excited, a current of 2 000 amps pk-pk was measured in the cable. This had no affect on the circuit operation. Even the transients caused by making and breaking the secondary circuit, (ie. the cable itself), had no noticeable effects. The magnitudes of the transients were not measured, but it was assumed that they were large enough to justify a field test.

5-20 ASSESMENT IN THE FIELD.

5-21 As a Measuring Device.

The initial field test showed that the system, as a contact wire measuring device, was a feasible proposition. On straight sections of track, and at speeds less than 40Km/hr, the system functioned acceptably. However it was clear that some minor modifications were necessary before any meaningful results could be obtained.

These entailed:

(a) Mechanical Rigidity:-

At first the lens housing, was fixed onto the pan at only one point. The reason for this was that the aiming of the light beam was rather critical, and this method of mounting provided a range of adjustment.

The mounting itself was firm enough, but the distributed weight of the housing resulted in a highly underdamped system which oscillated at each impact of the pan against the contact wire. The offset from the central axis, magnified by the dis= tance, was sufficient to cause the light beam to miss some of the detectors.

Not only did this occur at points and at cross-overs, where impact was unavoidable, but also on straight sections of track at speeds in excess of about 40 Km/hr.

The mounting was forthwith changed to a two-point system, with the front one controlling the elevation by means of a screw-thread. Once the light beam has been correctly aimed, the lens housing can be secured in position by means of a lock-nut. This, together with the larger lens mentioned below, enabled satisfac= tory readings to be obtained at speeds of up to 60 Km/hr.

(b) Size of Lens:-

With a good 2,5 mm of the 40 mm lens obscured all round by the "pop-out" window holder, the net diameter of the light beam was about 35 mm. Considering that the detectors are evenly spaced inside a circle of diameter 24 mm, only 5,5 mm "leeway" was left between the edge of the detectors' circle and the edge of the beam. Hence the maximum deviation that could be tolerated

AT THE/

at the light source approximately 1 metre away, was about $0,3^{o}$.

It was therefore decided to use a larger diameter lens. Inspection of the protective ramps showed that if they were lif= ted a few mm, a 60 mm lens could be tolerated. Since 5 mm must be deducted to account for the "pop-out" window holder, the light beam would then have a diameter of 55 mm.

The resultant "leeway" on either side of the detector circle then became about 15,5 mm, and the maximum allowable deviation of the light beam became $0,9^{o}$ - a factor of 3 greater.

Like the previous lens, this one also had the radius of curvature of one face, six times that of the other. It was not possible to extend the focal length though, because of the lack of space. However measurement showed the new focal length to be 125 mm, instead of 120 mm.

Using the actual diameter of the light beam, the effects of spherical aberration can be calculated from equation 3-8. The circle of least confusion has a diameter

$$b = \frac{0,07f}{N^3} = \frac{(0,07)(125)}{(2,27)^3} = 0,75 \text{ mm} \qquad (5\text{-}1)$$

which is acceptable.

Subsequent field tests yielded satisfactory results, as can be seen from Table 5-2. Here measurements of the contact wire between Maitland and Goodwood Stations made by the device, are compared with the accurate records of that section supplied by the S.A.R.

It must be borne in mind that though the records of the S.A.R. are quoted to the nearest hundredth of a mm, they are spot readings taken at the centre of each span. The distance between each reading is therefore about 67 metres. On the other hand, the readings of the device are only accurate to the nearest $1\frac{1}{2}$ mm, but they are only 1 cm apart. Also the S.A.R. records were taken in March 1975, while those of the device were taken in July 1975.

It is therefore understandable that many of the readings

show a worse state of wear than is shown in the records, especially since the information is "time-lengthened" by the device, and the worst case always takes predominance. However the TRENDS are clearly the same.

During the test, no bouncing of the contact wire on the pan was noticed, but on many occasions information was lost when the contact wire slid up the ramp and hence out of the light beam. This did not only occur at points and at cross overs, but also where stagger was more pronounced and at curves due to centrifuge.

Because of the staggering of the photodetectors in the "vertical" array, any slight tilting of the pan during such excursions caused the contact wire to appear much thinner than it actually was. Fortunately these errors were easily recognisable because they were accompanied by a bounce signal. They are the ringed readings in Table 5-2.

A section of the pen recorder chart from which the device readings of Table 5-2 were taken, is shown in Fig 5-2. The dotted lines refer to the six conditions of wear, (-, 0, 1, 2, 3 and 4). Superimposed on the chart are the March records of the S.A.R. (Represented by a series of connected dots.)

The fact that the pen recorder trace is seldom at one of its prescribed levels is due to its poor frequency response (of the order of one Hz), and the rapidly fluctuating contact wire condition. The ringed negative going peaks are the error readings mentioned above.

5-22 Mechanical Features.

(a) Weight Problem:-

The excess weight of the pan did not pose the problem originally visualised, though it did contribute significantly in degrading the system's performance.

To raise the pantograph, all that was required was some extra tensioning of its springs. However it did not have the same dynamic performance as an unloaded pantograph.

Modifications made to the pan included replacing the cadmium copper contact strips with longer steel ones (5 mm thick by about 30 mm wide), which were bowed up at each end to form the ramps,

AND EXTENDED/

MAITLAND —> GOODWOOD (1)

TABLE 5-2

POLE No.	THICKNESS (mm)	TRUE STATE OF WEAR (March, 1975)	MEASURED STATE OF WEAR (July, 1975)
7/17 - 8/1	14,28	4	4 —> 3
8/1 - 8/2	14,20	3	4 —> (-)
8/2 - 8/3	14,44	4	Bounce
8/3 - 8/4	13,06	3	Bounce
8/4 - 8/5	10,06	1	1 —> 0
8/5 - 8/6	10,28	1	0 —> 0
8/6 - 8/7	9,77	0-1	0 —> 0
8/7 - 8/8	10,15	1	0 —> 1
8/8 - 8/9	10,07	1	1 —> 0
8/9 - 8/10	10,09	1	0 —> 1
8/10 - 8/11	13,08	3	3 —> (-)
8/11 8/12	12,72	2-3	(-) —> 1
8/12 - 8/13	12,80	3	2 —> 1
8/13 - 8/14	12,56	2	3 —> 1
8/14 - 8/15	12,65	2	3 —> 2
8/15 - 8/16	12,67	2	3 —> 2
8/16 - 8/17	12,27	2	3 —> 2
8/17 - 9/1	12,35	2	2 —> 3
9/1 - 9/2	12,49	2	1 —> 2
9/2 - 9/3	12,63	2	2 —> (-)
9/3 - 9/4	12,52	2	2 —> 1
9/4 - 9/5	12,37	2	3 —> 2
9/5 - 9/6	12,34	2	2 —> (0)
9/6 - 9/7	12,39	2	2 —> 2
9/7 - 9/8	12,37	2	2 —> 1
9/8 - 9/9	12,30	2	1 —> 2
9/9 - 9/10	13,24	3	2 —> 1
9/10 - 9/11	10,11	1	1 —> 0
9/11 - 9/12	10,48	1	0 —> (-)
9/12 - 9/13	10,65	1	0 —> (-)
9/13 - 9/14	11,16	1	1 —> 0

MAITLAND —> GOODWOOD (2)

TABLE 5-2

POLE No.	THICKNESS (mm)	TRUE STATE OF WEAR (March, 1975)	MEASURED STATE OF WEAR (July, 1975)
9/14 - 9/15	14,56	4	0 —> 3
9/15 - 10/1	14,73	4	3 —> 4
10/1 - 10/2	14,84	4	3 —> 4
10/2 - 10/3	14,81	4	3 —> 4
10/3 - 10/4	14,74	4	3 —> 4
10/4 - 10/5	14,81	4	4 —> 3
10/5 - 10/6	12,79	2-3	Bounce
10/6 - 10/7	12,27	2	4 —> (-)
10/7 - 10/8	12,87	3	2 —> 1
10/8 - 10/9	12,40	2	2 —> 2
10/9 - 10/10	12,13	2	2 —> (0)
10/10 - 10/11	12,27	2	2 —> 1
10/11 - 10/12	12,25	2	1 —> 2
10/12 - 10/13	11,82	2	2 —> 2
10/13 - 10/14	12,74	2-3	2 —> 1
10/14 - 10/15	11,57	2	1 —> 2
10/15 - 10/16	11,57	2	2 —> 1
10/16 - 10/17	12,50	2	1 —> 2
10/17 - 10/18	13,33	3	2 —> 3
10/18 - 11/1	12,86	3	4 —> 3
11/1 - 11/2	13,15	3	2 —> 1
11/2 - 11/3	13,56	3	3 —> 2
11/3 - 11/4	12,47	2	3 —> 1
11/4 - 11/5	12,00	2	1 —> 2
11/5 - 11/6	12,86	3	3 —> 2
11/6 - 11/7	13,61	3	(0) —> 3
11/7 - 11/8	12,87	2	(0) —> 3
11/8 - 11/9	12,66	2	Ramp or Bounce

GOODWOOD → MAITLAND (1)

TABLE 5-2

POLE No.	THICKNESS (mm)	TRUE STATE OF WEAR (March, 1975)	MEASURED STATE OF WEAR (July, 1975)
10/15 - 10/14	14,27	3-4	3 → 4
10/14 - 10/13	14,27	3-4	4 → 3
10/13 - 10/12	14,48	4	4 → 3
10/12 - 10/11	14,21	3	4 → 3
10/11 - 10/10	14,34	4	4 → 3
10/10 - 10/9	14,34	4	3 → 4
10/9 - 10/8	14,36	4	3 → 4
10/8 - 10/7	14,29	3-4	3 → 4
10/7 - 10/6	14,52	4	4 → 3
10/6 - 10/5	14,56	4	4 → 3
10/5 - 10/4	14,47	4	4 → 3
10/4 - 10/3	14,03	3	4 → 3
10/3 - 10/2	14,51	4	3 → 4
10/2 - 10/1	14,50	4	3 → 4
10/1 - 9/15	14,36	4	3 → 4
9/15 - 9/14	14,33	4	4 → 3
9/14 - 9/13	14,34	4	4 → 3
9/13 - 9/12	14,36	4	3 → 4
9/12 - 9/11	14,33	4	4 → 3
9/11 - 9/10	14,29	4	4 → 2
9/10 - 9/9	12,56	2	2 → 3
9/9 - 9/8	10,70	1	2 → ⊖
9/8 - 9/7	10 16	1	2 → 0
9/7 - 9/6	12,38	2	1 → 2
9/6 - 9/5	11,37	2	2 → 1
9/5 - 9/4	11,27	1-2	1 → 3
9/4 - 9/3	11,80	2	3 → 1
9/3 - 9/2	11,08	1	2 → 0
9/2 - 9/1	11,28	1-2	1 → 1

See Fig. 5-2

GOODWOOD → MAITLAND (2)

TABLE 5-2

Pole No.	THICKNESS (mm)	TRUE STATE OF LINE (March, 1975)	MEASURED STATE OF LINE (July, 1975)
9/1 - 8/17	11,24	See Fig. 5-2: 1-2	1 → 3
8/17 - 8/16	11,13	See Fig. 5-2: 1	2 → 1
8/16 - 8/15	10,75	See Fig. 5-2: 1	1 → 0
8/15 - 5/14	10,98	1	2 → 0
8/14 - 8/13	10,89	1	1 → 0
8/13 - 8/12	11,19	1	2 → 1
8/12 - 8/11	10,91	1	0 → 1
8/11 - 8/10	10,24	1	0 → 1
8/10 - 8/9	12,24	2	1 → (-)
8/9 - 8/8	14,43	4	(-) → 4
8/8 - 8/7	11,60	2	4 → 3
8/7 - 8/6	12,08	2	2 → 3
8/6 - 8/5	12,22	2	3 → 2
8/5 - 8/4	13,00	3	3 → (-)
8/4 - 8/3	12,60	2	(0) → 2
8/3 - 8/2	11,41	2	2 → (0)
8/2 - 8/1	11,30	2	2 → 1
8/1 - 7/17	11,25	1-2	1 → 2
7/17 - 7/16	11,90	2	2 → 3
7/16 - 7/15	13,19	3	2 → (0)
7/15 - 7/14	10,98	1	(0) → 2
7/14 - 7/13	11,12	1	(-) → 1
7/13 - 7/12	11,01	1	1 → 2
7/12 - 7/11	10,71	1	2 → 1
7/11 - 7/10	11,96	2	1 → 2

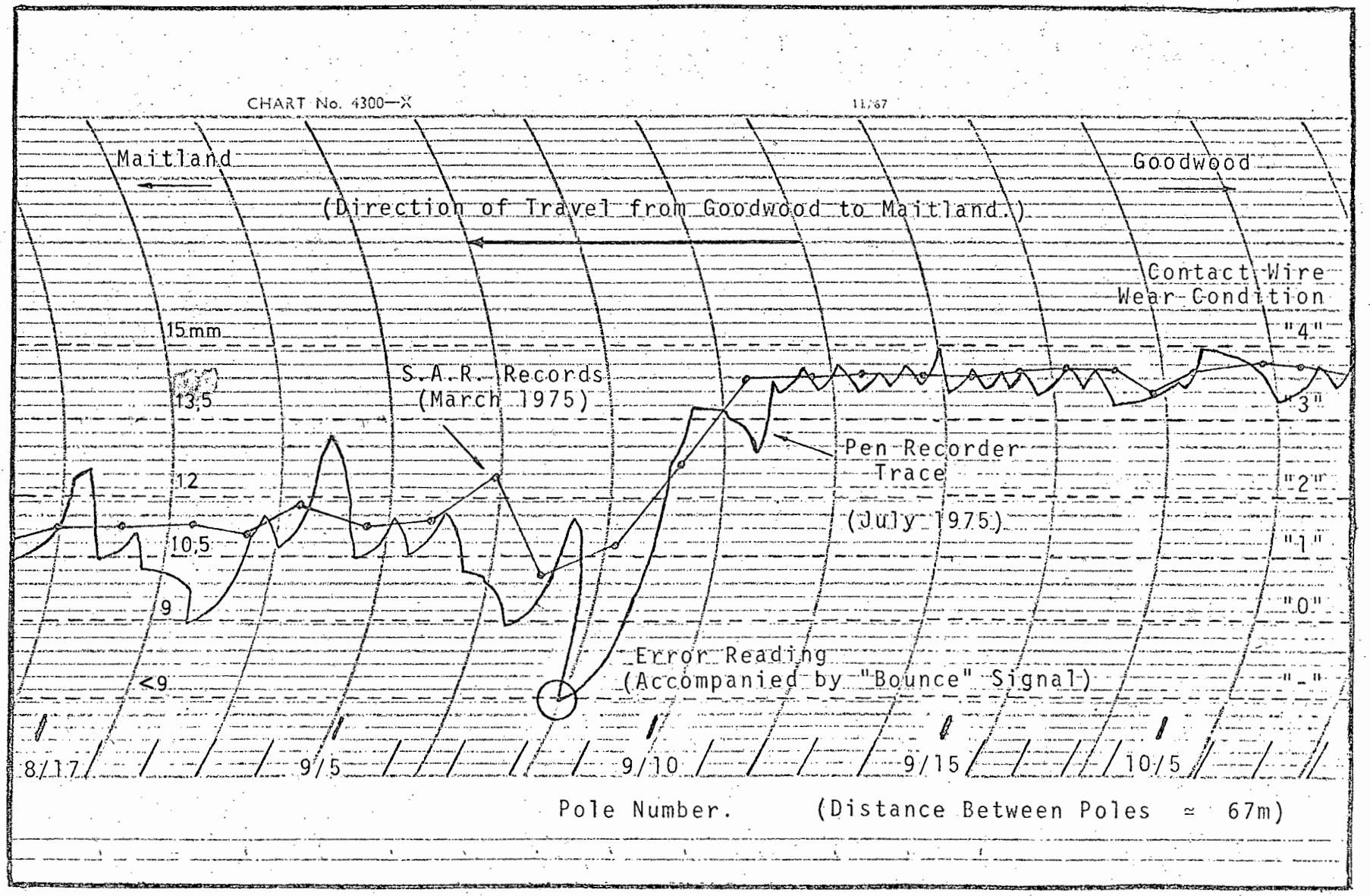

Fig 5-2: Section of Pen Recorder Chart Showing Contact Wire Wear Condition Between Pole Numbers 8/16 and 10/7 on Goodwood-to-Maitland Line.

and extended down to the ends of the horns.

Another modification involved its mounting onto the pantograph. The depth of the box did not allow a normal fit, so spacers of about 3 cm had to be used to lift the pan relative to the mounting point. The result, which is shown diagramatically in Fig 5-3, clearly leads to greater instability.

(b) Ramps:-

A great deal of concern had initially been felt as to whether the ramps protecting the optical equipment, would stand up to the harsh treatment meted out by the overhead line - especially at points and at cross-overs. These fears proved groundless, as the pan manoeuvred its way under these obstacles at normal running speeds with ease.

A more serious danger however, is the possibility of a contact wire supporting arm which has not been bowed up sufficiently, catching on a ramp and causing the contact wire to be pulled from its mountings. Although this is very unlikely to happen since the maximum height of the ramps is only 5 cm above the level of the contact strips, with the type of ramp framework in the prototype, it is nonetheless a distinct possibility. Clearly later models will require more thought in this direction if continued safe operation is to be guaranteed. They could possibly be made more streamlined as shown in Fig 5-4, so that a supporting arm would slide over it rather than hooking onto it. This would naturally mean that they should be made from a metal sheet instead of their present framework construction.

(c) Grease:-

Care had to be taken not to lift the pantograph in the vicinity of the Railway sheds where the grease on the contact wire was very thick.

This was actually done by way of an experiment, and within 5 minutes so much grease had accumulated on the top of the pan as to obscure part of the light beam.

The problem was hardly noticeable between stations however,

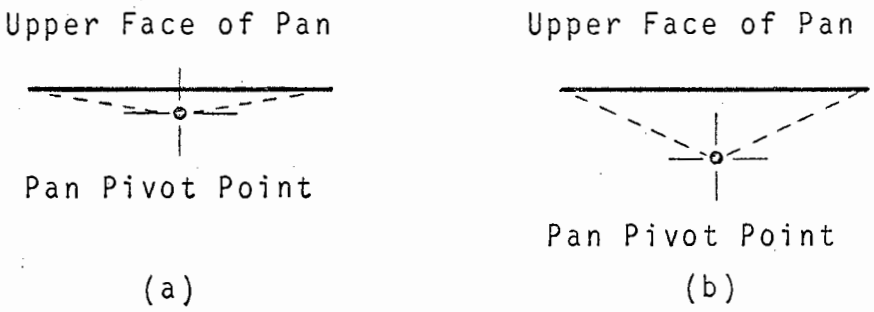

Fig 5-3: Standard Pan Mounting - (a)
Modified Pan Mounting - (b)

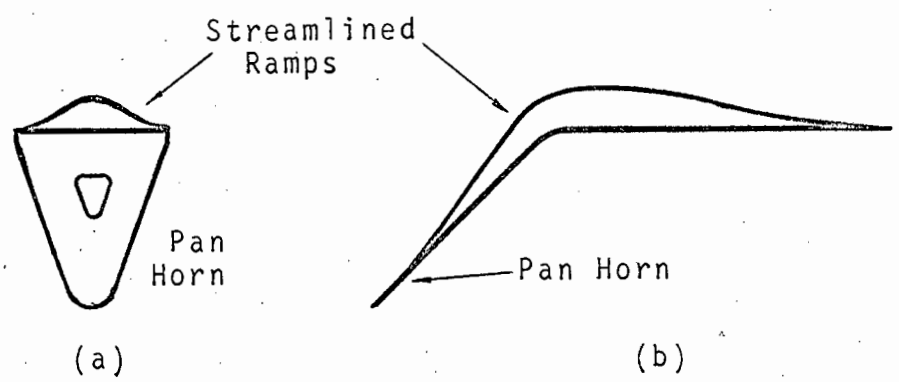

Fig 5-4: Pantograph Pan with Streamlined Ramps.
(a) End View.
(b) Side View.

and inspection of the pan after a 20 Km trip showed only a small build up of grease which did not affect the device at all. Nonetheless, future models should have the section of the pan under the light beam cut away to allow the grease to fall through.

(d) Vibration:-

The vibrations associated with the pantograph motion are, for reasons already mentioned, far more severe than normal.

During the device's first field test, half an hour's operation caused one of the bolts fixing the box to the underside of the pan, to rattle loose. Fortunately there was no damage done. (Later inspection showed that no spring washer had been placed on that particular bolt, and this mistake was duly rectified.)

(e) Rain:-

The device should not be used in the rain, because raindrops passing through the light beam refract and/or reflect the light away from the detectors.

5-23 Electrical Features.

As far as could be ascertained, there were no problems of an electrical nature. There are however, two features worthy of note.

(a) The screening proved adequate - even when the locomotive on which the device was mounted was being powered via its second pantograph.

(b) The optical data link to ground proved successful. As a precaution against a possible flashover being caused by dirt settling on the protective PVC hosepipe however, it is recommended that an earthed metal hose-clip be attached somewhere between the isolation gap and the receiving device.

CHAPTER 6

CONCLUSION.

6-10 General.

A full-scale prototype was constructed for gauging the wear on the overhead contact wire. Non-contact measurement was achieved by optical means, and the data was kept in digital form from start to finish.

The results show that the system is a viable proposition which should prove invaluable, especially on the long sections of electrified track between towns where manpower is low. Also it is relatively cheap to construct, the component cost alone totalling less than R600, of which the most expensive single item is the fibre-optic light guide.

The prototype scans the contact wire once every 0,7 ms, which at 50 Km/hr is once every centimetre. Hence it can be said to be a continuous measuring device.

The resolution is defined mainly by the vertical spacing of the photodetectors which is of the order of 1½ mm (10% of the thickness of the new contact wire). This can be considerably improved as will be described in Section 6-20.

Peak-signal-to-rms-noise ratios at the outputs of the photodetector amplifiers were of the order of 200:1, rendering the probability of error due to optical or internal electrical noise negligible. This was derated by a factor of 10 when the phototransistors were pointed directly at the sun. Such severe conditions should never occur in practice however, because of the protective cylinder at the back of which are housed the detectors. The cylinder served a dual purpose by also keeping the detectors free of the grease which sprays from the leading contact edge of the pan on the contact wire. A similar cylinder was used to keep the collimating lens clean.

The electromagnetic screening against the large fields associated with the currents in the live contact wire under normal running conditions proved adequate. It was also effective against severe transient magnetic fields generated in the laboratory.

THE METHOD/

The method of displaying and recording the data, which involved pre-processing it by first time-lengthening it, and then selecting only the worst condition in "memory" at any instant of time, was quite satisfactory. A pen recorder provided a permanent record of the contact wire profile, while a visual display of panel-mounted visible LED's provided a more convenient "on-the-spot" reading facility.

The increased weight of the box mounted on the overhead pan (because of the necessity for heavy magnetic screening) derated the dynamic behaviour of the pantograph at speeds above 60 Km/hr. Consequently no useful information could be obtained above this speed because of the vibrations induced in the pan. It should however, be possible to improve this in future models.

The railway engineers can use this prototype gauge to evaluate the usefulness of the system to their maintenance staff. If they decide that more of these devices are required, the following inprovements are recommended for future models.

6-20 IMPROVEMENTS FOR FUTURE MODELS.

(a) Finer Resolution:-

The uncertainty associated with an inter-detector spacing of 1½ mm is too great for any real reliance to be placed on any reading. (See Table 5-1). It should be reduced to a maximum of ½ mm, which is easily achieved with an integrated array of photodetectors. If even finer resolution than this is required however, there are integrated arrays available with elements spaced ¼ mm apart (5 thou).

(b) Improved Optics:-

Such a fine resolution would require a lens which is better compensated for spherical aberration. By varying the radius of curvature of each face in such a way as to cause parallel incident light on any zone of the lens to converge to the same point, the diameter of the circle of least confusion can be reduced right down to the μm level. Naturally this lens would cost a great deal more than those with faces of constant radii. It would also require a smaller source.

(c) Smaller Source Emission Area:-

Continued research into opto-semiconductor technology has resulted in LED's being developed with diameters of emission area as small as 13 μm.[1] As do the relatively large-area commercial LED's, they emit incoherently, but at brightness or radiance levels two to three orders of magnitude larger. This does not mean that they feature better quantum efficiencies, but is a result of brightness being proportional to current density, which is inversely proportional to emitting area. Hence the actual emitted optical power would be of the same order of magnitude for both types, if they were excited by equal currents. However their smaller sources permit shorter focal length lenses to be used, which permits a greater amount of flux to be captured.

There is no evidence that these devices are commercially available as yet. Their present day cost would probably be measured in hundreds of Rands - compared to the R2 of the ME 7121 used in the prototype.

THEIR ADVENT/

Their advent does introduce a new thought for the future. This is explained in Appendix IV, and involves mounting a number of such emitters, or better ones if possible, onto an integrated array.

(d) Circuit Modifications:-

The use of low current logic (eg. CMOS.) instead of TTL, would enable the circuit to be powered from a physically smaller voltage regulator with less heatsinking. This would allow the device to operate for longer periods between battery charges.

A further supply current reduction could be affected by using quad-comparators (4 in a 14-pin package), instead of the individual LM311's at the output of each amplifier. This too would help to conserve circuit space.

(e) Weight:-

The above modifications together with an improved circuit lay-out in general, would result in the size of the overhead box being reduced by at least a factor of two, implying a corresponding reduction in its weight.

Some thought should also be given to using some lightweight but strong alloy in the construction of a special pan, of which the box would form an integral part. If aerodynamic considerations are incorporated into the design, there is no reason why the device should not operate successfully at speeds even exceeding 100 Km/hr.

(f) Accumulation of Grease:-

To prevent grease accumulating on the pan and blocking the light path, the portion of the pan under the light beam should be cut away. This will allow the grease to fall through.

(g) Data Recording:-

If the pan recorder were run off the locomotive wheels, (geared down by some convenient ratio), then the chart displacement would be proportional to the distance travelled. This would make the location of any point very much easier.

REFERENCES.

1. C.A. BURRUS: "Radiance of Small-Area High Current Density Electroluminescent Diodes", Proc. I.E.E.E., Feb., 1972, Vol 60, No 2, pp 231 - 2.

A P P E N D I C E S

I REJECTED METHODS OF CONTACT WIRE WEAR MEASUREMENT.

I-1 Resistance Measurement.

The expression for the resistance of any material is:

$$R = \frac{\rho l}{A}$$

$$\text{ie. } A = \frac{\rho l}{R} \qquad \text{(I-1)}$$

where ρ = resistivity of material
l = length
A = cross-sectional area.

Since the cross-sectional shape of the conductor is known, a relationship between the residual area and thickness can be drawn up.

The resistivity being a constant of the material, all that is required is to determine R by measuring the voltage between two points on the line a distance l apart, and dividing by the current flowing through the cable. (The latter quantity could possibily be measured with a Hall-effect device.)

Taken at face value therefore, it seems that this is a plausible approach to contact wire thickness measurement. However there are some inherent difficulties that make it very unlikely to succeed.

1. Consider first the orders of magnitude involved. For new contact wire at $20^{o}C$,

$$R = 112 \text{ milli-ohms/metre} \quad \text{(max)}.^{1}$$

Hence the voltage developed across one metre of wire by a current of 1 000 amps is

V =/

$$V = IR = 112 \text{ milli-volts (max)}$$

This is certainly measurable under normal circumstances, but no reliability can be guaranteed when there is a sliding contact between voltage probes and contact wire, especially with the contact surface covered in grease. (This would cause variations in contact resistance ranging from near zero to almost infinity, which would make accurate voltage measurement impossible - even if very high input impedance amplifiers were used.)

Reliability would also suffer because of the inevitable contact loss between probes and cable due to bouncing.

2. Even assuming the voltage to be accurately measurable, the corresponding value of A would be the average over the length l. If this were as long as a metre, then hard spots (the most treacherous type of wear), would go by unnoticed. Reducing l by a factor of 10 or even 100 would only reduce the voltage by the respective amount, making its measurement even more difficult.

3. The temperature coefficient of copper is 0,226% per degree Centigrade.[2] Hence a change in ambient temperature of $20^{o}C$ would result in a change in resistivity ρ of almost 5%.

The overhead cable is also subject to Joule-heating, which is proportional to the square of the current flowing through it. ($P = I^2R$) (a 1 000 amps flowing through a new cable would cause 112 watts to be dissipated per metre length.)

Hence for this method to succeed, the temperature of the overhead cable would have to be continuously monitored, and the resistivity adjusted accordingly.

4. With regard to current measurement, the best solution would be to use a Hall-Effort device, which has the advantage of being able to measure direct current.

Its principle of operation is as follows. When an external magnetic field B is applied perpendicularly to a current I_s flowing in the device (a semiconductor bar), an electric field is produced, perpendicular to both B and I and proportional to BI, and a transverse open circuit voltage V is consequently

observed. Hence if I_s is kept constant, V will be proportional to B alone.

The expression relating B to the current flowing in the contact wire I_c, is

$$B = \frac{\mu I_c}{4\pi r} \qquad (I-2)$$

where μ is the permeability of the medium, and r is the radial distance from the cable.

To function accurately therefore, the device would have to be kept a constant distance from the contact wire, so that B would be proportional to I_c alone. This would prove very difficult because of "stagger", though the problem is not insur= mountable.

Two possible solutions exist. The first is to use a servomechanism to drive a mechanical follower which could track the contact wire as it moves from side to side across the panto= graph head. This would necessitate an optical detector device to monitor the position of the contact wire, which makes the method too complicated for further consideration.

The second method is possibly more feasible, requiring an array of matched Hall-effect devices mounted at equal intervals along the head. The largest output could then be selected at any instant of time.

5. The contact wire is electrically connected to the catenary via the droppers and feeder connections which occur at regular intervals along the line. Hence the resistance measured will not be that of the contact wire alone, but of a variable parallel combination of droppers, catenary and contact wire.

On the above grounds the method was rejected as being impracticable.

I-2 DEFLECTION MEASUREMENT.

This idea entails the use of two pantographs a distance l apart, which press upward against the contact wire with a constant force P, causing it to deflect upward by an amount y_B at the midpoint. The deflection can then be measured either mechanically, or by an ultra-sonic radar device and related to the wear.

What makes it so appealing is that measurement can be affected from below the level of the pantograph head. The fact that there is a fourth power dependence on diameter can also be exploited, since a small change in wear will hopefully cause a large change in deflection.

Figure 1-6 describes how the tension in the contact wire is measured by a deflection method, which also relates to the thickness of the wire. It has the advantage of only taking stationary measurements. The following analysis considers what can be expected under dynamic conditions.

Fig I-1 shows the schematic approach. It can be seen that the distance between B and the droppers will vary continuously, so for a first approximation the case of symmetry about the point B will be considered. Another simplification that will be made will be to neglect the reactions at points A and C due to rubbing friction. (In any event this could be minimised by using very smooth and frictionless rollers to make contact with the overhead wire). Thirdly the points A, B and C will be considered to lie on the arc of a circle, which is a reasonable assumption provided l is made small enough.

Deriving an expression for the deflection entails taking moments about point B.

Hence

$$\begin{aligned} M_B &= P(\tfrac{1}{2}l) + T(\Delta + y_B) - w(x + \tfrac{1}{2}d)\{\tfrac{1}{2}(x + \tfrac{1}{2}d)\} + tx \\ &= P(\tfrac{1}{2}l) + T(\Delta - y_B) - \tfrac{1}{2}w(x + \tfrac{1}{2}d)^2 + tx \end{aligned} \qquad \text{(I-3)}$$

where

T = tension in the contact wire

t = tension in first effective dropper. (The weight of contact wire supported by the second effective dropper does not affect M_B to any appreciable extent.)

$(t = \frac{wd}{2})$

P = THE/

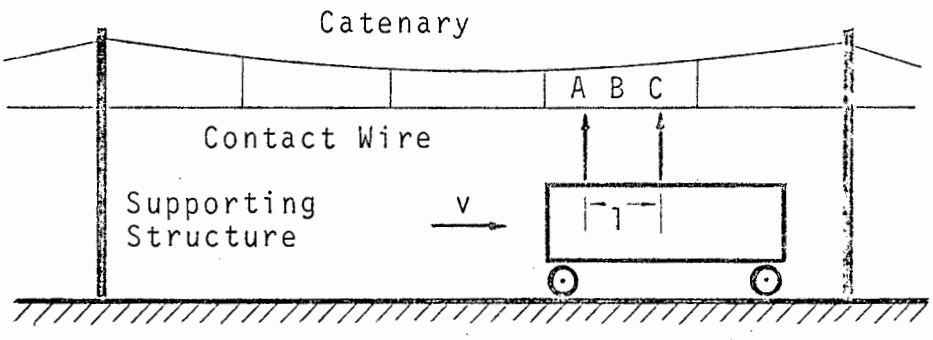

Fig I-1: Schematic Approach of Contact Wire Wear Determination by Measuring Deflection.

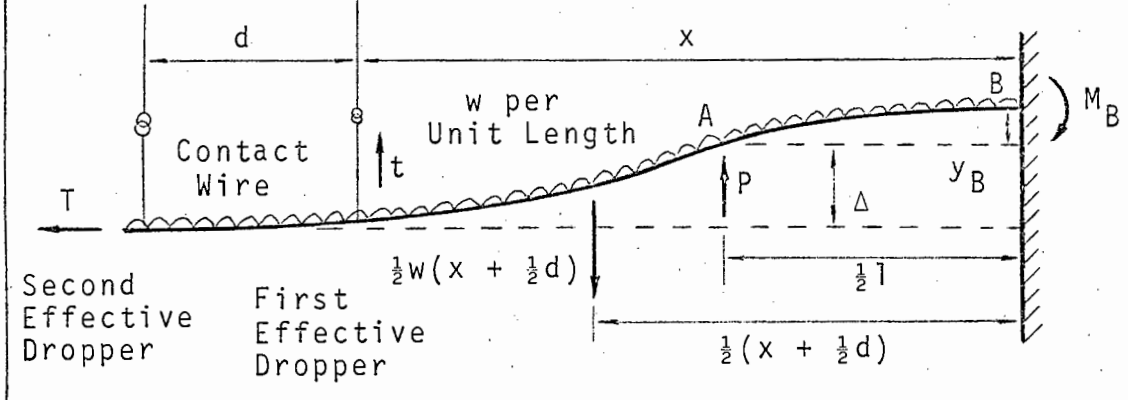

Fig I-2: Diagram Showing Distances and Forces Involved in Deflection Measurement Technique.

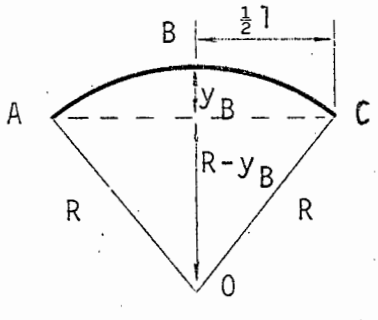

Fig I-3: Diagram Showing Relation Between y_B, l and R. It is Assumed that the Upward Forces Cause the Contact Wire to Form an Arc of a Circle.

P = the upward force supplied by the pantograph.

w = the weight of the contact wire per unit length.

Δ = The height of the pantograph head above normal contact wire height.

y_B = deflection of the contact wire

Using the formula for the bending of beams, it is possible to cancel M_B.

$$M_B/I = E/R \qquad \text{(I-4)}$$

M_B = moment above B

I = second moment of area about the neutral axis of the contact wire

E = Youngs Modulus

R = Radius of curvature at point B.

Also from Fig I-3.

$$(\tfrac{1}{2}l)^2 + (R - y_B)^2 = R^2$$

$$l^2/4 - 2Ry_B + y_B^2 = 0 \quad \{\text{Since } y_B \text{ is small, } y_B^2 \text{ is negligible}\}$$

$$\therefore y_B \simeq l^2/8R \qquad \text{(I-5)}$$

Combining equations (I-4) and (I-5), we get

$$y_B = \frac{l^2 M_B}{8EI} \qquad \text{(I-6)}$$

Then from (I-6) and (I-3)

$$y_B = \left(\frac{l^2}{8EI}\right)\{P(\tfrac{1}{2}l) + T\Delta - \tfrac{1}{2}w(x + \tfrac{1}{2}d)^2 + tx\}$$

$$= \frac{l^2\{P(\frac{1}{2}l) + T\Delta - \frac{1}{2}w(x + \frac{1}{2}d)^2 + tx\}}{\{8EI - Tl^2\}} \qquad \text{(I-7)}$$

Equation (I-7) is the important one, as it shows how y_B is dependant on the other parameters, some of which are characterised by wide variations.

THE TENSION/

The tension T for instance, can vary markedly from line to line.[3] The weight per unit length can change by almost 50% as it wears down to its critical thickness. Possibly the most serious factor however, is the variation in x - the distance between B and the first effective dropper - which follows a type of saw-tooth pattern as the locomotive moves along the line. the frequency of this fluctuation is proportional to train speed.

For the method to work with any accuracy at all, the term Pl/2 must be much larger than any other term in the bracket

$$\{\frac{Pl}{2} + T\Delta - w/2(x + \tfrac{1}{2}d)^2 + tx\} ,$$

in order to swamp out the effects of their variations.

The following typical values may be assumed.

$$\begin{aligned} 0{,}75 \text{ Kg/metre} &\leqslant w \leqslant 1{,}49 \text{ Kg/metre} \\ 600 \text{ Kg} &< T \leqslant 1\,200 \text{ Kg} \\ 2{,}5 \text{ metres} &< x < 5 \text{ metres} \end{aligned}$$

$$\begin{aligned} l &= 1 \text{ metre} \\ d &= 5 \text{ metres} \\ \Delta &= 0{,}05 \text{ metres (say)} \\ t &= wd/2 \text{ Kg} \end{aligned}$$

Then

$$\begin{aligned} 30 \text{ Kg-metres} &\leqslant T\Delta \leqslant 60 \text{ Kg-metres} \\ 9 \text{ Kg-metres} &< \tfrac{1}{2}w(x + \tfrac{1}{2}d)^2 < 42 \text{ Kg-metres} \\ 1 \text{ Kg-metre} &< tx < 4 \text{ Kg-metres} \end{aligned}$$

Hence for a minimum of 10% accuracy, Pl/2 must be at least 10 times larger than the sum of the maximum values.

$$\text{ie. } Pl/2 > 220 \text{ Kg-metres}$$
$$P > 440 \text{ Kg}$$

This by itself is prohibitive, since the contact wire would be lifted so high that other factors would be brought into play. For instance Δ and x would both increase, so the terms involving them which, in the above analysis have been relatively small,

WOULD/

would suddenly play a major part. Such an upward force could also cause the tension mounting of the cable to be strained, and the contact wire would experience excessive wear.

The tension T also appears in the denominator of equation (I-7), and, because it is so large, any variations in it must certainly affect y_B.

Other factors against the idea are listed below.

1. The new contact wire is supplied rolled on to large drums, so when it is straightened, it will have in it a series of bow-like bends and kinks, which no amount of tensioning will remove. These would cause errors in the measurement of y_B.

2. The carriage is a heavy vehicle and is subject to a great deal of bouncing on its suspension, especially around corners and on uneven sections of track. Hence it will be very difficult for the pantographs to maintain a constant upward thrust P, since they are themselves heavy frameworks and subject to swaying and bouncing.

3. Even assuming a special pantograph (probably hydraulic) was built for this purpose, it would have to be able to maintain a constant upward pressure regardless of the variations in contact wire height. Hydraulic devices are not always very reliable either, as they often suffer from "stiction", or static friction.

4. Finally, this method only looks at the average thickness of the cable between the two supports, A and B, so any isolated hard spots would pass undetected. Needless to say this method was not pursued further.

I-3 USING TELEVISION.

This entails mounting a television camera on the roof of a coach, and using it to scan the width of the contact surface of the overhead contact wire. Each line on the television screen then interrogates the contact surface.

The method shown in Fig I-4 has been tried by the Japanese[4], with a certain amount of success. They claim a resolution of 0,8 mm (which implies a 5% accuracy for the contact wire used by the S.A.R.), and that this can be maintained at speeds of up to 200 Km/hr. Also the apparatus is immune to interference from the fields generated by the currents in the overhead wires.

A very important advantage of such a system is that it requires nothing mounted on top of the pantograph head. Also the average thickness of the line is not measured, but rather it is scanned at intervals a distance d apart, which is dependent on the line frequency of the TV screen and the train speed. (They mention a frequency of 500 Hz, which at 200 Km/hr means that d is 11 cm).

However the method is not without its problems, one of them being the continuous variations in contact wire height. This was eventually satisfactorally compensated for by using a pantograph to monitor height & a strain gauge to give a proportional electrical signal.

Another problem which they had not yet solved when the paper was published was the phenomenon of stagger, but this they proposed to deal with by using some servomechanism to make the lens follow the wire. They also complained that the camera lenses became periodically fogged up and required constant attention. To improve the signal to noise ratio a light was shone upward against the contact surface.

Although this method seems promising in many respects, it was not pursued because it was thought that the approach finally decided upon might prove cheaper, and even more accurate. Also this one had already been taken to its logical conclusion by the Japanese.*

*Unfortunately letters sent to them requesting further information drew no response. Letters sent to other Japanese institutions which had attempted to solve the problem by other methods[4] were also unsuccessful.

IT IS/

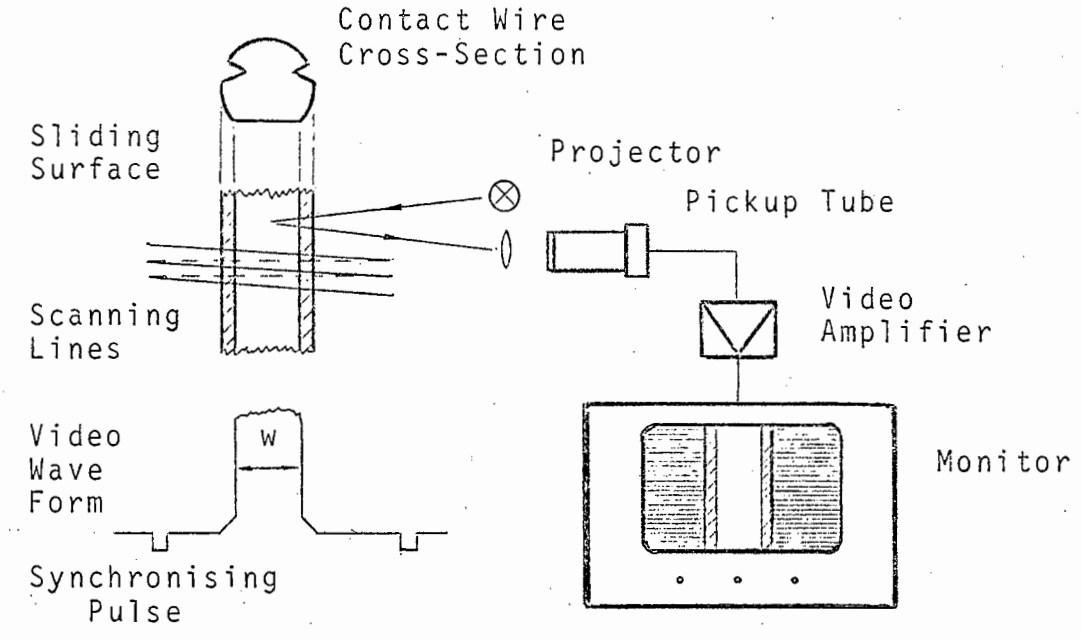

Fig I-4: Principle of Wear Assesment Using Closed Circuit Television to Scan Sliding Surface Width of Contact Wire.

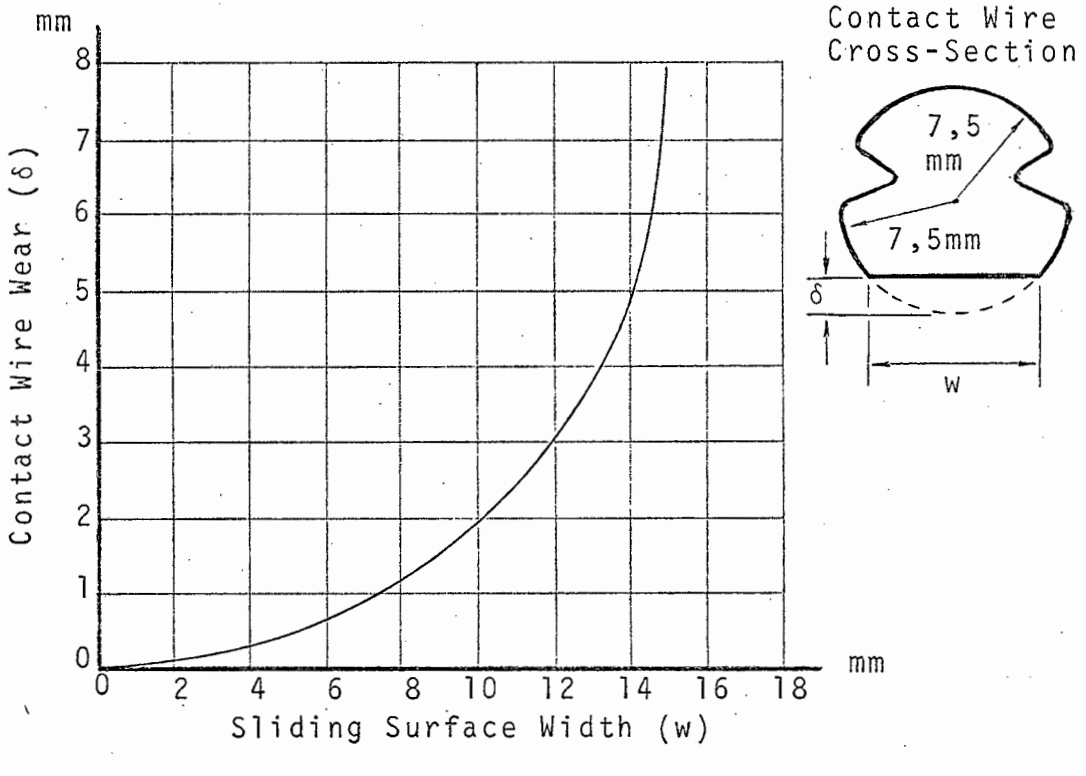

Fig I-5: Relation Between Contact Wire Wear (δ) and Sliding Surface Width (w).

It is also possible that the section of line on which this was tested had no lubricant on it, making the television approach a practical proposition. With thick deposits of dirty castor oil on the cable however, it is quite possible that the camera will not be able to distinguish the boundaries of the contact surface, and errors will result.

Another shortcoming of the method is that the contact width changes more and more slowly per unit change in thickness as the wear approaches its critical value. As can be seen from Fig I-5, for the first 50% of the allowable wear, the sliding surface width changes through 12 mm, while for the second 50% it only changes through 2,6 mm - hence the most critical part of the measurement is compressed into the last 18% of its range. Also an accuracy of 0,8 mm on the sliding surface width only implies a resolution of 1,4 mm on the wire thickness near the wear limit.

A method which measures the vertical thickness directly therefore seems preferable.

I-4 USING ULTRASONICS.

This method is appealing since measurement can also be made from below the level of the pantograph head.

The principle of operation would be to inject a pulse "packet" of ultrasonic waves into the contact surface of the wire by means of a transducer on top of the pantograph, and then to measure the time taken for it to bounce off the upper surface and return.

Such a technique has been successfully employed by the British Railways to detect rail flaws.[5] The ultrasonic probes are mounted on a trolley which is suspended from the underside of the coach, and is attached to it by means of a tow bar. The axles of the trolley are spring loaded to ensure that the probes follow the rail surface accurately, and the probes run on a thin film of water which acts both as a lubricant and an ultrasonic conductor. This is important since without the fluid, an air gap would exist between transducer and rail which would attenuate the signal.

Another solution to this problem has been to mount the transducer rigidly to the axle of a liquid-filled tyre,[6] which maintains sonic contact as it rolls along the rail. This has the advantage that it does not need a constant fluid supply, but has the disadvantage of decreased sensitivity.

Consider the orders of magnitude involved.

Velocity of Sound in Cadmium	=	$2{,}4 \times 10^5$ cm/sec
Velocity of Sound in Copper	=	$3{,}6 \times 10^5$ cm/sec
Hence velocity of Sound in Cadmium Copper	≃	3×10^5 cm/sec
Thickness of new cable	=	1,5 cm
Hence Delay Time	≃	10 µs
Thickness of Critically Worn Cable	=	0,9 cm
Hence Delay Time	≃	6 µs.

This means that the contact wire would be interrogated at least once every millisecond. At 50 Km/hr this amounts to once every 1,4 cm of length, which is sufficient resolution for detecting hard spots. The transducer frequency would have to be of the order of 100 MHz to produce sufficiently short pulse "packets" to measure the above delay times.

HOWEVER/

However, although this method has proved satisfactory for rail surveillance, it would be very difficult to implement on the overhead system. The main difficulty is of course, the way the contact wire is staggered.

A possible solution would be to use an elongated tyre, but for an acceptable signal to be transmitted across the interface, the rubber would have to be sufficiently pliable to allow a large surface area to be kept in contact with the wire. For good ultrasonic contact, it would also have to be firmly pressed against the cable. This would result in it wearing away extremely rapidly as a result of rubbing friction due to the wire continuously wiping across it - especially since it is so much softer than the copper.

Also for the method to operate satisfactorally, very little contact loss could be tolerated. However pantographs are subject to a certain amount of lurching and bouncing, particularly in areas where wear is severe. If the contact pressure were increased to counter this, it would only result in more rapid tyre wear; so this idea was also abandoned at an early stage.

II METHODS OF SETTING THE LIGHT SOURCE AT THE FOCAL POINT OF THE LENS.

II-1 Method 1

As has been mentioned in Section 3-23, this method was rejected because it did not prove very effective.

The idea in itself was simple enough, and merely entailed taking 2 readings, from which it was hoped the offset of the LED could have been read off from a table.

All that would have been required was a pair of cylindrical rods of different, but accurately known diameters. Each rod would then be set in turn, at the midpoint between the lens and detector array, as shown in Fig II-1; and its apparent diameter would be measured. The difference between the two apparent thicknesses would then be used to calculate the offset.

(It was thought important to use the difference between the two readings, as this was supposed to compensate for any errors caused by the sloping sides of the intensity distributions shown in Figs 3-6 & II-1. This assumption however proved incorrect.)

As will be appreciated, at first glance the idea does appear mathematically sound, (and indeed it would be for the ideal case.) It was only when it came to its application that its shortcomings were discovered, and then subsequent analysis of the uncertainties showed why it did not work.

The mathematical development of the idea follows.

(a) To Determine the Offset of the LED from the Focal Point.

The following quantities are defined with respect to Fig II-2.

r_1, r_2 = True radii of rods.
R_1, R_2 = Apparent radii of rods.
$2l$ = Distance between principal plane of lens and detector.
f = Focal length of lens.
u = Distance of LED to principal plane of lens.
v = Distance of LED image to principal plane of lens.
D = Offset of LED along principal axis.
$\delta = r_2 - r_1 \quad (r_2 \geq r_1)$
$\Delta = R_2 - R_1 \quad (R_2 > R_1)$

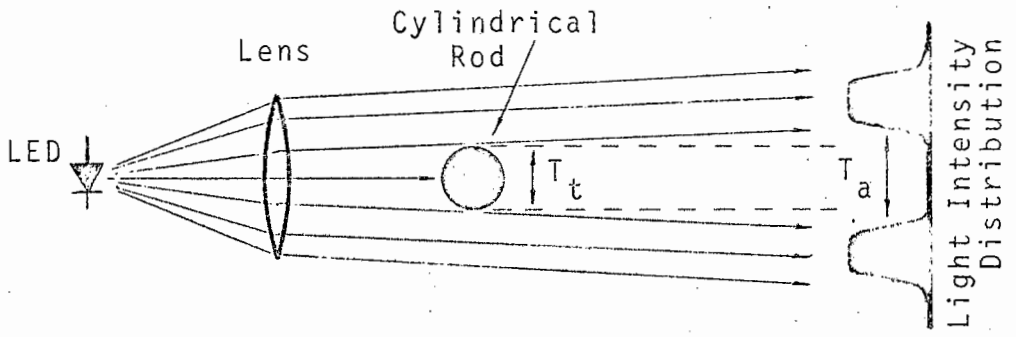

Fig II-1: Principle of Determination of Offset of LED from Focal Point of Lens.
(T_t = True thickness)
(T_a = Apparent thickness)

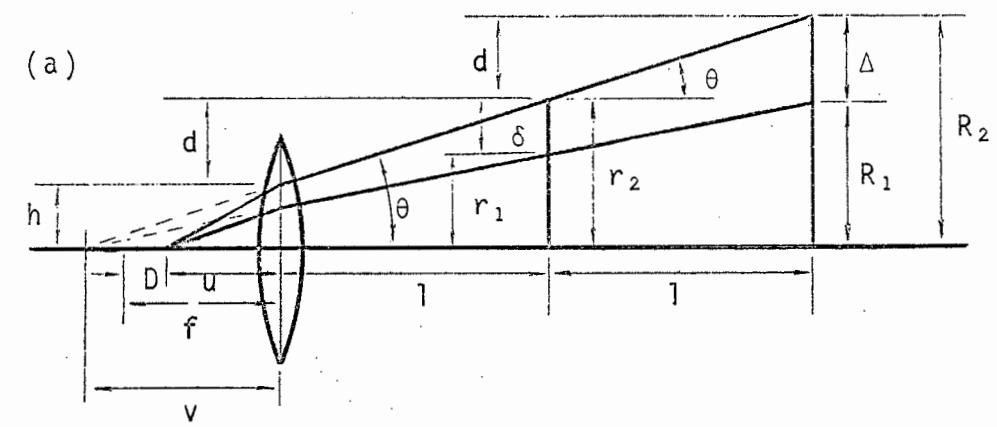

(u = distance of LED from focal plane of lens)

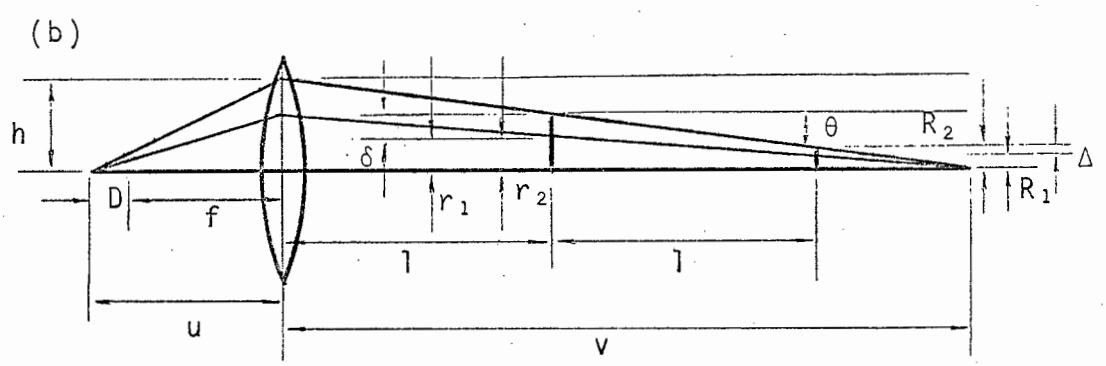

Fig II-2: Geometry of Light Rays Emitted from Point Source for:

(a) $u < f$
(b) $u > f$

As can be seen in Fig II-2, two distinct cases occur.

(i) LED too Close to Lens $(u < f)$

First find an expression for v in terms of δ, Δ and l.

$$\frac{\delta}{r_2} = \frac{\Delta}{R_2} \quad \Longrightarrow \quad R_2 = (\frac{\Delta}{\delta})r_2 \tag{II-1}$$

$$\text{Define} \quad d = (R_2 - r_2) = \{(\frac{\Delta}{\delta})r_2 - r_2\} = \frac{r_2(\Delta-\delta)}{\delta} \tag{II-2}$$

$$h = (r_2 - d) = \frac{(2\delta-\Delta)r_2}{\delta} \tag{II-3}$$

$$\text{Then} \quad \tan\theta = \frac{d}{l} = \frac{r_2(\Delta-\delta)}{\delta l} \tag{II-4}$$

$$\text{But} \quad \tan\theta = \frac{h}{v} \tag{II-5}$$

$$\text{Hence} \quad v = \{\frac{(2\delta-\Delta)r_2}{\delta}\}\cdot\{\frac{\delta l}{(\Delta-\delta)r_2}\} = \frac{(2\delta-\Delta)l}{(\Delta-\delta)} \tag{II-6}$$

Since the image in this case is virtual, v turns out to be negative. This is because $\Delta > \delta$.

(ii) LED too Far from Lens.

Again v must be found in terms of Δ, δ and l.

$$\frac{\delta}{r_2} = \frac{\Delta}{R_2} \quad \Longrightarrow \quad R_2 = (\frac{\Delta}{\delta})r_2 \tag{II-7}$$

$$\text{Define} \quad d = (r_2 - R_2) = \frac{r_2(\delta-\Delta)}{\delta} \tag{II-8}$$

$$h = (r_2 + d) = \frac{(2\delta-\Delta)r_2}{\delta} \tag{II-9}$$

$$\text{Again} \quad \tan\theta = \frac{d}{l} = \frac{(\delta-\Delta)r_2}{\delta l} \tag{II-10}$$

$$\text{But} \quad \tan\theta = \frac{h}{v}$$

$$\text{Hence} \quad v = \{\frac{(2\delta-\Delta)r_2}{\delta}\}\cdot\{\frac{\delta l}{(\delta-\Delta)r_2}\} \tag{II-11}$$

This time the image is real, so v is positive, since $\delta > \Delta$. Hence the only difference between the two expressions for v is one of sign.

Note too, that as $\delta \to \Delta$, so $v \to \infty$. This is in keeping with theory as when the object (a point source), is at the focal point of a lens, the light should emerge from the lens as a parallel beam.

The next step is to find u, the distance from the object to the lens, in terms of v. The expression for this depends on whether a thin lens or a thick lens is used, since for a thin lens the focal length on each side can be assumed to be equal. This need not necessarily be the case for a thick one.

Hence for a thin lens:

$$\frac{1}{f} = \frac{1}{u} + \frac{1}{v} \quad \Longrightarrow \quad u = \frac{fv}{v-f} \qquad \text{(II-12)}$$

But for a thick lens:

$$1 = \frac{f_1}{u} + \frac{f_2}{v} \quad \Longrightarrow \quad u = \frac{f_1 v}{v-f_2} \qquad \text{(II-13)}$$

The required parameter D, can now be calculated.

THIN LENS:- $D = (u - f) = \frac{f^2}{v-f} = \frac{f^2(\delta-\Delta)}{(2\delta-\Delta)1 - f(\delta-\Delta)}$ (II-14)

THICK LENS:- $D = (u - f_1) = \frac{f_1 f_2}{v-f_2} = \frac{f_1 f_2(\delta-\Delta)}{(2\delta-\Delta)1 - f_2(\delta-\Delta)}$ (II-15)

As can be seen, these two expressions are very similar.

Since the lens described in Section 3-13 is a thin one, Equation II-14 is the one to use. However, when an attempt was made to apply it in practice, the results it rendered were com=pletely wrong.

Further analysis shows why!

(b) To Determine the Uncertainty in D.

Since none of the parameters f, l, Δ or δ can be measured with absolute accuracy, it is instructive to estimate the uncer=tainty that can be expected in D. To do this Equation II-14 must first be broken up into its component terms as shown overleaf, and the uncertainty of each term calculayed independently. The resultant uncertainty can then be obtained.

COMPONENT/

Component Term.	Uncertainty.
$A = \delta - \Delta$	$\Delta A = \lvert\Delta\delta\rvert + \lvert-\Delta(\Delta)\rvert$ $= \lvert\Delta\delta\rvert + \lvert\Delta(\Delta)\rvert$
$B = 2\delta - \Delta$	$\Delta B = \lvert 2\Delta\delta\rvert + \lvert\Delta(\Delta)\rvert$
$C = Bl$ $\ln C = \ln B + \ln l$	$\left\lvert\frac{\Delta C}{C}\right\rvert = \left\lvert\frac{\Delta B}{B}\right\rvert + \left\lvert\frac{\Delta l}{l}\right\rvert$ $\therefore \Delta C = \lvert C\rvert\{\left\lvert\frac{\Delta B}{B}\right\rvert + \left\lvert\frac{\Delta l}{l}\right\rvert\}$
$E = fA$	$\Delta E = \lvert E\rvert\{\left\lvert\frac{\Delta f}{f}\right\rvert + \left\lvert\frac{\Delta A}{A}\right\rvert\}$
$F = C + E$	$\Delta F = \lvert\Delta C\rvert + \lvert\Delta E\rvert$
$D = \frac{f^2 A}{F}$ $\ln D = 2\ln f + \ln A - \ln F$	$\left\lvert\frac{\Delta D}{D}\right\rvert = \left\lvert\frac{2\Delta f}{f}\right\rvert + \left\lvert\frac{\Delta A}{A}\right\rvert + \left\lvert\frac{-\Delta F}{F}\right\rvert$

Hence

$$\Delta D = \lvert D\rvert\{2\left\lvert\frac{\Delta f}{f}\right\rvert + \left\lvert\frac{\Delta A}{A}\right\rvert + \left\lvert\frac{\Delta F}{F}\right\rvert\} \qquad \text{(II-16)}$$

Typical values were then substituted for the various parameters, together with reasonable estimates of their respective uncertainties.

Note that the largest relative uncertainties will be in the measured values of R_1 and R_2. For the purposes of this analysis however, the resolution of the measuring system will be assumed to be 0,25mm (10 thou), which from Section 3-22 is probably the best that can be expected with the trigger voltage of the comparator set at an intermediate 45% of the maximum signal voltage.

Table II-1 lists the results for various values of Δ.

$r_1 = 4\text{mm} \pm 0{,}01\text{mm}$
$r_2 = 8\text{mm} \pm 0{,}01\text{mm}$

$\therefore \delta = 4\text{mm} \pm 0{,}02\text{mm}$

$\Delta = R_2 - R_1$ $\Longrightarrow$ $\Delta(\Delta) = \lvert\Delta R_2\rvert + \lvert\Delta R_1\rvert$
$= (0{,}25 + 0{,}25)\text{mm}$
$= 0{,}5\text{mm} \ldots (\text{II-17})$

$f = 120\text{mm} \pm 2\text{mm}$

$l = 500\text{mm} \pm 5\text{mm}$

Δ (mm)	D (mm)	ΔD (mm)	$(\frac{100\ \Delta D}{D})\%$
1	13,8	4,8	33%
2	10,4	4,5	43%
3	6,1	4,3	70%
4	0,0	3,7	∞%
5	-8,9	6,8	-77%
6	-23,2	13,3	-57%
7	-50,2	30,4	-61%

TABLE II-1:- Relating Offset of LED from Focal Point of Lens to Difference in Rod Radii, together with Associated Uncertainties.

Note: $D < 0 \implies u < f$
$\implies$ the image of the LED is real.
$D > 0 \implies u > f$
$\implies$ the image is virtual.

As can be seen from Table II-1, the uncertainties are so big that they render the calculations almost meaningless. This can mainly be attributed to the fact that the difference between R_1 and R_2 is used, so the uncertainty in Δ is double that of either R_1 or R_2. Hence the relative uncertainty $\frac{\Delta(\Delta)}{\Delta}$ is much larger than the others and tends to dominate the expression. It is even worse in cases like

$$\frac{\Delta A}{A} = \frac{\Delta(\Delta) + \Delta\delta}{\Delta - \delta},$$

especially as δ approaches Δ.

A second attempt at the problem is shown in Appendix II-2.

II-2 Method 2.

(a) To Determine the Offset of the LED from the Focal Point.

Since the idea of having to measure the diameters of two rods and using the difference proved fallacious, it was decided to attempt to repeat the idea using only one rod, as shown in Fig II-3. Not surprisingly the resultant expression is of similar form.

From Fig II-3, define

R_1 = true radius of rod
R_2 = apparent radius of rod
$2l$ = distance from principal plane of lens to detector
f = focal length of lens
u = distance of LED to principal plane of lens
v = distance of image of LED to principal plane of lens
D = distance LED is offset along principal axis.

Then $$r = R_1 - R_2 \qquad \text{(II-18)}$$

$$\tan\theta = \frac{r}{l} = \frac{R_1+r}{v} \qquad \text{(II-19)}$$

Hence $$v = \frac{(2R_1 - R_2)l}{(R_1 - R_2)} \qquad \text{(II-20)}$$

(Note:- This time, only the case of the real image will be considered, since the only difference in the virtual case is that v will be negative.)

From the lens formula,

$$\frac{1}{f} = \frac{1}{u} + \frac{1}{v}$$

it is possible to find D.

$$D = u - f$$
$$= \frac{f^2}{v - f}$$
$$= \frac{f^2(R_1-R_2)}{(2R_1-R_2)l - f(R_1-R_2)} \qquad \text{(II-21)}$$

(Compare Equation II-21 with Equation II-14.)

(b) TO DETERMINE

(b) To Determine the Uncertainty in D

Proceeding in a similar vein to Appendix II,1(b):

Component Term.	Uncertainty.
$A = R_1 - R_2$	$\Delta A = \lvert\Delta R_1\rvert + \lvert\Delta R_2\rvert$
$B = 2R_1 - R_2$	$\Delta B = \lvert 2\Delta R_1\rvert + \lvert\Delta R_2\rvert$
$C = lB$ $\ln C = \ln B + \ln(l)$	$\left\lvert\frac{\Delta C}{C}\right\rvert = \left\lvert\frac{\Delta B}{B}\right\rvert + \left\lvert\frac{\Delta l}{l}\right\rvert$ $\Delta C = \lvert C\rvert\{\left\lvert\frac{\Delta B}{B}\right\rvert + \left\lvert\frac{\Delta l}{l}\right\rvert\}$
$E = fA$	$\Delta E = \lvert E\rvert\{\left\lvert\frac{\Delta f}{f}\right\rvert + \left\lvert\frac{\Delta A}{A}\right\rvert\}$
$F = C - E$	$\Delta F = \lvert\Delta C\rvert + \lvert\Delta E\rvert$
$D = \frac{f^2 A}{F}$ $\ln D = 2(\ln f) + \ln A - \ln F$	$\left\lvert\frac{\Delta D}{D}\right\rvert = \left\lvert\frac{2\Delta f}{f}\right\rvert + \left\lvert\frac{\Delta A}{A}\right\rvert + \left\lvert\frac{\Delta F}{F}\right\rvert$

Hence

$$\Delta D = \lvert D\rvert\{2\left\lvert\frac{\Delta f}{f}\right\rvert + \left\lvert\frac{\Delta A}{A}\right\rvert + \left\lvert\frac{\Delta F}{F}\right\rvert\} \qquad \text{(II-22)}$$

Again typical values were substituted into the Equations for D and ΔD. The results are listed in Table II-2.

In columns 3 & 4 the ultimate limit of 0,25mm was assumed for the uncertainty in R_2. However columns 5 & 6 show the accuracy that could be expected if the resolution was that used in the finished product. (For reasons given in Section 3-24 this was chosen to be 1,5mm.)

Hence

$R_1 = 8\text{mm} \pm 0{,}01\text{mm}$

$f = 120\text{mm} \pm 2\text{mm}$

$l = 500\text{mm} \pm 5\text{mm}$

$\Delta R_2 = 0{,}25\text{mm}$ (Columns 3 & 4)

$\Delta R_2 = 1{,}50\text{mm}$ (Columns 5 7 6)

1	2	3	4	5	6
R_2 (mm)	D (mm)	ΔD (mm)	$(\frac{100\ \Delta D}{D})\%$	ΔD (mm)	$(\frac{100\ \Delta D}{D})\%$
2	13,8	1,6	12%	6,3	45%
4	10,4	1,5	14%	6,2	59%
6	6,1	1,3	21%	6,0	100%
8	0,0	0,9	∞%	5,4	∞%
10	-8,9	2,0	-23%	9,7	-109%
12	-23,2	4,1	-18%	18,6	-80%
14	-50,2	9,3	-19%	42,4	-85%

Table II-2: Relating Offset of LED from Focal Point of Lens to R_2, together with Expected Accuracies.

The results of columns 3 and 4 are appreciably better than those of Table II-1, and are accurate enough to be useful, though some fine adjustment may still be necessary.

However those of columns 5 and 6 are completely unacceptable for anything other than a very rough guide. Consequently the process of trial and error described in Section 3-23 turned out to be the only practical solution to the problem.

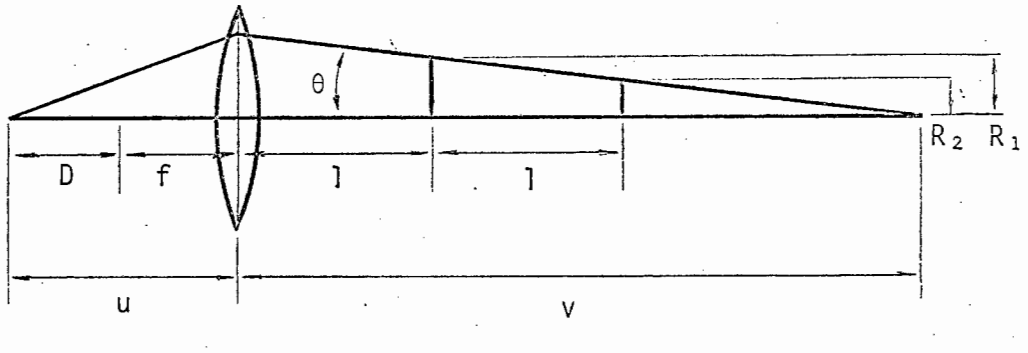

Fig II-3: Diagram Showing Convergence of Light Rays when LED Further Away from Lens than Focal Length (ie. u > f)

III MISCELLANEOUS CIRCUITS

III-1 LED Pulsing Circuits.

(a) The first circuit that was built for pulsing the LED is shown in Fig III-1. It also operated from voltage pulses of 1% duty cycle from a TTL source.

The principle of its operation is as follows. Each time the TTL gate output goes high, transistor T_7 is switched on, allowing base current ot flow from T_8 and hence causing T_9 to turn on. This causes current to flow through the LED.

When the TTL voltage drops to zero T_7 turns off, hence turning off T_8 and T_9, and the LED is given a chance to cool down before the advent of the next pulse.

T_5 and T_6 are included to protect the LED from destruction each time the power supply is switched on. (The 5 volt TTL rail is derived from the main 12 volt rail by means of an LM309 voltage regulator.)

Inspection of the TTL circuitry shows why they are neces= sary. (See the section of the circuit enclosed by the dashed line in Fig III-1.) The minimum supply voltage required to turn T_2 and T_4 on is the sum of the three PN junction conduction voltages

$$V_{min} = V_{be4} + V_{be2} + V_{bc1} \qquad \text{(III-1)}$$

While these transistors are still off, T_3 is quite able to conduct via the current path through R_2, D_1, R_5 and the base-emitter junction of T_7. T_7 is therefore turned on, and a large, continuous dc current is permitted to flow through the LED, causing its destruction.

With T_5 and T_6 in the circuit however, this is prevented. The zero diode Z_1 prevents T_5 from turning on until the main supply rail has risen to at least 7,5 volts, which is sufficient to allow the TTL rail to reach its 5 volts. While T_5 is off, T_6 receives base current from R_7, which turns it on, and causes it to rob T_7 of any base current it might have got from T_3.

R_8 AND/

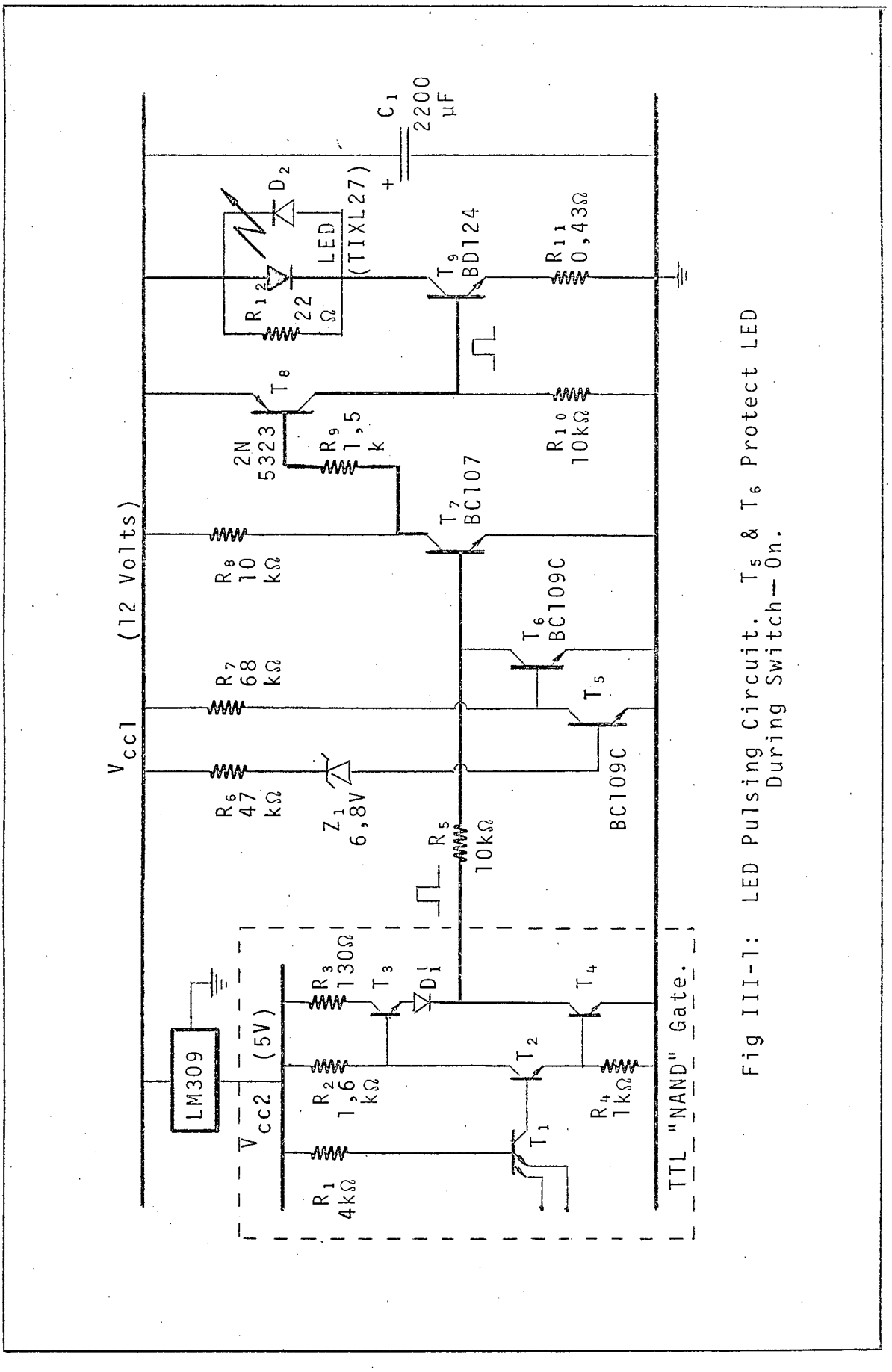

Fig III-1: LED Pulsing Circuit. T_5 & T_6 Protect LED During Switch—On.

R_8 and R_{10} are "bleeder" resistances, which tie the bases of T_8 and T_9 to their respective voltage rails when they are not conducting, thus protecting them from possible damage from stray electric fields. The function of R_{12} is to discharge the junction capacitance of the LED each time it is pulsed, and the diode D_2 ensures that the reverse voltage spikes that develop across the LED during switching do not exceed 0,7 volts. (Inverse voltages of as little as three volts can destroy a GaAs semiconductor junction.)

The decoupling capacitor C_1 must be large so that it can supply the energy demanded by the LED each time it is pulsed.

The current flowing through the LED can be calculated as follows. Each time the circuit is pulsed, T_9 is driven into saturation.

Hence $$I_{LED} = \frac{V_{cc1} - V_{LED} - V_{ce(sat)9}}{R_{11}} \qquad \text{(III-2)}$$

Since $$V_{LED} = V_j + I_{LED}R_D \qquad \text{(III-3)}$$

where V_j = junction voltage of LED

R_D = dynamic resistance of LED

$$I_{LED} = \frac{V_{cc1} - V_j - V_{ce(sat)9}}{R_{11} + R_D} \qquad \text{(II-4)}$$

The LED used at the time was the TIXL 27, which had a dynamic resistance of 2Ω, a junction voltage of 1,3 volts and a peak current carrying capability of 4 amps. Hence assuming $V_{cc(sat)9}$ to be about 1 volt,

$$4A = \frac{(12 - 1{,}3 - 1)V}{R_{11} + 2\ \Omega}$$

$$R_{11} = 0{,}43\ \Omega.$$

Transistor T_9 (type BD124) is also rated at a peak current

CAPABILITY/

capability of 4 amps.

The collector current of T_8 is then

$$I_{c8} = \frac{V_{cc} - V_{ce(sat)8}}{R_{10}} + \frac{I_{LED}}{h_{fe9}} \qquad \text{(III-5)}$$

$$= \frac{(12 - 0,4)V}{10\ \Omega} + \frac{4\ 000 mA}{25}$$

$$\simeq 160\ mA.$$

This is well within the current rating of T_8 (type 2N5323), which is 2 amps.

The collector current of T_7 can also be determined

$$I_{c7} = \frac{V_{cc} - V_{ce(sat)7}}{R_8} + \frac{V_{cc} - V_{ce(sat)7} - V_{be8}}{R_9}$$

$$= \frac{(12 - 0,2)V}{10\ \Omega} + \frac{(12 - 0,2 - 0,8)V}{1,5\ \Omega}$$

$$= 8,5\ mA. \qquad \text{(III-6)}$$

This is well within the capabilities of a BC107 transistor, which has a maximum rating of 100 mA.

Transistors T_5 and T_6, both BC109's, have collector current rating of 100 mA too, so they are quite safe with the small currents passing through them.

The circuit worked well enough in practice, but was rejected because it could not supply any protection to the LED in the event of a TTL failure at its input. Also it relied on the continued operation of T_5 and T_6 for protection, which are both active devices; it is far safer to rely on passive resistors and capacitors as in the circuit shown in Fig 4-1.

(b) The second attempt at a pulsing circuit for the LED is shown in Fig III-2. As can be seen, it incorporates the automatic switch-off mechanism described in Section 4-10.

THE OPERATION/

The operation of the circuit is quite simple. When the input voltage drops suddenly, base current from T_1 is able to flow onto the right hand plate of C_1. The resultant collector current from T_1 then activates the darlington pair, T_2 and T_3, causing current to flow through the LED.

When the input voltage V_{in} rises again, T_1 switches off, thus turning T_2 and T_3 off and terminating the LED current. Even if V_{in} fails to rise again however, C_1 will automatically charge up via R_1 and automatically turn T_1 off.

R_2 is included to ensure that C_1 charges right up to the positive rail after the base-emitter voltage of T_1 has become too small to allow it to pass any more current. The diode D_1 clamps C_1 to the 5 volt rail each time the input voltage rises.

R_3 and R_4 are "bleeder" resistances which tie the base terminals of T_2 and T_3 to ground respectively, when the circuit is off; hence protecting these transistors from being damaged by stray electric fields, as before.

An attractive feature about the circuit is that it uses a voltage rail which is already there to set the LED current - unlike the circuit of Fig 4-1 which incorporates a zener diode for this purpose. The LED current can therefore be determined as follows.

$$I_{LED} = \frac{V_{cc2} - V_{ce(sat)1} - V_{be2} - V_{be3}}{R_5} \qquad \text{(III-7)}$$

The LED used for testing the circuit was also a TIXL 27, which has a peak current carrying capability of 4 amps. This is also within the limits of the BD124 transistor.

$$4\ A = \frac{(5 - 0{,}2 - 0{,}8 - 0{,}9)V}{R_5}$$

$$R_5 = 0{,}8\ \Omega$$

The collector current of T_1 is then

$$I_{c2} = \frac{I_{c1}}{h_{fe1}} + \frac{V_{cc2} - V_{ce(sat)1} - V_{be2}}{R_4}$$

=/

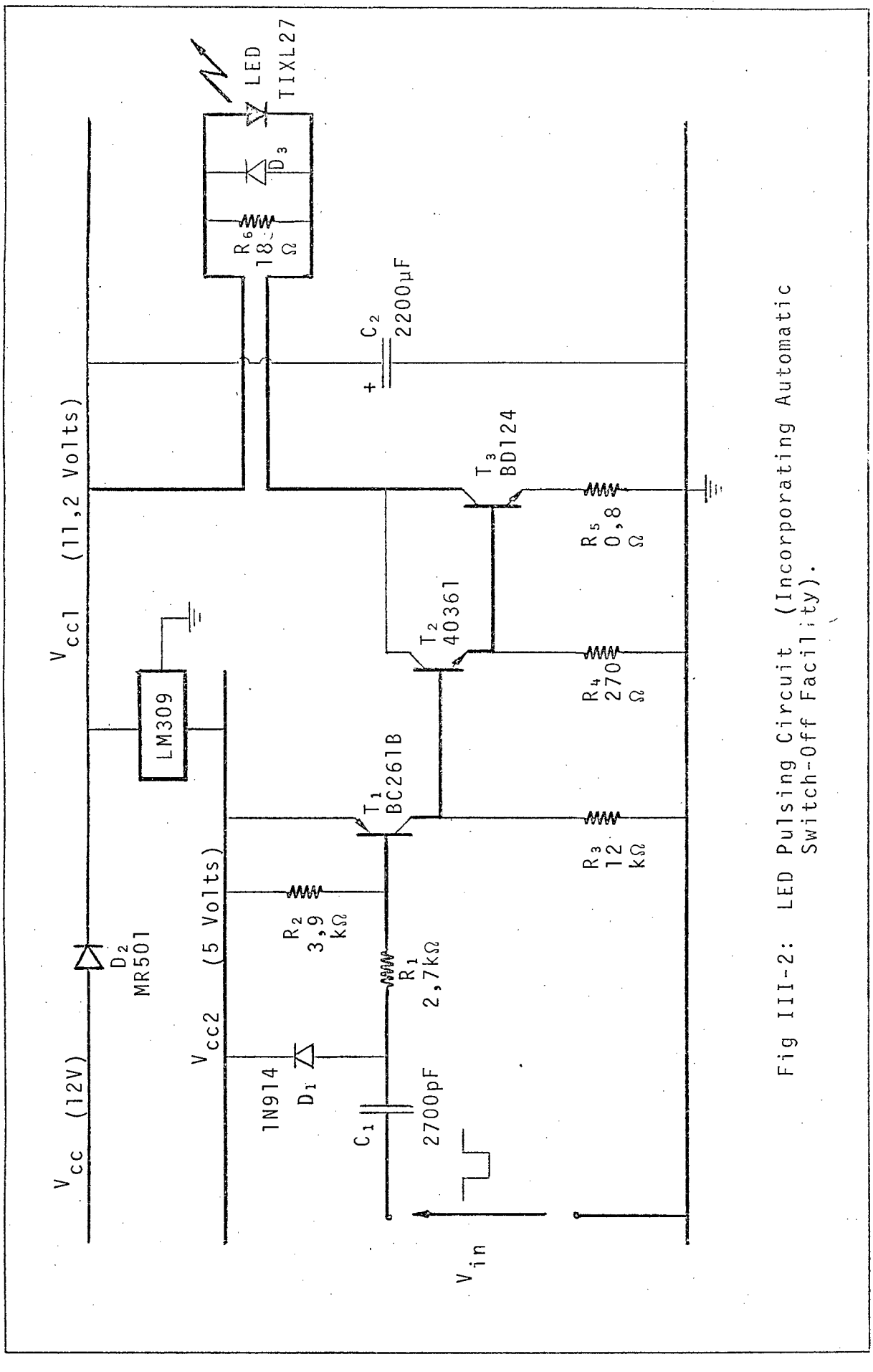

Fig III-2: LED Pulsing Circuit (Incorporating Automatic Switch-Off Facility).

$$= \frac{(4\,000)\ \text{mA}}{25} + \frac{(5 - 0{,}2 - 0{,}8)\text{V}}{0{,}27\ \Omega}$$

$$= 175\ \text{mA}. \qquad \text{(III-8)}$$

This is well within the capabilities of the 40361 transistor, which is rated at 700 mA for I_c.
The collector current of T_1 is

$$I_{c1} = \frac{I_{c2}}{h_{fe2}} + \frac{V_{cc2} - V_{ce(sat)1}}{R_3} \qquad \text{(III-9)}$$

$$= \frac{(175)\ \text{mA}}{70} + \frac{(5 - 0{,}2)\text{V}}{12\ \text{k}\Omega}$$

$$\simeq 3\ \text{mA}.$$

This is well within the capabilities of the BC261B transistor, which has a collector current rating of about 250 mA.

Unfortunately the transmission line effect of the long wires between the LED and T_3 caused large reverse voltages across the LED which even the diode D_3 could not suppress effec= tively. This was mainly because there was a connecting plug and socket in the middle of the line, which presented a dangerous mismatch that caused large reflections in the line - especially at the switching frequencies used.

(Even the power transistor T_8 (type BD124) was switching in about 0,2 µs - although it did have storage times of about 2 µs. This was because the current determining resistor R_5 was in its emitter, so its collector was not allowed to saturate.)

To safeguard the LED it was then decided to purposely slow down the current pulse and also to mount the pulsing circuitry right next to the LED itself, it being far safer to transmit the commanding TTL voltage pulses over the long leads rather than the large current pulses.

The circuit eventually used has been described in Section 4-10.

III-2 Photodetector Circuit.

The circuit described in Fig III-3* was considered for the first stage of the amplifier described in Section 4-22, but was eventually rejected because its bandwidth was too large for optimum match-filtering.

A useful feature about the circuit is that it automatically sets up its own bias conditions. The quiescent collector current of T_1 is given by

$$I_{c1} = \frac{V_{be2}}{R_3} \qquad \text{(III-10)}$$

The base current of T_1 can then be determined by dividing I_{c1} by h_{FE}, and the quiescent collector potential of T_2 is then

$$V_{c2} = V_{be1} + V_{be2} + I_{c1}(R_2 + \frac{R_1}{h_{FE}}) \qquad \text{(III-11)}$$

The open loop gain of the circuit (obtained by omitting R_1) is found to be

$$A = -(\frac{R_2}{R_3})(g_{m2}R_4) \qquad \text{(III-12)}$$

This is sufficiently high for the output signal voltage of the circuit to be merely taken as the product of the signal base current of T_1 and R_1. Hence if the phototransistor has sensitivity s, and is excited by an irradiance H,

$$i_{c1} = SH \qquad \text{(III-13)}$$

$$\frac{V_{out}}{H} = \frac{SR_1}{h_{fe1}} \qquad \text{(III-14)}$$

*This circuit is a modified version of one described in an article published by Hewlett Packard.[7] The basic difference lies at the front end, where the phototransistor T_1 is replaced by an ordinary transistor and a photodiode connected between its base and V_{cc}. In this configuration the article claims rise times of about 15 ns.

BECAUSE/

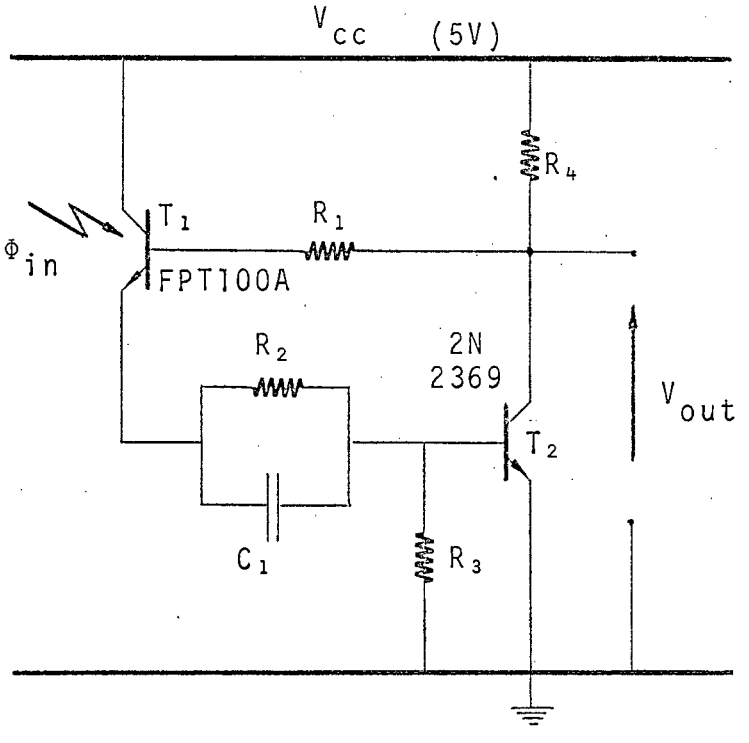

Fig III-3: High Speed First Stage for Opto-Amplifier.

Because of the high open loop gain however, overshoot will occur. In order to counter this a phase lead circuit in the form of R_2 and C_1 is incorporated, with a breakpoint at the upper limit of the circuit bandwidth.

The bandwidth of the circuit is given by

$$B = \frac{1}{2\pi R_{in} C_{in}}$$

where R_{in} = Input Resistance "seen" looking into base of T_1.

C_{in} = Input Capacitance "seen" looking into base of T_1.

B is high because the input resistance is reduced by the feedback (in the form of R_1). In general

$$R_{in} = \frac{R_1}{A} \qquad \text{(III-16)}$$

The feedback also reduces the output resistance of the circuit. This may be calculated as follows:

$$i_{c1} = h_{fe1}\left(\frac{V_{out}}{R_1}\right) \qquad \text{(III-17)}$$

$$\begin{aligned} i_{c2} &= g_{m2} V_{be2} \qquad \text{(III-18)} \\ &= g_{m2} i_{c1} R_3 \\ &= i_{out} \end{aligned}$$

Hence $$R_{out} = \frac{V_{out}}{i_{out}}$$

$$= \frac{R_1}{h_{fe1} g_{m2} R_3} \qquad \text{(III-19)}$$

IV OPTICAL MEASUREMENT OF CONTACT WIRE WEAR USING EMITTING AND DETECTING ARRAYS.

A possible future approach to the problem would require matched emitter and detector arrays as shown in Fig IV-1. This would have the advantage of eliminating the problems associated with producing the parallel light beam described in the main text. It would also be more accurate.

The proposed method requires each array to have the same number of elements, equally spaced; and it basically involves time-multiplexing the emitter-detector pairs. Hence each emitter would be sequentially pulsed, and while emitter E_i was on, only detector D_i would be receptive. This would eliminate the need for having a parallel light beam, since the light incident on the detector would have travelled in a straight line from its corresponding emitter.

Previously the irradiance at the detectors was the same as at the lens, which was 12 cm away from the source. In this case however, the detectors would be about 100 cm away, so by the inverse-square law, the new irradiance would be about 70 times less. Also, because of the inevitably smaller size of the detectors in the array, their sensitivities would be that much less, so far stronger emitters would be required. This could be compensated for, to a certain extent, by using a drum lens in front of each array, as shown in Fig IV-2. These would concen= trate the light in the horizontal plane only, while in the verti= cal plane it would diverge as before. Hence the principle of operation would be unaffected.

Assuming the inter-element spacing of both arrays to be 0,25 mm,* and the detectors to be photodiodes, then

Length of array	≈	25 mm
Inter-element spacing	≈	0,25 mm
No. of elements/array	=	100
On-time of emitter	=	½ µs
Relaxation time	=	½ µs
Time to sequentially pulse every element of array	=	100 µs.

*Optical semiconductor arrays commercially available today boast spacings of 0,127 mm or 5 thou. They are made by such firms as I.P.L., Texas Instruments, Motorola Opto, and many others.

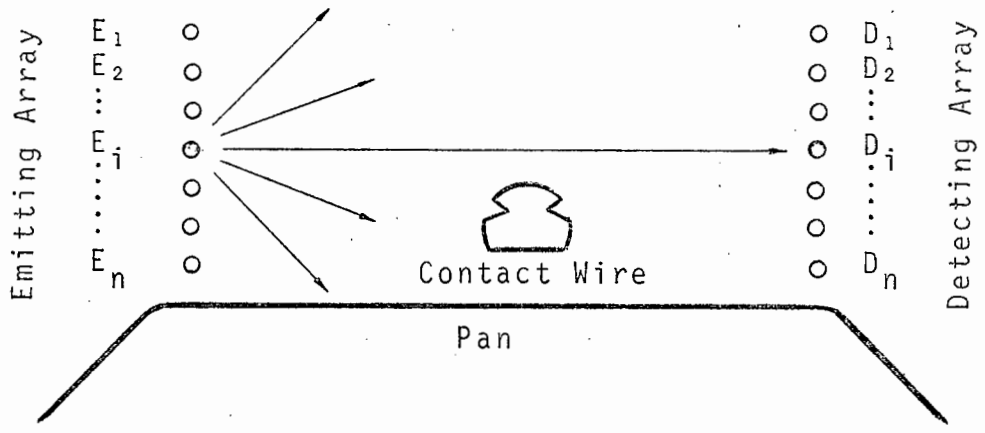

Fig IV-1: Contact Wire Wear Measurement Using Emitting & Detecting Arrays, and Time-Multiplexing Each Emitter-Detector Pair.

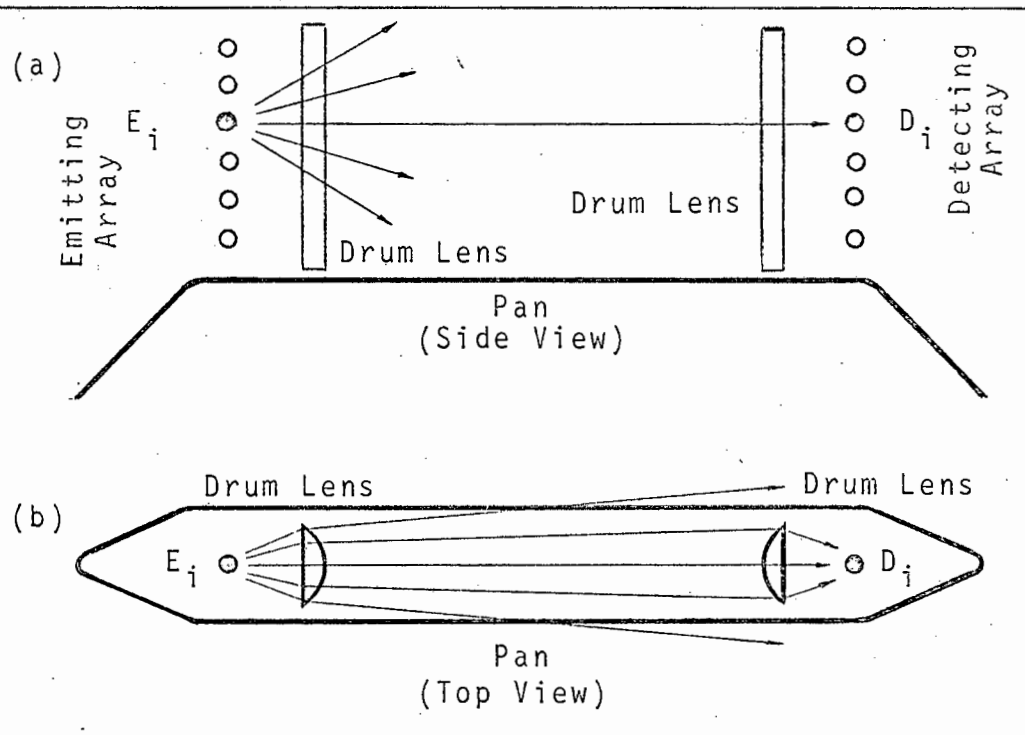

Fig IV-2: Contact Wire Wear Measurement Using Arrays, with Drum Lenses to Collect the Light in the Horizontal Plane.

In 100 µs, a vehicle travelling at 100 Km/hr would cover a distance of 2,8 mm, which is small enough to make the method feasible. Also, if the cycle was repeated every 500 µs, 400 µs would be available for data analysis, and the duty cycle of each individual emitter would only be 0,1%.

Since it would prove unwieldy to pulse 100 bits of information down to ground each cycle, this could first be converted to a 7-digit binary number at CMOS or if necessary, Shottky Logic speeds. (A 1 MHz clock could pulse 100 bits out of a shift register in 100 µs).

The binary number could be transmitted down to ground via the same single channel optical link as before by pulse-width modulation - a wide pulse corresponding to a logical "1", and a narrow one to a logical "0".

Further data manipulation would proceed as before.

It must be appreciated that this method would prove very difficult to implement if one uses discrete components. Because of the limited space available in the vicinity of the detecting array, and the six-fold increase in the number of optical amplifiers, long signal wires would have to be used to link the detectors to the amplifiers, which might introduce problems at the increased speeds. Also the decreased irradiance would require an extra stage on each amplifier, which would demand even more space.

A possible solution would be to integrate the amplifiers, and shift registers into the same chip* as the detectors. This would eliminate the large number of long leads required, since most of the interconnecting could be done internally. Access however would have to be provided for the following:

(a) Power supply,

(b) Clock to pulse information out of shift registers,

(c) Serial signal output from shift registers.

(d) Clock for a second shift register to turn each amplifier on in turn.

(e) Preset and reset facilities for shift registers.

*Such integrated circuits are commercially available today, but they operate in the charge-storage-mode and not the pulse-mode, so they would clearly be unsuitable for this application.

(f) Coherent detection facility for amplifier outputs, (this could possibly be incorporated with d.)

Problems may arise in the fine adjustment of the amplifier gains, but this could possibly be done at the sending end by varying the current through the individual emitters.

The possibility of using an array of Laser Diodes to achieve higher signal levels, should also be investigated.

REFERENCES.

1. "Specification for Hard Drawn, Grooved Copper Contact Wire for Electrical Traction Purposes", S.A.R. Electrical Dept., Dec.,1966, Spec. No. CEE-CIA-1.

2. "Reference Data for Radio Engineers - Fifth Edition", Howard W. Sams and Co., Inc. (a Subsidiary of ITT.)

3. "Contact Wire Tension Chart - Hans Schmidt Gauge", S.A.R. Electrical Department, Ref. No. ET 1/500/12.

4. KENJI HORIKI and MATSUTARO ICHIKAWA: "ITV Technique for Measurement of Trolley Wire Wear", J.R.T.R.I. Quart. Reports, 1971, Vol 12, No 2, p 84.

5. "Engineering Spotlight - Ultrasonic Probe Detects Rail Flaws", I.E.E. Electronics and Power, June 1971.

6. RICHARD GOLDMAN: "Ultrasonic Technology", pp 168 - 179.

7. "Electrical Isolation Using the H.P. 5082-4310", Hewlett Packard, Application Note 909.

NPN Planar* Phototransistors

FPT 100/100A/100B
FPF 110/110A/110B

General Description

The FPT 100 and FPF 110 are three-terminal NPN Planar phototransistors having exceptionally stable characteristics and high illumination sensitivity. The availability of the base lead gives wide latitude for flexible circuit design. The case is a special plastic compound with transparent resin encapsulation which exhibits stable characteristics under high humidity conditions. The range of sensitivities offered in the A and B versions gives the circuit designer increased flexibility.

Absolute Maximum Ratings (Note 1)

Maximum Temperatures/Humidity

Storage Temperature	−40°C to +100°C
Operating Junction Temperature	−40°C to +85°C
Relative Humidity at Temperature	95% at 65°C

Maximum Power Dissipation (Notes 2 and 3)

Total Dissipation at 25°C Case Temperature	200 mW
at 25°C Ambient Temperature	100 mW

Maximum Voltages (Note 6)

V_{CBO}	Collector to Base Voltage	80 Volts
V_{CEO}	Collector to Emitter Sustaining Voltage (Note 4)	30 Volts
V_{ECO}	Emitter to Collector Voltage	5.0 Volts

Maximum Current

I_C	Collector Current	25 mA

Physical Dimensions
FPT 100/100A/100B

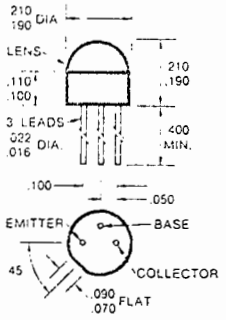

NOTES: 1. All dimensions in inches
2. All leads electrically isolated from case

Physical Dimensions
FPF 110/110A/110B

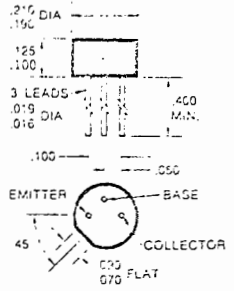

NOTES: 1. All dimensions in inches
2. All leads electrically isolated from case
3. Flatness variation of top of cap is ± .015
4. Photosensitive area is within a .080 diameter circle with center of circle coincident with the center of package

Electrical Characteristics (25°C Free Air Temperature unless otherwise noted)

Symbol	Characteristic	FPT 100/100A/100B			FPF 110/110A/110B			Units	Test Conditions
		Minimum	Typical	Maximum	Minimum	Typical	Maximum		
I_{CBO}	Collector Dark Current		0.25	25		0.25	25	nA	V_{CB} = 10 V (Note 6)
I_{CBO} 65°C	Collector Dark Current		0.025	0.5		0.025	0.5	μA	V_{CB} = 10 V (Note 6)
I_{CEO}	Collector Dark Current		2.0	100		2.0	100	nA	V_{CE} = 5.0 V (Note 6)
R_{CB}	Responsivity (Tungsten)	0.6	1.6		0.6	1.0		μA/mW/cm²	V_{CB} = 10 V H = 5.0 mW/cm² (Notes 4 and 9)
$R_{CB(.92)}$	Responsivity (GaAs)	1.8	5.3		1.8	3.3		μA/mW/cm²	V_{CB} = 10 V H = 5.0 mW/cm² (Notes 5 and 9)
$I_{CE(L)}$	Photo Current (Tungsten)	0.2	1.4		0.2	.88		mA	V_{CE} = 5.0 V H = 5.0 mW/cm² (Notes 4 and 8)
$I_{CE(L)}$	Photo Current (GaAs)	0.6	4.3		0.6	2.9		mA	V_{CE} = 5.0 V H = 5.0 mW/cm² (Notes 5 and 8)
t_r	Light Current Rise Time		2.8			2.8		μS	(Note 7)
t_f	Light Current Fall Time		2.8			2.8		μS	(Note 7)
$V_{CE(sat)}$	Collector to Emitter Saturation Voltage		0.16	0.3		0.16	0.33	Volts	I_C = 500 μA H = 20 mW/cm²
BV_{CBO}	Collector to Base Breakdown Voltage	80	150		80	150		Volts	I_C = 100 μA (Note 6)
$V_{CEO(sus)}$	Collector to Emitter Sustaining Voltage	30	50		30	50		Volts	I_C = 1.0 mA (Pulsed) (Note 6)
BV_{ECO}	Emitter to Collector Breakdown	5.0	10		5.0	10		Volts	I_{EC} = 100 μA (Note 6)

The following values affect the A and B versions only:

		FPT 100A			FPF 110A			
$I_{CE(L)}$	Photo Current (Tungsten Source)	1.0		3.0	0.6		1.8	mA	V_{CE} = 5.0 V H = 5.0 mW/cm²
		FPT 100B			FPF 110B			
$I_{CE(L)}$	Photo Current (Tungsten Source)	1.3		2.6	0.8		1.6	mA	V_{CE} = 5.0 V H = 5.0 mW/cm²

*Planar is a patented Fairchild process

FAIRCHILD MICROWAVE AND OPTOELECTRONICS DIVISION

500 Deer Creek Road, Palo Alto, California 94304, (415) 493-3100, TWX: 910-373-1278

TYPICAL ELECTRICAL CHARACTERISTICS

PHOTO CURRENT CHARACTERISTICS

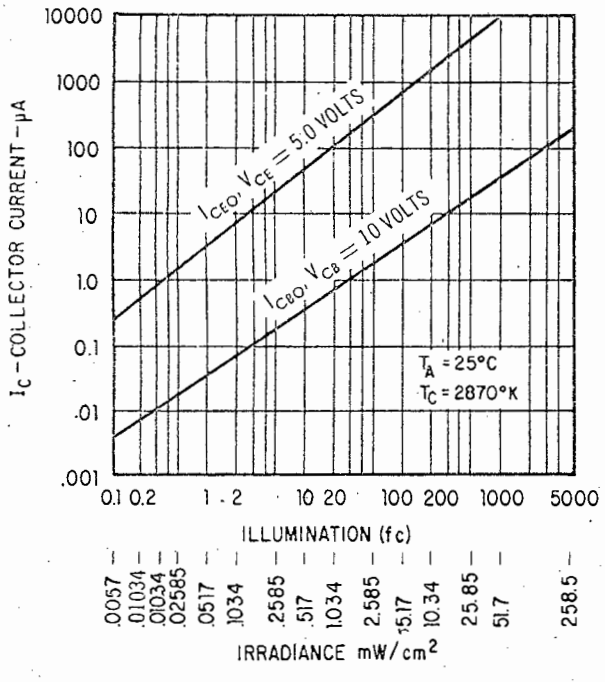

COLLECTOR CURRENT VERSUS COLLECTOR VOLTAGE

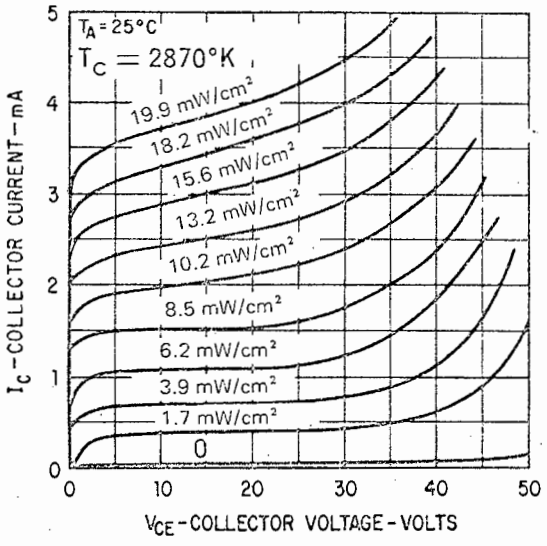

COLLECTOR BASE CHARACTERISTICS

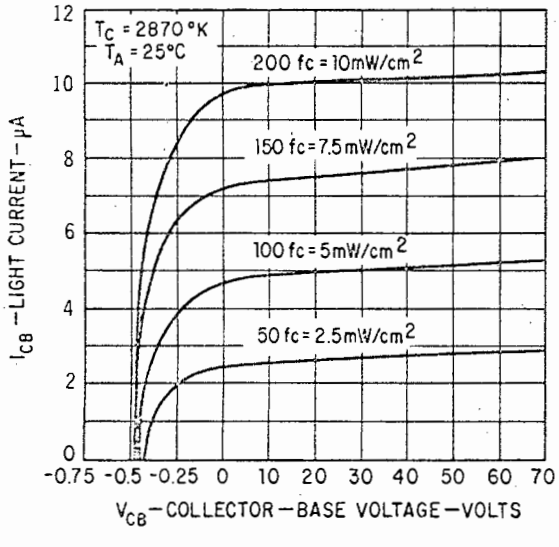

ANGULAR RESPONSE

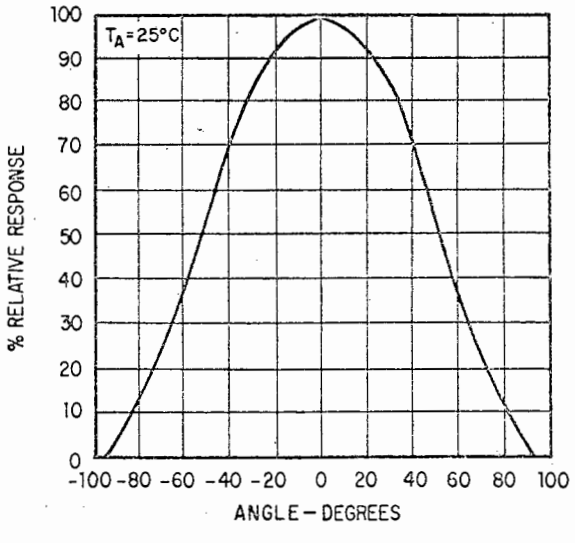

llector Dark Current Versus Temperature

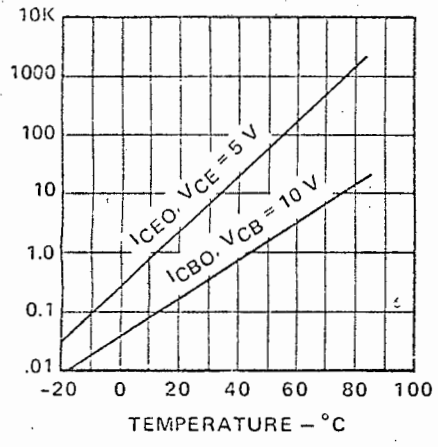

Spectral Characteristics

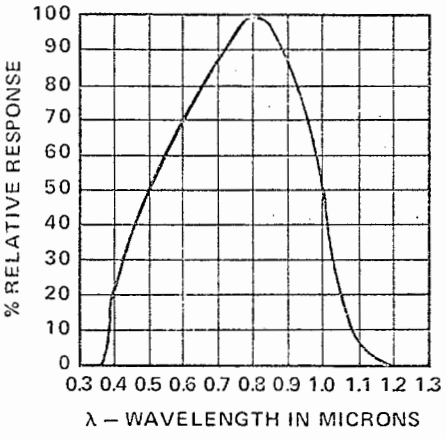

Rise and Fall Time Versus Collector Current

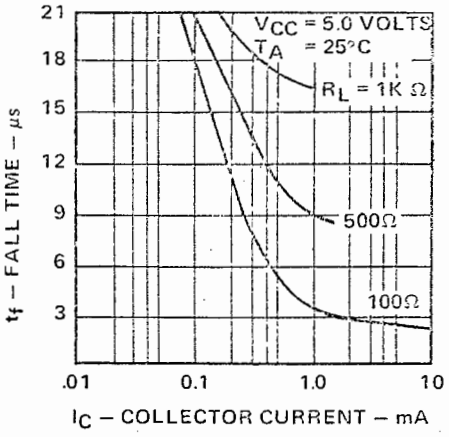

Turn-Off and Turn-On Delay Times for Circuit Shown

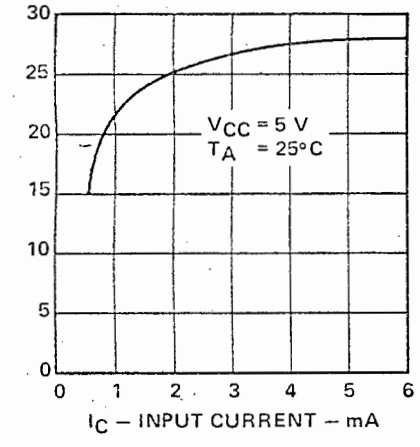

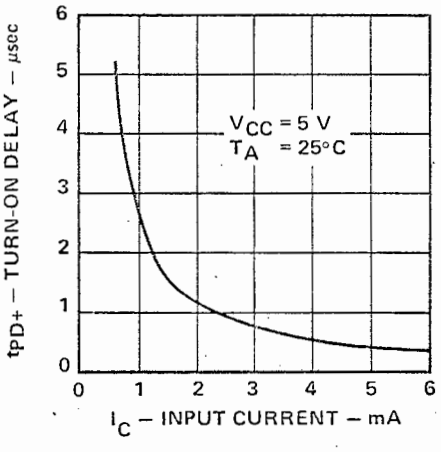

Switching Current for Rise and Fall Times

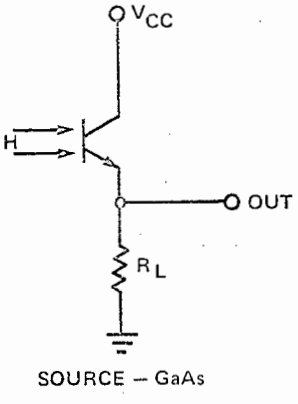

tes

These ratings are limiting values above which the serviceability of the device may be impaired.

These are steady state limits. The factory should be consulted on applications involving pulsed or low duty cycle operations.

These ratings give a maximum junction temperature of 85°C and junction to case thermal resistance of 300°C/Watt (derating factor of 3.33 mW/°C), and a junction to ambient thermal resistance of 600°C/Watt (derating factor of 1.67 mW/°C).

Measured at noted irradiance as emitted from a tungsten filament lamp at a color temperature of 2870°K. The effective photosensitive area is typically 1.25 mm² (FPT 100) and 0.78 mm² (FPF 110).

These are values obtained at noted irradiance as emitted from a GaAs source at 0.9μ.

Measured with radiation flux intensity of less than .1 μW/cm² over the spectrum from 0.1 micron to 1.5 microns.

Rise time is defined as the time required for I_{CE} to rise from 10% to 90% of peak value. Fall time is defined as the time required for I_{CE} to decrease from 90% to 10% of peak value. Test conditions are: I_{CE} = 4.0 mA, V_{CE} = 5.0 V, R_L = 100Ω, GaAs Source (FLD 100).

No electrical connection to base lead.

No electrical connection to emitter lead.

Circuit for Turn-On and Turn-Off Data

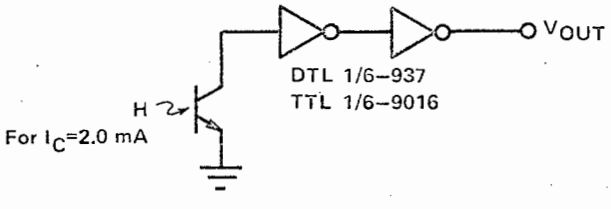

FAIRCHILD MICROWAVE AND OPTOELECTRONICS DIVISION
)0 Deer Creek Road, Palo Alto, California 94304, (415) 493-3100, TWX: 910-373-1278

©FAIRCHILD MICROWAVE AND OPTOELECTRONICS 1971 • PRINTED IN U.S.A. • 871-15M • MANUFACTURED UNDER ONE OR MORE OF THE FOLLOWING U.S PATENTS: 291077, 3015048, 3025589, 3064167, 3108359, 3117260; OTHER PATENTS PENDING

Monsanto

HIGH POWER INFRARED EMITTERS

ME7121, ME7122, ME7123, ME7124

PRODUCT DESCRIPTION

This family of high power liquid phase epitaxial IR Emitters is designed to accommodate all needs of the emitter detector relationship. Products range from a wide angle power spread for non-critical detector location to sharp-angle concentration of power for detectors located a significant distance from the emitter. The devices can be mounted with a plastic pop-in, furnished upon request.

PACKAGE DIMENSIONS

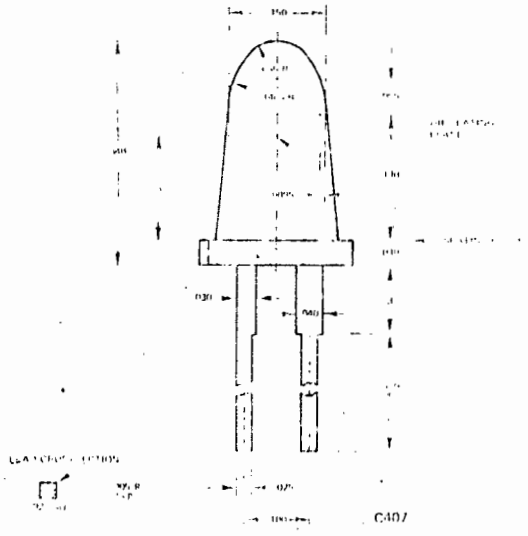

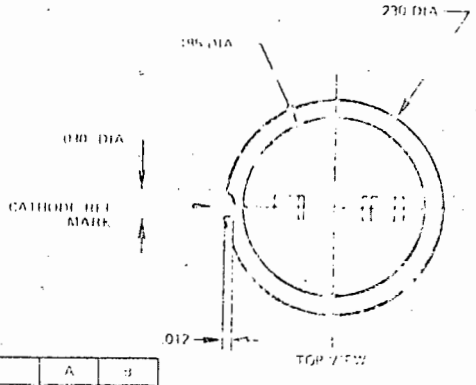

DIM	A	B
ME7121	190	190
ME7122	185	185
ME7123	180	180
ME7124	185	185

ABSOLUTE MAXIMUM RATINGS

Maximum power dissipation @ 25°C ambient	150 mW
Derate linearly from 50°C	2.8 mW/°C
Maximum storage & operating temperature	-55° to 100°C
Maximum lead solder time @ 260°C (Note 3)	5 sec
Maximum continuous forward current	100 mA
Maximum reverse voltage	3.0 V
Peak forward current (PW - 1.0 μsec, Duty Cycle = 0.1%)	6.0 A

ELECTRO-OPTICAL CHARACTERISTICS

	TYPICAL HALF ANGLE (DEGREES)	TYPICAL ON AXIS INTENSITY (MW/STR.) @ 50 mA	
• ME7121	15°	10.8	into cone @ 1/2 power points @ I_F = 50 mA, ROP = 3 mW
ME7122	10°	26.4	
ME7123	6°	105.6	
ME7124	4°	243.6	

	MIN.	TYP.	MAX.	UNITS	TEST CONDITIONS
Total External Output Power (Note 2)	1.0	3.0		mW	I_F = 50 mA
Peak Emission Wavelength		940		nm	I_F = 50 mA
Spectral Line Half Width		50		nm	I_F = 50 mA
Forward Voltage		1.4	1.8	V	I_F = 50 mA
Light Turn On & Turn Off Time		500		nsec	50 Ω Load

NEL
OUNTING
CHNIQUES

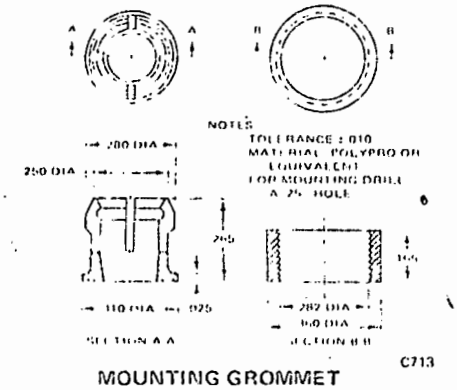

MOUNTING GROMMET

PANEL MOUNTING

TYPICAL ELECTRO-OPTICAL CHARACTERISTIC CURVES

(25°C Free air temperature unless otherwise specified.)

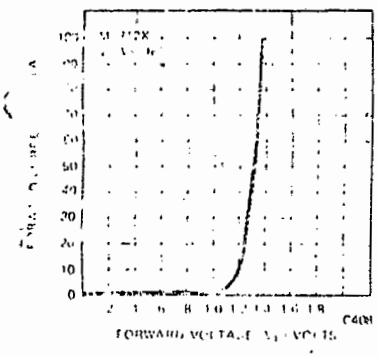

Fig. 1. I_F vs. V_F

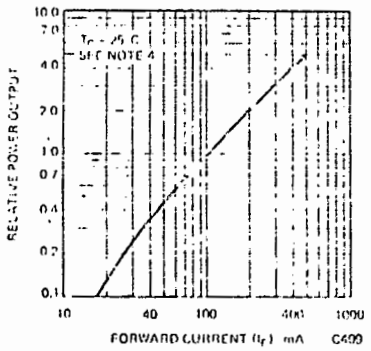

Fig. 2. ROP vs. I_F Peak

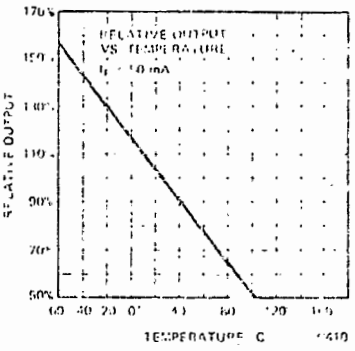

Fig. 3. ROP vs. Temperature (Note 1)

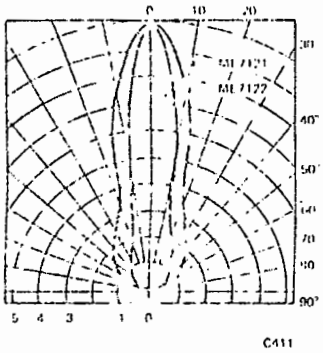

Fig. 4. Spatial Distribution (ME7121 and ME7122)

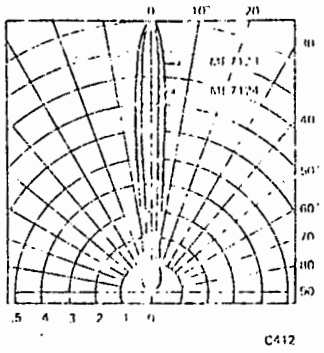

Fig. 5. Spatial Distribution (ME7123 and ME7124)

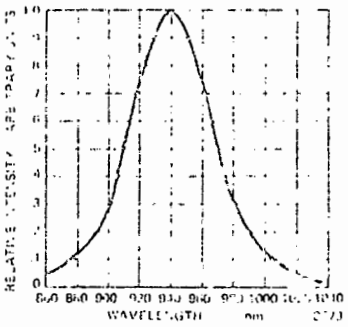

Fig. 6. Spectral Distribution

NOTES

1. *The curves in figure 3 are normalized to the power output at 25°C to indicate the relative efficiency over the operating temperature range.*
2. *The total external radiated power output measurements are made with a Centralab 110C solar cell terminated into a 100Ω impedance.*
3. *The leads of the ME7121, ME7122, ME7123, and ME7124 were immersed in molten solder, heated to 260°C, to a point 1/16 inch from the body of the device, per MIL-S-750.*
4. *This parameter is measured using pulse techniques tw=40 μsec duty cycle ≤10%.*